

Novel Block Copolymer Nanoparticles *via* RAFT Aqueous Emulsion Polymerization



Amy Alice Cockram

Department of Chemistry
The University of Sheffield

**Submitted to the University of Sheffield in fulfilment of the
requirements for the award of Doctor of Philosophy**

November 2018

Declaration

The work described in this Thesis was carried out at the University of Sheffield under the supervision of Professor Steven P. Armes FRS between October 2014 and November 2018 and has not been submitted, either wholly or in part, for this or any other degree. All the work is the original work of the author, except where acknowledged by references.

Signature:.....

Amy Alice Cockram

November 2018

Acknowledgements

I am incredibly grateful to many people who have helped and supported me since I first started out as a Chemistry undergraduate nine years ago. Firstly, thank you to my supervisor, Prof. Steve Armes. Thank you for taking a chance on me and offering me a summer project, for helping me get my first job in industry and then having me back to start a PhD. It has been an amazing opportunity to work with someone who has so many ideas, such incredible knowledge and excellent proof reading skills. I originally chose to study science because writing was not my strong suit. I think I can safely say that after four years of red pen my writing has improved significantly! I would also like to thank you for providing me with all the opportunities that came with being part of the CDT program and for the opportunity to travel to some amazing places for conferences.

A huge thank you to my industrial supervisors Neal Williams, Martin Murray and Simon Emmett. Thank you for providing me with an insight to a whole other world of research and for taking the time to impart some of your wisdom to me. I would also like to thank you and every other person who made me feel so welcome during my six-month placement at AkzoNobel, especially to Sylvie, Trish, Rob, Krystina, Dee, Sahar, Mojdeh, Agnieszka, Dawn, Jo, Damien and Julie. You all helped to make my time in Slough an enjoyable and fruitful experience. Thank you also to Seb Spain, Sasha Mykhaylyk and Tony Ryan for your contributions during our update meetings with AkzoNobel.

Thank you to all the support and technical staff who keep the department running smoothly. For everyone who has helped me with analytical techniques including Derry, Yin, Jeppe and James. Thank you to Sandra Marshall for all of your NMR help and career advice. A huge thank you to Dr Nick Penfold, for all the proof reading, advice and support. A huge thank you to Tom Neal for all the SAXS data, lab help and meeting prep and for always being there.

I feel extremely privileged to have been a part of the CDT in Polymers, Soft Matter and Colloids. I have had many wonderful experiences and the opportunity to meet many amazing people. In particular, I would like to thank Dr Joe Gaunt for your advice and unwavering support and for always having an open door policy. A special thanks to Dom, Matt, Luke and Ste for the many coffee breaks, support and understanding.

A huge thank you to every member of the Armes group past and present who I have had the privilege to work with. The advice and tutelage from the experienced members of the group has been invaluable. Thank you to past members Kate, Andrew, Dave, Lee, Nick, Mark, Lizzy, Vicki, Joe and Liam for helping to start me out on the right track. To everyone who has helped create a fun, friendly and supportive group; Shannon, Reb, Olly, Craig, Derek, Izzy, Greg, Irene, Sarah, Yin, Erik, Saul and Debs. To everyone else on F floor for making the office a more bearable place to be Canning, Rheanna, Emma, Jasmine, Anna, Marissa and Naomi. Thank you to Matt, Lucy, Fiona and Emma for your friendship and support over the last year. A special thank you to Charlotte, for your continued friendship since that first day of our summer project. To Kat, my thesis buddy, you have made this whole process considerably easier with your optimism and friendship. Thank you for every cup of tea, writing session, chat, text and hug.

To all my friends and family who have supported me unconditionally, even when they had no idea what I was going on about. To Rach, Harini, Sophie and Helen for your amazing friendship and always being there for me. To Robin and Bethany for your wonderful friendship. To Liz, without you I would not have found my way back into research, let alone on the road to becoming a Dr. To Mellie, for encouraging me to pursue my dreams. A special thanks to Andy, Jill and Katie for making me feel like part of the family. To my Nan, for always believing in me without a doubt. To my baby sister, for always being there through thick and thin. I know that with you by my side I can do anything. An enormous thank you to my Mum and Dad. Without you I would not be the person I am today. Thank you for everything you have done for me, for your constant encouragement, support, patience, love and support. I hope I have made you very proud.

Finally, to my Steve. Thank you for being by my side for the last 9 years. For always making me laugh and see the bright side. You have made the entire process of doing a PhD and writing a thesis easier. Thank you for being there for every up and down. With you everything is an adventure.

Publications

Primary Publications resulting from work in this thesis:

“Effect of monomer solubility on the evolution of copolymer morphology during polymerization-induced self-assembly in aqueous solution”, A. A. Cockram, T. J. Neal, M. J. Derry, O. O. Mykhaylyk, N. S. J. Williams, M. W. Murray, S. N. Emmett and S. P. Armes, *Macromolecules*, **2017**, 50, 796-802.

“Optimization of the high-throughput synthesis of multiblock copolymer nanoparticles in aqueous media via polymerization-induced self-assembly”, A. A. Cockram, R. D. Bradley, S. A. Lynch, P. C. D. Fleming, N. S. J. Williams, M. W. Murray, S. N. Emmett, S. P. Armes, *RSC reaction chemistry and engineering*, **2018**, 3, 645

Publications resulting from work conducted on other projects:

“Are block copolymer worms more effective Pickering emulsifiers than block copolymer spheres?” K. L. Thompson, C. J. Mable, A. Cockram, N. J. Warren, V. J. Cunningham, E. R. Jones, R. Verber and S. P. Armes, *Soft Matter*, **2014**, 10, 8615-8626.

“In Situ SAXS Studies During the RAFT Aqueous Emulsion Polymerization of 2-Methoxyethyl Methacrylate” E. E. Brotherton, F. L. Hatton, A. A. Cockram, M. J. Derry, P. D. Topham, O. O. Mykhaylyk, S. P. Armes, *manuscript in preparation*

Oral presentations at Conferences

“Effect of monomer solubility on the evolution of copolymer morphology during polymerization-induced self-assembly in aqueous solution”, Macro Group Young Researcher’s Meeting, April 2016, Liverpool, UK

“Effect of monomer solubility on the evolution of copolymer morphology during polymerization-induced self-assembly in aqueous solution”, 30th ECIS Conference, Sept 2016, Rome, Italy

“Effect of monomer solubility on the evolution of copolymer morphology during polymerization-induced self-assembly in aqueous solution”, 253rd ACS National Meeting, Spring 2017, San Francisco, USA

“Multiblock Copolymer Nanoparticles via RAFT Polymerization in Water for Low VOC coatings”, Polymer, Soft Matter and Colloids CDT Annual Summer School, August 2017, Sheffield, UK

“Optimization of the high-throughput synthesis of multiblock copolymer nanoparticles in aqueous media via polymerization-induced self-assembly”, CDT Industrial Showcase Day, Sept 2017, Sheffield, UK

“Optimization of the high-throughput synthesis of multiblock copolymer nanoparticles in aqueous media via polymerization-induced self-assembly”, 255th ACS National Meeting, Spring 2018, New Orleans, USA

Poster presentations at Conferences

“Effect of monomer solubility on the evolution of copolymer morphology during polymerization-induced self-assembly in aqueous solution”, Armes Festival 500, July 2015, Sheffield, UK.

“Effect of monomer solubility on the evolution of copolymer morphology during polymerization-induced self-assembly in aqueous solution”, The Polymer Conference, July 2016, Warwick, UK.

Abstract

Polymerization-induced self-assembly (PISA) has become a widely used technique for the rational design of diblock copolymer nano-objects in concentrated aqueous solution. Depending on the specific PISA formulation, reversible addition–fragmentation chain transfer (RAFT) aqueous dispersion polymerization typically provides straightforward access to either spheres, worms, or vesicles. In contrast, RAFT aqueous emulsion polymerization formulations often lead to just kinetically-trapped spheres. This limitation is currently not understood, and only a few empirical exceptions have been reported in the literature.

In the present work, the effect of monomer solubility on copolymer morphology is explored for an aqueous PISA formulation. More specifically a water-soluble poly(methacrylic acid) (PMAA_x) stabilizer block is chain-extended with six methacrylic monomers exhibiting a range of water solubilities; benzyl methacrylate (BzMA), 2,2,2-trifluoroethyl methacrylate (TFEMA), *n*-butyl methacrylate (BMA), methyl methacrylate (MMA), 2-hydroxybutyl methacrylate (HBMA) and 2-hydroxypropyl methacrylate (HPMA). These studies demonstrated that non-spherical (anisotropic) nanoparticles were only obtained during polymerization of HBMA. Using HBMA (aqueous solubility = 20 g dm⁻³ at 70 °C) for the core-forming block allows access to an unusual “monkey nut” copolymer morphology over a relatively narrow range of target degrees of polymerization when using a poly(methacrylic acid) RAFT agent at pH 5. These new anisotropic nanoparticles have been characterized by transmission electron microscopy, dynamic light scattering, aqueous electrophoresis, shear-induced polarized light imaging (SIPLI), and small-angle X-ray scattering (SAXS). Polymerization of each of the other five monomers only lead to the formation of spherical nanoparticles, indicating that aqueous monomer solubility is indeed a key parameter for the synthesis of higher-order morphology nanoparticles *via* PISA in aqueous media. The PMAA_x-PMMA_y series of spherical block copolymer nanoparticles are characterized in more detail by SAXS and DSC and also evaluated as Pickering emulsifiers for the stabilization of oil-in-water emulsions.

The PISA formulations described above are sufficiently robust to enable high-throughput experiments to be performed using a commercial synthesis robot (Chemspeed Autoplant A100). More specifically, RAFT aqueous emulsion polymerization of either BMA and/or BzMA is used to prepare various examples of methacrylic multiblock copolymer nanoparticles using a PMAA_x stabilizer block. Adequate stirring is essential to generate sufficiently small monomer droplets for such heterogeneous polymerizations to proceed efficiently. Good reproducibility can be achieved under such conditions, with well-defined spherical morphologies being obtained at up to 45% w/w solids. GPC studies indicated high blocking efficiencies but relatively broad molecular weight distributions ($\bar{M}_w = 1.36 - 1.85$), suggesting the formation of well-defined (albeit rather polydisperse) block copolymer chains. These preliminary studies provide a sound basis for high-throughput screening of RAFT-mediated PISA formulations, which is likely to be required for commercialization of this technology. Our results indicate that PISA formulations enable the synthesis of methacrylic diblock and triblock copolymer nanoparticles in high overall yield (94–99%) within 1–3 h at 70 °C. However, tetrablocks suffer from incomplete conversions (87–96% within 5 h) and hence most likely represent the upper limit for this approach.

Finally, BMA is replaced with hexyl methacrylate (HxMA) in order to prepare a series of diblock, triblock and tetrablock copolymer nanoparticles that form films at room temperature. The resulting block copolymers are evaluated by NMR, DLS, TEM and GPC, and the corresponding films are analyzed by visible absorption spectroscopy, DSC and SAXS.

List of Abbreviations

Abbreviation	Description
a_0	optimal head group area
AA	acrylic acid
ACVA	4,4-azobis(4-cyanovaleric acid)
AIBN	2,2'-azobisbutyronitrile
ATRP	atom transfer radical polymerization
BA	butyl acrylate
BHT	butylhydroxytoluene
BMA	butyl methacrylate
<i>BPO</i>	benzoyl peroxide
<i>bpy</i>	bipyridine
BzMA	benzyl methacrylate
CPCP	4-cyano-4-(phenylcarbonothioylthio)pentanoic acid
CTA	chain transfer agent
<i>cumyl</i>	2-phenylprop-2-yl dithiobenzoate
<i>d</i>	domain spacing
\bar{D}	molar-mass dispersity
DEAEMA	2-(diethylamino)ethyl methacrylate
DLS	dynamic light scattering
DNA	deoxyribonucleic acid
DP	number-average degree of polymerization
DSC	differential scanning calorimetry
ϵ_{AA}	interaction energy between blocks A and A
ϵ_{AB}	interaction energy between blocks A and B
ϵ_{BB}	interaction energy between blocks B and B
EMA	2-(ethoxycarbonyl)propyl-2-yl dithiobenzoate
<i>f</i>	Initiator efficiency
f_A	relative volume fraction of block A
f_B	relative volume fraction of block B
GlyMA	glycidyl methacrylate
HBMA	hydroxybutyl methacrylate (1:1 ratio of 2- and 4- isomers)
H-bond	hydrogen bond
HEMA	hydroxyethyl methacrylate
HPLC	high-performance liquid chromatography
HPMA	2-hydroxypropyl methacrylate
HxMA	hexyl methacrylate
<i>i</i>	total number of species
I·	Initiator radical
ICI	Imperial Chemical Industries
IPGMA	isopropylidenglycerol
IUPAC	International Union of Pure and Applied Chemistry
<i>K</i>	an empirical parameter that is related to the free volume present in the polymer sample

List of Abbreviations

k_{act}	rate constant of activation
k_B	Boltzmann constant
k_d	rate constant for initiator decomposition
k_{deact}	rate constant of deactivation
k_p	rate constant for propagation
KPS	potassium persulfate
k_t	rate constant for termination
k_{tc}	rate constant for termination by combination
k_{td}	rate constant for termination by disproportionation
L	complexing ligand
l_c	maximum effective length of the chains
M	molecular weight of monomer repeat unit
M	monomer
MAA	methacrylic acid
macro-CTA	macromolecular chain transfer agent
MADIX	macromolecular design <i>via</i> the interchange of xanthates
MFET	minimum film-forming temperature
MMA	methyl methacrylate
M_n	number-average molecular weight
MOEMA	2-methoxyethyl methacrylate
Mt^n	transition metal
Mt^n/L	transition metal complex
Mt^{n+1}	transition metal complex in a higher oxidation state
$Mt^{n+1}X/L$	higher oxidation state metal halide complex
M_w	weight-average molecular weight
MWD	molecular weight distribution
n	total number of monomer repeat units
N	aggregation number
N	total degree of polymerization of the two blocks
n -BA	n -butyl acrylate
NMP	nitroxide-mediated polymerization
NMR	nuclear magnetic resonance
p	packing parameter
P(AA-co-BA)	poly(acrylic acid-co-butyl acrylate)
P(AA-co-PEGA)	poly((acrylic acid-co-poly(ethylene glycol methyl ether acrylate)
P(HEAA-co-PEGA)	poly(ethylene glycol methyl ether acrylate)-co-poly(N -hydroxyethyl acrylamine)
P(MAA-co-PEOMA)	poly(methacrylic acid-co-poly(ethylene oxide) methyl ether methacrylate)
PAA	poly(acrylic acid)
PBA	poly(n -butyl acrylate)
PBzMA	poly(benzyl methacrylate)

List of Abbreviations

PDEAEMA	poly(2-(diethylamino)ethyl methacrylate)
PDI	polydispersity
PDMAAm	poly(N,N-dimethylacrylamide)
PDMAC	poly(dimethyl acrylamide)
PEGA	poly(ethylene glycol) methyl ether acrylate)
PEGA- <i>co</i> -PHEAA	poly(ethylene glycol) methyl ether acrylate)- <i>co</i> -poly(<i>N</i> -hydroxyethyl acrylamine)
PEO	poly(ethylene oxide)
PETTC	4-cyano-4-(2-phenylethanesulfanylthiocarbonyl)sulfanylpentanoic acid
PGMA	poly(glycerol monomethacrylate)
PhA	phenyl acrylate
PHxMA	poly(hexyl methacrylate)
PISA	polymerization-induced self-assembly
PLIs	polarized light images
P_m	propagating polymer radical
PMAA	poly(methacrylic acid)
PMAA-DB	poly(methacrylic acid) macro-CTA made utilizing CPCP
PMAA-TTC	poly(methacrylic acid) macro-CTA made utilizing PETTC
P_n	propagating polymer radical
P_{n+m}	dead polymer chain
PNAM	poly(<i>N</i> -acryloylmorpholine)
PNVP	poly(<i>N</i> -vinylpyrrolidone)
PPDTA	(2-phenylprop-2-ylphenyldithioacetate
PRE	persistent radical effect
PS	polystyrene
PVA	poly(vinyl alcohol)
q	scattering length vector
$R\cdot$	organic radical
RAFT	reversible addition-fragmentation chain transfer polymerization
RDRP	reversible deactivation radical polymerization
R_i	rate of initiation
R_p	rate of propagation
R_{polym}	rate of polymerization
R_t	rate of transfer
S	solvent
SAXS	small angle X-ray scattering
SDS	sodium dodecyl sulfate
SEM	scanning electron microscopy
SIPLI	shear-induced polarized light imaging
T	temperature
$t_{1/2}$	half-life
TEA	triethylamine
TEM	transmission electron microscopy
TEMPO	2,2,6,6-tetramethyl-1-piperidiny1-N-oxyl

List of Abbreviations

TFEMA	2,2,2-trifluoroethyl methacrylate
T_g	the glass transition temperature
$T_{g,\infty}$	the maximum glass transition temperature that can be achieved at a theoretically infinite molecular weight
THF	tetrahydrofuran
TIMT	temperature-induced morphological transition
TTCA	(2-(dodecylthiocarbonothioylthio)-2-methylpropanoic acid)
ν	kinetic chain length
V	volume occupied by the hydrocarbon chain
VA	vinyl acetate
VA-044	2,2'-Azobis[2-(2-imidazolin-2-yl)propane]dihydrochloride
χ_{AB}	Flory-Huggins parameter
X	deactivating species
$X\cdot$	persistent radicals

Table of Contents

1.	Introduction	1
1.1.	Polymer Science	2
1.2.	Polymerization Techniques	3
1.2.1.	Free Radical Polymerization	3
1.2.2.	Conventional Dispersion Polymerization	8
1.2.3.	Conventional Emulsion Polymerization	10
1.2.4.	Living Anionic Polymerization	13
1.2.5.	Reversible Deactivation Radical Polymerization	14
1.3.	Reversible Addition-Fragmentation Chain Transfer Polymerization	17
1.3.1.	Mechanism	18
1.3.2.	RAFT Polymerization Techniques	20
1.4.	Block Copolymer Self-Assembly	21
1.4.1.	Water and the hydrophobic effect	21
1.4.2.	Surfactants and Packing Parameter	22
1.4.3.	Self-Assembly of AB Diblock Copolymers	24
1.4.4.	Polymerization-Induced Self-Assembly (PISA)	26
1.4.5.	PISA by RAFT Aqueous Dispersion Polymerization	28
1.4.6.	PISA by RAFT Aqueous Emulsion Polymerization	32
1.5.	Thesis Outline	43
1.6.	References	45
2.	Synthesis of Diblock Copolymer Nanoparticles <i>via</i> RAFT-Mediated PISA in Water	53
2.1.	Introduction	54
2.2.	Experimental	55
2.2.1.	Materials	55
2.2.2.	Preparation of poly(methacrylic acid) (PMAA _x) macro-CTA agent	56
2.2.3.	Synthesis of PMAA _x -PBzMA _y diblock copolymer nanoparticles <i>via</i> RAFT aqueous emulsion polymerization	56
2.2.4.	Synthesis of PMAA _x -PBzMA _y diblock copolymer nanoparticles <i>via</i> RAFT aqueous emulsion polymerization in the presence of CaCl ₂ salt	56
2.2.5.	Chain extension of PMAA _x macro-CTA with monomers of varying aqueous solubility	57
2.2.6.	Synthesis of PMAA _x -PBzMA _y diblock copolymer nanoparticles <i>via</i> RAFT alcoholic dispersion polymerization	57
2.2.7.	Preparation of Pickering Emulsions	57

Table of Contents

2.3.	Copolymer Characterization	58
2.3.1.	¹ H NMR Spectroscopy	58
2.3.2.	Methylation of copolymers for GPC analysis	58
2.3.3.	Gel Permeation Chromatography (GPC)	58
2.3.4.	Dynamic Light Scattering (DLS)	58
2.3.5.	Aqueous Electrophoresis	58
2.3.6.	Transmission Electron Microscopy (TEM)	58
2.3.7.	Differential Scanning Calorimetry (DSC)	59
2.3.8.	Acid titration to determine the effective pKa values of the MAA monomer units	59
2.3.9.	Determination of aqueous monomer solubility by visual inspection	59
2.3.10.	Laser diffraction	59
2.3.11.	Optical microscopy	60
2.4.	Results and Discussion	60
2.4.1.	Synthesis of PMAA _x macro-CTA <i>via</i> RAFT solution polymerization	60
2.4.2.	Kinetics of PMAA _x -PBzMA _y synthesis <i>via</i> RAFT aqueous emulsion polymerization	63
2.4.3.	Investigation into the anionic behavior of PMAA _x macro-CTAs and PMAA _x -PBzMA ₂₀₀ diblock copolymers.	67
2.4.4.	Synthesis of PMAA _x -PBzMA _y diblock copolymer nanoparticles <i>via</i> RAFT aqueous emulsion polymerization at 10% w/w copolymer concentration	70
2.4.5.	Synthesis of PMAA ₅₄ -PBzMA ₅₀₀ diblock copolymer nanoparticles <i>via</i> RAFT aqueous emulsion polymerization at varying copolymer concentrations	77
2.4.6.	Synthesis of PMAA _x -PBzMA _y diblock copolymer nanoparticles in the presence of CaCl ₂ salt	80
2.4.7.	Chain extension of PMAA ₅₆ macro-CTA with monomers of varying aqueous solubility	83
2.4.7.1.	Synthesis of PMAA ₅₆ -PTFEMA _y diblock copolymer nanoparticles <i>via</i> RAFT aqueous emulsion polymerization at 20% w/w copolymer concentration	85
2.4.7.2.	Synthesis of PMAA ₅₆ -PBMA _y diblock copolymer nanoparticles <i>via</i> RAFT aqueous emulsion polymerization at 20% w/w copolymer concentration	89
2.4.7.3.	Synthesis of PMAA ₅₆ -PMMA _y diblock copolymer nanoparticles <i>via</i> RAFT aqueous emulsion polymerization of MMA at 20% w/w copolymer concentration	93
2.4.7.4.	Synthesis of PMAA ₅₆ -PHBMA _y diblock copolymer nanoparticles <i>via</i> RAFT aqueous emulsion polymerization of HBMA at 20% w/w copolymer concentration	103

2.4.7.5. Synthesis of PMAA ₅₆ -PHPMA _y diblock copolymer nanoparticles <i>via</i> RAFT aqueous dispersion polymerization at 20% w/w copolymer concentration	105
2.4.8. Synthesis of PMAA ₅₆ -PBzMA _y diblock copolymer <i>via</i> RAFT alcoholic dispersion polymerization	109
2.5. Conclusions	111
2.6. References	113
3. Effect of monomer solubility on the evolution of copolymer morphology during polymerization-induced self-assembly in aqueous solution	118
3.1. Introduction	119
3.2. Experimental	121
3.2.1. Materials	121
3.2.2. Preparation of poly(methacrylic acid) (PMAA) macro-CTA agent	121
3.2.3. RAFT polymerization of HBMA in water	121
3.2.4. Purification of HBMA monomer	121
3.3. Copolymer Characterization	122
3.3.1. ¹ H NMR Spectroscopy	122
3.3.2. Methylation of copolymers for GPC Analysis	122
3.3.3. Gel Permeation Chromatography (GPC)	122
3.3.4. Dynamic Light Scattering (DLS)	122
3.3.5. Aqueous Electrophoresis	123
3.3.6. Transmission Electron Microscopy (TEM)	123
3.3.7. Scanning Electron Microscopy (SEM)	123
3.3.8. Reverse-Phase High-Performance Liquid Chromatography (HPLC)	123
3.3.9. Shear-Induced Polarized Light Imaging (SIPLI)	123
3.3.10. Small-angle x-ray scattering (SAXS)	124
3.4. Results and Discussion	125
3.4.1. Synthesis of non-spherical nanoparticles <i>via</i> RAFT aqueous emulsion polymerization of HBMA	125
3.4.2. Anionic character of monkey nuts	129
3.4.3. Synthesis of non-spherical nanoparticles <i>via</i> RAFT aqueous emulsion polymerization of purified HBMA	130
3.4.4. Analysis using Shear-Induced Polarized Light Imaging to confirm the presence of non-spherical nanoparticles	133
3.4.5. Confirmation of diblock copolymer nanoparticle morphologies by Small Angle X-ray Scattering (SAXS)	135

3.4.6.	Synthesis of PMAA ₅₆ -PHBMA ₁₅₀ diblock copolymer nanoparticles at varying copolymer concentrations	138
3.4.7.	Comparison of reaction kinetics for the RAFT aqueous emulsion polymerization of HPMa and HBMA	140
3.4.8.	Changing the stabilizer block to a shorter PMAA ₂₉ macro-CTA or to a PGMA ₅₀ macro-CTA.	143
3.5.	Conclusions	147
3.6.	References	147
4.	Optimization of the high-throughput synthesis of multiblock copolymer nanoparticles in aqueous media <i>via</i> polymerization-induced self-assembly	150
4.1.	Introduction	151
4.2.	Experimental	153
4.2.1.	Materials	153
4.2.2.	Synthesis of poly(methacrylic acid) (PMAA) macro-CTA at 40% w/w polymer concentration.	153
4.2.3.	Laboratory-scale synthesis of PMAA ₅₆ -PBzMA ₅₀₀ diblock copolymer nanoparticles at 20% w/w copolymer concentration <i>via</i> RAFT aqueous emulsion polymerization of benzyl methacrylate.	154
4.2.4.	Laboratory-scale one-pot synthesis of tetrablock copolymer nanoparticles <i>via</i> RAFT aqueous emulsion polymerization.	154
4.2.5.	High-throughput syntheses of diblock copolymer nanoparticles <i>via</i> RAFT aqueous emulsion polymerizations using the Chemspeed Autoplant A100.	155
4.2.6.	High-throughput syntheses of triblock and tetrablock copolymers <i>via</i> RAFT aqueous emulsion polymerization using the Chemspeed Autoplant A100.	155
4.3.	Instrumentation and Copolymer Characterization	156
4.3.1.	The Chemspeed Autoplant A100 high-throughput robot.	156
4.3.2.	¹ H NMR Spectroscopy.	156
4.3.3.	Dynamic Light Scattering (DLS).	156
4.3.4.	Transmission Electron Microscopy (TEM).	157
4.3.5.	High-Performance Liquid Chromatography (HPLC) for Monomer Conversion	157
4.3.6.	Gel Permeation Chromatography (GPC).	157
4.4.	Results and Discussion	158
4.4.1.	Synthesis of PMAA macro-CTA on a large scale	158
4.4.2.	Laboratory-scale syntheses of di-, tri- and tetra-block copolymers	161
4.4.3.	Optimization of high-throughput protocol	166
4.4.4.	Stirring	168

4.4.5.	Reproducibility of high-throughput syntheses	174
4.4.6.	Synthesis of diblock, triblock and tetra-block copolymers <i>via</i> high-throughput method	179
4.5.	Conclusions	185
4.6.	References	186
5.	Synthesis and characterization of film-forming block copolymer nanoparticles <i>via</i> RAFT aqueous emulsion polymerization	190
5.1.	Introduction	191
5.2.	Experimental	195
5.2.1.	Preparation of poly(methacrylic acid) (PMAA) macro-CTA agent	195
5.2.3.	Synthesis of PMAA ₅₆ -PBzMA ₁₀₀ -PHxMA _y triblock copolymer nanoparticles <i>via</i> seeded RAFT aqueous emulsion polymerization	195
5.2.5.	¹ H NMR Spectroscopy	196
5.2.6.	Dynamic Light Scattering (DLS)	196
5.2.7.	Differential Scanning Calorimetry (DSC)	196
5.2.8.	Transmission Electron Microscopy (TEM)	197
5.2.9.	Methylation of copolymers for GPC Analysis	197
5.2.10.	Benzylation of copolymers for GPC Analysis	197
5.2.11.	Gel Permeation Chromatography (GPC)	197
5.2.12.	Casting and annealing of films	198
5.2.13.	Optical transmission measurements on copolymer films	198
5.2.14.	SAXS analysis	198
5.3.	Results and Discussion	199
5.3.1.	Synthesis of diblock, triblock and tetrablock copolymers	199
5.3.2.	Analysis of block copolymer films	209
5.4.	Conclusions	216
5.5.	References	217
6.	Conclusions and Future Work	220
6.1.	References	227
7.	Appendices	228

Chapter One

1. Introduction

1.1. Polymer Science

Polymers are ubiquitous in modern life. They can be found in a vast array of items from the everyday (e.g. cooking utensils, clothing, plastic bags, food packing, new bank notes) to more specialty items (e.g. bullet-proof vests, resins, coatings and medical devices). Polymers are also prevalent in nature and help form the basis of life (e.g. deoxyribonucleic acid (DNA), proteins, carbohydrates, polysaccharides and cellulose).

A single polymer is formed of many repeat units (monomers) covalently-bonded together to form a long chain molecule.¹ The mean number of repeat units per chain is termed the number-average degree of polymerization (DP). If a polymer is composed of only one monomer (all the repeat units are identical) it is known as a homopolymer. A polymer containing two or more monomers is known as a copolymer. The order and sequence of such monomers determines whether linear copolymers have statistical, alternating or block architectures (Figure 1.1).²

Homopolymer	A-A-A-A-A-A-A-A-A-A-A
Statistical copolymer	A-B-A-A-A-B-A-B-B-A-B-B
Alternating copolymer	A-B-A-B-A-B-A-B-A-B-A-B
AB diblock copolymer	A-A-A-A-A-A-B-B-B-B-B-B
ABA triblock copolymer	A-A-A-A-A-A-B-B-B-B-B-B-A-A-A-A-A
ABC triblock copolymer	A-A-A-A-A-A-B-B-B-B-B-B-C-C-C-C-C

Figure 1.1 Schematic representation of various linear copolymer architectures, where A, B and C represent different monomers.^{1,2}

As each polymer chain can have a different number of monomer repeat units, polymers do not have a finite molecular weight but a distribution of molecular weights. Typically, molecular weight averages are reported as the number-average molecular weight (M_n) and the weight-average molecular weight (M_w). These terms are defined

by Equation 1.1 and Equation 1.2 respectively, where n_i is the number of chains consisting of i repeat units and M_i is the molar mass of these chains.

$$M_n = \frac{\sum n_i M_i}{\sum n_i} \quad 1.1$$

$$M_w = \frac{\sum n_i M_i^2}{\sum n_i M_i} \quad 1.2$$

The breadth of the molecular weight distribution (MWD) is often reported as the polydispersity (PDI) or the molar-mass dispersity (\mathfrak{D}). The International Union of Pure and Applied Chemistry (IUPAC) recommends the use of dispersity (\mathfrak{D}) therefore this term will be used exclusively in this Thesis.³ The dispersity is given by the ratio of M_w to M_n as shown in Equation 1.3.

$$\mathfrak{D} = \frac{M_w}{M_n} \quad 1.3$$

In an ideal synthesis, the molecular weight of every single polymer chain would be identical, giving a \mathfrak{D} value of unity. However, such perfect control cannot be achieved in practice. For current polymerization techniques, broad MWDs are characterized by $\mathfrak{D} \geq 1.5$ and narrow MWDs are characterized by $\mathfrak{D} \leq 1.5$.⁴

1.2. Polymerization Techniques

1.2.1. Free Radical Polymerization

Free radical polymerization is a widely-used technique for the synthesis of polymers on an industrial scale.⁵ It is applicable to a wide range of functional vinyl monomers, can be performed in both protic and aprotic solvents and is tolerant to trace impurities (such as inhibitors).⁶ In addition, it can be performed under a range of physical conditions such as bulk, solution, dispersion, emulsion or suspension.⁷ The polymerization involves three distinct steps: (i) *initiation*, (ii) *propagation* and (iii) *termination*, as outlined by the mechanism shown in Figure 1.2.

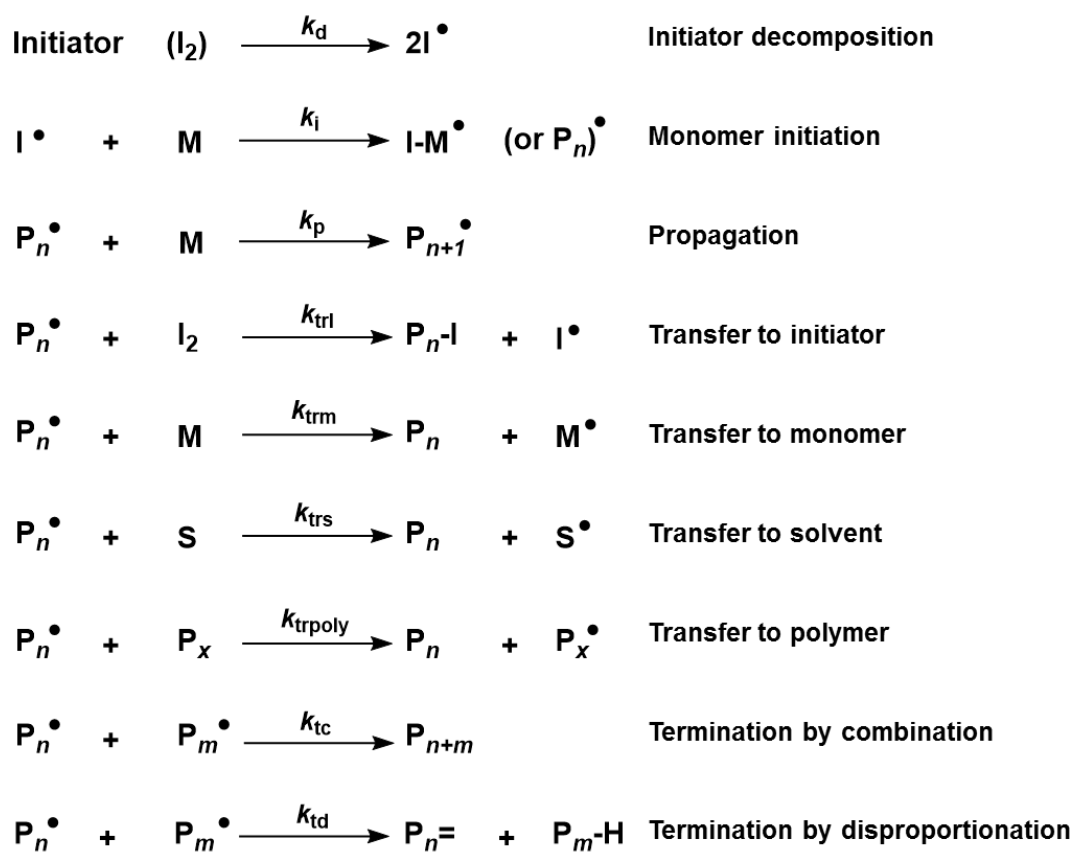


Figure 1.2 The free radical polymerization mechanism consists of three main steps: (i) initiation, (ii) propagation and (iii) termination. Possible radical transfer steps are also shown. I^\bullet = initiator radical, M = monomer, P_n^\bullet and P_m^\bullet = propagating polymer radical, P_x and P_{n+m} = dead polymer chain and S = solvent.

An initiator is typically added to the formulation to act as the radical source. Azo compounds or peroxides are often used as free radical initiators (Figure 1.3). These undergo homolytic scission *via* thermolysis to generate two radicals.¹ Other initiator decomposition methods can be used to generate radicals such as photolysis, redox chemistry or electromagnetic radiation. However, these will not be discussed further as only thermal initiators have been used in this Thesis.

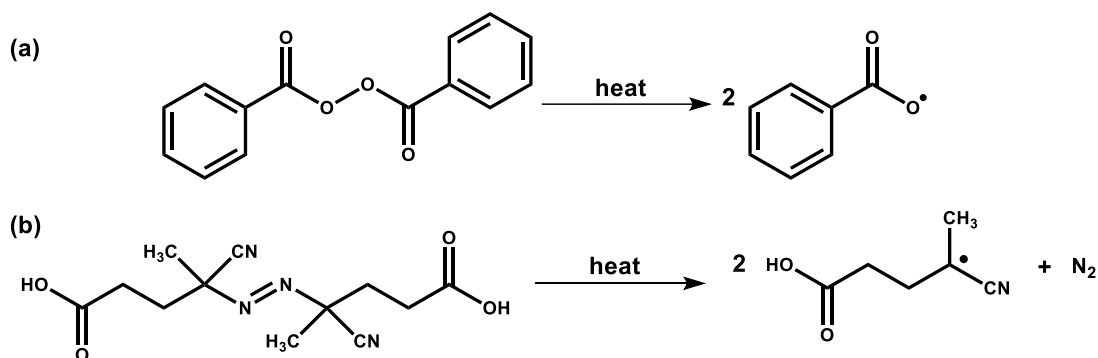


Figure 1.3 Formation of free radicals *via* thermal decomposition of two common types of free radical initiators; (a) benzoyl peroxide and (b) 4,4'-azobis-4-cyanopentanoic acid.

The thermal initiator and reaction temperature are carefully selected in order to provide an adequate radical flux at the desired polymerization temperature. Typically, the rate constant for initiator decomposition (k_d) should be approximately 10^{-4} - 10^{-6} s^{-1} .⁸ The half-life, $t_{1/2}$, is often used to express the decomposition rates of different initiators. It describes the time taken for the initiator concentration to reduce to half its original value and is calculated using Equation 1.4. Initiators are often ranked according to the characteristic temperature at which their half-life is equal to 10 h. For example, 4,4'-azobis(4-cyanovaleric acid) (ACVA) has a 10 h half-life of 69 °C, 2,2'-azobisbutyronitrile (AIBN) has a 10 h half-life of 65 °C, 2,2'-azobis(2-(2-imidazolin-2-yl)propane dihydrochloride (VA-044) has a 10 h half-life of 44 °C.

$$t_{1/2} = \frac{\ln 2}{k_d} \quad 1.4$$

The rate of thermal decomposition of the initiator is slow compared to the rate of monomer initiation. Therefore, the overall rate of initiation (R_i) for a thermal initiation can be expressed by Equation 1.5. This takes into account k_d , the initiator efficiency (f) and the generation of two radicals per initiator molecule. The initiator efficiency describes the ability of the radical to react with monomer as opposed to undergoing recombination. The rate of initiator decomposition is relatively slow; hence this is considered to be the rate-determining step.

$$R_i = - \frac{d[I]}{dt} = 2k_d f [I] \quad 1.5$$

Once the initiator radical ($I\cdot$) has been generated, it can react with a vinyl monomer (M) to produce an active radical center ($I\text{-}M\cdot$). This active radical center then reacts with further monomer to become the propagating polymer radical ($P_n\cdot$). The rate for the addition of each monomer unit (R_p) is assumed to be independent of DP, as outlined in Equation 1.6.

$$R_p = -\frac{d[M]}{dt} = k_p[P_n\cdot][M] \quad 1.6$$

Propagation continues until two polymer radicals react with each other, causing chain termination. There are two mechanisms for chain termination: combination and disproportionation. When chain termination occurs *via* combination, the resulting polymer chain (P_{n+m}) has a molecular weight equal to the sum of that of the two polymer radicals ($P_n + P_m$). In contrast, if termination occurs *via* disproportionation, a hydrogen atom is abstracted by one polymer radical from the other. This results in one polymer chain with a terminal vinyl group ($P_n=$) and one hydrogen-capped polymer chain ($P_m\text{-}H$). Partly as a result of these two termination mechanisms the molecular weight distribution of the final polymer can be relatively broad. These termination reactions occur to differing degrees depending on the monomer type. Termination by combination is the predominant mechanism for styrene, whereas disproportionation is more prevalent for methacrylates.⁹ The overall rate of termination (R_t) is given by in Equation 1.7, where $k_t = k_{tc} + k_{td}$.

$$R_t = -\frac{d[P\cdot]}{dt} = 2k_t[P\cdot]^2 \quad 1.7$$

Typically, the rate of termination is considerably faster than the rate of propagation.⁷ Therefore, in order to synthesize high molecular weight polymers, polymerizations must be performed under conditions where $R_t < R_p$. As R_t is second-order with respect to radical concentration (Equation 1.7) but R_p is first-order (Equation 1.6) this can be achieved by keeping the radical flux relatively low. During free radical polymerization, chain transfer reactions can also occur between the polymer radicals and the initiator, monomer, solvent or dormant polymer chains (see Figure 1.2). These side reactions can result in cross-linking or branching, thus impacting the molecular

weight and the dispersity (\mathfrak{D}) of the final polymer chains. However, these reactions do not have a significant impact on the overall rate of polymerization. Instead, only the rates of initiation, propagation and termination influence the overall rate of polymerization (R_{polym}). Accordingly, R_{polym} can be expressed by Equation 1.8.

$$R_{polym} = k_p[M] \sqrt{\frac{fk_d[I]}{k_t}} \quad 1.8$$

The kinetic chain length (ν) is defined as the average number of monomer units consumed per active radical and is given by the ratio of the rate of propagation to the rate of termination.⁸ For a thermally-initiated polymerization, this can be calculated using Equation 1.9, and depends on the initiator efficiency (f) and the rate constants for initiator decomposition (k_d), propagation (k_p) and termination (k_t).

$$\nu = \frac{R_p}{R_t} = \frac{k_p[M]}{2\sqrt{fk_d k_t[I]}} \quad 1.9$$

The kinetic chain length can be used to calculate the DP, dependent on whether the mechanism of termination occurs by combination (Equation 1.10) or by disproportionation (Equation 1.11).⁸

$$\text{Combination} \quad DP = 2\nu \quad 1.10$$

$$\text{Disproportionation} \quad DP = \nu \quad 1.11$$

Despite being widely used in industry, there are some significant drawbacks to free radical polymerization. In particular, control over the molecular weight distribution is difficult to achieve and it is impossible to synthesize pure block copolymers.⁷ Broad molecular weight distributions result from the short life-time of the propagating chains ($\ll 1$ s), and the slow rate of initiation relative to the rate of propagation ($R_i < R_p$) which causes high molecular weight polymers to be formed relatively quickly.⁷

1.2.2. Conventional Dispersion Polymerization

Free radical dispersion polymerization has been widely used since it and was first reported by scientists working for Imperial Chemical Industries (ICI) in 1962.¹⁰ The development of dispersion polymerization has important applications for the coatings industry. By identifying the conditions required for the synthesis of stable latex particles in either non-polar or polar solvents, coating formulations could be prepared with high polymer content (> 50% by mass) without a substantial increase in solution viscosity.

Fundamental research into dispersion polymerization was also conducted by Rohm & Haas in the USA.¹¹ This company examined the synthesis of latex particles in organic solvents with the aim of formulating coatings for use in extreme temperatures (cold climates or inside drying ovens) and pressures. Rohm & Haas scientists also investigated aqueous dispersion polymerization in order to simplify aqueous syntheses which required numerous purification steps.

The mechanism of particle formation *via* dispersion polymerization was studied by Shen *et al.*¹² In a dispersion polymerization, the reaction solution is initially homogeneous with the monomer, initiator and stabilizer all being soluble in the continuous phase (Figure 1.4, Stage 1). Initially, the polymerization proceeds in solution because the shorter chains (oligomers) are soluble (Figure 1.4, Stage 2). As the chains grow they become increasingly hydrophobic causing the polymer chains to aggregate and form particle nuclei (Figure 1.4, Stage 3).¹³ In the absence of any polymeric stabilizer, these nuclei would simply form a macroscopic precipitate. Initially, the nuclei are not fully stabilized by the polymeric stabilizer, this makes them unstable with respect to aggregation. The polymeric stabilizer adsorbs onto the aggregated nuclei to form fully-coated colloiddally stable particles (Figure 1.4, Stage 4). These particles become monomer-swollen as monomer diffuses from the aqueous phase into the particle cores. As the polymerization proceeds, the particles continue to grow until all monomer has been consumed (Figure 1.4, Stage 5), forming sterically-stabilized latex particles (Figure 1.4, Stage 6).

Initially the majority of dispersion polymerizations were performed in non-aqueous solvents (e.g. non-polar solvents or alcohol).^{12, 14-17} Subsequently, aqueous dispersion polymerizations were also conducted,¹⁸⁻²² including the polymerization of

2-hydroxypropyl methacrylate (HPMA) using poly(*N*-vinylpyrrolidone) (PNVP) as the steric stabilizer.¹⁸ The steric stabilizer can be a soluble homopolymer,²¹ a block¹⁵ or a graft polymer¹³, or it can be a polymer containing a polymerizable functionality.^{13, 16} The effect of the steric stabilizer on the polymerization of styrene in both polar solvents¹³ and aqueous¹⁴ media has been well-studied. One limitation of dispersion polymerization is that it requires a solvent-miscible monomer that forms an insoluble polymer. For aqueous dispersion polymerization, there are only a few *water-miscible* monomers that form *water-insoluble* polymers.²³

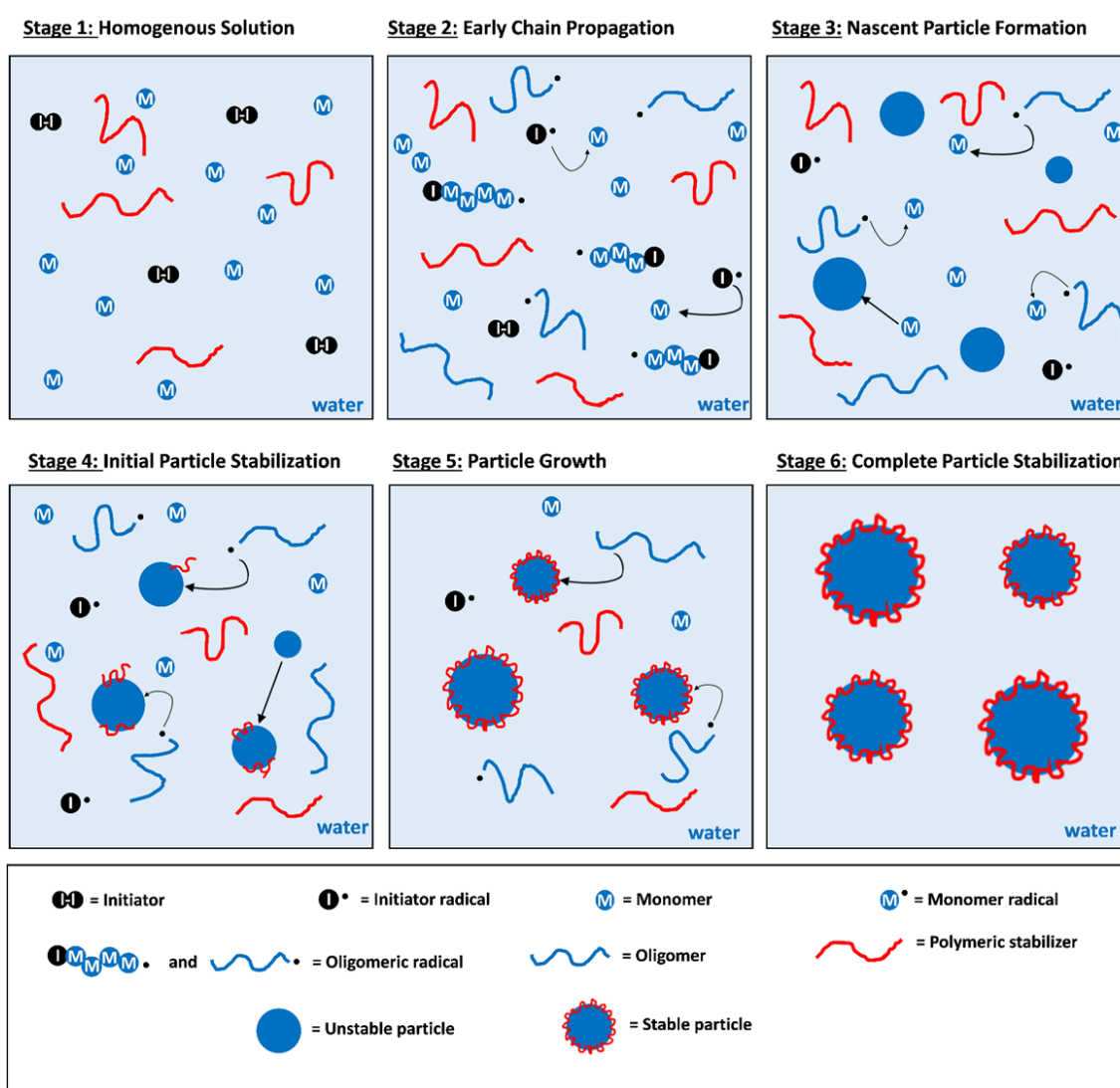


Figure 1.4 Cartoon representing the mechanism for aqueous dispersion polymerization.¹²

1.2.3. *Conventional Emulsion Polymerization*

Conventional emulsion polymerization is widely used in industry to produce polymer latexes for use in many applications such as coatings, pigments, adhesives and rheology modifiers.²⁴⁻²⁶ A typical aqueous emulsion polymerization requires a *water-immiscible* monomer, *water-soluble* initiator, surfactant and water and proceeds as a free radical polymerization. The use of water as the continuous phase is a key reason why emulsion polymerization is ideally suited to industrial scale-up. It is cheap, non-toxic, environmentally-friendly, non-flammable and has a high heat capacity. Surfactant is usually required in the formulation to stabilize the growing polymer particles and prevent coagulation. However, high levels of surfactant can be detrimental to the final polymer properties, e.g. film formation.^{26, 27} Surfactant-free emulsion polymerization formulations have also been reported.²⁸⁻³¹ However, such formulations typically involve the synthesis of a surface-active species *in situ* during the polymerization.

The mechanism for emulsion polymerization can be considered in terms of three key stages; Intervals I, II and III (Figure 1.5).²⁴⁻²⁷ Interval I involves the particle nucleation stage. Firstly, the *water-immiscible* monomer and surfactant are emulsified to generate surfactant-stabilized monomer droplets (approximately 1-10 μm in diameter) and surfactant micelles.²⁷ These monomer droplets contain the majority of the monomer present in the system and act as monomer reservoirs during the polymerization. A small amount of monomer also resides in monomer-swollen micelles (5-10 nm in diameter), if the surfactant concentration is above the critical micelle concentration. Depending on its aqueous solubility, a low concentration of monomer will also be dissolved in the aqueous phase.²⁴ This soluble monomer fraction is available to react with the radicals in the aqueous phase generated by the initiator. As the polymerization proceeds, these oligomers become increasingly hydrophobic and, at some critical chain length, migrate into the surfactant-stabilized micelles. As the polymer chains continue to propagate, the micelles are transformed into growing particle nuclei. The micelles are the main locus of polymerization and minimal polymerization occurs inside the monomer droplets. This is owing to the large oil-water interfacial area of the micelles in comparison to the monomer droplets, making them more efficient at capturing free radicals.²⁴ Monomer diffuses from the monomer droplets into these nuclei to feed the growing polymer chains. Interval I is complete once all micelles are

either transformed into latex particles or undergo dissociation to supply the increasing demand for surfactant as the latex surface area increases.

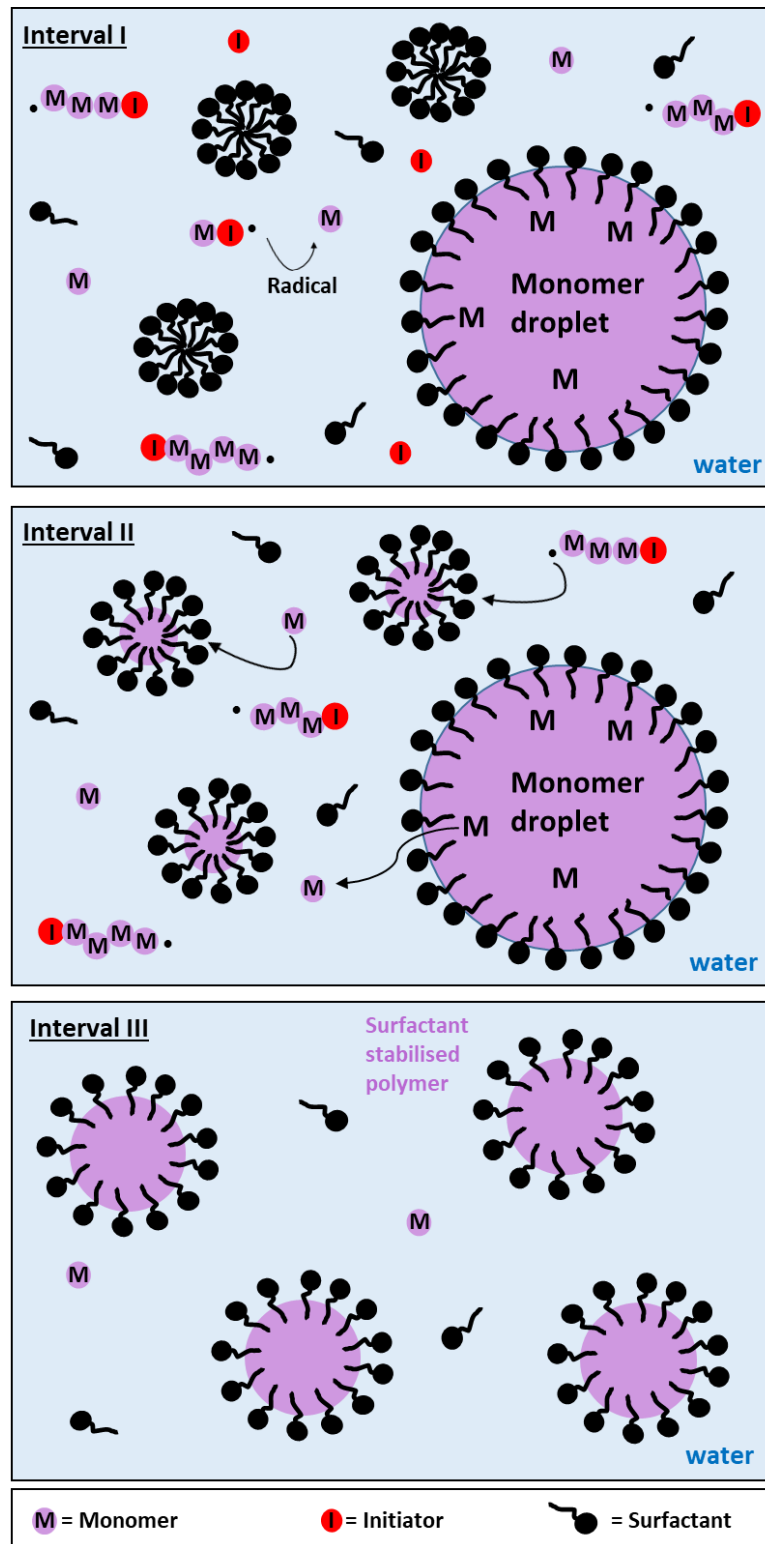


Figure 1.5 Scheme representing the three intervals (I, II, III) that occur during conventional emulsion polymerization.²⁴⁻²⁷

Interval II is the particle growth stage (Figure 1.5). The number of latex particles remains constant and the polymer chains continue to grow inside these particles. As monomer is consumed, it is replenished by monomer diffusing from the aqueous phase. The concentration of dissolved monomer in the aqueous phase remains relatively constant as it continually diffuses from the surfactant-stabilized monomer droplets to the aqueous phase. Thus, the rate of polymerization during Interval II remains constant (Figure 1.6). Once all monomer droplets have been consumed and only monomer-swollen latex particles remain, Interval II is complete.

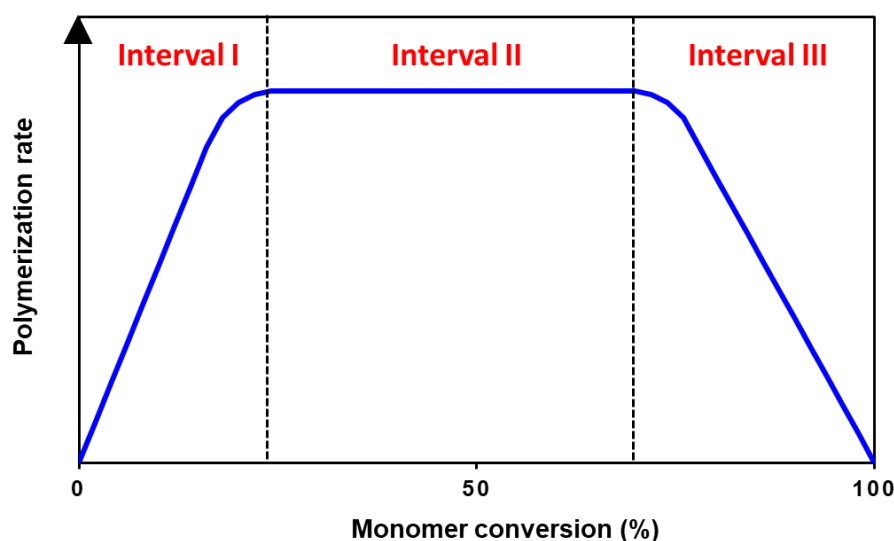


Figure 1.6 Relationship between polymerization rate and monomer conversion during the three key intervals (I, II and III) of a conventional emulsion polymerization.^{8, 24}

The final stage of the polymerization is Interval III. The remaining monomer inside the particles is consumed, leaving colloiddally stable latex particles. The reduction in monomer concentration during Interval III causes a reduction in the polymerization rate (Figure 1.6).²⁷

The mechanism of particle formation described above is termed ‘micellar nucleation’.²⁷ The growing oligomers migrate into monomer-swollen surfactant micelles and continue to propagate to form polymer particles. Particle formation can also occur by a ‘heterogeneous nucleation’ mechanism.²⁷ In this case, when the growing oligomer chains become sufficiently hydrophobic, they collapse to form particles. These particles are then stabilized by the adsorption of surfactant and absorb monomer to become the main locus of polymerization.

1.2.4. *Living Anionic Polymerization*

In contrast to free radical polymerization, living polymerization techniques afford much more control over copolymer composition, architecture and molecular weight.⁵ In order for a polymerization to be considered living, termination must be eliminated and the rate of initiation must be much faster than the rate of propagation. Rapid initiation results in simultaneous initiation of all chains, which then have equal probability to grow, leading to a linear evolution of molecular weight with conversion and a relatively narrow final MWD.^{1, 8} Conversely, in the case of free radical polymerization, high molecular weight polymers are formed even at low conversions.³² After all monomer is consumed, the living character of the chains is retained, enabling the synthesis of well-defined block copolymers *via* sequential monomer addition. In addition, selective termination of living chain-ends can yield functionalized polymers.

The concept of a living polymerization was first exemplified for anionic polymerization by Szwarc and co-workers in 1956.³³ Styrene was polymerized in dry tetrahydrofuran (THF) using sodium naphthalenide as the initiator. The anionic naphthalenide ions act as electron transfer agents to generate styrene radical anions. The anions are unstable and almost instantaneously dimerize to generate a dicarbanion. Continuous addition of styrene monomer to both ends of this dicarbanion initiator occurs to form polystyrene chains comprising a reactive carbanion at each chain-end.

Under appropriate conditions, anionic polymerization fulfils all the criteria of a living polymerization and can be employed to synthesize polymers with a high degree of both structural and compositional control. In addition, intrinsic termination is prevented by mutual electrostatic repulsion from the anionic reactive centers, leading to the formation of polymers with low dispersity ($\mathfrak{D} \leq 1.12$).^{8, 34}

For a monofunctional initiator, the DP of the polymer chains can be calculated using Equation 1.12.³⁵ Unlike free radical polymerization, the DP is not dependent on the rate constants for initiator decomposition (k_d), propagation (k_p) or termination (k_t) or the initiator efficiency (f), see Equations 1.9 to 1.11. It follows that the M_n can be simply calculated using Equation 1.13.

$$DP = \frac{[M]}{[I]} \quad 1.12$$

$$M_n = \frac{[M]}{[I]} \cdot \text{monomer molar mass} \quad 1.13$$

Living anionic polymerization can be used to polymerize styrene,³⁶ 2-vinyl pyridine,³⁷ isoprene,³⁸ butadiene,³⁸ methacrylates,³⁹ acrylates,³⁹ ethylene oxide⁴⁰ and lactones,³² typically using initiators such as *n*-butyllithium or sodium naphthalenide (Figure 1.7).⁸ However, living anionic polymerization cannot be easily used to polymerize functional monomers.^{41, 42} This is because many functional groups are incompatible with carbanions. In more recent work, strategies have been developed to facilitate the living anionic polymerization of functional monomers *via* protecting group chemistry.^{41, 42}

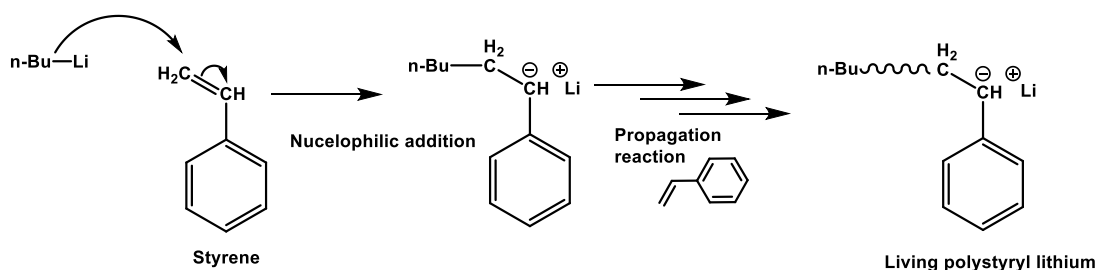


Figure 1.7 Living anionic polymerization of styrene utilizing *n*-butyllithium as the electron transfer agent.⁸

1.2.5. Reversible Deactivation Radical Polymerization

Controlled radical polymerization methods offer comparable control over molecular weight to living anionic polymerization but afford the versatility of free radical polymerization. As in living anionic polymerization, termination needs to be suppressed relative to propagation. This is achieved through reversibly deactivating the active polymer radicals by establishing a rapid equilibrium between active and dormant polymer chains.⁴³ To describe polymerizations utilizing this equilibrium, IUPAC recommends the use of the term ‘reversible deactivation radical

polymerization' (RDRP).⁴⁴ IUPAC describes a living polymerization as “a chain polymerization from which irreversible chain transfer and irreversible chain termination (deactivation) are absent”.⁴⁴ This definition does not accurately describe RDRP therefore the use of terms such as living, controlled living, controlled/living, pseudo-living and quasi-living are discouraged.

In recent years, RDRP methods have become increasingly popular,^{7, 43-45} because they offer numerous advantages.⁴⁶ RDRP provides a high level of control over the polymerization, leading to reliable targeting of molecular weights and narrow MWDs ($\mathcal{D} \leq 1.2$). This occurs as there is a constant number of chains, all with an equal opportunity to grow throughout the polymerization.

Finally, block copolymers can be synthesized *via* sequential monomer addition. These attractive features, along with the ease of implementation and tolerance of many monomer functionalities, impurities and solvents make RDRP ideally suited to the synthesis of functional copolymers of various architectures, such as block copolymers,^{7, 47} star polymers,^{48, 49} and graft polymers^{48, 50} (Figure 1.8).^{2, 5, 51}

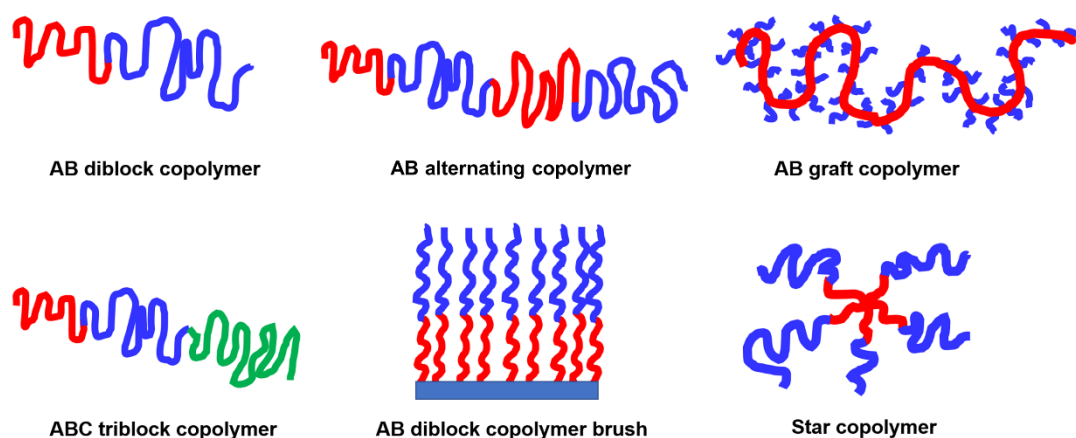


Figure 1.8 Examples of various block copolymer architectures prepared using RDRP techniques reported in the literature^{2, 5, 47-51}

All RDRP formulations involve a rapid equilibrium between propagating radical chains and dormant species. This can occur *via* two mechanisms; polymer radicals either participate in a reversible deactivation/activation process (Figure 1.9) or in a reversible transfer process (Figure 1.10).^{5, 7, 44}

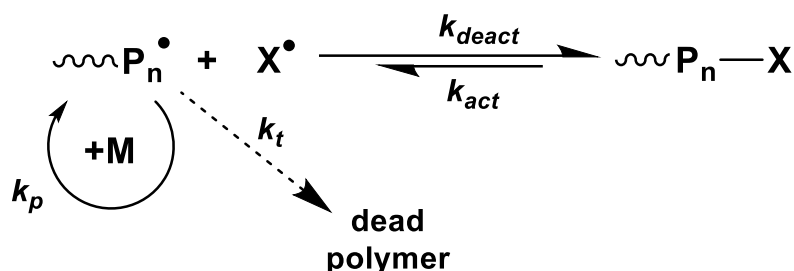


Figure 1.9 Reversible deactivation/activation of propagating polymer radicals by radicals X·.^{5, 44}

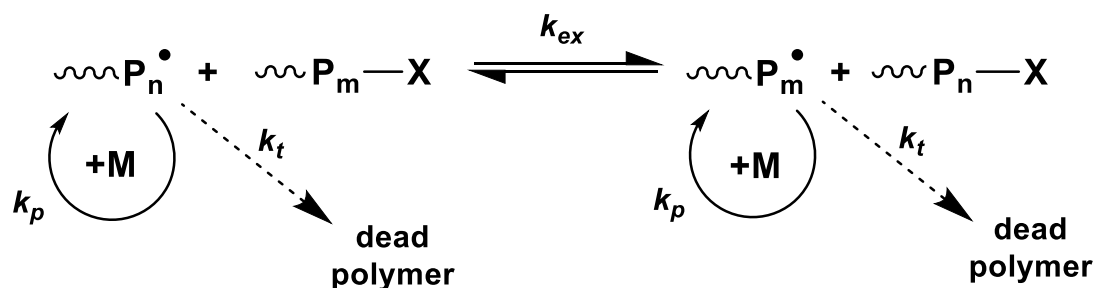


Figure 1.10 Reversible transfer mechanism of propagating polymer radicals.^{5, 44}

Polymerizations that proceed *via* the reversible deactivation/activation mechanism rely on the persistent radical effect (PRE).^{7, 52} A deactivating species (X), such as a nitroxide or organometallic complex, is employed to rapidly deactivate (k_{deact}) the propagating radicals (P_n^\bullet). These dormant species can then be activated (k_{act}) to reform the propagating radicals. The propagating radical can continue to grow (k_p) or terminate (k_t). Species X forms persistent radicals (X^\bullet) which cannot react with each other to terminate, leading to an increase in the concentration of X^\bullet as the reaction proceeds. This causes a reduction in the concentration of propagating radicals. Propagating radicals are therefore more likely to react with X^\bullet than to undergo self-termination. RDRP techniques such as nitroxide-mediated polymerization (NMP)⁵²⁻⁵⁹ and atom transfer radical polymerization (ATRP)^{7, 60-64} utilize the PRE to confer control over radical polymerization.^{52, 65}

Alternatively, RDRP techniques can proceed *via* a second mechanism (Figure 1.10).^{5, 44, 65} This involves reversible transfer of a labile end-group (X) between a dormant chain and a transfer agent.⁴⁶ This can occur as a direct exchange *via* degenerative transfer or *via* an addition-fragmentation process. A well-studied example based on the latter mechanism is reversible addition-fragmentation chain transfer (RAFT) polymerization, which utilizes various thiocarbonylthio compounds as the chain transfer agents.⁴⁴ This is the technique that has been utilized for all the synthetic work carried out in this Thesis.

1.3. Reversible Addition-Fragmentation Chain Transfer Polymerization

RAFT polymerization was first reported in 1998 by Chiefari *et al.*⁶⁶ In comparison to other RDRP techniques (NMP and ATRP), RAFT is often considered to be more convenient and versatile.⁶⁷ It is compatible with a wide range of functional monomers, solvents and conditions (bulk, solution, dispersion, emulsion etc.).⁶⁶ RAFT polymerizations are based on the addition of a RAFT agent (Figure 1.13) which acts as a chain transfer agent (CTA) throughout the polymerization.⁶⁶ A conventional free radical polymerization can be converted into a RAFT polymerization simply by adding a suitable RAFT agent. All other components and conditions (monomer, initiator, solvent and temperature) can be kept the same.⁶ RAFT polymerizations demonstrate key characteristics of RDRP, including linear evolution of molecular weight with conversion and narrow molecular weight distributions.⁶ They also afford good control over the target molecular weight and allow access to various copolymer architectures.

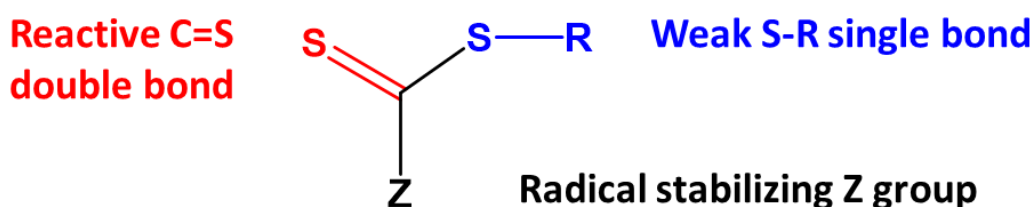


Figure 1.13 General chemical structure of a thiocarbonylthio RAFT chain transfer agent (CTA). Depending on the Z group, there are four main classes of RAFT CTA: dithioester (Z = alkyl or aryl), trithiocarbonates (Z = SR), dithiocarbamates (Z = NR₂) and xanthates (Z = alkyl). The R group = alkyl.^{68, 69}

The RAFT CTA must be carefully selected for each monomer class to ensure good control.⁶⁹ The generic chemical structure of a RAFT CTA is shown in Figure 1.13. The R group and Z group are very important in ensuring the effectiveness of a RAFT agent. The R group must be a good radical leaving group that is also capable of reinitiating polymerization.⁶⁶ The Z group activates the C=S double bond towards radical addition, ensuring a high chain transfer constant.^{66, 68} Based on the Z group, these RAFT CTAs can be split into four classes: dithioesters (Z= alkyl or aryl), trithiocarbonates (Z = SR), dithiocarbamates (Z= NR₂) or xanthates (Z= O-alkyl). The R group is an alkyl group.⁷⁰ For example, to polymerize a methacrylate or methacrylamide monomer it is best to use a dithioester (e.g. 4-cyano-4-(phenylcarbonothioylthio)pentanoic acid) or a trithiocarbonate CTA (e.g. (4-cyano-4(2-phenylethanesulfanylthiocarbonyl)sulfanyl)pentanoic acid). In contrast, a trithiocarbonate CTA would be a more suitable choice for the polymerization of acrylates or acrylamides, whereas dithiocarbamates are most effective for styrenic monomers. Finally, to achieve a well-controlled polymerization of a vinyl ester or vinyl amide then a xanthate CTA would be the ideal choice.⁷¹

1.3.1. Mechanism

For work carried out in this thesis, thiocarbonylthio RAFT agents were used. The RAFT agent interacts with the growing polymer radicals through a rapid reversible addition-fragmentation process,⁷² which suppresses irreversible termination. As RAFT polymerization does not make use of the PRE, an external source of radicals is required to initiate the polymerization (eg. azo initiators, redox initiation) (Figure 1.14, step 1). Reaction between the initiator and monomer leads to the formation of a propagating radical ($P_n\cdot$) which then undergoes addition to the thiocarbonylthio compound. This intermediate carbon-centered radical (Figure 1.14, step 2) fragments via β -scission to generate a new radical ($R\cdot$) and a dormant polymeric thiocarbonylthio compound (Figure 1.14, step 3). This $R\cdot$ radical reacts with monomer to form a new propagating radical ($P_m\cdot$). The key mechanistic step is the rapid equilibrium between the two active propagating radicals ($P_n\cdot$ and $P_m\cdot$) and the dormant thiocarbonylthio compounds (Figure 1.14, steps 3 and 4). This rapid equilibrium provides equal opportunity for all chains to grow leading to the synthesis of polymers with narrow molecular weight distributions. Upon termination (Figure 1.14, step 5) of the polymerization, the thiocarbonylthio moieties are retained at the end of the polymer

The target DP is simply calculated as the ratio of monomer concentration to RAFT CTA concentration, see Equation 1.16. As for other RDRP techniques, it is not dependent on rate constants or other kinetic parameters.⁶²

$$DP = \frac{[M]}{[CTA]} \quad 1.16$$

The main disadvantages of RAFT polymerization are the physical properties of the sulfur-based RAFT CTA end-groups, which make the polymer chains intrinsically colored and malodorous. However, various chemistries have been developed to remove these chain ends after polymerization.^{70, 73-82}

1.3.2. RAFT Polymerization Techniques

RAFT polymerizations can be performed in many solvents, including alcohols,⁸³⁻⁸⁶ *n*-alkanes,⁸⁷ and water.^{23, 88-95} This body of work focuses solely on using water as the solvent so only aqueous conditions will be discussed in any detail.

Aqueous RAFT polymerizations can occur under different conditions depending on the water solubility of the monomer and the corresponding polymer. If the monomer is *water-miscible* and polymerizes to form a water-insoluble polymer, such as HPMA (aqueous solubility $\sim 100 \text{ g dm}^{-3}$ at $70 \text{ }^\circ\text{C}$)⁹⁶ then chain growth proceeds *via* RAFT aqueous dispersion polymerization. On the other hand, if the monomer is *water-immiscible* and polymerizes to form a water-insoluble polymer, such as benzyl methacrylate (BzMA, aqueous solubility $\sim 0.40 \text{ g dm}^{-3}$ at $70 \text{ }^\circ\text{C}$),⁹⁷ then the chain growth proceeds *via* RAFT aqueous emulsion polymerization. In addition, bulk polymerization (when the monomer itself is used as the solvent) can be used, while RAFT solution polymerization is where both the monomer and its resulting polymer are fully soluble in the solvent.

1.4. Block Copolymer Self-Assembly

The term ‘self-assembly’ has been widely used in various contexts. Herein, we use self-assembly to describe the autonomous organization of components into patterns or structures without human intervention, as defined by Whitesides and Grzybowski.⁹⁸

1.4.1. Water and the hydrophobic effect

In order to understand the underlying principles of self-assembly in aqueous media, it is first important to consider the unique behavior and properties of water. Each water molecule is composed of two hydrogen atoms covalently bonded to a central oxygen atom. A distorted tetrahedral structure is adopted due to the two lone pairs of electrons on the oxygen atom (Figure 1.15). The covalent bonds between the oxygen and hydrogen atoms are polarized due to difference in electronegativity of the atoms. Hydrogen bonds (H-bonds) can be formed between the oxygen lone pair of one water molecule and a hydrogen atom on a neighboring water molecule.^{99, 100} With each molecule able to form four such bonds, liquid water forms one of the densest H-bond networks of all solvents.¹⁰¹ These hydrogen bonds explain many of the unusual properties of water, such as its unexpectedly high boiling and melting point and that the density of ice is less than that of the liquid water.^{102, 103}

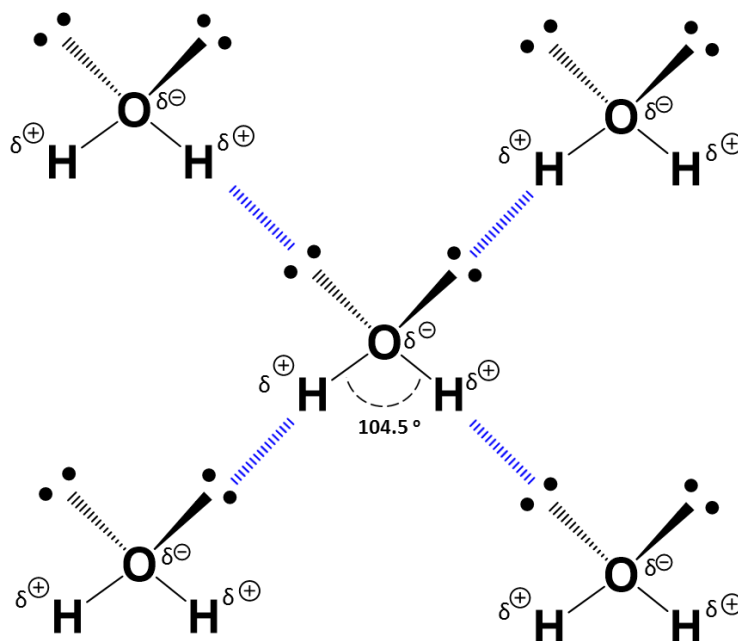


Figure 1.15 Water has two lone pairs on its oxygen atom and a bond angle of 104.5° between the two hydrogen atoms. The blue dashed lines represent hydrogen bonds between the oxygen lone pair of one water molecule and a hydrogen atom on a neighboring water molecule.¹⁰³

Of particular relevance here is the behavior of water as a solvent.¹⁰³ Many *hydrophilic* (water-loving) molecules have a strong propensity to form H-bonds with water. In contrast, many *hydrophobic* molecules are incapable of forming H-bonds with water and are therefore insoluble in aqueous media. Typically, these are non-polar molecules such as alkanes, aromatic hydrocarbons or fluorocarbons. The presence of such molecules disrupts the extensive H-bond network in liquid water. This is often referred to as the *hydrophobic effect*.^{104, 105} Non-polar molecules are only sparingly water-soluble owing to the highly unfavorable free energy of solubilization as a result of the entropic cost of increasing order in the system.¹⁰³

1.4.2. Surfactants and Packing Parameter

Amphiphilic molecules undergo spontaneous self-assembly in aqueous solution. An amphiphilic molecule is composed of a hydrophilic component and a hydrophobic component, which are covalently connected by one or more chemical bonds. Surfactants are a common example: here a hydrophilic head-group is connected to a hydrophobic alkyl tail.¹⁰⁶ The head-group is solvated by water whereas the non-polar tail group is not solvated by the water molecules. Surfactants are classified as anionic, cationic, zwitterionic or neutral, depending on the properties of the hydrophilic head-group.

Surfactant aggregation in aqueous solution is a thermodynamically-driven process; the entropic cost of the formation of higher order structures is less than the enthalpy of solubilization. The micellar aggregates are sometimes known as association colloids.¹⁰³ They are held together by van der Waals forces, H-bonding and the hydrophobic effect. Moreover, rapid exchange occurs between the individual surfactant molecules and the micelles (Figure 1.16). A surfactant molecule spends only 10^{-5} to 10^{-3} seconds inside a micelle.¹⁰³

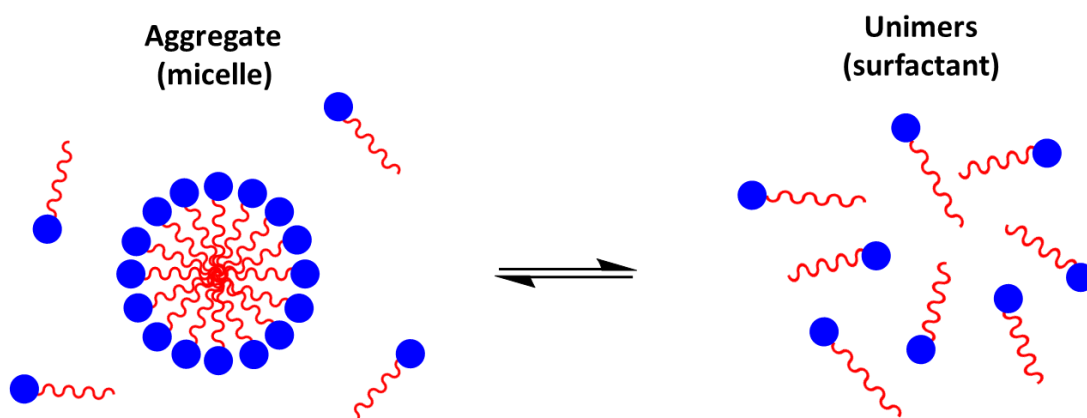


Figure 1.16 Schematic cartoon demonstrating the dynamic equilibrium between unimers (surfactant) and their colloidal aggregates (micelles).¹⁰³

Surfactant micelles can form various structures (spheres, worms, vesicles or bilayers), as shown in Figure 1.17. The micelle morphology depends on the surfactant concentration and is also influenced by solution pH or electrolyte concentration.

The amphiphilic nature of a surfactant molecule creates two opposing forces.¹⁰⁵ The hydrocarbon tails cluster together to form the micelle cores in order to minimize contact with the water molecules. In contrast, the hydrophilic head-groups remain in contact with the water.¹⁰³ Micellar self-assembly is driven by the balance between these two opposing forces, for which there is a minimum interaction energy that is related to an optimal head group area (a_0).¹⁰³

The micelle structure depends on the geometric packing of the surfactant molecules (Figure 1.17), which depends on the optimal head-group area (a_0), the volume occupied by the hydrocarbon chain (V) and the maximum effective length of the chains, also known as the critical chain length (l_c). Generally speaking, smaller structures with lower aggregation numbers (N) are entropically favored.

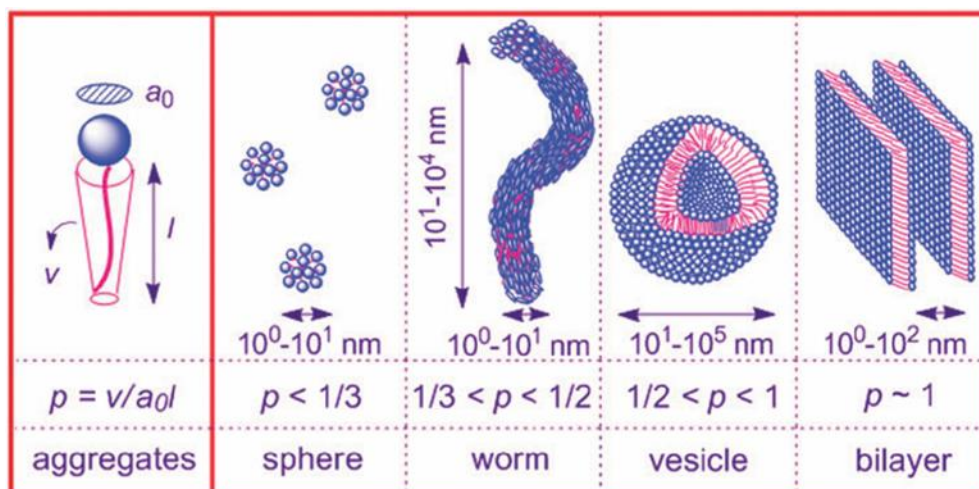


Figure 1.17 Schematic representation of self-assembled surfactant aggregates. Four morphologies (spheres, worms, vesicles and bilayers) and their approximate dimensions and corresponding packing parameters (p) are shown as described by Israelachvili.^{103, 107}

These three parameters can be used to define the dimensionless *packing parameter* (p), see Equation 1.17.

$$p = \frac{v}{a_0 l_c} \quad 1.17$$

The fractional value of p determines the aggregate structure corresponding to the minimum free energy (Figure 1.17). Different micelle structures are obtained as p increases: spherical micelles ($p \leq 1/3$), worm-like micelles ($1/3 \geq p \leq 1/2$), vesicles ($1/2 \geq p \leq 1$) and bilayers ($p \sim 1$). If p exceeds unity, then ‘inverted’ micelles are formed.

1.4.3. Self-Assembly of AB Diblock Copolymers

The self-assembly of AB block copolymers has been extensively studied.¹⁰⁸⁻¹¹¹ In the bulk, this leads to microphase separation as the enthalpic incompatibility between the two comonomers exceeds the entropy of mixing.^{109, 112} Macroscopic separation is prevented by the covalent bond connecting the two blocks. The resulting copolymer morphology depends on three parameters (Figure 1.18). Firstly, the relative volume fraction of each block (f_A and f_B), where the total volume fraction equals unity ($f_A + f_B = 1$). Secondly, the total DP (N) of the two blocks (where $N = DP_A + DP_B$). Thirdly, the Flory-Huggins parameter (χ_{AB}), which indicates the degree of incompatibility between the two blocks, as defined in Equation 1.18.^{108, 111, 113}

$$\chi_{AB} = \frac{1}{k_B T} \left[\varepsilon_{AB} - \frac{1}{2} (\varepsilon_{AA} + \varepsilon_{BB}) \right] \quad 1.18$$

The Flory-Huggins parameter depends on Boltzmann's constant (k_B), the absolute temperature (T) and the three interaction energies between the A and B blocks (ε_{AB} , ε_{AA} and ε_{BB}).¹¹³ When an AB diblock copolymer has equal volume fractions for each block, then a lamellae structure is observed (Figure 1.18). When the f_A is less than 0.5, either spheres or worms are obtained, and if f_A is higher than 0.5, then inverted structures are formed (Figure 1.18).

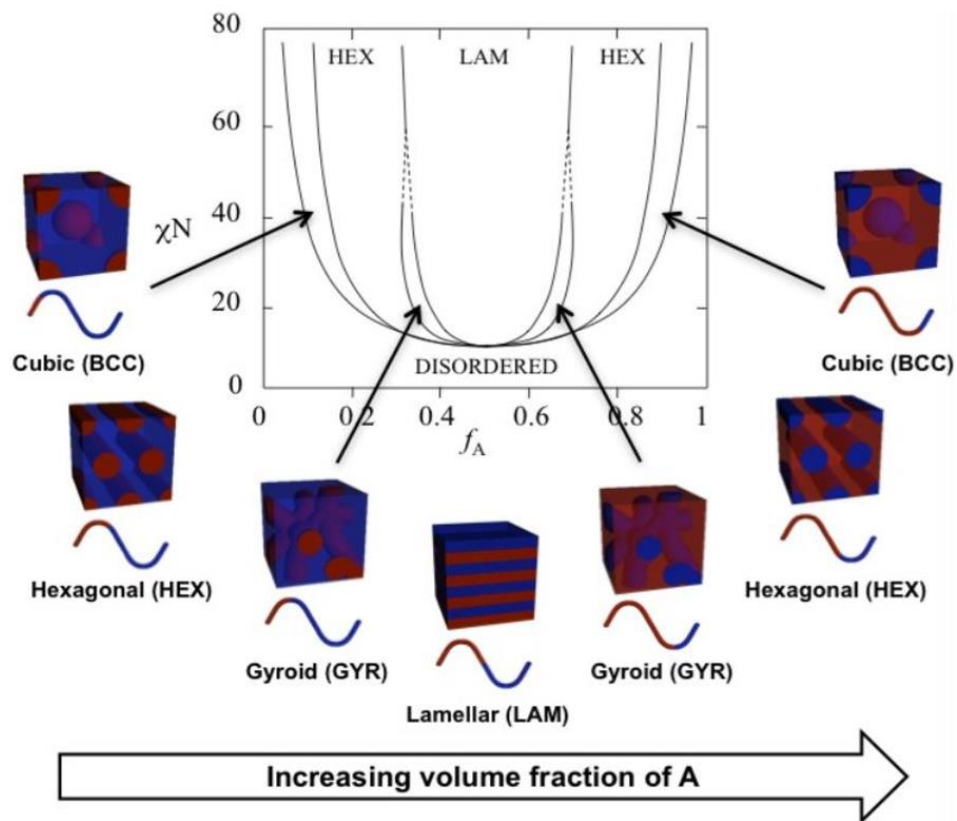


Figure 1.18 Theoretical AB diblock copolymer morphology as a function of volume fraction of the A block (f_A).¹¹²

In aqueous solution, amphiphilic AB diblock copolymers self-assemble like surfactants, where the final block copolymer morphology depends on the balance between the hydrophilic and hydrophobic components of the diblock copolymer.¹¹⁴ The concept of a packing parameter (previously discussed in Section 1.4.2), can also be applied here to predict the final copolymer morphology. Each of the terms in Equation 1.17 can be related to the block copolymer; a_0 is the cross-sectional area of the hydrophilic block, V is the volume occupied by the hydrophobic block and l_c is the effective length of the hydrophobic chain. Various copolymer morphologies can be obtained as p increases; spherical micelles ($p \leq 1/3$), worm-like micelles ($1/3 \geq p \geq 1/2$) and vesicles ($1/2 \geq p \geq 1$).¹¹⁴

Traditionally, the self-assembly of block copolymers to obtain such morphologies has been achieved by post-polymerization processing techniques such as a solvent switch,¹³ pH switch^{14, 115, 116} or thin film hydration.¹⁶ However, these processes are often time-consuming and typically conducted in dilute solution (< 1% w/w block copolymer). This is a significant limitation with regards to potential industrial applications of the resulting nanoparticles.

1.4.4. Polymerization-Induced Self-Assembly (PISA)

Over the last fifteen years, polymerization-induced self-assembly (PISA) has become a powerful and versatile method for the formation of sterically-stabilized block copolymer nanoparticles. PISA offers an attractive alternative to post-polymerization processing because it can be performed at significantly higher copolymer concentrations (10 - 50% w/w).^{94, 117-119} First reported by Ferguson *et al.* in 2002, PISA is based on the chain extension of a soluble homopolymer using a second monomer, whose corresponding polymer is insoluble, thus driving *in situ* self-assembly to form polymeric nanoparticles (Figure 1.19).¹²⁰ This technique can be used to prepare a wide range of organic polymeric nanoparticles of various morphologies, including spheres, worms and vesicles. In practice, the copolymer morphology depends on the stabilizer block DP, the core-forming block DP and the copolymer concentration.¹¹⁴

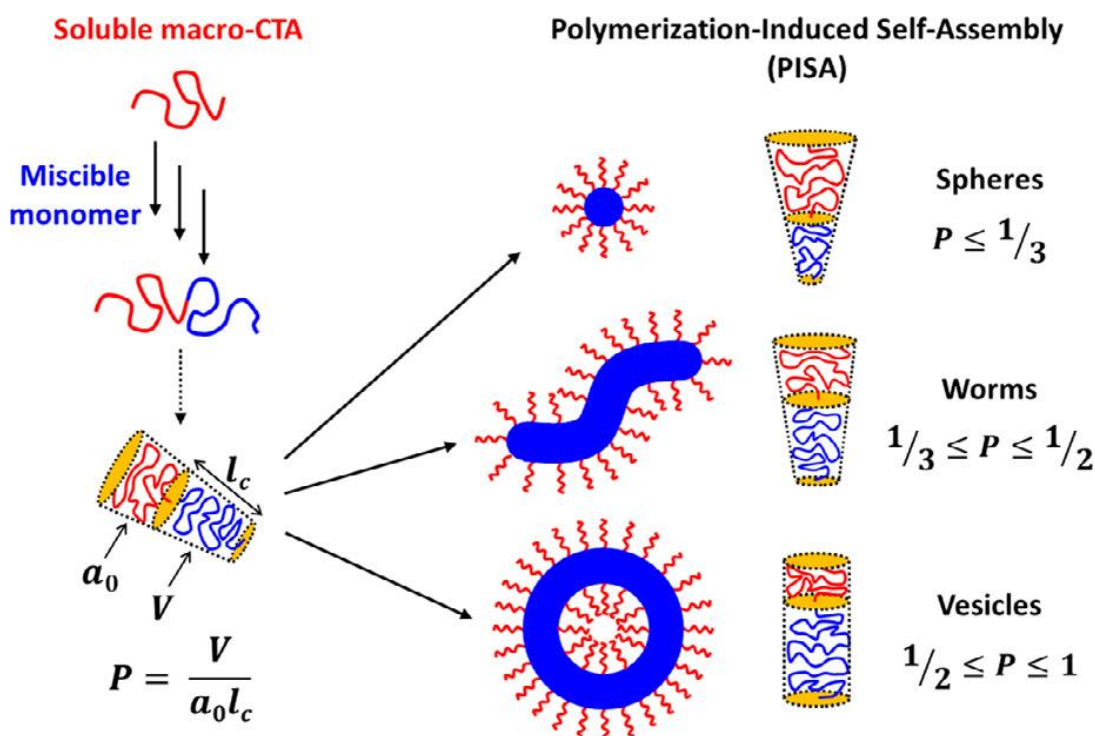


Figure 1.19 Schematic representation of the formation of diblock copolymer nanoparticles via polymerization-induced self-assembly (PISA). Chain extension of a soluble homopolymer with a second monomer, whose corresponding polymer is insoluble, drives *in situ* self-assembly to form sterically-stabilized diblock copolymer nanoparticles, whose morphology can be related to the *packing parameter* (p). Reproduced from Reference.¹¹⁷

To determine the conditions required for the reproducible synthesis of each nanoparticle morphology, a phase diagram can be constructed.¹²¹ This is achieved by systematically varying two of the three parameters. For example, the stabilizer block DP can be fixed and the core-forming block DP and copolymer concentration can be systematically varied. By analyzing the diblock copolymer nanoparticles *via* dynamic light scattering (DLS) and transmission electron microscopy (TEM), the copolymer morphology can be determined and mapped out to produce a phase diagram.

PISA can be conducted using NMP, ATRP or RAFT polymerization.^{23, 92, 117} Of particular relevance to this Thesis is the recent review by Canning *et al.* on RAFT-mediated PISA.¹²² There are numerous examples of such PISA formulations under various conditions including both aqueous^{23, 88-95} and non-aqueous media.^{83-86, 117, 123-127} For this Thesis, polymers were prepared by PISA using RAFT aqueous dispersion polymerization and RAFT aqueous emulsion polymerization, thus these formulations are discussed in more detail in the following sections.

1.4.5. PISA by RAFT Aqueous Dispersion Polymerization

RAFT aqueous dispersion polymerization involves the chain extension of a water-soluble polymer with a *water-miscible* monomer which forms a water-insoluble polymer.^{23, 89} The growing core-forming block is initially soluble but at some critical DP it becomes water-insoluble, thus driving *in situ* self-assembly. The water-soluble precursor polymer is first synthesized by RAFT solution polymerization. Thus, it is capped with RAFT end-groups and can act as a macromolecular chain transfer agent (macro-CTA). In contrast to a conventional dispersion polymerization, addition of a polymeric stabilizer is not required as the water-soluble macro-CTA acts as a steric and/or electrostatic stabilizer.

Over the last ten years, there have been numerous PISA reports involving RAFT-mediated aqueous dispersion polymerization.^{23, 89, 90, 122, 128, 129} For example, Li and Armes reported the chain extension of a water-soluble poly(glycerol monomethacrylate) (PGMA) macro-CTA with HPMA to form PGMA₆₅-PHPMA_y diblock copolymer nanoparticles, where $y = 30 - 300$ (Figure 1.20).¹³⁰ When synthesized at 10% w/w copolymer concentration, only spherical nanoparticles were formed, whose mean diameter increased with PHPMA DP. However, vesicles could be obtained by targeting a relatively asymmetric diblock composition (PGMA₆₅-PHPMA₃₀₀) at 20% w/w copolymer concentration. The synthesis of PGMA_x-PHPMA_y diblock copolymer nanoparticles *via* RAFT aqueous dispersion polymerization has been extensively studied as a model system.^{121, 130-133} One reason for this is the limited number of monomers that are suitable for PISA under these conditions; it requires a *water-miscible* monomer that polymerizes to form a water-insoluble polymer.^{65, 122}

RAFT aqueous dispersion polymerization

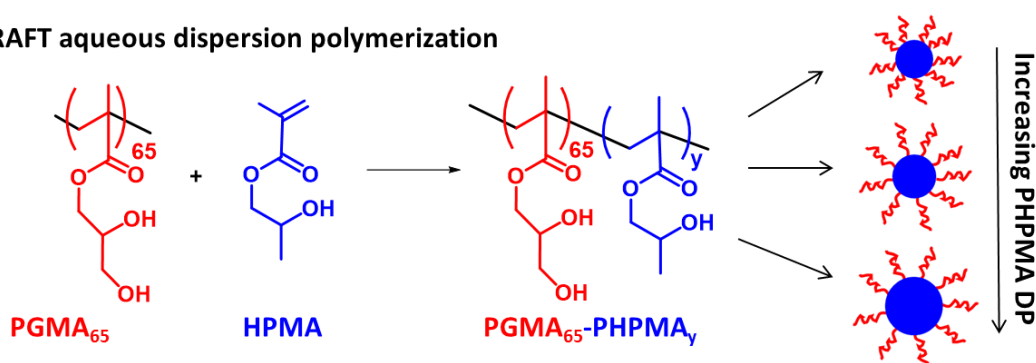


Figure 1.20 Synthesis of sterically-stabilized poly(glycerol monomethacrylate)-poly(2-hydroxypropyl methacrylate) (PGMA₆₅-PHPMA_y) diblock copolymer nanoparticles (where $y = 30-300$) *via* PISA utilizing RAFT aqueous dispersion polymerization.¹³⁰

In-depth studies regarding the evolution of copolymer morphology during PISA were conducted. Blanazs *et al.* performed a detailed kinetic study during the synthesis of PGMA₄₇-PHPMA₂₀₀ vesicles.¹³¹ Aliquots of the reaction solution were taken at regular time intervals throughout the HPMa polymerization. ¹H nuclear magnetic resonance (NMR) spectroscopy was used to monitor the kinetics of polymerization, with > 99% monomer conversion being achieved within 2 h at 70 °C. Self-assembly was monitored by DLS and TEM, see Figure 1.21. This study showed the gradual evolution of copolymer morphology from molecularly-dissolved chains, to spheres, to dimers and trimers, to worms. These worms then began to branch, forming bilayer ‘octopi’ which underwent ‘wrap-up’ to form jellyfish and subsequently formed vesicles.

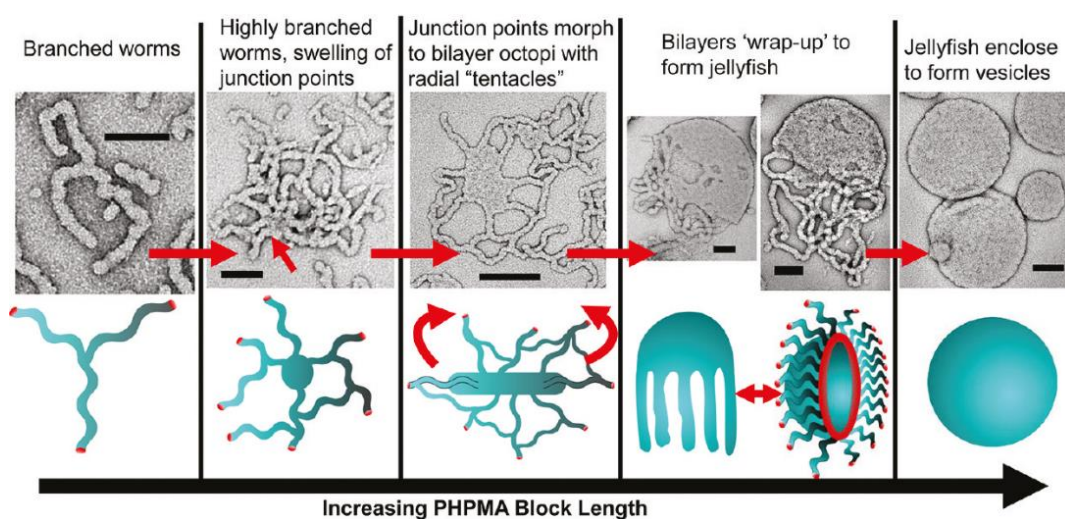


Figure 1.21 Evolution of diblock copolymer morphology during the synthesis of PGMA₄₇-PPMA₂₀₀ vesicles by RAFT dispersion polymerization. Reproduced from Reference.¹³¹

Blanazs *et al.* constructed three phase diagrams to demonstrate that the systematic variation of the PHPMA DP and the copolymer concentration enables pure phases of each of the three main morphologies to be obtained (Figure 1.22).¹²¹

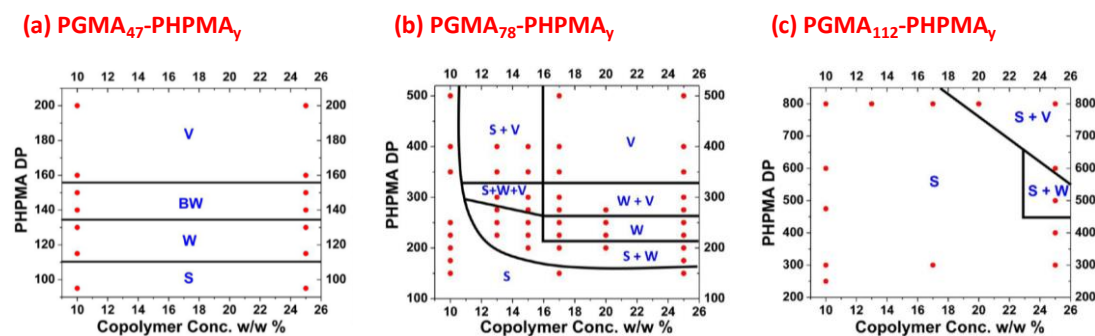


Figure 1.22 Three phase diagrams for (a) PGMA₄₇-PHPMA_y (b) PGMA₇₈-PHPMA_y and (c) PGMA₁₁₂-PHPMA_y diblock copolymer nanoparticles synthesized by RAFT aqueous dispersion polymerization. Morphologies were assigned by TEM (S = spheres, W = worms, BW = branched worms and V = vesicles). Reproduced from Reference.¹²¹

The phase diagram constructed using the PGMA₇₈ macro-CTA (Figure 1.22b) indicates that different copolymer morphologies can be formed by identical diblock copolymers. For example, PGMA₇₈-PHPMA₅₀₀ can form either spherical nanoparticles or vesicles depending on the copolymer concentration. Clearly, only one of these morphologies can be the equilibrium morphology. Given this copolymers compositional asymmetry, this must be the vesicle morphology, which suggests that the spherical morphology is kinetically-trapped. In this case, sphere-sphere fusion does not occur, which is the essential first step required for the transition from spheres to worms.¹³¹ Similarly, if the stabilizer block is too long (e.g. PGMA₁₁₂), then predominantly spherical nanoparticles are obtained regardless of the PHPMA DP or copolymer concentration (Figure 1.22c). The longer macro-CTA provides more effective steric stabilization and also hinders sphere-sphere fusion. It was also demonstrated that, for a shorter macro-CTA DP (PGMA₄₇), the copolymer concentration had no influence over the morphology. This is presumably because sphere-sphere fusion occurs much more readily in this case (Figure 1.20a).

The various diblock copolymer nanoparticles synthesized by RAFT aqueous dispersion polymerization have potential applications. These often require the identification of pure phases of each morphology, in particular the higher order morphologies (worms and vesicles) which have more interesting properties. Worm-like particles typically form soft free-standing gels at room temperature owing to multiple inter-worm contacts.^{107, 134} Interestingly, these worms can undergo a reversible morphology transition to spheres on cooling to 4 °C, causing a gel-sol transition (Figure 1.23).¹³² Variable temperature ¹H NMR studies suggest that this

thermal transition is caused by an increase in surface plasticization of the PGMA₅₄-PHPMA₁₄₀ worms. This results in an increase in the volume fraction of the stabilizer block relative to the core, thus reducing the effective p . Numerous publications by Armes and co-workers have explored novel applications of these worms (or worm gels), including as effective Pickering emulsifiers,¹³⁵ for the cryopreservation of red blood cells¹³⁶ and as a cost-effective storage medium for the transportation of human stem cells without loss of pluripotency.¹³⁷

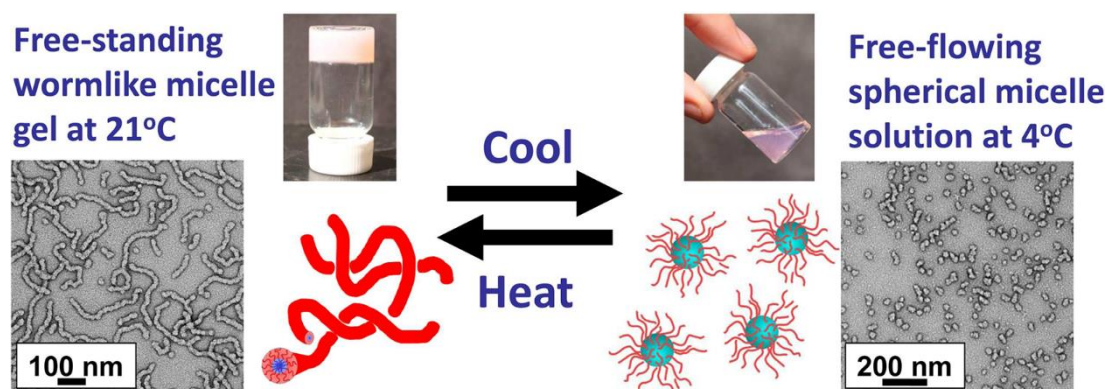


Figure 1.23 PGMA₅₄-PHPMA₁₄₀ diblock copolymer worms form free-standing gels at 21°C. Upon cooling these worms undergo a worm-to-sphere transition, resulting in a free-flowing solution at 4 °C. This transition was fully reversible. Reproduced from Reference.¹³²

The vesicular morphology also has interesting applications in the context of encapsulation. Mable *et al.* showed that silica nanoparticles can be encapsulated inside PGMA₅₈-PHPMA₂₅₀ vesicles during their PISA synthesis.¹³⁸ These vesicles also exhibit thermoresponsive behavior, enabling the thermally-triggered release of the silica nanoparticles on cooling to 0 °C.¹³⁸ In addition, by further chain-extending PGMA₆₃-PHPMA₃₅₀ vesicles with BzMA (PBzMA DP 25 - 400) the preparation of well-defined framboidal vesicles was achieved, as a result of microphase separation between the PHPMA and PBzMA blocks co-located within the vesicle membrane (Figure 1.24).¹³⁹

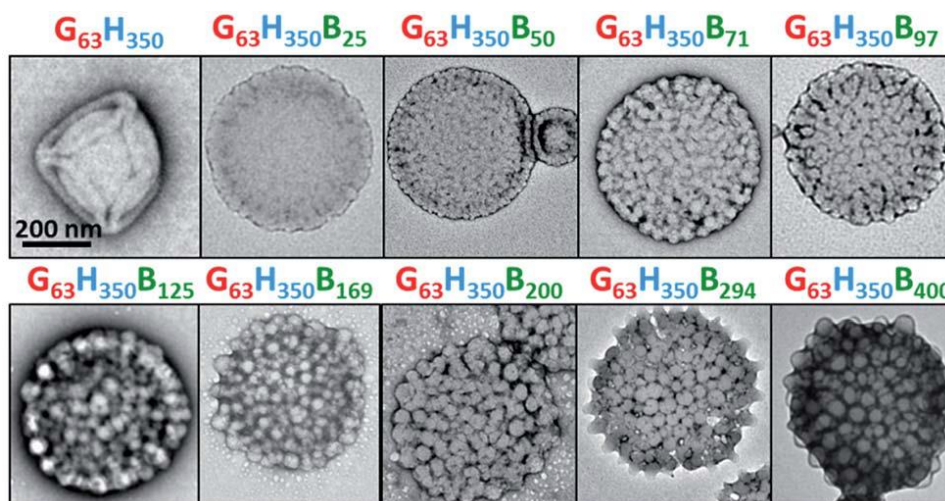


Figure 1.24 Representative TEM images of a $\text{PGMA}_{63}\text{-PHPMA}_{350}$ vesicle precursor and a series of framboidal $\text{PGMA}_{63}\text{-PHPMA}_{350}\text{-PBzMA}_z$ vesicles (where $z = 25 - 400$). Scale bar is the same for all images. Reproduced from Reference, where G = PGMA, H = PHPMA and B = PBzMA.¹³⁹

Despite being restricted to a limited number of monomers, an important advantage of RAFT aqueous dispersion polymerization is the ability to synthesize stimuli-responsive nanoparticles such as those described above. For thermally-induced copolymer morphology transitions, the solvent must be able to diffuse into the nanoparticle core. This is not possible *via* RAFT aqueous emulsion polymerization, owing to the much greater hydrophobicity of the core-forming blocks in such syntheses.

1.4.6. PISA by RAFT Aqueous Emulsion Polymerization

For both conventional emulsion and dispersion polymerization, either a surfactant or a polymeric stabilizer is required for the formation of stable polymer particles. For RAFT aqueous dispersion polymerization, as discussed previously, addition of a polymeric stabilizer is not required as the water-soluble macro-CTA acts as a (electro)steric stabilizer enabling the formation of colloidally stable particles *via* PISA.

The first successful RAFT aqueous emulsion polymerization was reported in the original RAFT publication by Rizzardo and co-workers.⁶⁶ However, during this polymerization of *n*-butyl methacrylate (BMA) two important experimental factors are worth considering; the presence of added surfactant (sodium dodecyl sulfate, SDS) and the gradual addition of BMA monomer *via* syringe pump. Thus, this polymerization was performed under monomer-starved conditions. Despite this initial

success, subsequent attempts to develop robust RAFT emulsion polymerization formulations proved to be problematic with substantially incomplete conversions, poor molecular weight control and broad MWD typically being observed.¹⁴⁰⁻¹⁴⁶

For example, Uzulina *et al.* aimed to adapt the RAFT polymerization of styrene in bulk to a RAFT emulsion polymerization using a commercial CTA (S-(thiobenzoyl-)thioglycolic acid).¹⁴¹ The CTA was dissolved in the styrene monomer and then suspended in an aqueous phase (pH < 7) containing both surfactant (SDS) and initiator (potassium persulfate, KPS). Although the observed polymerization displayed living characteristics it proceeded relatively slowly, only reaching low conversion. The precipitation of unreacted CTA also resulted in a partial flocculation.

The fundamental issue with RAFT aqueous emulsion polymerizations was considered to be the solubility of the CTA in the monomer and its ability to diffuse through the aqueous phase. For a successful RAFT emulsion polymerization, the CTA needs to be adequately water-soluble to enable its transport with the monomer to the growing polymer particles. However, if the CTA is too water-soluble it may diffuse out of the particles during the polymerization. It was found that using the triethyl amine salt of this CTA addressed both of these issues. The salt form of the CTA is sufficiently water-soluble to enable its diffusion through the aqueous phase, where it readily dissociates to yield the monomer-soluble CTA and triethyl amine. Application of this triethylamine CTA salt enabled the RAFT aqueous emulsion polymerization of styrene (17% conversion), methyl methacrylate (MMA, 17% conversion), and vinyl acetate (VA, up to 40% conversion). This study indicated that RAFT polymerization could be performed under emulsion conditions with acrylic, styrenic or vinylic monomers, but was limited to rather low levels of monomer conversion.

To further investigate the effect of exit of the CTA from the growing polymer particles on the rate of polymerization and the MWD of the polymer chains, Monteiro *et al.* studied the seeded emulsion polymerization of styrene.¹⁴² These polymerizations were carried out using a poly(methyl methacrylate) seed in the presence of surfactant. Two different CTAs were compared: 2-(ethoxycarbonyl)propyl-2-yl dithiobenzoate (EMA) and 2-phenylprop-2-yl dithiobenzoate (cumyl dithiobenzoate). Both CTAs resulted in a significant reduction in polymerization rate, relative to the rate of

conventional emulsion polymerization, which was explained by the exit of the CTA from the particles after fragmentation. Broad MWDs and coagulum were also observed, most likely resulting from polymerization occurring within the monomer droplets throughout the polymerization. Monteiro and co-workers concluded that, in order to improve their results, larger seed particles were required to further reduce exit of the CTA.

In order to facilitate transport of the CTA to latex seed particles, Prescott *et al.* utilized acetone as a co-solvent.¹⁴⁷ During the seeded emulsion polymerization of styrene, acetone was added to the polystyrene seed latex (previously prepared by conventional aqueous emulsion polymerization and surfactant-stabilized) in addition to solid crystals of the RAFT agent (2-phenylprop-2-ylphenyldithioacetate, PPPDTA). This method gave reasonable control over the molecular weight distribution ($1.2 \leq \bar{D} \leq 1.4$) and was identified as a living system, owing to the linear evolution of molecular weight with conversion (Figure 1.25). In addition, little or no coagulum was formed during the polymerization. By assisting transport of the CTA into the particles, less polymerization could occur in the monomer droplets due to the absence of the CTA. Despite these improvements, long inhibition periods (45 min to 3 h) were observed along with a 30 to 50% reduction in rate, as reported previously for RAFT emulsion formulations.^{142, 148} However, these effects were minimized by increasing the initiator (sodium persulfate) concentration by a factor of nine up to 1.39 mM.

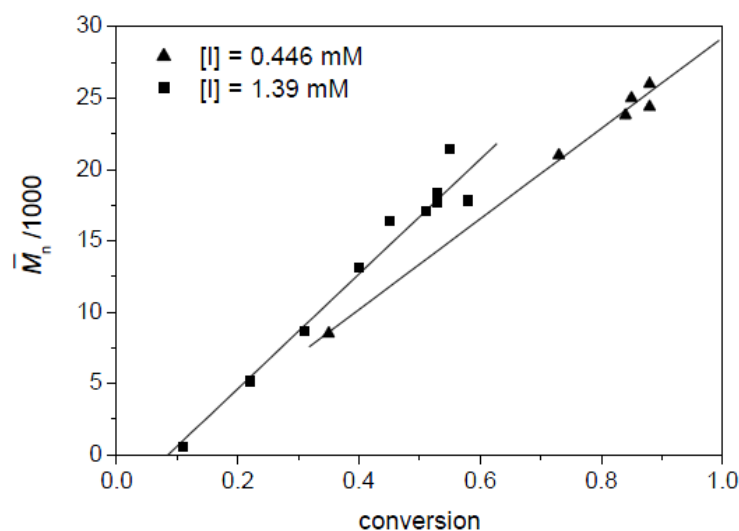


Figure 1.25. Molecular weight (\bar{M}_n) evolution with conversion for the seeded RAFT emulsion polymerization of styrene, using a sodium persulfate initiator concentration of either 0.446 mM or 1.39 mM. The linear evolution of molecular weight with conversion indicates living character. For each data point, \bar{D} varied from 1.20 to 1.40. Reproduced from Reference.¹⁴⁷

The use of acetone as a co-solvent (also termed nanoprecipitation) was adapted by Szkurhan *et al.* to polymerize styrene.^{149,150} The CTA (PPPDTA) was used to prepare RAFT-agent terminated polystyrene (PS) oligomers. This hydrophobic macro-CTA was then dissolved in acetone and added drop wise to a stirred aqueous solution of poly(vinyl alcohol) (PVA). This protocol resulted in the formation of PVA-stabilized particles, with the PS macro-CTA chains located in the particle core. After removal of acetone, these particles were swollen with styrene monomer and polymerized. Originally, these polymerizations were initiated by the addition of KPS. However, this initiator resulted in both poor control and reproducibility issues. These results were attributed to the high water-solubility of KPS, which caused a delay in entry to the growing polymer particles until PS oligomers were formed. Better results were achieved at higher temperatures (105 °C), by employing the auto-initiation mechanism of styrene. This increased the conversion to 74% within 54 h and led to the synthesis of living polymers with narrow molecular weight distributions, which formed stable particle latexes of ~150 nm (Figure 1.26). These high temperature reactions were performed in a pressurized Parr bomb reactor at 6.9 bar.

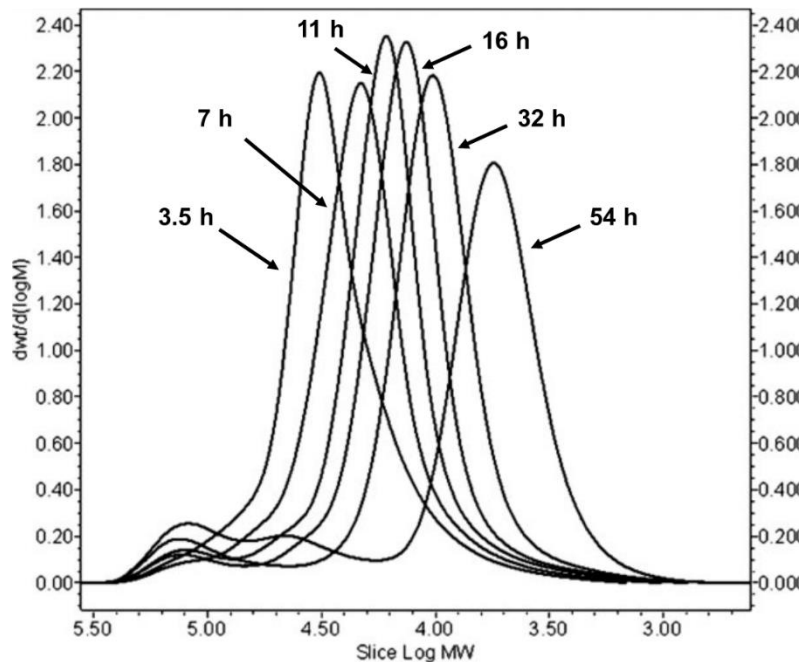


Figure 1.26. GPC chromatograms obtained for the RAFT emulsion polymerization of styrene under RAFT emulsion polymerization conditions, using autoinitiation as a radical source. The chromatograms correspond to 3.5, 7, 11, 16, 32, and 54 h of polymerization from right to left. Reproduced from Reference.¹⁵⁰

Although these seeded emulsion polymerizations helped to gain insight into the mechanism of RAFT emulsion polymerization, significant problems remain unresolved.^{144, 148-150} The main issues include poor monomer conversions ($\leq 74\%$), polymer seed contamination of the final product and the limitations of the acetone-assisted monomer transport technique on an industrial scale. The majority of these formulations also still required addition of surfactant. Prior to 2002, the only successful *ab initio* RAFT emulsion polymerization reported was the polymerization of BMA, as described in the seminal RAFT publication.⁶⁶ As discussed above, all other attempts at unseeded RAFT aqueous emulsion polymerization were susceptible to multiple issues.^{5, 120, 141, 142, 144, 146}

These mechanistic insights were used by Ferguson *et al.* to develop a novel *ab initio* RAFT emulsion polymerization method which overcame the impracticalities of the seeded mechanism (Figure 1.27).^{120, 151, 152} The seeded emulsion polymerization studies indicated that, for a successful RAFT emulsion polymerization, all of the CTA must be located inside the particles as they form, rather than in the monomer droplets, thus allowing the polymerization to proceed under RAFT control.^{147, 152, 120} The new concept explored by Ferguson *et al.* was to stabilize the growing polymer particles using a water-soluble precursor block, instead of relying on the surfactants typically used in conventional emulsion polymerization.

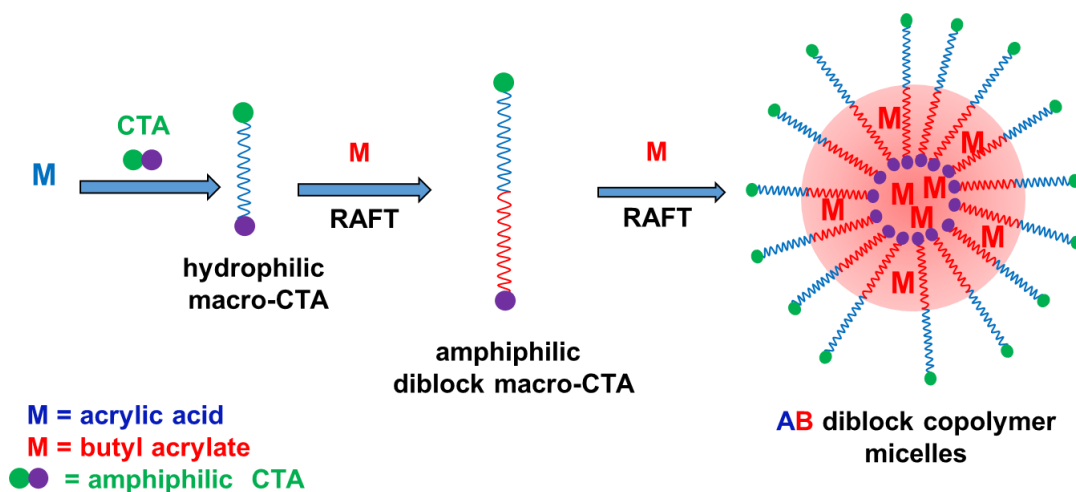


Figure 1.27. *Ab initio* RAFT aqueous emulsion polymerization of a poly(acrylic acid) macro-RAFT agent with butyl acrylate.^{120, 152}

Thus, a water-soluble monomer (acrylic acid, AA) was polymerized using an amphiphilic CTA (2-[(butylsulfanyl)-carbonothioyl]sulfanyl propanoic acid or 2-[(dodecylsulfanyl)-carbonothioyl]sulfanyl propanoic acid) to form a PAA_x macro-CTA with a low DP ($x = 5$). This precursor was then chain-extended with a hydrophobic monomer (butyl acrylate, BA) to form PAA_x-PBA_y oligomers. At a critical PBA DP, the second block becomes sufficiently hydrophobic to form micelles *via in situ* self-assembly. These micelles act as a seed and contain the hydrophobic CTA. Under monomer-starved conditions, no monomer droplets form and the BA monomer diffuses into the growing particles. The particles then continue to grow as the PBA block increases in length, allowing emulsion polymerization to proceed rapidly under RAFT control.

This first example of *ab initio* RAFT aqueous emulsion polymerization was a considerable improvement on previous formulations. The polymerization proceeded under living conditions to high conversion within 6 h, resulting in polymers of controlled molecular weight and low dispersity ($\mathcal{D} \leq 1.5$). The particles formed during the polymerization were colloidally stable and ~60 nm diameter, as judged by capillary hydrodynamic fractionation.¹²⁰ This *ab initio* method successfully eliminated the need for added surfactant and co-solvent, improving the quality of the polymer product. This advance paved the way for a considerable increase in research activity focused on RAFT aqueous emulsion polymerization.

Many such reports utilize styrene as the hydrophobic monomer. A range of non-ionic macro-CTAs has been investigated, based on poly(ethylene oxide) (PEO),¹²⁹ polyacrylamide¹⁵³ and poly(*N,N*-dimethylacrylamide).¹¹⁸ The use of both anionic and cationic macro-CTAs was also investigated, including PAA,^{154, 155} poly(sodium acrylate),¹⁵⁶ poly(sodium 4-styrenesulfonate),¹⁵⁷ poly(4-vinylpyridine)¹⁵⁸ and poly[2-(diethylamino)ethyl methacrylate] (PDEAEMA).¹⁵⁹ [N.B. The latter two macro-CTAs become water-soluble in their protonated form below their respective pK_a values]. This research showed that either ionic or non-ionic homopolymers can act as efficient stabilizers in the absence of surfactant, see Figure 1.28.

Jing *et al.* adapted this method further by applying ultrasonic irradiation to the RAFT aqueous emulsion polymerization of styrene.¹⁶⁰ Ultrasonic irradiation led to the formation of a stable emulsion, where the styrene droplets were stabilized by a

polyacrylamide macro-CTA. This enabled RAFT aqueous emulsion polymerization to proceed without the need for a surfactant or organic co-solvent. The resulting spherical nanoparticles had relatively narrow particle size distributions.

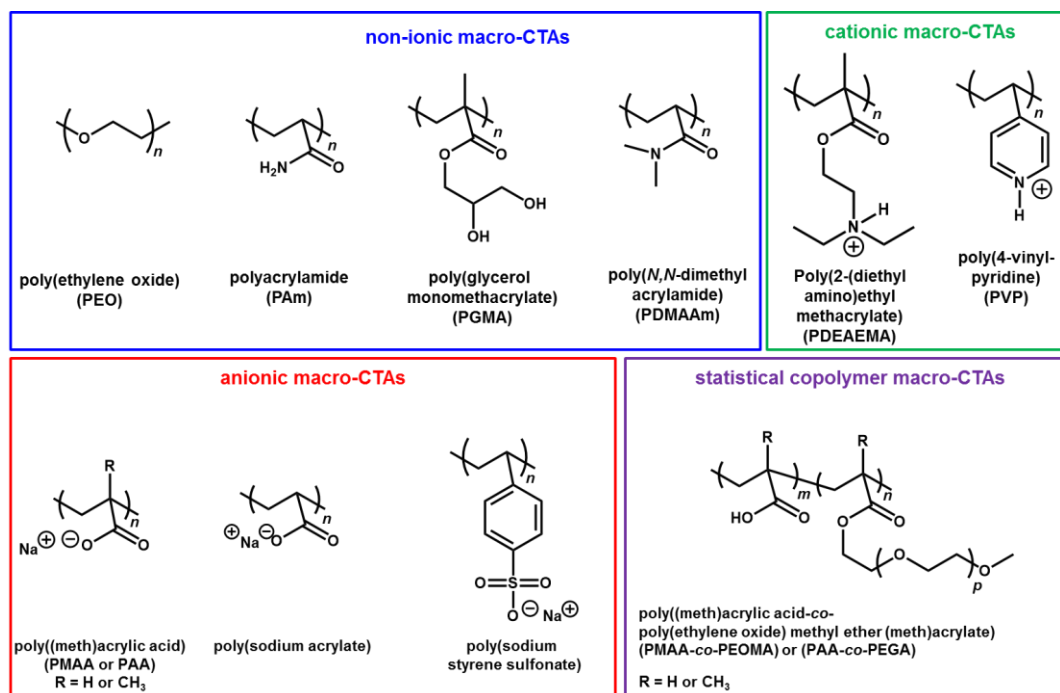


Figure 1.28 Chemical structures of various types of water-soluble macromolecular chain transfer agents (macro-CTAs) utilized in RAFT aqueous emulsion polymerization. These macro-CTAs form the stabilizer block of sterically-stabilized nanoparticles synthesized by polymerization-induced self-assembly.^{118, 129, 153-159, 161, 162}

The Charleux group has conducted extensive research into the synthesis of diblock copolymer nanoparticles *via* RAFT aqueous emulsion polymerization. They utilized a water-soluble PEO macro-CTA for the RAFT aqueous emulsion polymerization of both styrene and *n*-butyl acrylate (*n*BA).¹²⁹ PEO was first coupled with (2-(dodecylthiocarbonothioylthio)-2-methylpropanoic acid) (TTCA) to produce an amphiphilic macro-CTA. This macro-CTA acts as both the chain transfer agent for the RAFT polymerization and the particle stabilizer, leading to the formation of core-shell latex particles. These nanoparticles are composed of a hydrophilic stabilizer shell (PEO) and a hydrophobic (styrene or *n*BA) core. Polymerizations were well-controlled, affording good control over target molecular weight and narrow molecular weight distributions. It was shown that the particle size could be tuned by systematically altering the macro-CTA to monomer molar ratio. Similarly, it was shown that altering the PEO macro-CTA DP influenced the nanoparticle size.¹⁶³

Other water-soluble macro-CTAs were also researched, including poly(AA),^{164, 165-167} poly(methacrylic acid) (PMAA),^{164, 168} poly[2-(diethylamino)ethyl methacrylate] (PDEAEMA),¹⁵⁹ PEO,¹⁶⁹ poly[methacrylic acid-*co*-poly(ethylene oxide) methyl ether methacrylate],¹⁷⁰ poly[ethylene glycol) methyl ether acrylate)]-*co*-poly(*N*-hydroxyethyl acrylamine) (PEGA-*co*-PHEAA)¹⁷¹ and poly(styrene-*co*-acrylic acid),¹⁵⁶ see Figure 1.28. All acted as effective stabilizers and CTAs for the RAFT aqueous emulsion polymerizations of hydrophobic monomers such as styrene, *n*BA or MMA.

This same method was utilized by Cunningham *et al.* who chain-extended a non-ionic PGMA macro-CTA (Figure 1.28) with BzMA *via* RAFT aqueous emulsion polymerization to form a series of spherical nanoparticles of increasing particle diameter with PBzMA DP, at up to 50% w/w copolymer concentration.⁹⁴ Similar PGMA macro-CTAs were also chain-extended with 2,2,2-trifluoroethyl methacrylate (TFEMA),¹⁷² glycidyl methacrylate (GlyMA)¹⁷³ or isopropylidenglycerol (IPGMA)¹⁷⁴ to give sterically-stabilized spherical nanoparticles by PISA. The RAFT aqueous emulsion polymerization of phenyl acrylate (PhA) was also reported using a poly(dimethyl acrylamide) (PDMAC) macro-CTA.¹⁷⁵ However, all of the RAFT aqueous emulsion polymerizations discussed above only led to the formation of spherical nanoparticles by PISA. This is in spite of the fact that equivalent or similar diblock copolymers have been synthesized *via* RAFT alcoholic dispersion polymerization and can form either worms or vesicle under appropriate conditions.

Considerable research has also been conducted into the use of macro-CTAs comprising a statistical mixture of monomers, see Figure 1.28. Use of these macro-CTAs typically enables access to non-spherical morphologies *via* RAFT aqueous emulsion polymerization. For example, the polymerization of styrene using a poly[(acrylic acid)-*co*-poly(ethylene glycol methyl ether acrylate)] (P(AA-*co*-PEGA)) macro-CTA led to the formation of ‘amphiphilic nano-fibers’ or worms.¹⁶¹ Similarly, chain-extending a poly[methacrylic acid-*co*-poly(ethylene oxide) methyl ether methacrylate] (P(MAA-*co*-PEOMA)) macro-CTA with styrene and/or MMA, enabled the formation of spheres, worms or vesicles *via* PISA (Figure 1.29).^{162, 176-178} During these syntheses, various parameters including the statistical copolymer composition, core-forming block DP, salt concentration, stirring rate, copolymer concentration and

pH were all determined to have a significant impact on polymerization control and the final diblock copolymer morphology.

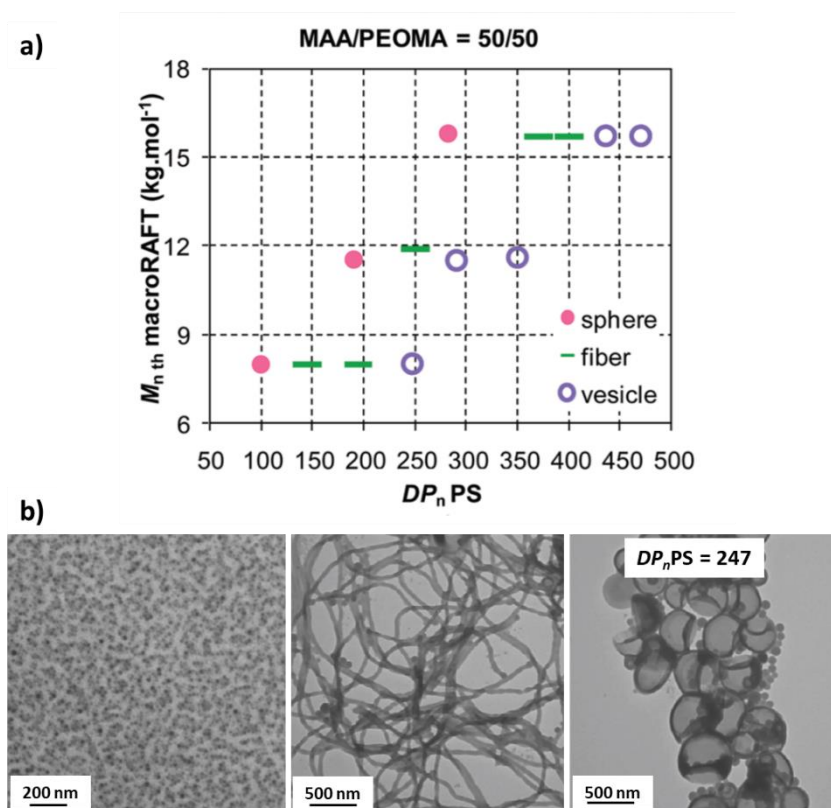


Figure 1.29. (a) Phase diagram showing the effect of macro-CTA molecular weight and degree of polymerization of styrene on the final nanoparticle morphology for the RAFT aqueous emulsion polymerizations of styrene at pH 5, in the presence of P(MAA-*co*-PEOMA). (b) TEM images showing the three morphologies depicted in (a). Reproduced from Reference.¹⁷⁹

It is not well understood why the use of statistical copolymers as macro-CTAs enables the synthesis of higher order morphologies by RAFT aqueous emulsion polymerization. Recent empirical experiments have aimed to gain further insights. Lesage de la Haye *et al.* investigated the effect of hydrophile structure on the morphology of diblock copolymer nanoparticles synthesized *via* RAFT aqueous emulsion polymerization of styrene.¹⁸⁰ Three different hydrophilic poly(*N*-acryloylmorpholine) (PNAM) macro-CTAs were synthesized, each containing three poly(ethylene glycol acrylate) (PEGA) units, see Figure 1.30. It was demonstrated that the position of the PEGA units had a dramatic effect on the final diblock copolymer morphology. For pure PNAM₂₆-PS diblock copolymers only spherical nanoparticles were obtained, but pure vesicles were observed by inserting

three PEGA units at the end of the PNMA chain. Mixed phases of spheres and vesicles were also obtained when the PEGA units were inserted either statistically or at the beginning of the PNMA chain.

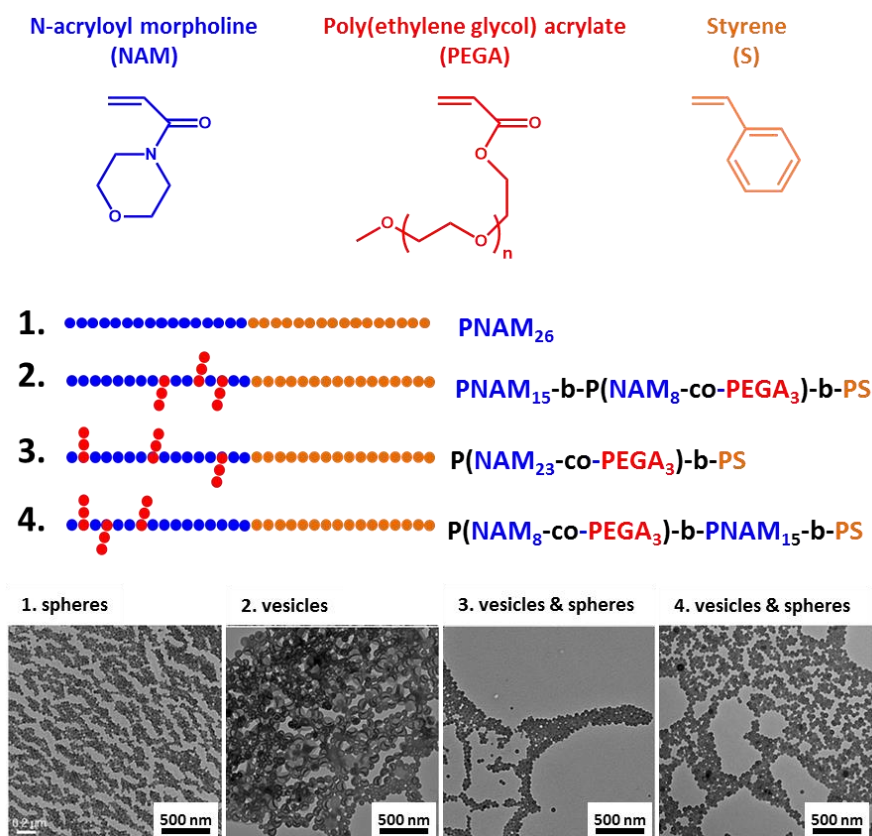


Figure 1.30 Influence of the position of poly(ethylene glycol acrylate) (PEGA) units along a poly(N-acryloylmorpholine) macro-CTA on the final copolymer morphology of P(NAM-co-PEGA)-PS diblock copolymer nanoparticles. Four different PNAM macro-CTAs were used; (1) pure PNAM, (2), PEGA units at end of PNAM chain, (3) PEGA units statistically throughout the PNAM chain and (4) PEGA units at the beginning of the PNAM chain. The TEM of the corresponding particle morphology is also shown for each macro-CTA. Taken in part from Reference.¹⁸⁰

Truong *et al.* also recently reported the synthesis of novel non-spherical ‘filomicelle nanomaterials’ by employing RAFT aqueous emulsion polymerization followed by a ‘temperature-induced morphological transition’ (TIMT).¹⁸¹ At the end of the initial polymerization, only spherical micelles were obtained. On cooling in the presence of additional monomer, a morphological transition from spheres to filomicelles (worms) and/or vesicles was observed. In this case, it appears that the additional monomer acts as a plasticizer for the frustrated core-forming block. However, application of this TIMT approach would not be particularly attractive from a commercial perspective due to the presence of residual monomer.

Another recently published article from the Davis group, demonstrated that spheres, worms and vesicles could be synthesized by RAFT aqueous emulsion polymerization provided that the macro-CTA end-group and the radical initiator concentration are carefully chosen.¹⁸² More specifically, two poly[*N*-hydroxyethyl acrylamide-*co*-poly(ethylene glycol) methyl ether acrylate] P(HEAA-*co*-PEGA) macro-CTAs were synthesized by RAFT solution copolymerization. A carboxylic acid-functionalized 4-cyano-4-(ethylthiocarbonothioylthio)pentanoic acid RAFT agent was used alongside its methylated analogue. For the subsequent RAFT emulsion polymerization of styrene, only spheres were obtained when using the carboxylic acid-terminated macro-CTA, whereas vesicles were formed when utilizing the methyl ester-terminated macro-CTA. Additionally, it was shown that halving the initiator concentration during the above vesicle synthesis (macro-CTA:initiator ratio adjusted from 1:0.25 to 1:0.125) resulted in the formation of spheres only. In this case, the synthesis of spheres is thought to occur as a result of the reduced number of growing polymer chains and thus, a lower number of chains aggregating in one particle.

More recently, diblock and triblock copolymers have been utilized as the macro-CTA for RAFT aqueous emulsion polymerizations, instead of homopolymers. For example, Qiao *et al.* synthesized a poly(acrylic acid)-poly(2,2,2-trifluoroethyl acrylate)-poly(acrylic acid) ABA triblock copolymer which was then chain extended with 2,2,3,4,4,4-hexafluorobutyl acrylate by RAFT aqueous emulsion polymerization to give ABCBA penta-block copolymer spherical nanoparticles *via* PISA.¹⁸³ Similarly, Pham *et al.* polymerized styrene from either a P(AA-*co*-BA)-PS AB diblock copolymer or a P(AA-*co*-BA)-PS-P(AA-*co*-BA) ABA triblock copolymer. The resulting polymers were shown to self-assemble to form not only spherical nanoparticles but worm and vesicles as well.¹⁸⁴

Although this empirical research¹⁸⁰⁻¹⁸² undoubtedly constitutes useful progress, the critical synthesis parameters that determine whether only kinetically-trapped spheres are obtained or the full range of morphologies are observed have not yet been established.

1.5. Thesis Outline

The work presented in this Thesis aims to better understand the synthesis of diblock copolymer nanoparticles in aqueous media. There is a considerable volume of work published on RAFT aqueous dispersion polymerization, involving the polymerization of a *water-miscible* monomer from a *water-soluble* homopolymer. Under these conditions, a wide range of diblock copolymer morphologies (spheres, worms and vesicles) can be accessed by PISA. This Thesis focuses on the polymerization of *water-immiscible* monomers *via* RAFT aqueous emulsion polymerization. The literature indicates that such formulations often only lead to the synthesis of kinetically-trapped spherical nanoparticles *via* PISA. The critical synthesis parameters that determine whether or not the full range of morphologies can be obtained have not yet been established.

In Chapter 2, the RAFT aqueous emulsion polymerization of a range of monomers is explored using a water-soluble PMAA_x macro-CTA. Anionic macro-CTAs are well-known to provide good electrosteric stability, required for the synthesis of stable nanoparticles. More specifically, PMAA was an attractive stabilizer block for my PhD sponsor (AkzoNobel) owing to its high glass transition temperature, an attractive property for potential applications in paints and coatings. Initially, BzMA was chosen as a suitable *water-immiscible* monomer. Two series of PMAA_x-PBzMA_y diblock copolymers are synthesized using different RAFT agents (CPCP and PETTC). The same PMAA_x-PBzMA_y diblock copolymers are then prepared at varying copolymer and salt concentrations. Six core-forming monomers of varying water solubility are then used to synthesize a series of diblock copolymer nanoparticles by chain-extending a PMAA_x macro-CTA. These six monomers were; BzMA, 2,2,2-trifluoroethyl methacrylate (TFEMA), *n*-butyl methacrylate (BMA), methyl methacrylate (MMA), 2-hydroxybutyl methacrylate (HBMA) and 2-hydroxypropyl methacrylate (HPMA). These monomers exhibit a range of water solubilities, enabling the influence of this parameter to be studied. All block copolymers are analyzed by NMR, GPC, DLS and TEM. The PMAA_x-PMMA_y series is investigated in more detail by Small-angle X-ray scattering (SAXS) and differential scanning calorimetry (DSC) and evaluated as Pickering emulsifiers for the stabilization of oil-in-water emulsions.

Chapter 3 examines the effect of aqueous monomer solubility on the diblock copolymer morphology obtained during PISA by investigating the RAFT aqueous

emulsion polymerization of HBMA in more detail. A novel ‘monkey-nut’ morphology is observed and these anisotropic nanoparticles are characterized by DLS, TEM, scanning emission microscopy (SEM), shear-induced polarized light imaging (SIPLI) and SAXS.

Chapter 4 examines the optimization of the high-throughput synthesis of diblock copolymer nanoparticles in aqueous media *via* PISA. The synthesis of PMAA₅₆-PBzMA_y and PMAA₅₆-PBMA_y diblock copolymer nanoparticles *via* RAFT aqueous emulsion polymerization is optimized using a high-throughput protocol combined with an automated Chemspeed Autoplant A100 synthesizer. The reproducibility of such high-throughput PISA syntheses is evaluated. This approach is then extended to the synthesis of diblock, triblock and tetrablock copolymer nanoparticles at up to 45% w/w copolymer concentration.

In Chapter 5, a PMAA₅₆ macro-CTA is chain-extended with BzMA and hexyl methacrylate (HxMA) in turn *via* RAFT aqueous emulsion polymerization to synthesize a series of diblock, triblock and tetrablock copolymer nanoparticles that film-form at room temperature to give highly transparent films (> 95% for triblock copolymer films and > 89 % transmittance for tetrablock copolymer films at 600 nm). The resulting block copolymers are evaluated by NMR, DLS, TEM and GPC, and the corresponding films are analyzed by visible absorption spectroscopy, DSC and SAXS.

1.6. References

1. J. M. G. Cowie, *Polymers: Chemistry & Physics of Modern Materials*, Nelson Thornes, Cheltenham, 2nd edn., 2001.
2. K. Matyjaszewski, *Science*, 2011, **333**, 1104-1105.
3. R. G. Gilbert, M. Hess, A. D. Jenkins, R. G. Jones, P. Kratochvil, R. F. T. Stepto, M. Baron, T. Kitayama, G. Allegra, T. Chang, C. dos Santos, A. Fradet, K. Hatada, J. He, K. H. Hellwich, R. C. Hiorns, P. Hodge, K. Horie, J. I. Jin, J. Kahovec, P. Kubisa, I. Meisel, W. V. Metanowski, V. Meille, I. Mita, G. Moad, W. Mormann, C. Ober, S. Penczek, L. P. Rebelo, M. Rinaudo, I. Schopov, M. Schubert, F. Schue, V. P. Shibaev, S. Slomkowski, D. Tabak, J. P. Vairon, M. Vert, J. Vohlidal, W. E. S. and W. J. Work, *Pure and Applied Chemistry*, 2009, **81**, 351-353.
4. P. C. Hiemenz and T. P. Lodge, *Polymer Chemistry*, CRC Press, New York, 2nd edn., 2007.
5. G. Moad and D. H. Solomon, *The Chemistry of Radical Polymerization*, Elsevier, Oxford, 2nd edn., 2006.
6. G. Moad, E. Rizzardo and S. H. Thang, *Australian Journal of Chemistry*, 2005, **58**, 379-410.
7. W. A. Braunecker and K. Matyjaszewski, *Progress in Polymer Science*, 2007, **32**, 93-146.
8. G. Odian, *Principles of Polymerization*, Wiley, New Jersey, 4th edn. edn., 2004.
9. Y. Nakamura and S. Yamago, *Macromolecules*, 2015, **48**, 6450-6456.
10. D. W. J. Osmond, *Dispersion Polymerisation*, GB893429, 1962.
11. Rohm and Haas, *Polymer dispersions in organic liquid media and methods of preparation*, GB934038, 1963.
12. S. Shen, E. D. Sudol and M. S. El-Aasser, *Journal of Polymer Science Part A: Polymer Chemistry*, 1994, **32**, 1087-1100.
13. A. J. Paine, Y. Deslandes, P. Gerroir and B. Henrissat, *Journal of Colloid and Interface Science*, 1990, **138**, 170-181.
14. Y. Almog and M. Levy, *Journal of Polymer Science Part A: Polymer Chemistry*, 1981, **19**, 115-126.
15. F. L. Baines, S. Dionisio, N. C. Billingham and S. P. Armes, *Macromolecules*, 1996, **29**, 3096-3102.
16. A. P. Richez, H. N. Yow, S. Biggs and O. J. Cayre, *Progress in Polymer Science*, 2013, **38**, 897-931.
17. J. V. Dawkins and G. Taylor, *Polymer*, 1979, **20**, 599-604.
18. A. M. I. Ali, P. Pareek, L. Sewell, A. Schmid, S. Fujii, S. P. Armes and I. M. Shirley, *Soft Matter*, 2007, **3**, 1003-1013.
19. S. P. Armes and B. Vincent, *Journal of the Chemical Society, Chemical Communications*, 1987, 288-290.
20. C. DeArmitt and S. P. Armes, *Langmuir*, 1993, **9**, 652-654.
21. A. J. Paine, *Macromolecules*, 1990, **23**, 3109-3117.
22. A. J. Paine, W. Luymes and J. McNulty, *Macromolecules*, 1990, **23**, 3104-3109.
23. N. J. Warren and S. P. Armes, *Journal of the American Chemical Society*, 2014, **136**, 10174-10185.
24. C. S. Chern, *Progress in Polymer Science*, 2006, **31**, 443-486.

25. W. D. Harkins, *Journal of the American Chemical Society*, 1947, **69**, 1428-1444.
26. P. A. Lovell and M. S. El-Aasser, *Emulsion Polymerization and Emulsion Polymers*, John Wiley & Sons Ltd, 1997.
27. R. G. Gilbert, *Emulsion Polymerization: A Mechanistic Approach*, Academic Press, London, 1995.
28. P. J. Feeney, D. H. Napper and R. G. Gilbert, *Macromolecules*, 1987, **20**, 2922-2930.
29. E. Marc and Z. Rudolf, *Macromolecular Chemistry and Physics*, 2004, **205**, 1479-1488.
30. K. Tauer, R. Deckwer, I. Kühn and C. Schellenberg, *Colloid and Polymer Science*, 1999, **277**, 607-626.
31. J. W. Goodwin, J. Hearn, C. C. Ho and R. H. Ottewill, *Colloid and Polymer Science*, 1974, **252**, 464-471.
32. O. W. Webster, *Science*, 1991, **251**, 887-893.
33. M. Szwarc, M. Levy and R. Milkovich, *Journal of the American Chemical Society*, 1956, **78**, 2656-2657.
34. R. Waack, A. Rembaum, J. D. Coombes and M. Szwarc, *Journal of the American Chemical Society*, 1957, **79**, 2026-2027.
35. M. Szwarc, *Journal of Polymer Science Part A: Polymer Chemistry*, 1998, **36**, ix-xv.
36. J. Smid, *Journal of Polymer Science Part A: Polymer Chemistry*, 2002, **40**, 2101-2107.
37. D. Honnore, J. C. Favier, P. Sigwalt and M. Fontanille, *European Polymer Journal*, 1974, **10**, 425-431.
38. I. Natori and S. Inoue, *Macromolecules*, 1998, **31**, 982-987.
39. S. K. Varshney, J. P. Hautekeer, R. Fayt, R. Jerome and P. Teyssie, *Macromolecules*, 1990, **23**, 2618-2622.
40. N. Hadjichristidis, M. Pitsikalis, S. Pispas and H. Iatrou, *Chemical Reviews*, 2001, **101**, 3747-3792.
41. A. Hirao, S. Loykulant and T. Ishizone, *Progress in Polymer Science*, 2002, **27**, 1399-1471.
42. A. Hirao, R. Goseki and T. Ishizone, *Macromolecules*, 2014, **47**, 1883-1905.
43. A. Goto and T. Fukuda, *Progress in Polymer Science*, 2004, **29**, 329-385.
44. G. Moad, E. Rizzardo and S. H. Thang, *Accounts of Chemical Research*, 2008, **41**, 1133-1142.
45. P. B. Zetterlund, Y. Kagawa and M. Okubo, *Chemical Reviews*, 2008, **108**, 3747-3794.
46. J. Qui, B. Charleux and K. Matyjaszewski, *Progress in Polymer Science*, 2001, **26**, 2083-2134.
47. E. E. Malmström and C. J. Hawker, *Macromolecular Chemistry and Physics*, 1998, **199**, 923-935.
48. C. J. Hawker, *Angewandte Chemie International Edition in English*, 1995, **34**, 1456-1459.
49. R. T. A. Mayadunne, J. Jeffery, G. Moad and E. Rizzardo, *Macromolecules*, 2003, **36**, 1505-1513.
50. A. Bhattacharya and B. N. Misra, *Progress in Polymer Science*, 2004, **29**, 767-814.
51. L. Barner, T. P. Davis, M. H. Stenzel and C. Barner-Kowollik, *Macromolecular Rapid Communications*, 2007, **28**, 539-559.

52. H. Fischer, *Chemical Reviews*, 2001, **101**, 3581-3610.
53. J. Nicolas, Y. Guillaneuf, C. Lefay, D. Bertin, D. Gigmes and B. Charleux, *Progress in Polymer Science*, 2013, **38**, 63-235.
54. M. K. Georges, R. P. N. Veregin, P. M. Kazmaier and G. K. Hamer, *Macromolecules*, 1993, **26**, 2987-2988.
55. D. H. Solomon, E. Rizzardo and P. Cacioli, *Free radical polymerization and the produced polymers*, 1985.
56. C. J. Hawker, *Journal of the American Chemical Society*, 1994, **116**, 11185-11186.
57. C. J. Hawker, G. G. Barclay, A. Orellano, J. Dao and W. Devonport, *Macromolecules*, 1996, **29**, 5245-5254.
58. D. Benoit, V. Chaplinski, R. Braslau and C. J. Hawker, *Journal of the American Chemical Society*, 1999, **121**, 3904-3920.
59. J. Nicolas, C. Dire, L. Mueller, J. Belleney and B. Charleux, *Macromolecules*, 2006, **39**, 8274-8282.
60. J.-S. Wang and K. Matyjaszewski, *Journal of the American Chemical Society*, 1995, **117**, 5614-5615.
61. K. Matyjaszewski, T. E. Patten and J. Xia, *Journal of the American Chemical Society*, 1997, **119**, 674-680.
62. T. E. Patten and K. Matyjaszewski, *Advanced Materials*, 1998, **10**, 901-915.
63. V. Coessens, T. Pintauer and K. Matyjaszewski, *Progress in Polymer Science*, 2001, **26**, 337-377.
64. K. Matyjaszewski and J. Xia, *Chemical Reviews*, 2001, **101**, 2921.
65. J. Qui, B. Charleux and K. Matyjaszewski, *Progress in Polymer Science*, 2001, **26**, 2083-2134.
66. J. Chiefari, Y. K. B. Chong, F. Ercole, J. Krstina, J. Jeffery, T. P. T. Le, R. T. A. Mayadunne, G. F. Meijs, C. L. Moad, G. Moad, E. Rizzardo and S. H. Thang, *Macromolecules*, 1998, **31**, 5559-5562.
67. E. Rizzardo, J. Chiefari, Y. K. Chong, F. Ercole, J. Krstina, J. Jeffery, T. P. T. Le, R. T. A. Mayadunne, G. F. Meijs, C. L. Moad, G. Moad and S. H. Thang, *Macromolecular Symposia*, 1999, **143**, 291-307.
68. J. Chiefari, R. T. A. Mayadunne, C. L. Moad, G. Moad, E. Rizzardo, A. Postma, M. A. Skidmore and S. H. Thang, *Macromolecules*, 2003, **36**, 2273-2283.
69. D. J. Keddie, G. Moad, E. Rizzardo and S. H. Thang, *Macromolecules*, 2012, **45**, 5321-5342.
70. H. Willcock and R. K. O'Reilly, *Polymer Chemistry*, 2010, **1**, 149-157.
71. G. Moad, E. Rizzardo and S. H. Thang, *Australian Journal of Chemistry*, 2006, **59**, 669-692.
72. C. Barner-Kowollik, *Handbook of RAFT Polymerization*, John Wiley & Sons, Weinheim, 2008.
73. C. P. Jesson, C. M. Pearce, H. Simon, A. Werner, V. J. Cunningham, J. R. Lovett, M. J. Smallridge, N. J. Warren and S. P. Armes, *Macromolecules*, 2017, **50**, 182-191.
74. W. Shen, Q. Qiu, Y. Wang, M. Miao, B. Li, T. Zhang, A. Cao and Z. An, *Macromolecular Rapid Communications*, 2010, **31**, 1444-1448.
75. D. Matioszek, P.-E. Dufils, J. Vinas and M. Destarac, *Macromolecular Rapid Communications*, 2015, **36**, 1354-1361.
76. Y. K. Chong, G. Moad, E. Rizzardo and S. H. Thang, *Macromolecules*, 2007, **40**, 4446-4455.

77. G. Moad, E. Rizzardo and S. H. Thang, *Polymer International*, 2011, **60**, 9-25.
78. T. D. Michl, K. E. S. Locock, N. E. Stevens, J. D. Hayball, K. Vasilev, A. Postma, Y. Qu, A. Traven, M. Haeussler, L. Meagher and H. J. Griesser, *Polymer Chemistry*, 2014, **5**, 5813-5822.
79. M. Chen, G. Moad and E. Rizzardo, *Journal of Polymer Science Part A: Polymer Chemistry*, 2009, **47**, 6704-6714.
80. T. M. Legge, A. T. Slark and S. Perrier, *Journal of Polymer Science Part A: Polymer Chemistry*, 2006, **44**, 6980-6987.
81. A. Postma, T. P. Davis, G. Moad and M. S. O'Shea, *Macromolecules*, 2005, **38**, 5371-5374.
82. K. M. Mattson, C. W. Pester, W. R. Gutekunst, A. T. Hsueh, E. H. Discekici, Y. Luo, B. V. K. J. Schmidt, A. J. McGrath, P. G. Clark and C. J. Hawker, *Macromolecules*, 2016, **49**, 8162-8166.
83. E. R. Jones, M. Semsarilar, A. Blanazs and S. P. Armes, *Macromolecules*, 2012, **45**, 5091-5098.
84. M. Semsarilar, E. R. Jones, A. Blanazs and S. P. Armes, *Advanced Materials*, 2012, **24**, 3378-3382.
85. C. Gonzato, M. Semsarilar, E. R. Jones, F. Li, G. J. P. Krooshof, P. Wyman, O. O. Mykhaylyk, R. Tuinier and S. P. Armes, *Journal of the American Chemical Society*, 2014, **136**, 11100-11106.
86. W. Zhao, G. Gody, S. Dong, P. B. Zetterlund and S. Perrier, *Polymer Chemistry*, 2014, **5**, 6990-7003.
87. M. J. Derry, L. A. Fielding and S. P. Armes, *Progress in Polymer Science*, 2016, **52**, 1-18.
88. S. Sugihara, S. P. Armes, A. Blanazs and A. L. Lewis, *Soft Matter*, 2011, **7**, 10787-10793.
89. S. Sugihara, A. Blanazs, S. P. Armes, A. J. Ryan and A. L. Lewis, *Journal of the American Chemical Society*, 2011, **133**, 15707-15713.
90. N. J. Warren, O. O. Mykhaylyk, D. Mahmood, A. J. Ryan and S. P. Armes, *Journal of the American Chemical Society*, 2014, **136**, 1023-1033.
91. M. Semsarilar, V. Ladmair, A. Blanazs and S. P. Armes, *Langmuir*, 2012, **28**, 914-922.
92. B. Charleux, G. Delaittre, J. Rieger and F. D'Agosto, *Macromolecules*, 2012, **45**, 6753-6765.
93. I. Chaduc, M. Lansalot, F. D'Agosto and B. Charleux, *Macromolecules*, 2012, **45**, 1241-1247.
94. V. J. Cunningham, A. M. Alswieleh, K. L. Thompson, M. Williams, G. J. Leggett, S. P. Armes and O. M. Musa, *Macromolecules*, 2014, **47**, 5613-5623.
95. J. Tan, H. Sun, M. Yu, B. S. Sumerlin and L. Zhang, *ACS Macro Letters*, 2015, **4**, 1249-1253.
96. L. P. D. Ratcliffe, A. J. Ryan and S. P. Armes, *Macromolecules*, 2013, **46**, 769-777.
97. A. A. Cockram, T. J. Neal, M. J. Derry, O. O. Mykhaylyk, N. S. J. Williams, M. W. Murray, S. N. Emmett and S. P. Armes, *Macromolecules*, 2017, **50**, 796-802.
98. G. M. Whitesides and B. Grzybowski, *Science*, 2002, **295**, 2418-2421.
99. C. B. Aakeroy and K. R. Seddon, *Chemical Society Reviews*, 1993, **22**, 397-407.
100. E. Arunan, G. R. Desiraju, R. A. Klein, J. Sadlej, S. Scheiner, I. Alkorta, D. C. Clary, R. H. Crabtree, J. J. Dannenberg, P. Hobza, H. G. Kjaergaard, A. C.

- Legon, B. Mennucci and D. J. Nesbitt, *Pure and Applied Chemistry*, 2011, **83**, 1637-1641.
101. T. H. Rehm and C. Schmuck, *Chemical Society Reviews*, 2010, **39**, 3597-3611.
102. R. Ludwig, *Angewandte Chemie International Edition*, 2001, **40**, 1808-1827.
103. J. Israelachvili, *Intermolecular & Surface Forces*, Academic Pres, 2nd edn., 1991.
104. D. Chandler, *Nature*, 2005, **437**, 640-647.
105. C. Tanford, *Science*, 1978, **200**, 1012-1018.
106. S. Puvvada and D. Blankschtein, *The Journal of Chemical Physics*, 1990, **92**, 3710-3724.
107. Z. Chu, C. A. Dreiss and Y. Feng, *Chemical Society Reviews*, 2013, **42**, 7174-7203.
108. F. S. Bates and G. H. Fredrickson, *Physics Today*, 1999, **52**, 32-38.
109. L. Leibler, *Macromolecules*, 1980, **13**, 1602-1617.
110. S. Lecommandoux, M. Lazzari and G. Liu, *Block Copolymers in Nanoscience*, Wiley-VCH, Weinheim, 2008.
111. Y. Mai and A. Eisenberg, *Chemical Society Reviews*, 2012, **41**, 5969-5985.
112. J. M. G. Swann and P. D. Topham, *Polymers*, 2010, **2**, 454-469.
113. F. S. Bates, *Science*, 1991, **251**, 898-905.
114. A. Blanazs, S. P. Armes and A. J. Ryan, *Macromolecular Rapid Communications*, 2009, **30**, 267-277.
115. Z. An, Q. Shi, W. Tang, C.-K. Tsung, C. J. Hawker and G. D. Stucky, *Journal of the American Chemical Society*, 2007, **129**, 14493-14499.
116. J. Rieger, C. Gazon, B. Charleux, D. Alaimo and C. Jérôme, *Journal of Polymer Science Part A: Polymer Chemistry*, 2009, **47**, 2373-2390.
117. M. J. Derry, L. A. Fielding and S. P. Armes, *Progress in Polymer Science*, 2016, **52**, 1-18.
118. J. Rieger, W. Zhang, F. Stoffelbach and B. Charleux, *Macromolecules*, 2010, **43**, 6302-6310.
119. S. Binauld, L. Delafresnaye, B. Charleux, F. D'Agosto and M. Lansalot, *Macromolecules*, 2014, **47**, 3461-3472.
120. C. J. Ferguson, R. J. Hughes, B. T. T. Pham, B. S. Hawkett, R. G. Gilbert, A. K. Serelis and C. H. Such, *Macromolecules*, 2002, **35**, 9243-9245.
121. A. Blanazs, A. J. Ryan and S. P. Armes, *Macromolecules*, 2012, **45**, 5099-5107.
122. S. L. Canning, G. N. Smith and S. P. Armes, *Macromolecules*, 2016, **49**, 1985-2001.
123. M. J. Derry, L. A. Fielding and S. P. Armes, *Polymer Chemistry*, 2015, **6**, 3054-3062.
124. L. A. Fielding, M. J. Derry, V. Ladmiral, J. Rosselgong, A. M. Rodrigues, L. P. D. Ratcliffe, S. Sugihara and S. P. Armes, *Chemical Science*, 2013, **4**, 2081-2087.
125. L. A. Fielding, J. A. Lane, M. J. Derry, O. O. Mykhaylyk and S. P. Armes, *Journal of the American Chemical Society*, 2014, **136**, 5790-5798.
126. Y. Pei, O. R. Sugita, L. Thurairajah and A. B. Lowe, *RSC Advances*, 2015, **5**, 17636-17646.
127. Y. Pei, L. Thurairajah, O. R. Sugita and A. B. Lowe, *Macromolecules*, 2015, **48**, 236-244.
128. M. Semsarilar, V. Ladmiral, A. Blanazs and S. P. Armes, *Langmuir*, 2013, **29**, 7416-7424.

129. J. Rieger, F. Stoffelbach, C. Bui, D. Alaimo, C. Jérôme and B. Charleux, *Macromolecules*, 2008, **41**, 4065-4068.
130. Y. Li and S. P. Armes, *Angewandte Chemie International Edition*, 2010, **49**, 4042-4046.
131. A. Blanazs, J. Madsen, G. Battaglia, A. J. Ryan and S. P. Armes, *Journal of the American Chemical Society*, 2011, **133**, 16581-16587.
132. A. Blanazs, R. Verber, O. O. Mykhaylyk, A. J. Ryan, J. Z. Heath, C. W. I. Douglas and S. P. Armes, *Journal of the American Chemical Society*, 2012, **134**, 9741-9748.
133. P. Chambon, A. Blanazs, G. Battaglia and S. P. Armes, *Macromolecules*, 2012, **45**, 5081-5090.
134. R. Verber, A. Blanazs and S. P. Armes, *Soft Matter*, 2012, **8**, 9915-9922.
135. K. L. Thompson, C. J. Mable, A. Cockram, N. J. Warren, V. J. Cunningham, E. R. Jones, R. Verber and S. P. Armes, *Soft Matter*, 2014, **10**, 8615-8626.
136. D. Mitchell, J. R. Lovett, S. P. Armes and M. I. Gibson, *Angewandte Chemie International Edition*, 2016, **55**, 2801-2804.
137. I. Canton, N. J. Warren, A. Chahal, K. Amps, A. Wood, R. Weightman, E. Wang, H. Moore and S. P. Armes, *ACS Central Science*, 2016, **2**, 65-74.
138. C. J. Mable, R. R. Gibson, S. Prevost, B. E. McKenzie, O. O. Mykhaylyk and S. P. Armes, *Journal of the American Chemical Society*, 2015, **137**, 16098-16108.
139. C. J. Mable, N. J. Warren, K. L. Thompson, O. O. Mykhaylyk and S. P. Armes, *Chemical Science*, 2015, **6**, 6179-6188.
140. J. Zhou, H. Yao and J. Ma, *Polymer Chemistry*, 2018, **9**, 2532-2561.
141. I. Uzulina, S. Kanagasabapathy and J. Claverie, *Macromolecular Symposia*, 2000, **150**, 33-38.
142. M. J. Monteiro, M. Hodgson and H. D. Brouwer, *Journal of Polymer Science Part A: Polymer Chemistry*, 2000, **38**, 3864-3873.
143. S. W. Prescott, M. J. Ballard, E. Rizzardo and R. G. Gilbert, *Australian Journal of Chemistry*, 2002, **55**, 415.
144. M. J. Monteiro and J. d. Barbeyrac, *Macromolecules*, 2001, **34**, 4416-4423.
145. M. J. Monteiro, M. Sjoberg, J. V. D. Vlist and C. M. Gottgens, *Journal of Polymer Science Part A: Polymer Chemistry*, 2000, **38**, 4206.
146. D. Charmot, P. Corpart, H. Adam, S. Z. Zard, T. Biadatti and G. Bouhadir, *Macromolecular Symposia*, 2000, **150**, 23-32.
147. S. W. Prescott, M. J. Ballard, E. Rizzardo and R. G. Gilbert, *Macromolecules*, 2002, **35**, 5417-5447.
148. W. Smulders, R. G. Gilbert and M. J. Monteiro, *Macromolecules*, 2003, **36**, 4309-4318.
149. A. R. Szkurhan and M. K. Georges, *Macromolecules*, 2004, **37**, 4776-4782.
150. A. R. Szkurhan, T. Kasahara and M. K. Georges, *Journal of Polymer Science Part A: Polymer Chemistry*, 2006, **44**, 5708-5718.
151. E. Sprong, J. S. K. Leswin, D. J. Lamb, C. J. Ferguson, B. Hawket, B. T. T. Pham, D. Nguyen, C. H. Such and R. G. Gilbert, *Macromolecular Symposia*, 2006, **231**, 84-93.
152. C. J. Ferguson, R. J. Hughes, D. Nguyen, B. T. T. Pham, R. G. Gilbert, A. K. Serelis, C. H. Such and B. S. Hawket, *Macromolecules*, 2005, **38**, 2191-2204.
153. J. Ji, L. Yan and D. Xie, *Journal of Polymer Science Part A: Polymer Chemistry*, 2008, **46**, 3098-3107.
154. Y. Luo, X. Wang, B.-G. Li and S. Zhu, *Macromolecules*, 2011, **44**, 221-229.

155. X. Wang, Y. Luo, B. Li and S. Zhu, *Macromolecules*, 2009, **42**, 6414-6421.
156. S. Fréal-Saison, M. Save, C. Bui, B. Charleux and S. Magnet, *Macromolecules*, 2006, **39**, 8632-8638.
157. N. Yeole, D. Hundiwale and T. Jana, *Journal of Colloid and Interface Science*, 2011, **354**, 506-510.
158. J. Božović-Vukić, H. T. Mañon, J. Meuldijk, C. Koning and B. Klumperman, *Macromolecules*, 2007, **40**, 7132-7139.
159. M. Manguian, M. Save and B. Charleux, *Macromolecular Rapid Communications*, 2006, **27**, 399-404.
160. J. Jing, Y. Lifeng and X. Dinghai, *Journal of Polymer Science Part A: Polymer Chemistry*, 2008, **46**, 3098-3107.
161. S. Boissé, J. Rieger, K. Belal, A. Di-Cicco, P. Beaunier, M.-H. Li and B. Charleux, *Chemical Communications*, 2010, **46**, 1950-1952.
162. S. Boissé, J. Rieger, G. Pembouong, P. Beaunier and B. Charleux, *Journal of Polymer Science Part A: Polymer Chemistry*, 2011, **49**, 3346-3354.
163. J. Rieger, G. Osterwinter, C. Bui, F. o. Stoffelbach and B. Charleux, *Macromolecules*, 2009, **42**, 5518-5525.
164. I. Chaduc, W. Zhang, J. Rieger, M. Lansalot, F. D'Agosto and B. Charleux, *Macromolecular Rapid Communications*, 2011, **32**, 1270-1276.
165. I. Chaduc, A. Crepet, O. Boyron, B. Charleux, F. D'Agosto and M. Lansalot, *Macromolecules*, 2013, **46**, 6013.
166. J. Zhou, R. He and J. Ma, *Polymers*, 2016, **8**, 207-220.
167. E. Velasquez, J. Rieger, F. Stoffelbach, F. D'Agosto, M. Lansalot, P.-E. Dufils and J. Vinas, *Polymer*, 2016, **106**, 275-284.
168. I. Chaduc, M. Girod, R. Antoine, B. Charleux, F. D'Agosto and M. Lansalot, *Macromolecules*, 2012, **45**, 5881-5893.
169. E. Velasquez, J. Rieger, F. Stoffelbach, B. Charleux, F. D'Agosto, M. Lansalot, P.-E. Dufils and J. Vinas, *Polymer*, 2013, **54**, 6547-6554.
170. W. Zhang, F. D'Agosto, O. Boyron, J. Rieger and B. Charleux, *Macromolecules*, 2011, **44**, 7584-7593.
171. N. P. Truong, M. V. Dussert, M. R. Whittaker, J. F. Quinn and T. P. Davis, *Polymer Chemistry*, 2015, **6**, 3865-3874.
172. B. Akpınar, L. A. Fielding, V. J. Cunningham, Y. Ning, O. O. Mykhaylyk, P. W. Fowler and S. P. Armes, *Macromolecules*, 2016, **49**, 5160-5171.
173. F. L. Hatton, J. R. Lovett and S. P. Armes, *Polymer Chemistry*, 2017, **8**, 4856-4868.
174. C. P. Jesson, V. J. Cunningham, M. J. Smallridge and S. P. Armes, *Macromolecules*, 2018, **51**, 3221-3232.
175. S. L. Canning, V. J. Cunningham, L. P. D. Ratcliffe and S. P. Armes, *Polymer Chemistry*, 2017, **8**, 4811-4821.
176. W. Zhang, F. D'Agosto, O. Boyron, J. Rieger and B. Charleux, *Macromolecules*, 2012, **45**, 4075-4084.
177. X. Zhang, S. Boissé, W. Zhang, P. Beaunier, F. D'Agosto, J. Rieger and B. Charleux, *Macromolecules*, 2011, **44**, 4149-4158.
178. W. Zhang, F. D'Agosto, P.-Y. Dugas, J. Rieger and B. Charleux, *Polymer*, 2013, **54**, 2011-2019.
179. W. Zhang, F. D'Agosto, O. Boyron, J. Rieger and B. Charleux, *Macromolecules*, 2012, **45**, 4075-4084.
180. J. Lesage de la Haye, X. Zhang, I. Chaduc, F. Brunel, M. Lansalot and F. D'Agosto, *Angewandte Chemie International Edition*, 2016, **55**, 3739-3743.

181. N. P. Truong, J. F. Quinn, A. Anastasaki, D. M. Haddleton, M. R. Whittaker and T. P. Davis, *Chemical Communications*, 2016, **52**, 4497-4500.
182. S. Y. Khor, N. P. Truong, J. F. Quinn, M. R. Whittaker and T. P. Davis, *ACS Macro Letters*, 2017, **6**, 1013-1019.
183. Z. Qiao, T. Qiu, W. Liu, L. Zhang, J. Tu, L. Guo and X. Li, *Polymer Chemistry*, 2017, **8**, 3013-3021.
184. B. T. T. Pham, D. Nguyen, V. T. Huynh, E. H. Pan, B. Shirodkar-Robinson, M. Carey, A. K. Serelis, G. G. Warr, T. Davey, C. H. Such and B. S. Hawkett, *Langmuir*, 2018, **34**, 4255-4263.

Chapter Two

2. Synthesis of Diblock Copolymer Nanoparticles *via* RAFT-Mediated PISA in Water

2.1. Introduction

There has been considerable research into RAFT polymerization conducted in a wide range of solvents, including alcohols,¹⁻⁴ *n*-alkanes,⁵⁻¹⁰ and water.¹¹⁻¹⁹ This Thesis focuses on using water as a solvent because it is cheap, non-toxic, environmentally-friendly, non-flammable and has a high heat capacity. Polymerization of a monomer in water, whose corresponding polymer is insoluble, from a water-soluble homopolymer leads to *in situ* self-assembly and the formation of nanoparticles *via* PISA.²⁰ This PISA can occur by two methods dependent on the aqueous solubility of the core-forming monomer. Either by RAFT aqueous dispersion polymerization,^{12, 13, 18, 21-23} when the monomer is *water-miscible* or by RAFT aqueous emulsion polymerization,^{17, 20, 21, 24-28} when the monomer is *water-immiscible*.

The synthesis of nanoparticles *via* RAFT aqueous dispersion polymerization is well-studied.^{12, 13, 18, 21-23} The resulting nanoparticles have a wide range of potential applications. In particular utilizing water as a solvent has increased the possibility for bio-applications.²⁹⁻³² A wide range of nanoparticle morphologies can be targeted (including spheres, worms and vesicles) by adjusting the hydrophilic (stabilizer) block DP, the hydrophobic (core-forming) block DP and the copolymer concentration.³⁰ During PISA, the core-forming chains are solvated by unreacted monomer which facilitates the evolution in copolymer morphology from spheres to worms to vesicles. These nanoparticles can also be stimulus-responsive, a desirable quality for many applications.^{6, 31, 33-36} However, RAFT aqueous dispersion polymerization is restricted to a limited number of monomers.²¹

In contrast, there are many more *water-immiscible* monomers which can be polymerized *via* RAFT aqueous emulsion polymerization. Although much research has been conducted in this area over recent years, there are fewer reports of higher order morphology nanoparticles (worms and vesicles), with most systems being limited to the synthesis of kinetically-trapped spherical nanoparticles.^{17, 23, 26, 28, 37-42} Of particular relevance to this body of work is the synthesis of PGMA₅₁-PBzMA_y diblock copolymers *via* RAFT aqueous emulsion polymerization of BzMA. A range of PBzMA DPs ($y = 50$ to 1000) and copolymer concentrations (10 to 50% w/w) were targeted but only spherical nanoparticles were obtained.¹⁷ During this polymerization the *water-immiscible* BzMA monomer may diffuse through the aqueous phase too slowly to provide sufficient plasticization/swelling of the core-forming block on the

timescale of the polymerization. If this is correct, then there may be insufficient solvation to enable the evolution of nanoparticle morphology from spheres to worms to vesicles.¹⁷ Despite this limitation, there are reports of higher order morphologies synthesized *via* RAFT aqueous emulsion polymerization. In many cases, these syntheses involve the use of a statistical copolymer macro-CTA.^{27, 43-47} The reasons for this are not well understood. Thus, recent empirical experiments have aimed to gain further insights.⁴⁷⁻⁴⁹ However, the critical synthesis parameters that determine whether only kinetically-trapped spheres are obtained or the full range of morphologies are observed have not yet been established.

This Chapter focuses on the chain extension of a water-soluble PMAA_x macro-CTA with a range of core-forming monomers *via* RAFT aqueous polymerization. Firstly, the RAFT aqueous emulsion polymerization of BzMA was studied in detail. Then the effect of increasing the core-forming monomer *aqueous solubility* was assessed with the aim of synthesizing higher order morphologies *via* aqueous PISA.

2.2. Experimental

2.2.1. Materials

Methacrylic acid (MAA), benzyl methacrylate (BzMA), 2-hydroxypropyl methacrylate (HPMA), methyl methacrylate (MMA), *n*-butyl methacrylate (BMA), 2,2,2-trifluoroethyl methacrylate (TFEMA), 2-hydroxybutyl methacrylate (HBMA; actually a 1:1 molar ratio of 2- and 4-isomers as judged by ¹H NMR spectroscopy),⁵⁰ 4,4'-azobis(4-cyanovaleric acid) (ACVA) and 4-cyano-4-(phenylcarbonothioylthio)pentanoic acid (CPCP) were purchased from Sigma-Aldrich UK and used as received unless otherwise specified. Deionized water was used in all experiments. 4-cyano-4-(2-phenylethanesulfanylthiocarbonyl)sulfanyl-pentanoic acid (PETTC) RAFT CTA was prepared in house, as described previously.⁵¹ The trimethylsilyldiazomethane solution (2.0 M in diethyl ether), THF (HPLC, ≥ 99.9%) and glacial acetic acid (≥ 99.85%) used for the preparation and analysis of the methylated diblock copolymers were also purchased from Sigma-Aldrich UK. *d*₄-Methanol, *d*₆-dimethyl sulfoxide and *d*₇-dimethylformamide (*d*₇-DMF) were purchased from Goss Scientific Instruments Ltd. (Cheshire, UK). All other solvents were purchased from Sigma-Aldrich UK.

2.2.2. Preparation of poly(methacrylic acid) (PMAA_x) macro-CTA agent

PETTC RAFT agent (3.169 g, 9.3 mmol), MAA (45.00 g, 0.5227 mol, target DP = 50), ACVA (0.523 g, 1.0 mmol; CTA/initiator molar ratio = 5.0), and ethanol (73.04 g, 40% w/w) were weighed into a 500 mL round-bottom flask and degassed with N₂ for 30 min in an ice bath. The reaction solution was then heated for 3 h at 70 °C in a pre-heated oil bath. The resulting macro-CTA was then purified by precipitation into diethyl ether (1.5 L). The insoluble polymer was isolated by filtration and redissolved in the minimum amount of ethanol, before a second precipitation step. The polymer was then collected and redissolved in the minimum amount of water for isolation by lyophilization. The mean degree of polymerization was calculated to be 56 for this PMAA₅₆ macro-CTA by ¹H NMR in *d*₄-methanol. This synthesis was also performed using 4-cyano-4-(phenylcarbonothioylthio)pentanoic acid (CPCP) as the RAFT agent. Throughout this Thesis PMAA₅₆-TTC macro-CTA refers to the macro-CTA made using PETTC and PMAA₅₄-DB macro-CTA refers to the macro-CTA made using CPCP.

2.2.3. Synthesis of PMAA_x-PBzMA_y diblock copolymer nanoparticles via RAFT aqueous emulsion polymerization

A typical protocol for the synthesis of PMAA₅₆-PBzMA₅₀₀-TTC nanoparticles was as follows: PMAA₅₆-TTC macro-CTA (0.0293 g, 0.0057 mmol), ACVA (0.30 mg; 0.0011 mmol, macro-CTA/initiator molar ratio = 5.0) and water (4.77 g, 10% w/w) were weighed into a 15 mL vial. The solution pH was adjusted to pH 5 using 1 M NaOH and BzMA monomer (0.50 g, 2.84 mol) was then added. A magnetic flea was added and the reaction vial was sealed using a rubber septum. The reaction solution was purged under N₂ for 15 min and the vial was then placed in a pre-heated water bath at 70 °C for 2 h, prior to its removal and exposure to air to quench the polymerization.

2.2.4. Synthesis of PMAA_x-PBzMA_y diblock copolymer nanoparticles via RAFT aqueous emulsion polymerization in the presence of CaCl₂ salt.

A typical protocol for the synthesis of PMAA₅₄-PBzMA₅₀₀-DB nanoparticles in the presence of 0.04 M CaCl₂ was as follows: PMAA₅₄-DB macro-CTA (0.0472 g, 0.01 mmol), ACVA (0.60 mg; 0.002 mmol, macro-CTA/initiator molar ratio = 5.0), CaCl₂ salt (0.0419 g; 0.40 mmol) and water (9.43 g, 10% w/w) were weighed into a 15 mL vial. The solution pH was adjusted to pH 5 using 1 M NaOH and BzMA

monomer (1.00 g, 5.7 mmol) was then added. A magnetic flea was added and the reaction vial was sealed using a rubber septum. The reaction solution was purged under N₂ for 15 min and the vial was then placed in a pre-heated water bath at 70 °C for 2 h, prior to its removal and exposure to air to quench the polymerization.

2.2.5. Chain extension of PMAA_x macro-CTA with monomers of varying aqueous solubility

A PMAA₅₆-TTC macro-CTA was chain-extended with various monomers (TFEMA, BMA, MMA, HBMA or HPMA) to form diblock copolymer nanoparticles in water *via* PISA. These diblock copolymer nanoparticles were synthesized by the same method used for the synthesis of PMAA_x-PBzMA_y nanoparticles, as described above. In all syntheses the same conditions were used: 20% w/w copolymer concentration, pH 5, macro-CTA/ACVA molar ratio = 5 and 70 °C

2.2.6. Synthesis of PMAA_x-PBzMA_y diblock copolymer nanoparticles via RAFT alcoholic dispersion polymerization

A typical protocol for the synthesis of PMAA₅₆-PBzMA₆₀-TTC nanoparticles was as follows: PMAA₅₆-TTC macro-CTA (0.5857 g, 0.1135 mmol), ACVA (6.36 mg; 0.0227 mmol, macro-CTA/initiator molar ratio = 5.0), BzMA monomer (1.00 g, 5.68 mmol) and ethanol (6.37 g, 20% w/w) were weighed into a 15 mL vial. A magnetic flea was added and the reaction vial was sealed using a rubber septum. The reaction solution was purged under N₂ for 15 min and the vial was then placed in a pre-heated water bath at 70 °C for 24 h, prior to its removal and exposure to air to quench the polymerization.

2.2.7. Preparation of Pickering Emulsions

2.0 mL of oil (methyl myristate or squalene) was homogenized with 2.0 mL of an aqueous dispersion of PMAA₅₆-PMMA₂₀₀ diblock copolymer nanoparticles (0.05 to 2.0% w/w) for 2 min using a IKA Ultra-Turraz T-18 homogenizer with a 10 mm dispersing tool operating at 12,000 rpm. Mean droplet diameter was determined by laser diffraction. The emulsions were imaged by optical microscopy.

2.3. Copolymer Characterization

2.3.1. ¹H NMR Spectroscopy

All ¹H NMR spectra were recorded using a 400 MHz Bruker Advance-400 spectrometer using either *d*₄-methanol, *d*₆-dimethyl sulfoxide or *d*₇-DMF as the solvent.

2.3.2. Methylation of copolymers for GPC analysis

Prior to GPC analysis, all copolymers were modified by methylation of the carboxylic acid groups in the PMAA block. Excess trimethylsilyldiazomethane was added dropwise to a solution of copolymer (20 mg) in THF (2.0 mL), until the yellow color persisted. This reaction solution was then stirred overnight until all THF had evaporated prior to analysis by ¹H NMR and THF GPC.

2.3.3. Gel Permeation Chromatography (GPC)

THF GPC at 30 °C was used to determine the molecular weights and dispersities of the modified copolymers. The GPC set-up consisted of two 5 μM Mixed C columns connected to a WellChrom K-2301 refractive index and UV detector (set to 298 nm). The mobile phase was HPLC-grade THF containing 0.05% w/v butylhydroxytoluene (BHT) and 2.0% v/v trimethylamine (TEA) at a flow rate of 1.0 mL min⁻¹. Molecular weights were calculated with respect to a series of near-monodisperse PMMA standards.

2.3.4. Dynamic Light Scattering (DLS)

Aqueous copolymer dispersions (0.20% w/w) in disposable plastic cuvettes were analyzed using a Malvern Zetasizer NanoZS instrument. Scattered light was detected at 173° and intensity-average hydrodynamic diameters were calculated using the Stokes-Einstein equation. Data were averaged over three consecutive measurements, comprising a minimum of ten runs per measurement.

2.3.5. Aqueous Electrophoresis

Measurements were performed using a Malvern Zetasizer NanoZs instrument on dilute (0.20% w/w) copolymer dispersions containing background salt (1 mM KCl). The solution pH was adjusted by addition of either NaOH or HCl.

2.3.6. Transmission Electron Microscopy (TEM)

One droplet (10 μL) of a dilute copolymer dispersion (0.20% w/w) was deposited onto a carbon-coated copper grid. The grid was then stained with 10 μL uranyl formate

for 10 seconds and dried using a vacuum hose. TEM images were then obtained using a Philips CM100 instrument operating at 100 kV and equipped with a Gatan 1 k CCD camera.

2.3.7. Differential Scanning Calorimetry (DSC)

The polymer dispersions were dried overnight on a glass slide. An accurate mass (between 6 and 10 mg) was weighted into an aluminium pan and sealed with a lid. The polymer sample was heated under N₂ in a TA instruments Q2000 model calorimeter. Thermograms were acquired at a rate of 10 °C per min from – 80 °C to 285 °C, 3 cycles were performed. These analyses were conducted by members of the analytical department at AkzoNobel (Slough).

2.3.8. Acid titration to determine the effective pK_a values of the MAA monomer units

Acid titrations were conducted on the dilute PMAA_x macro-CTA solutions and the PMAA_x-PBzMA₂₀₀ diblock copolymer dispersions (1.0% w/w). Each solution was titrated from pH 11 to pH 2 using a 0.1 M HCl solution with continuous stirring. The pH was measured using a Thermo Scientific Orion Star A211 pH meter. The effective pK_a values for the PMAA block in each of the polymers were calculated based on the pH at 50% ionization.

2.3.9. Determination of aqueous monomer solubility by visual inspection

The aqueous solubility of the various monomers (HPMA, HBMA, MMA, BMA, TFEMA and BzMA) was determined at both 20 °C and 70 °C. The monomer (0.019 - 13 g) was added dropwise to a known quantity of water (100 g) at either 20 or 70 °C with vigorous stirring (an oil bath was used for heating to 70 °C). The aqueous solubility was determined by visual inspection as the point at which the monomer no longer dissolved fully but could be observed as a haze or as emulsion droplets. From this protocol, the aqueous solubility can be determined (g dm⁻³) at any given temperature.

2.3.10. Laser diffraction

Mean droplet diameter (D_[4,3]) of the emulsions was determined using a Malvern Mastersizer 3000 instrument equipped with a Hydro EV flexible wet dispersion unit, a He-Ne laser operating at 633 nm, and a solid-state blue laser operating at 466 nm. The stirring rate was adjusted to 1,750 rpm in order to avoid creaming of the emulsion

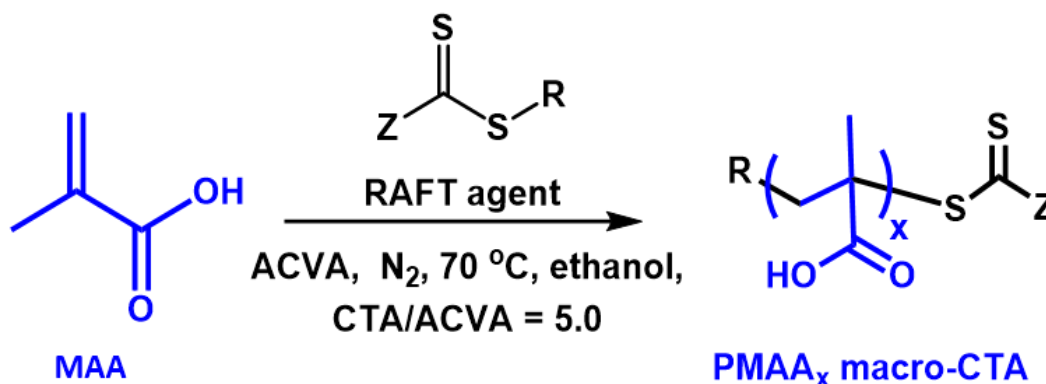
during analysis. After each measurement, the cell was rinsed twice with ethanol, followed by once with distilled water; the glass walls of the cell were carefully wiped with lens cleaning tissue to avoid cross-contamination and the laser was aligned centrally to the detector prior to data acquisition. The volume-average diameter was measured and repeated five times for each emulsion.

2.3.11. Optical microscopy

Emulsions were imaged by optical microscopy using a Motic DMBA300 digital biological microscope with a built-in camera and equipped with Motic Images Plus 2.0 ML software.

2.4. Results and Discussion

2.4.1. Synthesis of PMAA_x macro-CTA via RAFT solution polymerization



Scheme 2.1 Synthesis of PMAA_x macro-CTA via RAFT solution polymerization in ethanol at 40% w/w polymer concentration. The RAFT agent structure shown is the generic structure where R is an alkyl group and the Z group varies depending on the class of chain transfer agent (trithiocarbonate vs. dithiobenzoate).

Methacrylic acid (MAA) monomer was polymerized *via* RAFT solution polymerization in ethanol with two different RAFT CTAs to yield the corresponding RAFT macro-CTAs (Scheme 2.1). The RAFT CTA must be carefully selected for each polymerization to ensure good control.⁵² The Z group activates the C=S double bond for radical addition, ensuring a high transfer constant.^{53, 54} Based on the Z group, these RAFT CTAs can be categorized into four classes: dithioesters (Z= alkyl or aryl), trithiocarbonates (Z = SR), dithiocarbamates (Z= NR₂) and xanthates (Z= O-alkyl). In this Thesis, both a dithobenzoate RAFT agent and a trithiocarbonate RAFT agent were used, see Figure 2.1. Although both types of RAFT agents have high transfer

constants, dithiobenzoates are more prone to hydrolysis which is not ideal for RAFT polymerizations conducted in aqueous media.^{52, 54} The dithiobenzoate and trithiocarbonate RAFT agents chosen were 4-cyano-4-(phenylcarbonothioylthio)pentanoic acid (CPCP) and 4-cyano-4(2-phenylethanesulfanylthiocarbonyl)sulfanylpentanoic acid (PETTC). The use of PETTC for the synthesis of PMAA_x-PBzMA_y diblock copolymers *via* RAFT alcoholic dispersion polymerization has been previously reported by Semsarilar *et al.*⁵¹ Another advantage is the ability to synthesize PETTC in-house making it considerably cheaper than purchasing CPCP.⁵¹

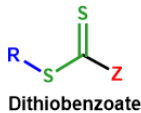
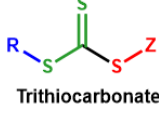
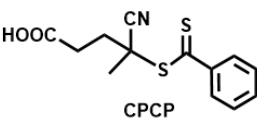
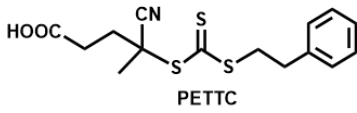
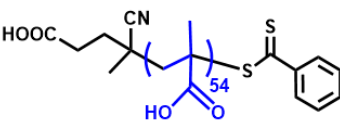
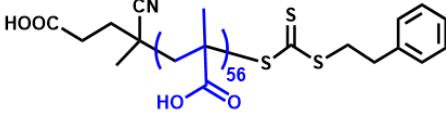
Type of RAFT agent	 <p>Dithiobenzoate</p>	 <p>Trithiocarbonate</p>
Chosen RAFT agent	 <p>CPCP</p>	 <p>PETTC</p>
PMAA _x macro-CTA	 <p>PMAA₅₄-DB macro-CTA</p>	 <p>PMAA₅₆-TTC macro-CTA</p>

Figure 2.1 Two poly(methacrylic acid) macromolecular chain transfer agents (macro-CTAs) were prepared *via* RAFT solution polymerization in ethanol using two different classes of RAFT CTAs. The chosen dithiobenzoate CTA was (4-cyano-4-(phenylcarbonothioylthio)pentanoic acid) (CPCP) and the selected trithiocarbonate CTA was (4-cyano-4(2-phenylethanesulfanylthiocarbonyl)sulfanylpentanoic acid) (PETTC).

The PMAA₅₄-DB and the PMAA₅₆-TTC macro-CTAs were synthesized by the same general method, see Scheme 2.1. In both cases, a PMAA DP of 50 was targeted. Polymerizations were allowed to proceed for 3 h at 70 °C resulting in MAA conversions of 89% and 82% for the CPCP and the PETTC CTAs respectively. Typically, macro-CTA syntheses are terminated prior to achieving full monomer conversion to ensure high RAFT chain-end fidelity.⁵⁵ This means that, on chain extension of the macro-CTA with a second monomer, high blocking efficiencies can be achieved. The crude macro-CTAs were purified by repeated precipitation into

excess diethyl ether to remove any residual monomer and unreacted CTA. Purified polymer was then dissolved in water and freeze-dried to render a PMAA_x macro-CTA powder. The thiocarbonylthio moiety of the CTA causes the resulting macro-CTAs to be strongly coloured.⁵⁶ The PMAA₅₄-DB macro-CTA is pink⁵⁷ whereas the PMAA₅₆-TTC macro-CTA is yellow.⁵⁸ Mean PMAA DPs were determined by ¹H NMR spectroscopy, in *d*₄-methanol, to be 54 and 56 when using the CPCP and the PETTC CTA, respectively, see Figure 2.2.

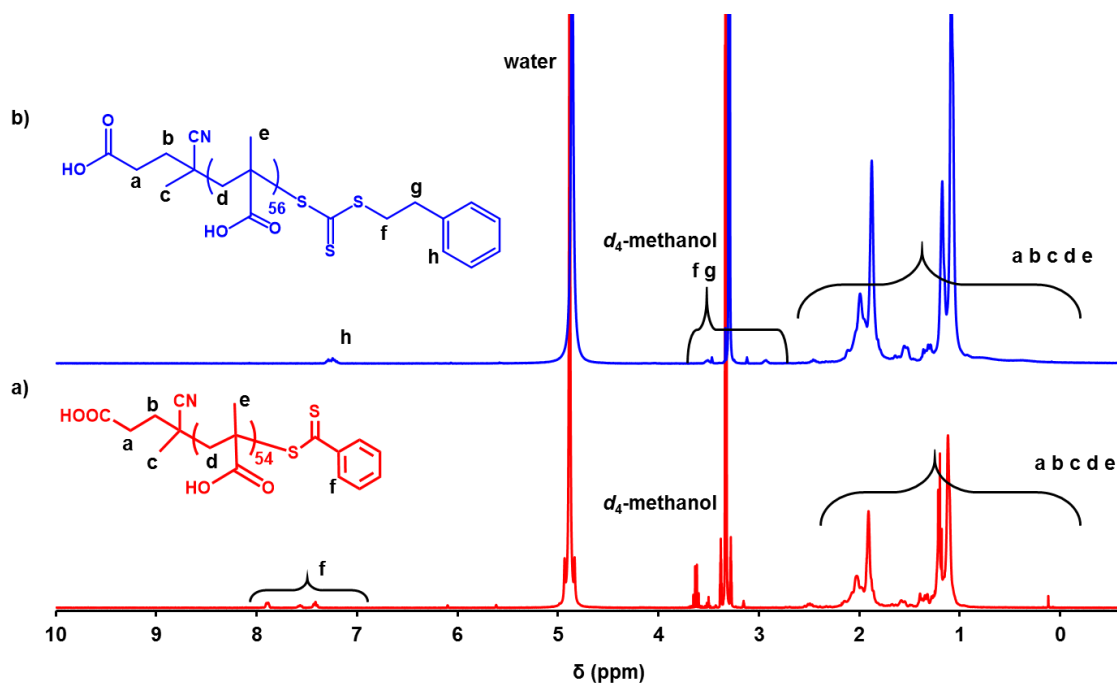


Figure 2.2 ¹H NMR spectra of (a) PMAA₅₄-DB macro-CTA and (b) PMAA₅₆-TTC macro-CTA. Both macro-CTAs were synthesized *via* RAFT solution polymerization in ethanol (a) was made using CPCP and (b) was made using PETTC as the chain transfer agent.

THF GPC analysis was used to determine the molecular weight (M_n) of the PMAA_x macro-CTAs. However, these PMAA_x macro-CTAs (and any corresponding block copolymers) had to be methylated prior to THF GPC analysis. This is owing to the anionic nature of the PMAA residues, which can interact with or adsorb onto the GPC column, disrupting the size exclusion mechanism. To prevent this problem, the PMAA residues are methylated and converted to PMMA *via* reaction with excess trimethylsilyldiazomethane, as previously reported by Couvreur *et al.*⁵⁹ THF GPC analysis of the methylated PMAA₅₄-DB macro-CTA indicated an M_n of 5,600 g mol⁻¹ and a dispersity of 1.17. Similarly, analysis of the methylated PMAA₅₆-TTC macro-CTA indicated an M_n of 7,000 g mol⁻¹ and a dispersity of 1.18.

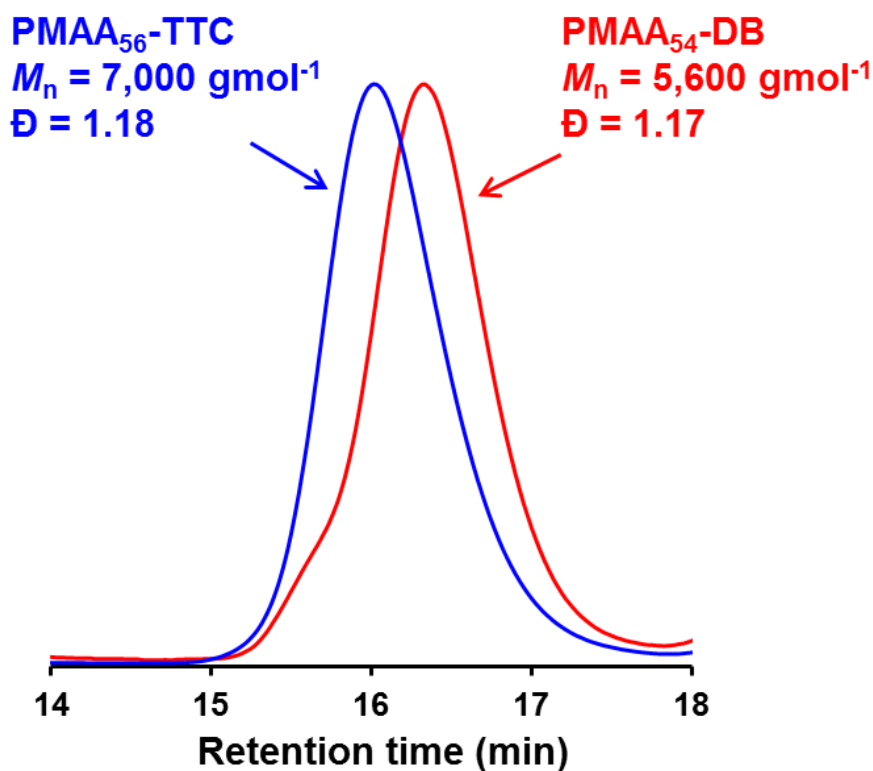
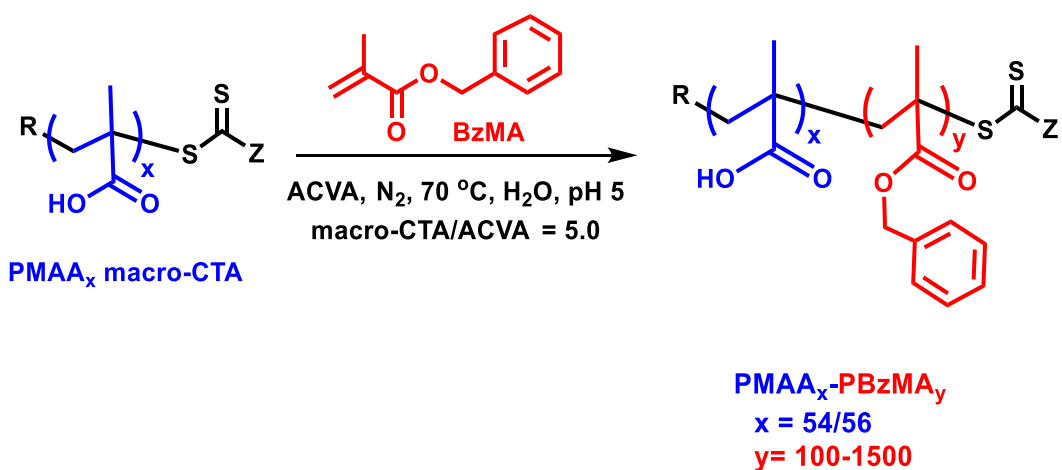


Figure 2.3 THF GPC chromatograms of methylated PMAA₅₄-DB macro-CTA and PMAA₅₆-TTC macro-CTA. Molecular weight (M_n) and dispersity (\mathcal{D}) are calculated relative to a series of near-monodisperse PMMA calibration standards.

2.4.2. Kinetics of PMAA_x-PBzMA_y synthesis via RAFT aqueous emulsion polymerization



Scheme 2.2. Synthesis of poly(methacrylic acid)-poly(benzyl methacrylate) (PMAA_x-PBzMA_y) diblock copolymer nanoparticles *via* RAFT aqueous emulsion polymerization of BzMA at 70 °C.

The PMAA₅₄-DB macro-CTA was chain-extended *via* RAFT aqueous emulsion polymerization of BzMA to form PMAA₅₄-PBzMA₂₀₀ diblock copolymer nanoparticles (Scheme 2.2). The kinetics of this polymerization at 70 °C were monitored by ¹H NMR spectroscopy at 10% w/w copolymer concentration (Figure 2.4). Samples were taken throughout the reaction and analyzed by ¹H NMR spectroscopy in d₇-DMF, which acts as a good solvent for both the PMAA and PBzMA blocks (thus fully dissolving the nanoparticles as copolymer chains). The PMAA₅₄ macro-CTA/ACVA molar ratio was varied from 3.0 to 10.0 to determine the effect of this parameter on the reaction kinetics and on the dispersity of the final PMAA₅₄-PBzMA₂₀₀ diblock copolymer. From Figure 2.4 it is clear that, at all macro-CTA/ACVA molar ratios, the polymerization proceeded to > 94% conversion within 135 min. At a macro-CTA/ACVA molar ratio of 3.0 faster polymerizations are observed, with > 94% conversion being achieved in just 60 min. Increasing this molar ratio to 5.0 or 10.0 reduces the rate, with > 94% conversion being achieved within 100 and 135 min, respectively. An increase in dispersity is often observed when using low macro-CTA/ACVA molar ratios owing to an increase in termination and a reduction in living character. The choice of macro-CTA/ACVA molar ratio therefore usually requires a compromise between polymerization rate and dispersity.¹⁷ In this case, the dispersity was the same for molar ratios of 3.0 and 5.0 ($\mathcal{D} = 1.40$) and only increased marginally ($\mathcal{D} = 1.45$) as the molar ratio was increased to 10.0, see Figure 2.5. An intermediate macro-CTA/ACVA molar ratio of 5.0 was selected for all subsequent experiments.

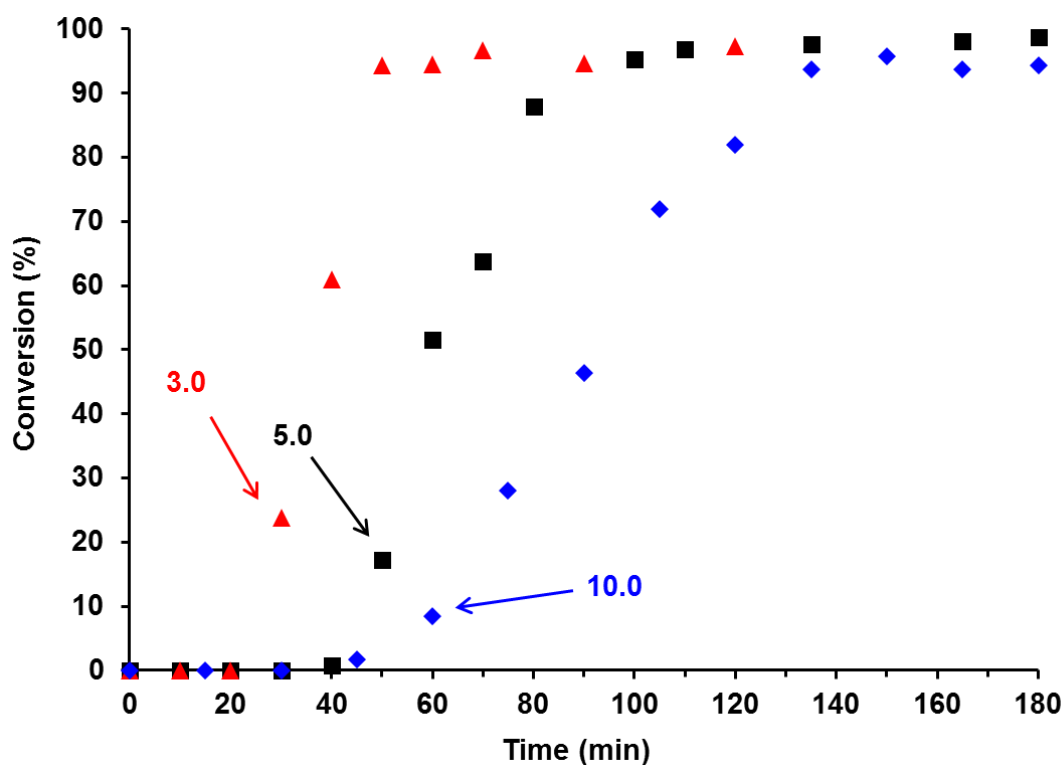


Figure 2.4 Kinetics of polymerization of BzMA at 70 °C in water (pH 5) at 10% w/w copolymer concentration with varying PMAA₅₄-DB macro-CTA/ACVA molar ratios of 3.0 (red ▲), 5.0 (black ■) and 10.0 (blue ◆). The target diblock copolymer in each case was PMAA₅₄-PBzMA₂₀₀.

For the BzMA polymerization conducted with a macro-CTA/ACVA molar ratio of 5.0, the evolution of molecular weight and dispersity was also monitored throughout the reaction, see Figure 2.5. A linear evolution of molecular weight with conversion was observed, indicative of a RDRP, see Figure 2.5c. Dispersities also increased throughout the polymerization (up to 1.53 at 96% conversion within 120 min). Despite this relatively high dispersity, high blocking efficiencies were achieved and GPC analyses also indicated unimodal MWD curves.

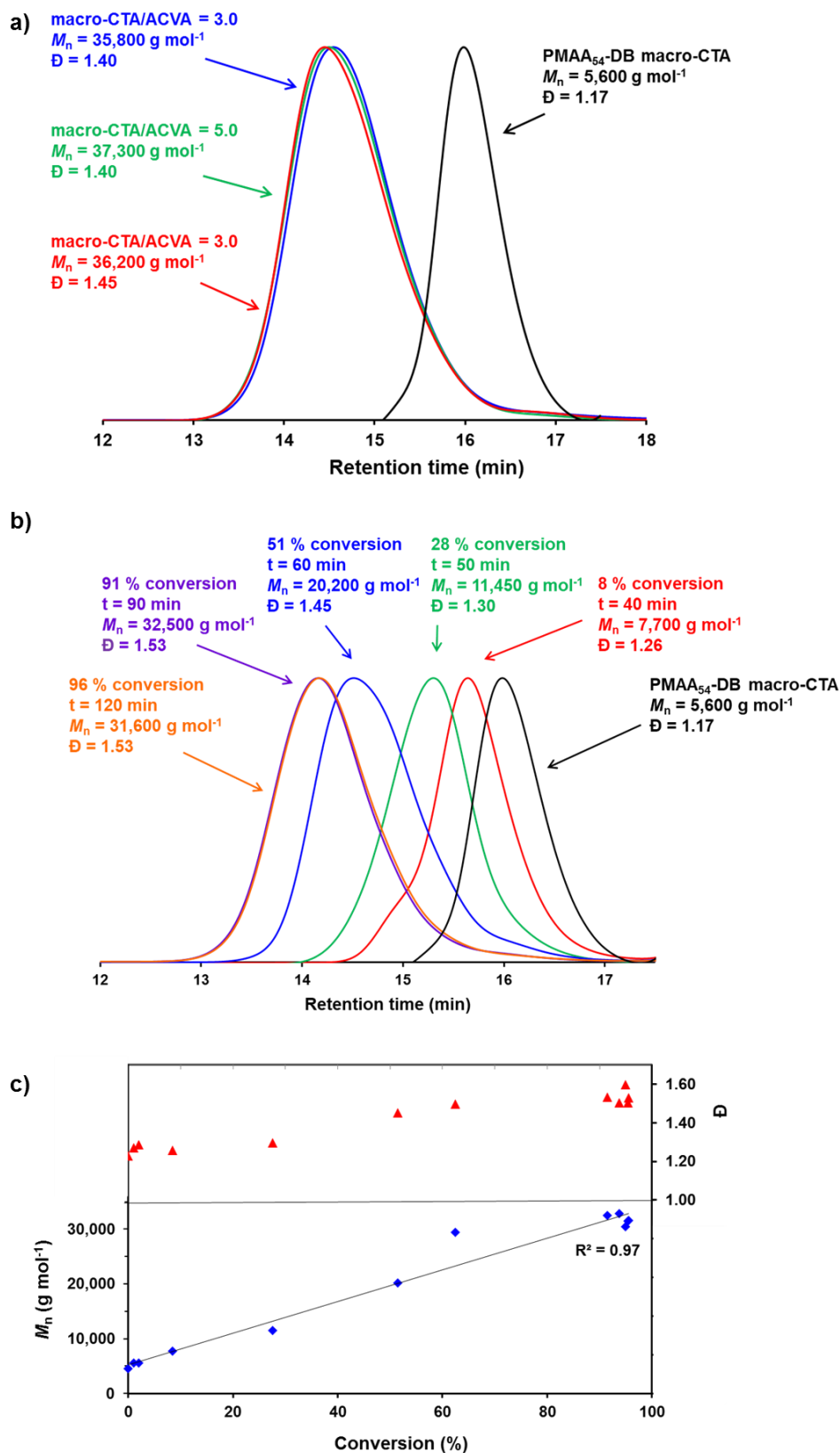


Figure 2.5 THF GPC chromatograms obtained for methylated PMAA₅₄-BzMA₂₀₀ diblock copolymers synthesized at 70 °C in water at 10% w/w using the PMAA₅₄-DB macro-CTA. (a) Effect of varying the macro-CTA/ACVA molar ratio (3.0, 5.0 or 10.0) on the polymerization rate. (b) a series of GPC chromatograms recorded for samples taken at various time points and (c) evolution of M_n and \bar{D} with conversion throughout the polymerization of BzMA using a macro-CTA/ACVA molar ratio of 5.0.

2.4.3. Investigation into the anionic behavior of $PMAA_x$ macro-CTAs and $PMAA_x$ -PBzMA₂₀₀ diblock copolymers.

Acid titration studies were performed on the PMAA₅₄-DB macro-CTA and the PMAA₅₆-TTC macro-CTA (Figure 2.5a) to determine the pK_a values.⁶⁰ These experiments indicated that the pK_a values were 6.12 for the former macro-CTA and 5.97 latter. The pK_a of PMAA_x-PBzMA₂₀₀ diblock copolymers synthesized using either a PMAA₅₄-DB macro-CTA or a PMAA₅₆-TTC macro-CTA were also determined, see Figure 2.5b. The pK_a values of the PMAA_x-PBzMA₂₀₀ nanoparticles were somewhat higher than that of the macro-CTAs at 6.65 and 6.72, respectively.

The increased pK_a values of the PMAA_x-PBzMA_y diblock copolymers relative to the PMAA_x macro-CTAs was expected.⁶¹ The MAA units in each case are in different environments, the PMAA_x macro-CTAs are essentially polyelectrolyte homopolymers whereas the block copolymers form spherical nanoparticles. The close proximity of the MAA acid units on the stabilizer block of the diblock copolymer nanoparticles results in an increase in the pK_a values.

Determination of the pK_a values is important as it gives an indication of the degree of ionization of the PMAA residues under the reaction conditions. The degree of ionization will have an effect on the electrostatic repulsion between adjacent chains which could influence the formation of nanoparticles *via* PISA. The level of electrosteric stabilization provided by the PMAA chains will also vary with the degree of ionization. The degree of ionization under the reaction conditions (pH 5.0), is 7.6% for the PMAA₅₄-DB macro-CTA and 10.7% for the PMAA₅₆-TTC macro-CTA (see Appendix 1).⁶⁰

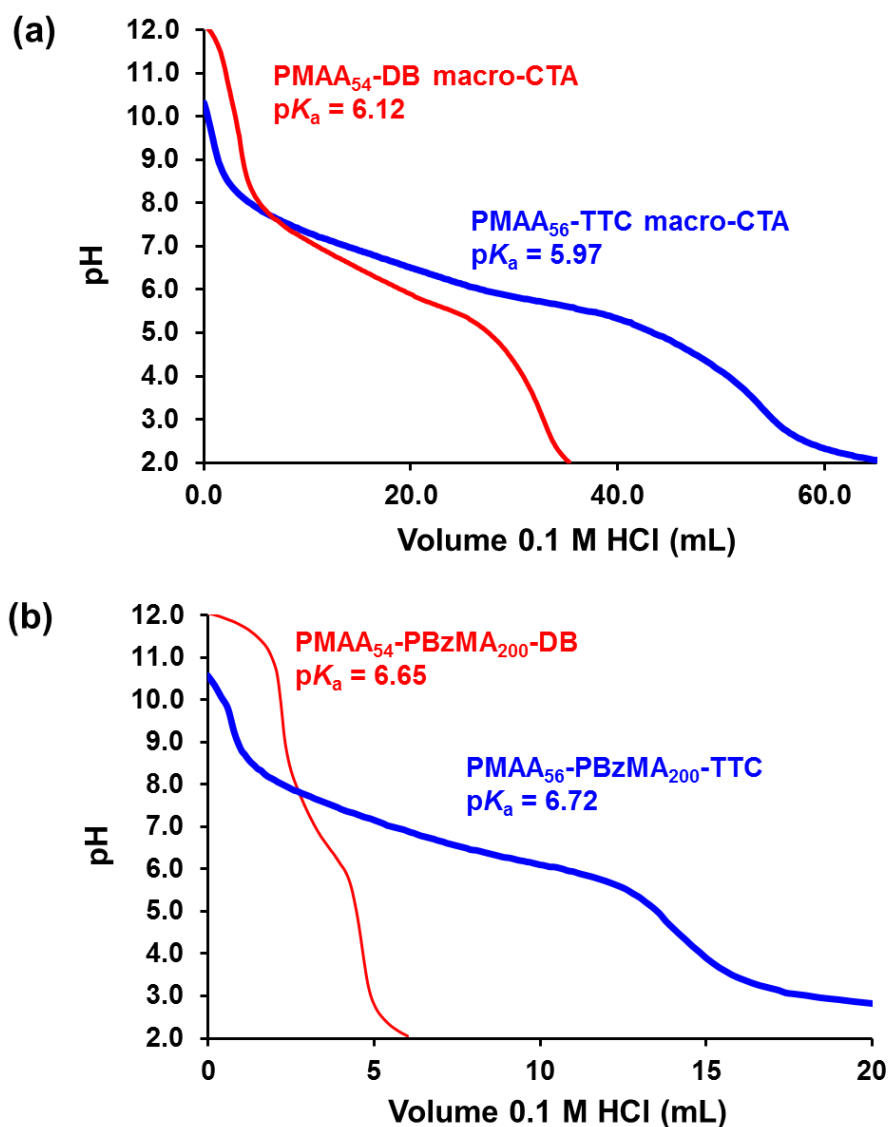


Figure 2.6 Acid titration used to determine the pK_a of (a) PMAA₅₄-DB macro-CTA and PMAA₅₆-TTC macro-CTA and (b) of PMAA_x-PBzMA₂₀₀ diblock copolymers synthesized from either a PMAA₅₄DB macro-CTA or a PMAA₅₆-TTC macro-CTA.

Aqueous electrophoresis was used to evaluate the surface anionic character of PMAA₅₆-PBzMA₂₀₀ nanoparticles, synthesized with the PMAA₅₆-TTC macro-CTA, with respect to pH (Figure 2.6). A pH titration was performed by starting at pH 10.0 and gradually reducing the dispersion pH to pH 2.0 by addition of acid. Between pH 10.0 and pH 6.5, the PMAA stabilizer chains are fully ionized and highly extended with particle diameter of ~45 nm and a zeta potential of ~ -40 mV. In this pH range, the particle diameter remains relatively constant at approximately 46 nm. As the pH is reduced from pH 6.5 to pH 4.5 the zeta potential changes from -40 mV to -30 mV as more of the PMAA chains become protonated. At the pK_a value of 6.12

approximately half of the PMAA residues per chain are protonated. The mean particle diameter in this pH range is reduced to approximately 35 nm as the PMAA chains begin to contract. Lowering the pH below 4.5 further reduces the zeta potential as the PMAA chains become more protonated and collapse. This leads to loss of electrosteric stabilization causing flocculation. The flocculated nanoparticles possess no net charge at approximately pH 2. Indeed, the apparent particle diameter measured below pH 4.0 exceeded $\sim 2 \mu\text{m}$. This nanoparticle aggregation proved to be reversible by conducting a pH titration in the reverse direction (pH 2.0 to pH 10.0). By gradually increasing the pH from 2.0 to 10.0 the PMAA chains become increasingly deprotonated with a zeta potential of -38 mV being observed at pH 7.5. The apparent particle diameter also decreases as the particles become stabilized by the highly anionic, extended PMAA chains. During this pH titration (from pH 10.0 to pH 2.0) some hysteresis was observed: the particle diameter did not return to its originally measured value but appeared to double in size ($\sim 80 \text{ nm}$ vs. $\sim 45 \text{ nm}$). However, on direct adjustment of the pH from pH 2.0 to 10.0 the particle diameter did return to its original value of 45 nm.

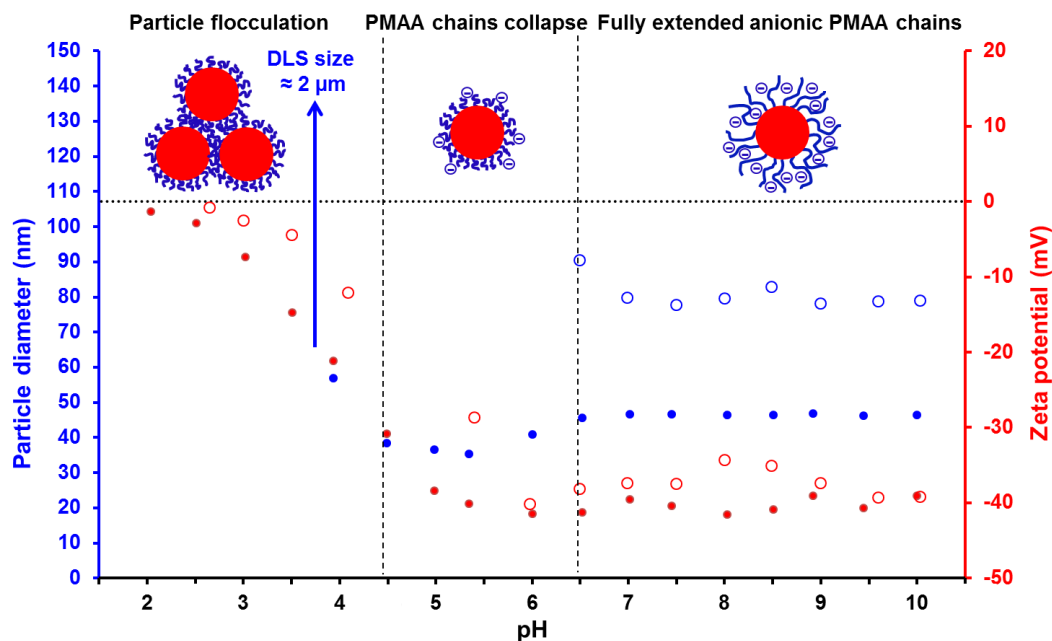


Figure 2.7 Variation in particle diameter and zeta potential with pH for PMAA₅₆-PBzMA₂₀₀ diblock copolymer spheres, synthesized with a PMAA₅₆-TTC macro-CTA. Closed spheres indicate titration from pH 10.0 to pH 2.0. Open spheres indicate titration from pH 2.0 to pH 10.0.

2.4.4. Synthesis of PMAA_x-PBzMA_y diblock copolymer nanoparticles via RAFT aqueous emulsion polymerization at 10% w/w copolymer concentration

Two series of PMAA_x-PBzMA_y diblock copolymer nanoparticles were prepared via RAFT aqueous emulsion polymerization of BzMA at 70 °C (Scheme 2.2). All reactions were performed at a macro-CTA/ACVA molar ratio of 5.0 and at 10% w/w copolymer concentration. In each series, either the PMAA₅₄-DB or the PMAA₅₆-TTC macro-CTA was used and the target PBzMA DP was varied from 100 to 1500. The resulting diblock copolymers were analyzed by ¹H NMR spectroscopy, THF GPC, DLS and TEM, see Table 2.1 and Table 2.2.

Previous work by Chaduc *et al.* indicated that pH has a strong influence on RAFT aqueous emulsion polymerizations conducted using an anionic macro-CTA such as PMAA.^{16, 62} Their work demonstrated that reaction pH has a significant effect on the formation of particles *via* PISA. Under acidic conditions (pH 3 to 5) the PMAA macro-CTA chains are in a hypercoiled conformation. This results in a higher local concentration of the core-forming monomer aiding the rapid formation of well-defined diblock copolymer chains that assemble into stable nanoparticles. In contrast at pH ≥ 6.5 the increased ionization of the PMAA macro-CTA chains leads to a more open water-swollen structure. The increased charge of the PMAA chains at high pH makes them more hydrophilic. Thus, a longer core-forming block DP is required for particle nucleation to occur, resulting in a long inhibition period. This causes a loss of control over the polymerization and the formation of polydisperse particles. In addition to this the RAFT chain end is also more susceptible to hydrolysis. It was therefore concluded that acidic conditions are favorable for RAFT aqueous emulsion polymerizations conducted using an anionic PMAA macro-CTA. The formation of coagulum was reported at acidic pH but the level of coagulum decreased with increasing pH.¹⁶ Given this all RAFT aqueous emulsion polymerizations in this Thesis utilizing a PMAA_x macro-CTA were conducted at pH 5.

Chapter 2: Synthesis of Diblock Copolymer Nanoparticles *via* RAFT-Mediated PISA in Water

Table 2.2 Monomer conversions, number-average molecular weights (M_n), dispersities (\mathcal{D}) and mean DLS and TEM diameter for a series of PMAA₅₄-PBzMA_y diblock copolymer nanoparticles prepared at 10% w/w *via* RAFT aqueous emulsion polymerization at pH 5 and 70 °C. All diblock copolymers were synthesized using a PMAA₅₄-DB macro-CTA.

Target Composition	Copolymer concentration (% w/w)	Conversion ^a (%)	M_n^b (g mol ⁻¹)	\mathcal{D}^b	DLS particle diameter (nm)	DLS polydispersity	TEM particle diameter (nm)
PMAA ₅₄ -DB	40	89	5,600	1.17	N/A	N/A	N/A
PMAA ₅₄ -PBzMA ₁₀₀	10	96	21,000	1.33	36	0.18	22
PMAA ₅₄ -PBzMA ₂₀₀	10	95	35,600	1.41	33	0.13	24
PMAA ₅₄ -PBzMA ₃₀₀	10	95	48,000	1.50	36	0.11	24
PMAA ₅₄ -PBzMA ₄₀₀	10	98	65,800	1.79	35	0.13	25
PMAA ₅₄ -PBzMA ₅₀₀	10	97	85,300	1.59	45	0.09	37
PMAA ₅₄ -PBzMA ₆₀₀	10	98	98,700	1.51	51	0.11	30
PMAA ₅₄ -PBzMA ₇₀₀	10	93	125,600	1.59	54	0.15	36
PMAA ₅₄ -PBzMA ₈₀₀	10	97	132,400	1.87	57	0.08	41
PMAA ₅₄ -PBzMA ₉₀₀	10	95	197,100	1.76	59	0.08	46
PMAA ₅₄ -PBzMA ₁₀₀₀	10	95	106,300	1.72	85	0.18	35
PMAA ₅₄ -PBzMA ₁₅₀₀	10	92	183,900	1.90	Flocculated	Flocculated	43

^aMonomer conversions determined by ¹H NMR spectroscopy.

^bDetermined by THF GPC analysis on methylated copolymer samples relative to a series of near-monodisperse PMMA standards

Chapter 2: Synthesis of Diblock Copolymer Nanoparticles *via* RAFT-Mediated PISA in Water

Table 2.3 Monomer conversions, number-average molecular weights (M_n), dispersities (\mathcal{D}) and mean DLS and TEM diameter for a series of PMAA₅₆-PBzMA_y diblock copolymer nanoparticles prepared at 10% w/w *via* RAFT aqueous emulsion polymerization at pH 5 and 70 °C. All diblock copolymers were synthesized using a PMAA₅₆-TTC macro-CTA.

Target Composition	Copolymer concentration (% w/w)	Conversion ^a (%)	M_n^b (g mol ⁻¹)	\mathcal{D}^b	DLS particle diameter (nm)	DLS polydispersity	TEM particle diameter (nm)
PMAA ₅₆ -TTC	40	82	7,000	1.18	N/A	N/A	N/A
PMAA ₅₆ -PBzMA ₁₀₀	10	94	22,800	1.34	34	0.25	23
PMAA ₅₆ -PBzMA ₂₀₀	10	97	38,500	1.41	46	0.14	25
PMAA ₅₆ -PBzMA ₃₀₀	10	98	57,100	1.39	53	0.10	30
PMAA ₅₆ -PBzMA ₄₀₀	10	99	62,500	1.37	62	0.15	31
PMAA ₅₆ -PBzMA ₅₀₀	10	98	90,700	1.32	64	0.11	38
PMAA ₅₆ -PBzMA ₆₀₀	10	99	101,300	1.48	63	0.08	40
PMAA ₅₆ -PBzMA ₇₀₀	10	97	129,100	1.50	72	0.10	40
PMAA ₅₆ -PBzMA ₈₀₀	10	99	150,100	1.52	75	0.09	44
PMAA ₅₆ -PBzMA ₉₀₀	10	99	153,400	1.59	75	0.09	45
PMAA ₅₆ -PBzMA ₁₀₀₀	10	99	129,900	1.71	84	0.07	45
PMAA ₅₆ -PBzMA ₁₅₀₀	10	98	230,000	1.89	92	0.05	52

^aMonomer conversions determined by ¹H NMR spectroscopy.

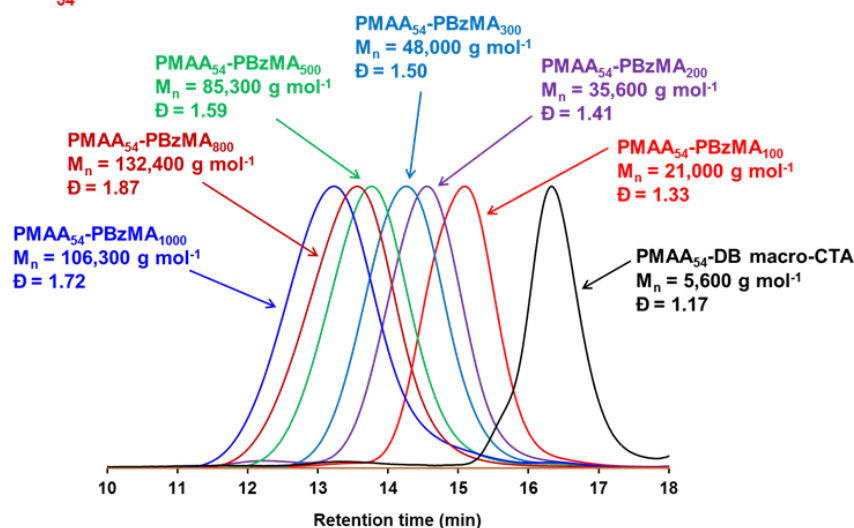
^bDetermined by THF GPC analysis on methylated copolymer samples relative to a series of near-monodisperse PMMA standards

Monomer conversions of at least 92% (as judged by ^1H NMR spectroscopy studies in d_7 -DMF) were achieved for the synthesis of all the $\text{PMAA}_x\text{-PBzMA}_y$ diblock copolymer nanoparticles. Typically, higher conversions were achieved when utilizing the $\text{PMAA}_{56}\text{-TTC}$ macro-CTA.

As discussed above, all $\text{PMAA}_x\text{-PBzMA}_y$ diblock copolymers were methylated prior to THF GPC analysis. A linear increase in molecular weight with PBzMA DP was observed for both series up to a PBzMA DP of 800, which is indicative of a RDRP (Figure 2.8). High blocking efficiencies were observed, indicating very little residual unreacted macro-CTA. For well-controlled RAFT polymerizations $\mathcal{D} \leq 1.50$ are expected. THF GPC chromatograms of the methylated block copolymers indicated a reduced level of control over the polymerization, with dispersities ranging between 1.33 and 1.90 for the series synthesized using the $\text{PMAA}_{54}\text{-DB}$ macro-CTA. The $\text{PMAA}_{56}\text{-TTC}$ macro-CTA afforded a similar level of control with dispersities between 1.32 and 1.89. These higher-than-expected dispersities could be the result of only partial methylation being achieved before GPC analysis.

Sterically-stabilized diblock copolymer nanoparticles were formed during RAFT aqueous emulsion polymerization of BzMA owing to the strongly amphiphilic nature of the $\text{PMAA}_x\text{-PBzMA}_y$ chains. These nanoparticles were analyzed by both DLS and TEM studies (Table 2.2 and Table 2.3). For the $\text{PMAA}_{54}\text{-PBzMA}_y$ diblock copolymer series (using the $\text{PMAA}_{54}\text{-DB}$ macro-CTA), the hydrodynamic diameter remained relatively constant (between 33 and 36 nm) for PBzMA DPs of 100 to 400, see Figure 2.9. At PBzMA DPs of 500 to 1000 the hydrodynamic particle diameter increased from 45 to 85 nm. A more linear increase in the hydrodynamic diameter of the spherical nanoparticles was observed for the $\text{PMAA}_{56}\text{-PBzMA}_y$ series (using the $\text{PMAA}_{56}\text{-TTC}$ macro-CTA) as the PBzMA DP increased from 100 to 1500 (34 nm up to 92 nm), see Figure 2.9. This relationship was supported by TEM studies, see Figure 2.8. All DLS analyses were conducted on dilute copolymer dispersions (0.20% w/w) adjusted to pH 8. If DLS analyses were conducted at the natural post-reaction pH (5-6), this led to greater scatter in the data caused by different degrees of ionization of the PMAA stabilizer chains in each sample. The pH titration previously discussed (Figure 2.7) indicates that there is minimal variation in particle diameter on adjusting from pH 6.5 to pH 10.0. Therefore, by choosing to conduct these analyses at pH 8.0 scatter in the data caused by pH variation is minimized.

(a) PMAA₅₄-DB macro-CTA



(b) PMAA₅₆-TTC macro-CTA

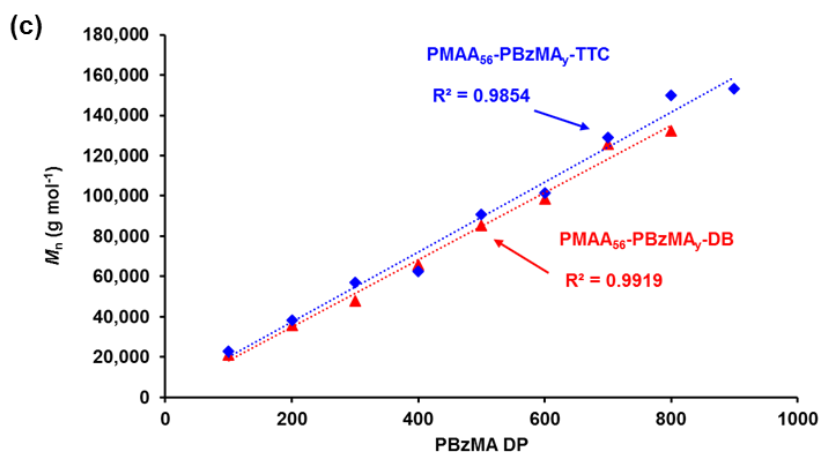
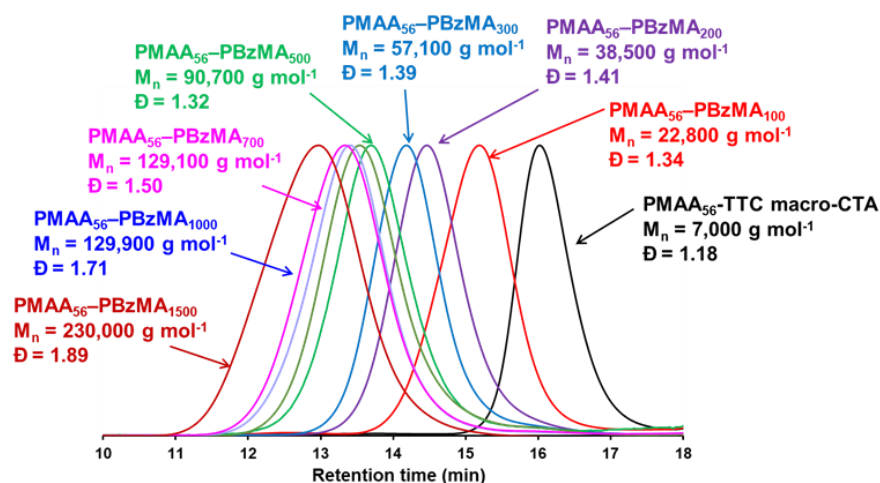
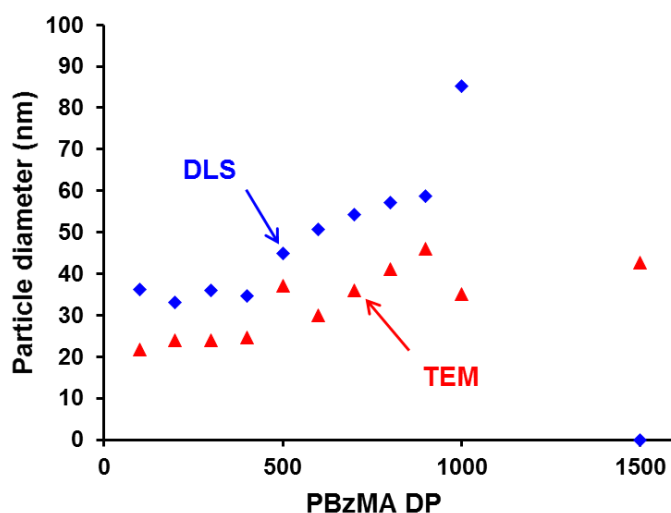


Figure 2.8 THF GPC chromatograms for PMAA_x-PBzMA_y diblock copolymer prepared at 10% w/w copolymer concentration *via* RAFT aqueous emulsion polymerization of BzMA using either (a) a PMAA₅₄-DB macro-CTA or (b) a PMAA₅₆-TTC macro-CTA, where $y = 100 - 1500$. (c) evolution of M_n with PBzMA DP for each series prepared with either the PMAA₅₄-DB macro-CTA or the PMAA₅₆-TTC macro-CTA. All diblock copolymers were modified by methylation prior to GPC analysis. Molecular weight data is relative to a series of near-monodisperse PMMA standards.

TEM studies indicated that only spherical nanoparticles were formed *via* PISA (Figure 2.10). Even by targeting highly asymmetric diblock copolymers such as PMAA₅₆-PBzMA₁₅₀₀, higher order morphologies such as worms or vesicles could not be accessed. Similar observations were reported by Cunningham *et al.* for the synthesis of PGMA₅₁-PBzMA_y nanoparticles and also by Chaduc *et al.* for PMAA_x-PS_y nanoparticles.^{17, 39}

(a) PMAA₅₄-PBzMA_y-DB diblock copolymers



(b) PMAA₅₆-PBzMA_y-TTC diblock copolymers

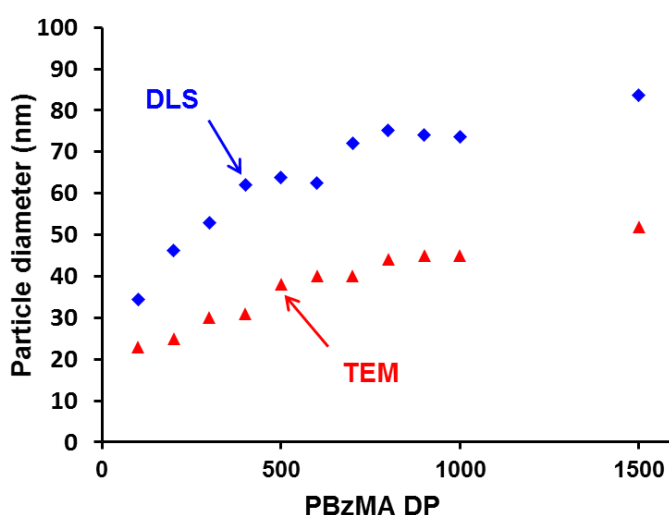
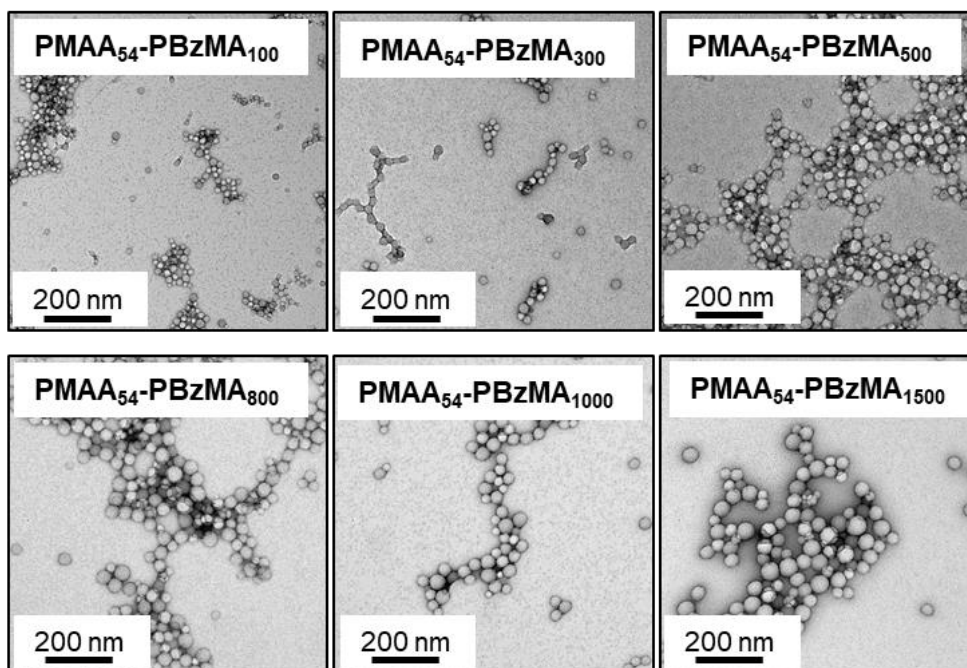


Figure 2.9 A comparison of mean particle diameter vs. mean degree of polymerization of the PBzMA block for two series of PMAA_x-PBzMA_y diblock copolymers prepared at 10% w/w copolymer concentration *via* RAFT aqueous emulsion polymerization using either (a) PMAA₅₄-DB macro-CTA or (b) PMAA₅₆-TTC macro-CTA. Data collected on dilute dispersions at pH 8.

(a) PMAA₅₄-PBzMA_y-DB



(b) PMAA₅₆-PBzMA_y-TTC

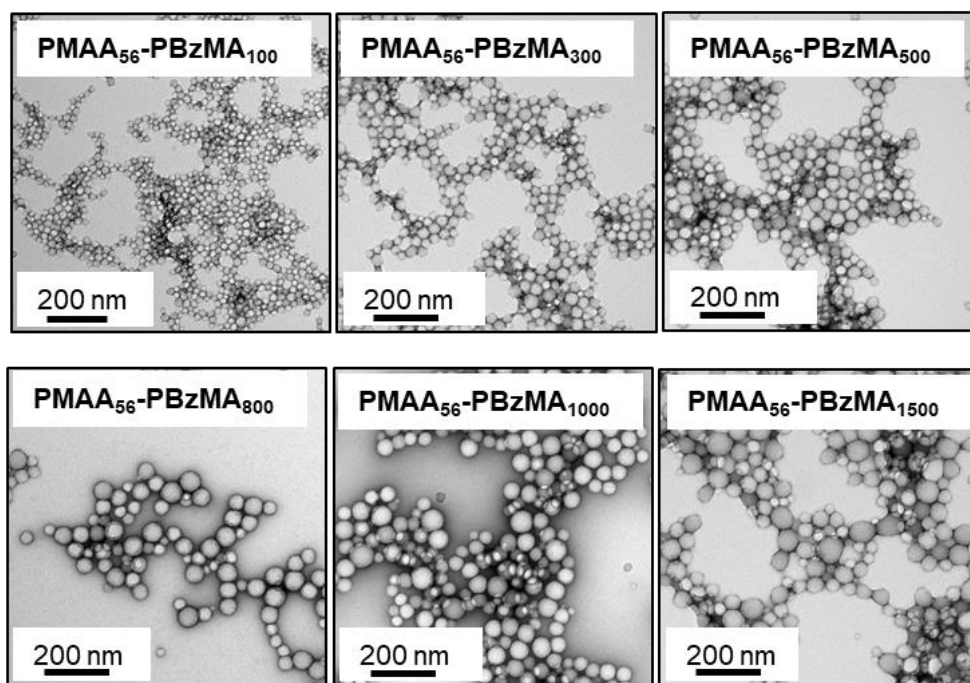


Figure 2.10 TEM images PMAA_x-PBzMA_y diblock copolymers prepared at 10% w/w copolymer concentration *via* RAFT aqueous emulsion polymerization of BzMA made utilizing either (a) PMAA₅₄-DB macro-CTA or (b) PMAA₅₆-TTC macro-CTA.

Synthesizing two series of PMAA_x-PBzMA_y diblock copolymer nanoparticles *via* RAFT aqueous emulsion polymerization of BzMA utilizing two different macro-CTAs enabled a direct comparison of the two RAFT agents to be made. The results described above indicate that better results are achieved when using the PMAA₅₆-TTC macro-CTA. More specifically, higher conversions were typically achieved and a slightly improved level of control over the polymerization was observed ($1.32 \leq \bar{D} \leq 1.89$). A more linear increase in the hydrodynamic diameter of the spherical nanoparticles was also observed as the PBzMA DP increased from 100 to 1500 (34 nm up to 92 nm). Therefore, the PMAA₅₆-TTC macro-CTA has been used in all subsequent experiments from Section 2.4.7 onwards.

2.4.5. Synthesis of PMAA₅₄-PBzMA₅₀₀ diblock copolymer nanoparticles via RAFT aqueous emulsion polymerization at varying copolymer concentrations

It has been reported that the copolymer concentration can have an effect on the particle morphology formed by PISA, with higher concentrations favoring the formation of worms and vesicles.⁵⁵ Thus a series of PMAA₅₄-PBzMA₅₀₀ diblock copolymers were prepared at 10 to 50% w/w copolymer concentration using the PMAA₅₄-DB macro-CTA. High conversions (> 97%) were achieved at 10, 20 and 30% w/w copolymer concentration with the conversion reducing to 86% and 84% at 40 and 50% w/w copolymer concentration, respectively (see Figure 2.11 and Table 2.4).

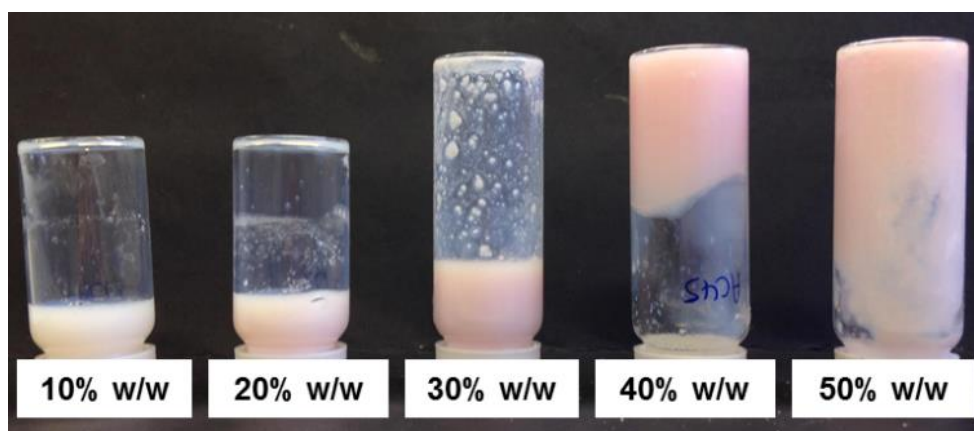


Figure 2.11 Digital photographs of PMAA₅₄-PBzMA₅₀₀-DB diblock copolymer dispersions prepared at copolymer concentrations of 10 to 50% w/w at pH 5.

THF GPC analysis of the methylated copolymers suggests high blocking at all total copolymer concentrations (Figure 2.11a). Reasonable control ($\mathcal{D} = 1.53$) was achieved at 10 and 20% w/w copolymer concentration. However, higher dispersities ($1.69 \leq \mathcal{D} \leq 1.99$) were observed at copolymer concentrations $\geq 30\%$ w/w. TEM studies showed a series of well-defined spherical nanoparticles of an approximately equal particle diameter (33 - 38 nm) at 10 to 40% w/w copolymer concentration and slightly larger spheres (48 nm) at 50% w/w (Figure 2.11c). In comparison, the DLS data showed increasing particle diameter with increasing copolymer concentration, Figure 2.11b. As this was not observed by TEM, it suggests incipient flocculation at higher copolymer concentration (Figure 2.11c). It is also worth noting that a higher viscosity was observed at increasing copolymer concentration. At 10% to 30% w/w, free-flowing dispersions were obtained. A more paste-like consistency was observed at 40% and 50% w/w concentration, see Figure 2.11. If the increase in viscosity caused inefficient stirring this could account for the lower degrees of conversions obtained at these concentrations. Similar observations on increasing viscosity were reported by Cunningham and co-workers when preparing $\text{PGMA}_x\text{-PBzMA}_y$ spheres at 10 to 50% w/w.¹⁷ However, in this system high conversions were achieved at all copolymer concentrations.

Table 2.4 Monomer conversions, number-average molecular weights (M_n), dispersities (\mathcal{D}) and mean DLS and TEM diameter for a series of $\text{PMAA}_{54}\text{-PBzMA}_{500}$ diblock copolymer nanoparticles prepared at 10 to 50% w/w copolymer concentration.

Target Composition	Copolymer concentration (% w/w)	Conversion ^a (%)	M_n^b (g mol ⁻¹)	\mathcal{D}^b	DLS particle diameter (nm)	DLS particle dispersity	TEM particle diameter (nm)
$\text{PMAA}_{54}\text{-PBzMA}_{500}$	10	98	81,100	1.53	64	0.11	38
$\text{PMAA}_{54}\text{-PBzMA}_{500}$	20	99	65,600	1.53	59	0.13	36
$\text{PMAA}_{54}\text{-PBzMA}_{500}$	30	97	61,200	1.99	105	0.31	38
$\text{PMAA}_{54}\text{-PBzMA}_{500}$	40	86	48,500	1.69	113	0.32	33
$\text{PMAA}_{54}\text{-PBzMA}_{500}$	50	84	79,000	1.89	131	0.15	48

^aMonomer conversions determined by ¹H NMR spectroscopy.

^bDetermined by THF GPC analysis on methylated polymer samples, relative to a series of near-monodisperse PMMA standards.

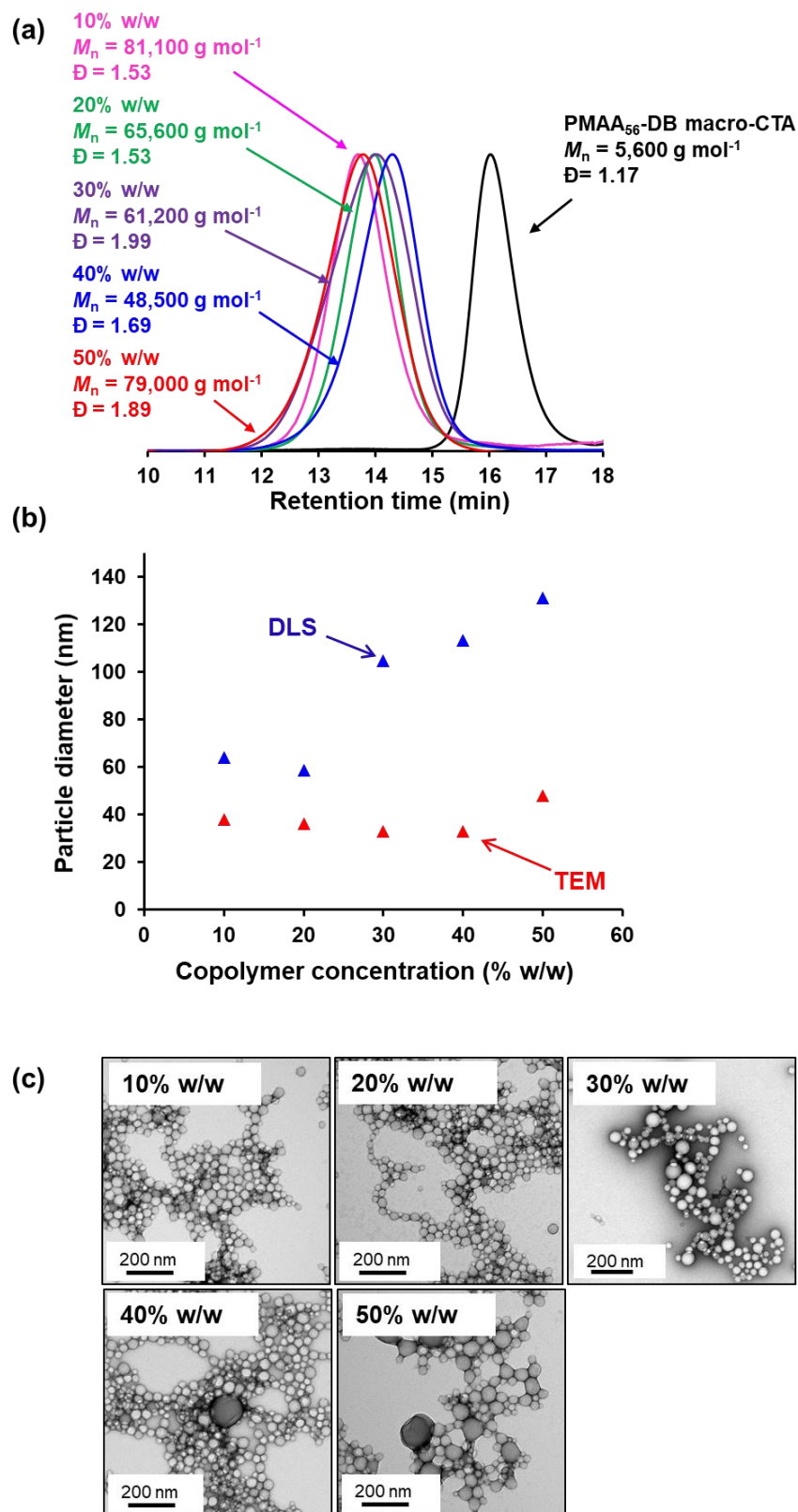


Figure 2.12 Characterization of PMAA₅₄-PBzMA₅₀₀ diblock copolymers prepared at 10, 20, 30, 40 and 50% w/w copolymer concentration *via* RAFT aqueous emulsion polymerization of BzMA: (a) THF GPC curves of methylated copolymers, (b) mean particle diameter vs. copolymer concentration and (c) TEM images showing well-defined spherical nanoparticles.

2.4.6. Synthesis of $PMAA_x$ - $PBzMA_y$ diblock copolymer nanoparticles in the presence of $CaCl_2$ salt

One method utilized by the Charleux research group to synthesize higher order morphology nanoparticles *via* RAFT aqueous emulsion polymerization was the addition of $CaCl_2$ salt to the reaction mixture.⁴⁴ When the appropriate salt concentration ($[CaCl_2] = 0.04$ to 0.072 M) was present during the synthesis of poly[acrylic acid-*co*-poly(ethylene oxide) methyl ether acrylate]-polystyrene (P(AA-*co*-PEOA)-PS) then fibres or vesicles were formed, whereas at low (or no) salt concentrations only spherical nanoparticles were obtained.

During the synthesis of $PMAA_x$ - $PBzMA_y$ diblock copolymer nanoparticles *via* PISA, the formation of higher order morphologies is most likely hindered by mutual electrostatic repulsion between the anionic PMAA stabilizer chains. The addition of Ca^{2+} ions screens this charge repulsion, enabling the PMAA chains to pack closer together in the coronal shell and resulting in a reduction in the stabilizer block volume fraction. Theoretically, this could favor the formation of worms or vesicles, see Figure 2.13.

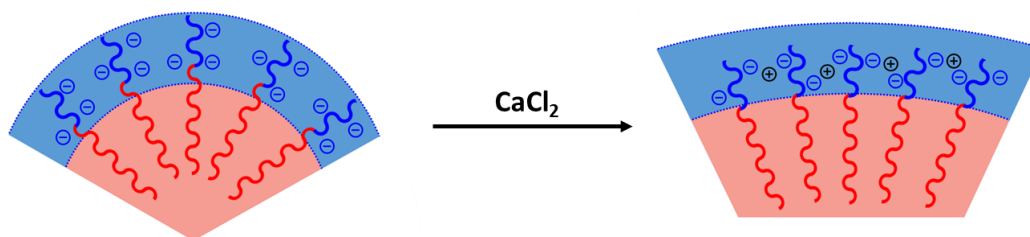


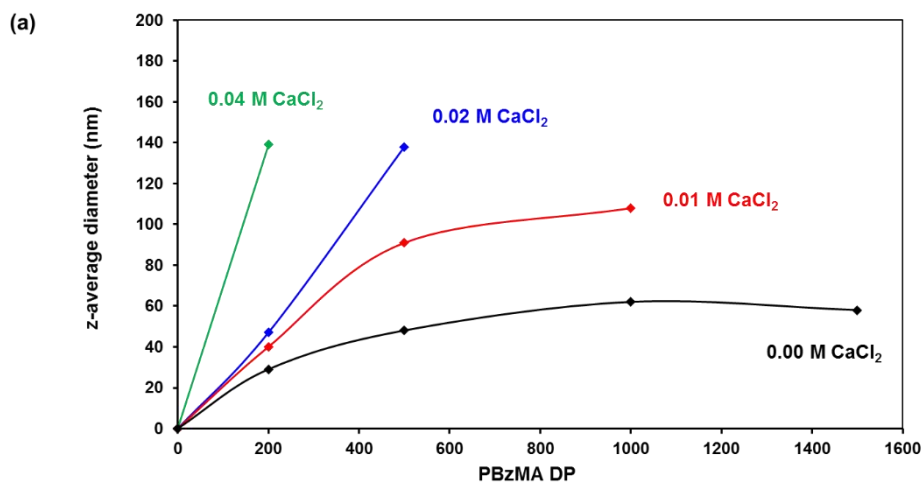
Figure 2.13 Schematic representation of the packing of $PMAA_{54}$ - $PBzMA_y$ chains to form electrosterically stabilized nanoparticles. The addition of $CaCl_2$ salt results in charge screening between the anionic PMAA chains, reducing repulsion and enabling closer packing. This could result in an increase in the packing parameter and a morphology transition from spheres to worms or vesicles.

To investigate this possibility, the $PMAA_{54}$ -DB macro-CTA was chain-extended *via* RAFT aqueous emulsion polymerization of BzMA in the presence of $CaCl_2$. $PBzMA$ DPs of 200 to 1500 were targeted at $CaCl_2$ concentrations of 0.01, 0.02 and 0.04 M, see Table 2.5. All syntheses were conducted at pH 5, with a macro-CTA/ACVA molar ratio of 5.0 and at a copolymer concentration of 10% w/w.

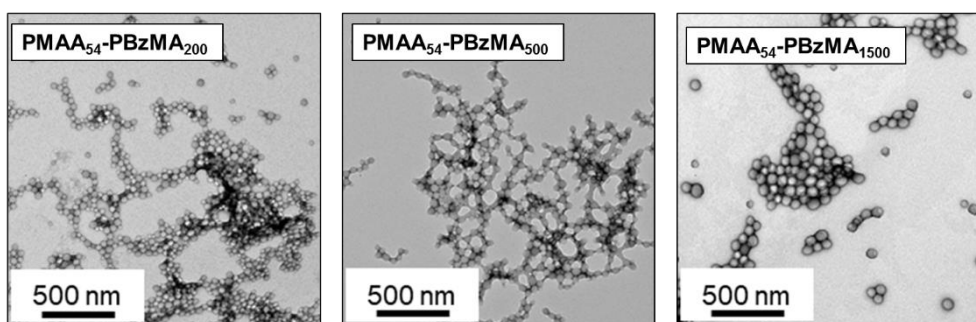
Table 2.5 Target compositions, CaCl₂ concentration and hydrodynamic particle diameters for PMAA₅₄-PBzMA_y diblock copolymer nanoparticles synthesized in the presence of CaCl₂ at 10% w/w copolymer concentration. All diblock copolymers were synthesized using the PMAA₅₄-DB macro-CTA.

Target Composition	CaCl ₂ Concentration (M)	DLS particle diameter (nm)	DLS particle polydispersity
PMAA ₅₄ -PBzMA ₂₀₀	0.04	139	0.10
PMAA ₅₄ -PBzMA ₅₀₀	0.04	Flocculated	-
PMAA ₅₄ -PBzMA ₁₀₀₀	0.04	Flocculated	-
PMAA ₅₄ -PBzMA ₁₅₀₀	0.04	Flocculated	-
PMAA ₅₄ -PBzMA ₂₀₀	0.02	47	0.09
PMAA ₅₄ -PBzMA ₅₀₀	0.02	138	0.14
PMAA ₅₄ -PBzMA ₁₀₀₀	0.02	Flocculated	-
PMAA ₅₄ -PBzMA ₁₅₀₀	0.02	Flocculated	-
PMAA ₅₄ -PBzMA ₂₀₀	0.01	40	0.06
PMAA ₅₄ -PBzMA ₅₀₀	0.01	91	0.08
PMAA ₅₄ -PBzMA ₁₀₀₀	0.01	108	0.35
PMAA ₅₄ -PBzMA ₁₅₀₀	0.01	Flocculated	-

Unfortunately, DLS and TEM analysis indicated that only spherical nanoparticles were formed irrespective of the target PBzMA DP or the CaCl₂ salt concentration (Figure 2.14). The presence of the CaCl₂ does have some effect on PISA, as an increase in nanoparticle diameter was observed for a given PBzMA DP with increasing salt concentration. This indicates that the Ca²⁺ ions reduce the repulsion between adjacent PMAA chains, enabling closer packing. However, the morphology transition from spheres to worms or vesicles was not observed under these conditions. Instead, the presence of CaCl₂ caused flocculation of the nanoparticles. This is most likely owing to excessive charge screening resulting in reduced electrosteric stabilization. Flocculation was observed at a lower PBzMA DP as the CaCl₂ concentration was increased, see Table 2.5. At higher PBzMA DPs, the particles have larger cores but are stabilized by the same PMAA₅₄ chains. It therefore follows that a smaller reduction in anionic charge density on the PMAA₅₄ chains results in loss of electrosteric stabilization of the particles.



(b) 0.01 M CaCl₂



(c) PMAA₅₄-PBzMA₅₀₀

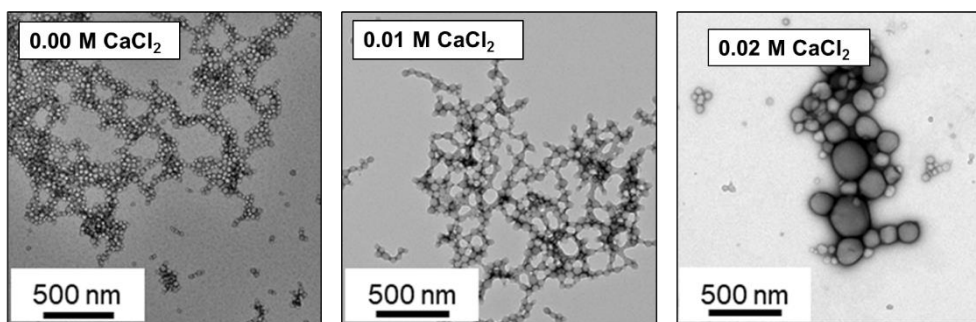


Figure 2.14 Effect of CaCl₂ concentration and PBzMA DP on the morphology and hydrodynamic particle diameter of PMAA₅₄-PBzMA_y diblock copolymer nanoparticles; (a) z-average particle diameter vs. PBzMA DP, where trendlines act only as a guide for the eye, (b) TEM images of PMAA₅₄-PBzMA_y diblock copolymer nanoparticles ($y = 200$ -1500) synthesized in the presence of 0.01 M CaCl₂ and (c) TEM images of PMAA₅₄-PBzMA₅₀₀ diblock copolymer nanoparticles synthesized in the presence of 0.01 – 0.04 M CaCl₂.

2.4.7. Chain extension of PMAA₅₆ macro-CTA with monomers of varying aqueous solubility

The results discussed on the PMAA_x-PBzMA_y system considered alongside previous work on the PGMA₅₁-PBzMA_y system suggest that often only kinetically-trapped spherical nanoparticles can be obtained *via* RAFT aqueous emulsion polymerization.¹⁷ In stark contrast, RAFT aqueous dispersion polymerization formulations, such as PGMA_x-PHPMA_y can be used to prepare the full wide range of morphologies including worms and vesicles.^{31, 55, 63-65} The key difference between these two systems is the aqueous solubility of the core-forming monomer. More specifically, the aqueous monomer solubility of BzMA at 70 °C is 0.40 g dm⁻³, which is considerably lower than the aqueous monomer solubility of HPMA at 70 °C (100 g dm⁻³).

Table 2.6 Density, aqueous monomer solubility and glass transition temperature (T_g) data for a series of six core-forming methacrylic monomers.

Monomer	Monomer	Density at 25 °C (g cm ⁻³) ^a	Aqueous monomer solubility at 20 °C (g dm ⁻³)	Aqueous monomer solubility at 70 °C (g dm ⁻³)	T _g (°C) ^f
2-Hydroxypropyl methacrylate	HPMA	1.03	130 ^b	100 ^b	76
2-Hydroxybutyl methacrylate	HBMA	1.01	31 ^b	20 ^b	-
Methyl methacrylate	MMA	0.94	15 ^c	13 ^b	105, 120
<i>n</i> -Butyl methacrylate	BMA	0.89	3 ^d	2 ^b	20
2,2,2-Trifluoroethyl methacrylate	TFEMA	1.18	2.92 ^e	2 ^b	80
Benzyl methacrylate	BzMA	1.04	0.19 ^b	0.40 ^b	54

^aall density values taken from Reference⁶⁶

^bvalue determined in the laboratory by the Armes group.

^cvalue taken from Reference⁶⁷

^dvalue taken from Reference⁶⁸

^evalue taken from Reference⁶⁹

^fall T_g values taken from Reference,⁷⁰ except for TFEMA value taken from Reference⁷¹

It was postulated that the aqueous solubility of the core-forming monomer could be a critical parameter for the attempted synthesis of higher order morphologies *via* PISA. To investigate this hypothesis, a series of diblock copolymer nanoparticles was prepared by chain-extending a PMAA₅₆-TTC macro-CTA with six core-forming monomers: BzMA, TFEMA, BMA, MMA, HBMA and HPMA. These monomers increase in aqueous solubility from BzMA to HPMA (Table 2.6). Their aqueous solubility can be determined by visual inspection at both room temperature (20 °C) and at the reaction temperature (70 °C). The monomer is added slowly to a known fixed quantity of water at the desired temperature. The point at which the monomer no longer fully dissolves and remains visible by eye is considered to be the limit of the monomer aqueous solubility. Above this saturation point, residual monomer is visible as either very fine droplets (HPMA and HBMA) or as relatively coarse droplets (MMA, BMA, TFEMA and BzMA), see Figure 2.15.

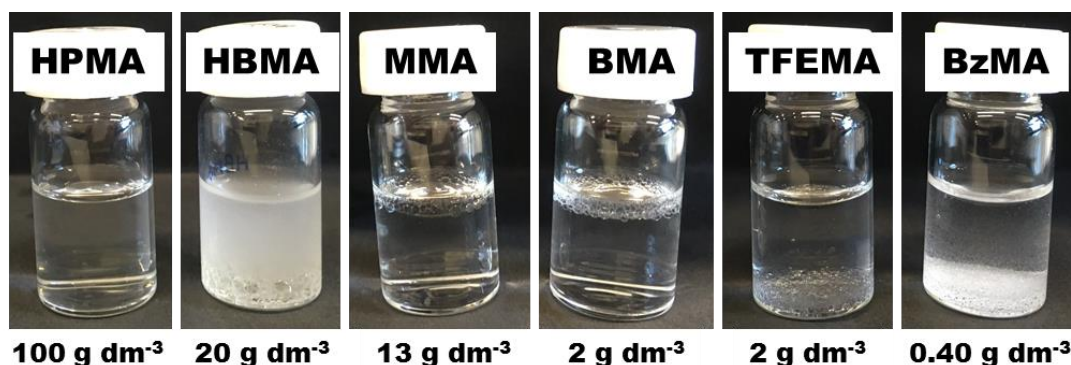
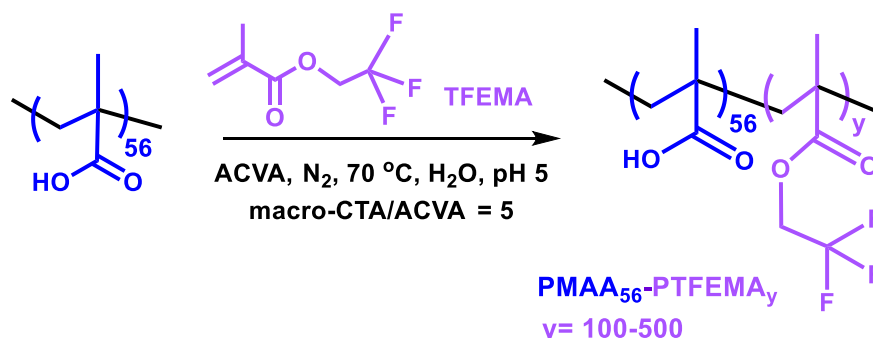


Figure 2.15 Digital photographs of various core-forming monomer aqueous mixtures showing either a dispersion (HPMA) or an emulsion (HBMA, MMA, BMA, TFEMA, BzMA) Values underneath each image correspond to the aqueous solubility of that monomer at 70 °C.

2.4.7.1. Synthesis of PMAA₅₆-PTFEMA_y diblock copolymer nanoparticles via RAFT aqueous emulsion polymerization at 20% w/w copolymer concentration



Scheme 2.3 Synthesis of poly(methacrylic acid)-poly(2,2,2-trifluorethyl methacrylate) diblock copolymers (PMAA₅₆-PTFEMA_y) via RAFT aqueous emulsion polymerization.

The first monomer chosen for investigation was TFEMA which has an aqueous solubility of 2 g dm⁻³ at 70 °C. This is more than ten times greater than that of BzMA (0.40 g dm⁻³ at 70 °C). A series of PMAA_x-PTFEMA_y diblock copolymer nanoparticles was prepared via RAFT aqueous emulsion polymerization where the target PTFEMA DP was varied from 100 to 500 (Scheme 2.3). All reactions were performed at 70 °C, with a macro-CTA/ACVA molar ratio of 5.0 at 20% w/w copolymer concentration and pH 5. The resulting diblock copolymers were analyzed by ¹H NMR spectroscopy, THF GPC, DLS and TEM, see Table 2.7.

Table 2.7 Monomer conversions, number-average molecular weights (M_n), dispersities (\mathcal{D}) and mean DLS and TEM diameters for a series of PMAA₅₆-PTFEMA₂₀₀ diblock copolymer nanoparticles prepared at 20% w/w copolymer concentration.

Target	Conversion ^a (%)	M_n^b (g mol ⁻¹)	\mathcal{D}^b	DLS particle diameter (nm)	DLS particle polydispersity	TEM particle diameter (nm)
PMAA ₅₆ -PTFEMA ₁₀₀	99	11,400	2.94	50	0.06	29
PMAA ₅₆ -PTFEMA ₂₀₀	99	17,000	3.36	48	0.08	30
PMAA ₅₆ -PTFEMA ₃₀₀	99	15,700	4.37	47	0.07	37
PMAA ₅₆ -PTFEMA ₄₀₀	99	23,400	4.45	54	0.06	44
PMAA ₅₆ -PTFEMA ₅₀₀	99	24,000	4.20	69	0.24	41

^aMonomer conversions determined by ¹H NMR spectroscopy.

^bDetermined by THF GPC analysis of methylated copolymer samples relative to a series of near-monodisperse PMMA standards.

Monomer conversions of $> 99\%$ were achieved for all syntheses, as judged by ^1H NMR spectroscopy studies in d_6 -DMSO. THF GPC analysis of the $\text{PMAA}_{56}\text{-PTFEMA}_y$ diblock copolymers is problematic compared to diblock copolymers based on other core-forming monomers. This is owing to the low refractive index (RI) of the PTFEMA block (1.42)⁷² compared to that of other non-fluorinated methacrylic polymers (RI = 1.49 - 1.59). Ideally, the two blocks should have comparable refractive indices and therefore generate an equal RI response. The difference in RI leads to an artificially high macro-CTA signal relative to the diblock copolymer, indicating apparently poor blocking efficiency for the macro-CTA.^{73, 74} To confirm that the high level of residual macro-CTA is an artefact owing to this RI difference, the diblock copolymers can be analyzed using a UV GPC detector at 298 nm (corresponding to the λ_{max} of the S=S in the CTA end-group).

A large residual macro-CTA peak and broad MWDs were observed in the GPC chromatograms for each $\text{PMAA}_{56}\text{-PTFEMA}_y$ diblock copolymer collected using the RI detector, see Figure 2.16a. Similar, chromatograms were collected using the UV detector set to 298 nm, see Figure 2.16b. In fact, the macro-CTA signal was increased relative to the block copolymer signal. This suggests that not all the block copolymer chains are capped by the PETTC RAFT agent and strongly indicates that FRP is taking place. Thus, the RAFT aqueous emulsion polymerization of TFEMA is not well-controlled.

Cornel *et al.* recently published that is also possible to set the UV detector to 260 nm, corresponding to the λ_{max} of the aromatic ring in the CTA end-group.⁷⁵ In hindsight, this wavelength is more suitable for UV GPC analysis as PS standards can be used as calibrants to collect molecular weight data. There are no UV calibration standards available for analysis at 298 nm.

TEM analysis of the resulting diblock copolymer nanoparticles indicated that only spherical nanoparticles were formed *via* PISA, see Figure 2.17. Typically, the particle size increases with increasing core-forming block DP. However, minimal variation in particle diameter was observed by DLS and TEM for this system, see Figure 2.17. The lack of control over the RAFT aqueous emulsion polymerization of TFEMA and the possibility of FRP indicated by GPC analysis could be responsible for this behavior.

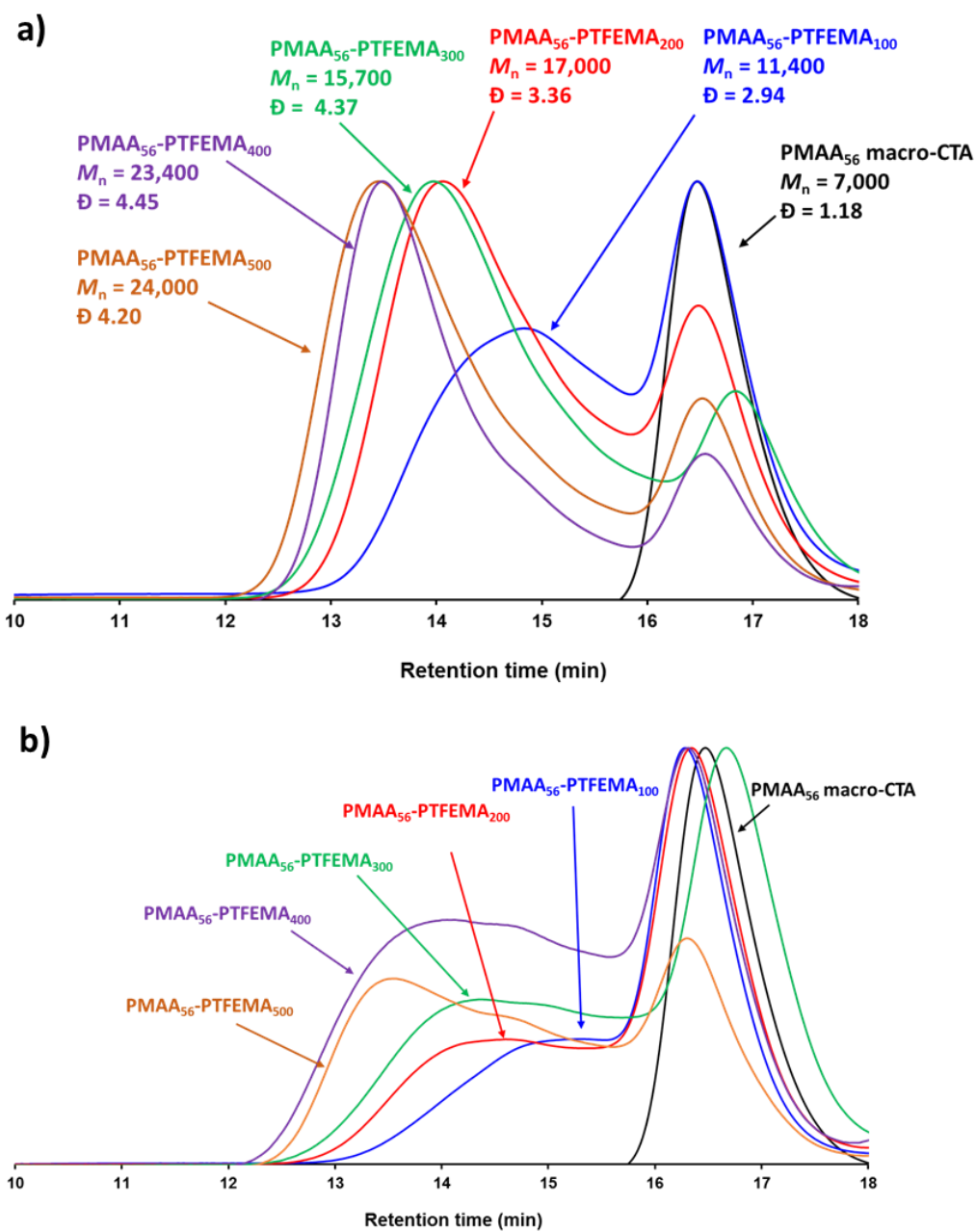


Figure 2.16 THF GPC chromatograms of PMAA₅₆-PTFEMA_y diblock copolymers synthesized *via* RAFT aqueous emulsion polymerization at 70 °C. (a) chromatograms collected using a refractive index detector and (b) chromatograms collected using a UV-detector at 298 nm.

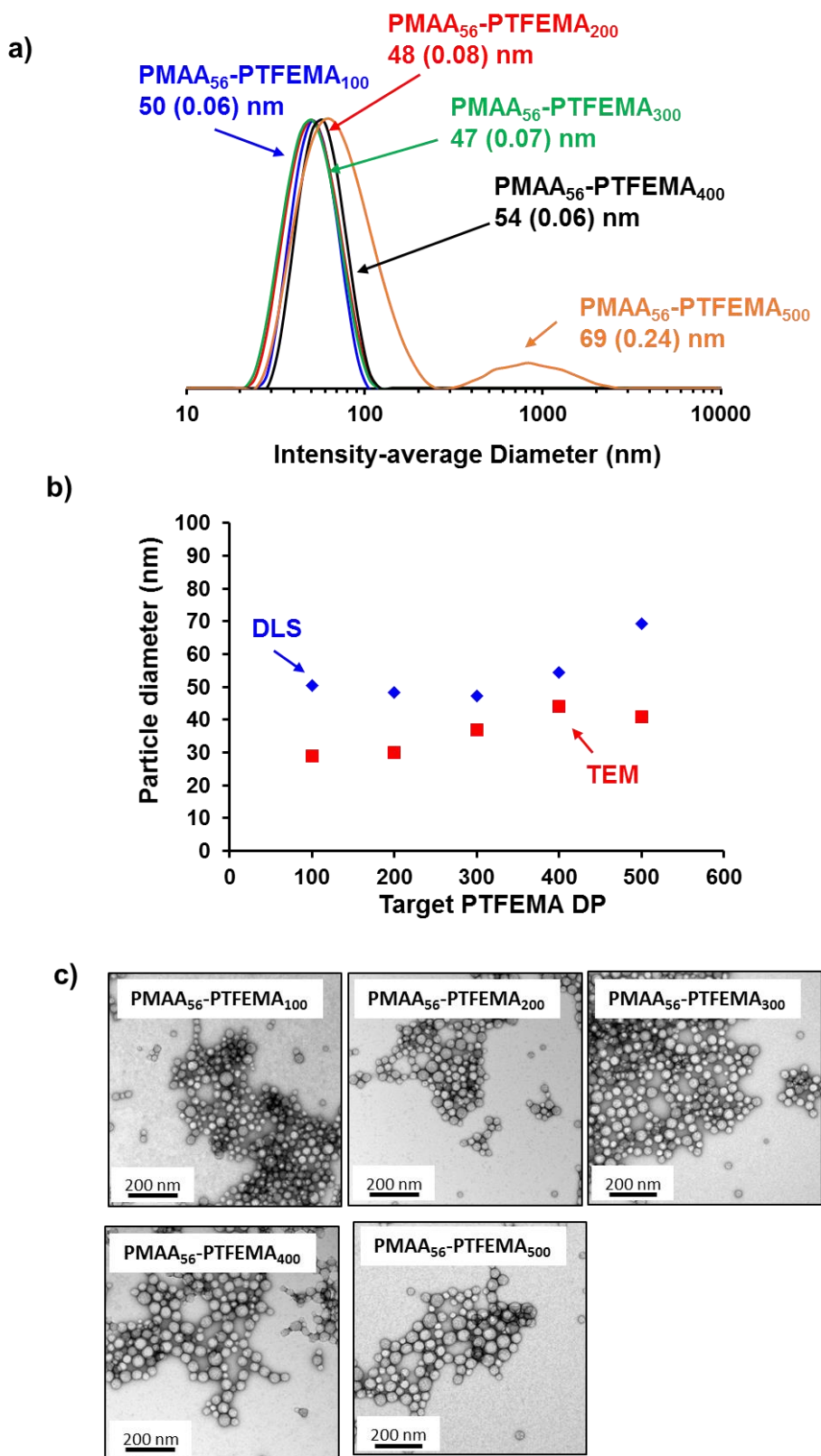
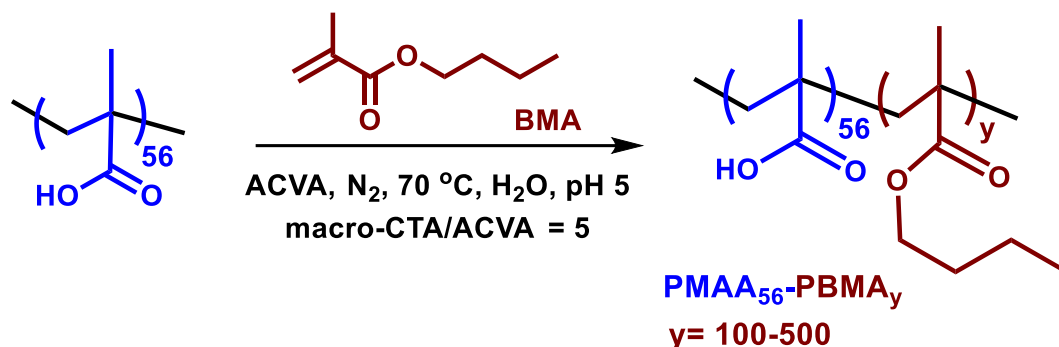


Figure 2.17 Characterization of PMAA₅₆-PTFEMA_y diblock copolymers ($y = 100-500$) prepared at 20% w/w copolymer concentration *via* RAFT aqueous emulsion polymerization: (a) DLS traces, (b) mean particle diameter vs. PTFEMA DP and (c) TEM images showing well-defined spherical nanoparticles.

2.4.7.2. *Synthesis of PMAA₅₆-PBMA_y diblock copolymer nanoparticles via RAFT aqueous emulsion polymerization at 20% w/w copolymer concentration*



Scheme 2.4 Synthesis of poly(methacrylic acid)-poly(butyl methacrylate) diblock copolymer nanoparticles *via* RAFT aqueous emulsion polymerization of butyl methacrylate at 70 °C.

Secondly, a series of PMAA_x-PBMA_y diblock copolymer nanoparticles was prepared *via* RAFT aqueous emulsion polymerization at 70 °C (Scheme 2.4). All reactions were performed at a macro-CTA/ACVA molar ratio of 5.0 and at 20% w/w copolymer concentration at pH 5. The target PBMA DP was varied from 100 to 500 and the resulting diblock copolymers were analyzed by ¹H NMR spectroscopy, THF GPC, DLS and TEM, see Table 2.8. The aqueous solubility of BMA is comparable to that of TFEMA (~3 g dm⁻³) but unlike BzMA and TFEMA, BMA is less dense than water (0.89 g cm⁻³). Instead of sedimenting at the bottom of the aqueous phase, the monomer droplets cream above the aqueous phase. It is therefore important to ensure that adequate stirring is applied to the reaction vessel to form sufficiently small monomer droplets in the early stages of the polymerization. Without this precaution, free radical polymerization could occur inside the monomer droplets resulting in suspension polymerization, rather than emulsion polymerization.

Table 2.8 Monomer conversions, number-average molecular weights (M_n), dispersities (\mathcal{D}) and mean DLS and TEM diameters obtained for a series of PMAA₅₆-PBMA_y diblock copolymer nanoparticles ($y = 100 - 500$) prepared at 20% w/w copolymer concentration.

Target	Conversion ^a (%)	M_n^b (g mol ⁻¹)	\mathcal{D}^b	DLS particle diameter (nm)	DLS polydispersity	TEM particle diameter (nm)
PMAA ₅₆ -PBMA ₁₀₀	99	18,600	2.44	41	0.08	24
PMAA ₅₆ -PBMA ₂₀₀	99	34,300	2.28	48	0.13	27
PMAA ₅₆ -PBMA ₃₀₀	99	47,600	1.98	47	0.17	30
PMAA ₅₆ -PBMA ₄₀₀	99	62,000	1.88	47	0.16	32
PMAA ₅₆ -PBMA ₅₀₀	99	127,800	1.69	40	0.17	28

^aMonomer conversions determined by ¹H NMR spectroscopy.

^bDetermined by THF GPC analysis on methylated copolymer samples relative to a series of near-monodisperse PMMA standards.

Monomer conversions of more than 99% were achieved in all syntheses, as judged by ¹H NMR spectroscopy studies in *d*₆-DMSO. THF GPC analysis of the methylated diblock copolymers indicated an increase in M_n with PBMA DP and good blocking efficiency for PBMA DP 200 to 500, see Figure 2.18. However, the dispersities are higher than expected ($1.69 \leq \mathcal{D} \leq 2.44$). In particular, the GPC chromatogram for PMAA₅₆-PBMA₁₀₀ is particularly broad and indicates poor blocking efficiency. The decrease in dispersity with PBMA DP presents an interesting trend. As the PBMA DP increases the relative fraction of the PMAA block decreases. This could suggest that the methylation protocol is not ideal for this series of block copolymers resulting in interactions between the PMAA residues and the column. These interactions will be more significant for the diblock copolymers with lower PBMA DP and thus, a higher relative fraction of PMAA.

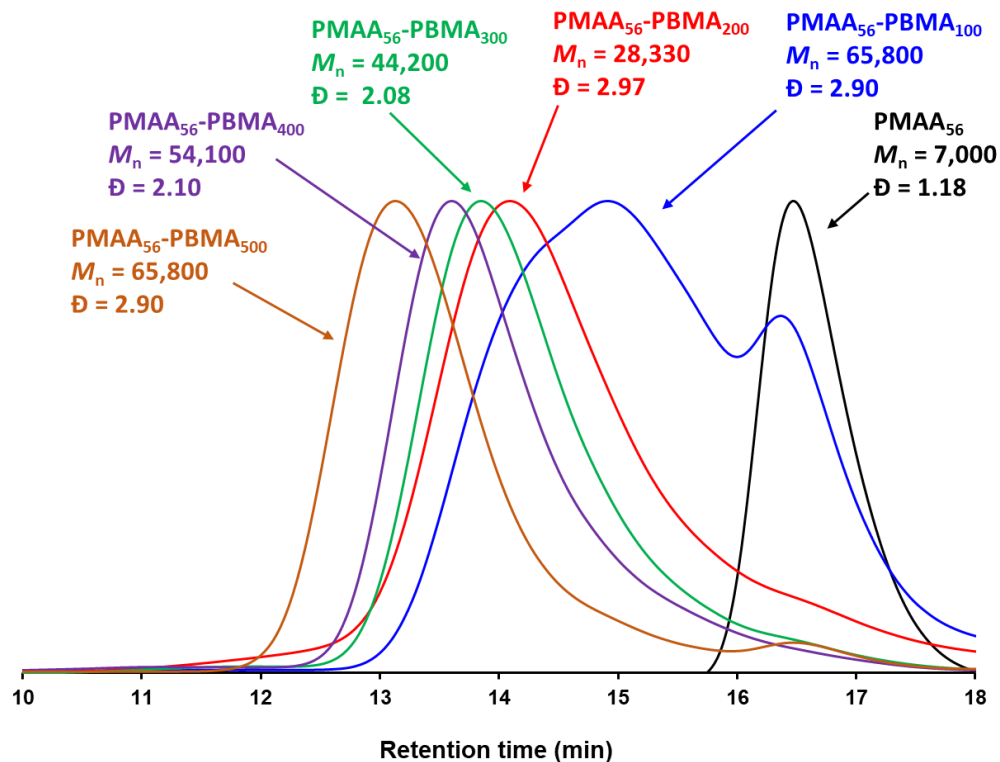


Figure 2.18 THF GPC chromatograms of methylated PMAA₅₆-PBMA_y diblock copolymers ($y = 100 - 500$) synthesized *via* RAFT aqueous emulsion polymerization. All molecular weight data was calculated relative to a series of near-monodisperse PMAA standards.

Sterically-stabilized nanoparticles were formed during the polymerization owing to the amphiphilic nature of the PMAA_x-PBMA_y chains. However, analysis by both DLS and TEM (Table 2.8 and Figure 2.19) indicated that only spherical nanoparticles were obtained. Strangely, the particle diameter did not increase with PBMA DP as expected but remained relatively constant. This is observed by both DLS and TEM. Either the core-forming chains are becoming more closely packed together at high PBMA DPs or more nanoparticles are formed at the beginning of the polymerization resulting in less diblock copolymer chains per nanoparticle at the end of the polymerization. This behavior was also reported for the RAFT aqueous emulsion polymerization of TFEMA.

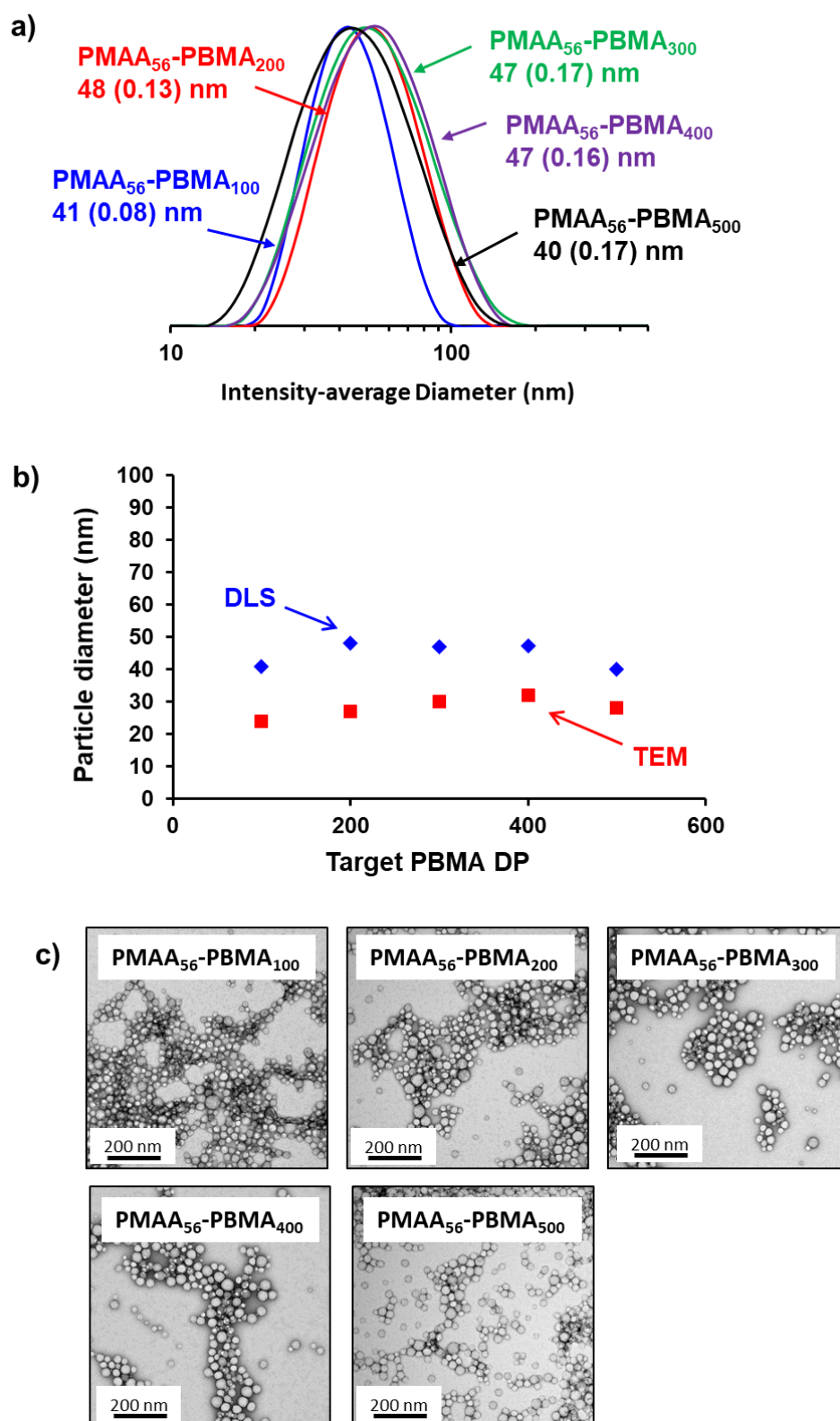
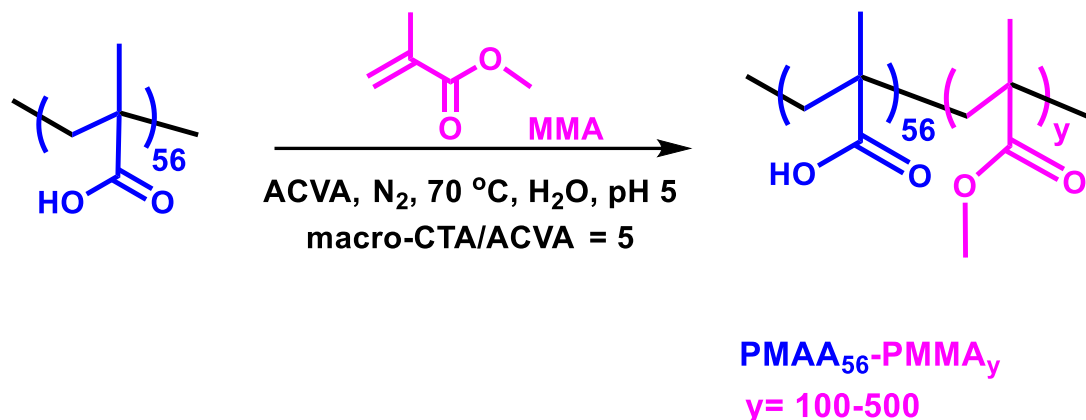


Figure 2.19 Characterization of PMAA₅₆-PBMA_y diblock copolymers ($y = 100 - 500$) prepared at 20% w/w copolymer concentration *via* RAFT aqueous emulsion polymerization of BMA: (a) DLS traces, (b) mean particle diameter vs. target PBMA DP and (c) TEM images showing well-defined spherical nanoparticles.

2.4.7.3. *Synthesis of PMAA₅₆-PMMA_y diblock copolymer nanoparticles via RAFT aqueous emulsion polymerization of MMA at 20% w/w copolymer concentration*



Scheme 2.5 Synthesis of poly(methacrylic acid)-poly(methyl methacrylate) diblock copolymer nanoparticles via RAFT aqueous emulsion polymerization at 70 °C.

The RAFT aqueous emulsion polymerization of MMA at 70 °C (Scheme 2.5) was investigated. All reactions were performed at a macro-CTA/ACVA molar ratio of 5.0 and a copolymer concentration of 20% w/w, at pH 5. The target PMMA DP was varied from 40 to 3000 and the resulting diblock copolymers were analyzed by ¹H NMR spectroscopy, THF GPC, DLS and TEM, see Table 2.9. The aqueous solubility of MMA (~15 g dm⁻³) is five times higher than that of BMA and TFEMA (~3 g dm⁻³). All syntheses yielded relatively high monomer conversions (≥ 95%), as judged by ¹H NMR studies. The PMAA₅₆-PMMA_y diblock copolymers were methylated prior to THF GPC analysis. Assuming complete methylation, this modification effectively converts the PMAA₅₆-PMMA_y diblock copolymer to PMMA_{56+y} homopolymers. As PMMA calibration standards are used to calculate the molecular weight and dispersity of these homopolymers, the resulting data should have no systematic error. THF GPC analyses indicate a linear increase in molecular weight with PMMA DP, see Figure 2.20. High blocking efficiencies were observed in all cases with reasonable control being maintained (1.46 ≤ Đ ≤ 2.00). A close correlation between the theoretical M_n and the measured M_n of the methylated PMAA₅₆-PMMA_y diblock copolymers was observed, see Figure 2.20.

Chapter 2: Synthesis of Diblock Copolymer Nanoparticles via RAFT-Mediated PISA in Water

Table 2.9 Monomer conversions, number-average molecular weights (M_n), dispersities (\mathcal{D}) and mean DLS, and TEM diameters for a series of PMAA₅₆-PMMA_y diblock copolymer nanoparticles ($y = 20$ -3000) prepared at 20% w/w copolymer concentration. Conditions: 70 °C, pH 5, macro-CTA/ACVA molar ratio = 5.0

Target Composition	Conversion (%) ^a	Theoretical M_n^b	M_n^c (g mol ⁻¹)	\mathcal{D}^c	DLS particle diameter (nm)	DLS particle polydispersity	TEM particle diameter (nm)	T_g^d (°C)
PMAA ₅₆ -PMMA ₄₀	99	9,100	3,800	2.00	24	0.14	14	116
PMAA ₅₆ -PMMA ₆₀	99	11,100	5,900	1.89	24	0.14	16	140
PMAA ₅₆ -PMMA ₈₀	99	13,000	7,600	1.84	24	0.15	17	115
PMAA ₅₆ -PMMA ₁₀₀	99	15,000	14,800	1.46	26	0.16	16	118
PMAA ₅₆ -PMMA ₂₀₀	99	24,900	24,200	1.71	36	0.36	21	121
PMAA ₅₆ -PMMA ₃₀₀	99	34,800	35,000	1.89	45	0.09	31	121
PMAA ₅₆ -PMMA ₄₀₀	99	44,800	45,000	1.79	49	0.10	35	123
PMAA ₅₆ -PMMA ₅₀₀	99	54,700	50,600	1.78	58	0.09	43	125
PMAA ₅₆ -PMMA ₈₀₀	99	84,400	93,600	1.58	70	0.14	41	126
PMAA ₅₆ -PMMA ₁₀₀₀	94	99,000	114,700	1.53	74	0.11	56	125
PMAA ₅₆ -PMMA ₁₅₀₀	99	153,800	149,300	1.59	84	0.09	69	127
PMAA ₅₆ -PMMA ₃₀₀₀	88	268,700	280,800	1.65	125	0.03	105	127

^aMonomer conversions determined by ¹H NMR spectroscopy.

^bTheoretical M_n of diblock copolymers, based on conversion by NMR.

^cDetermined by THF GPC analysis on methylated copolymers relative to a series of near mono-disperse PMMA standards

^dDetermined by DSC

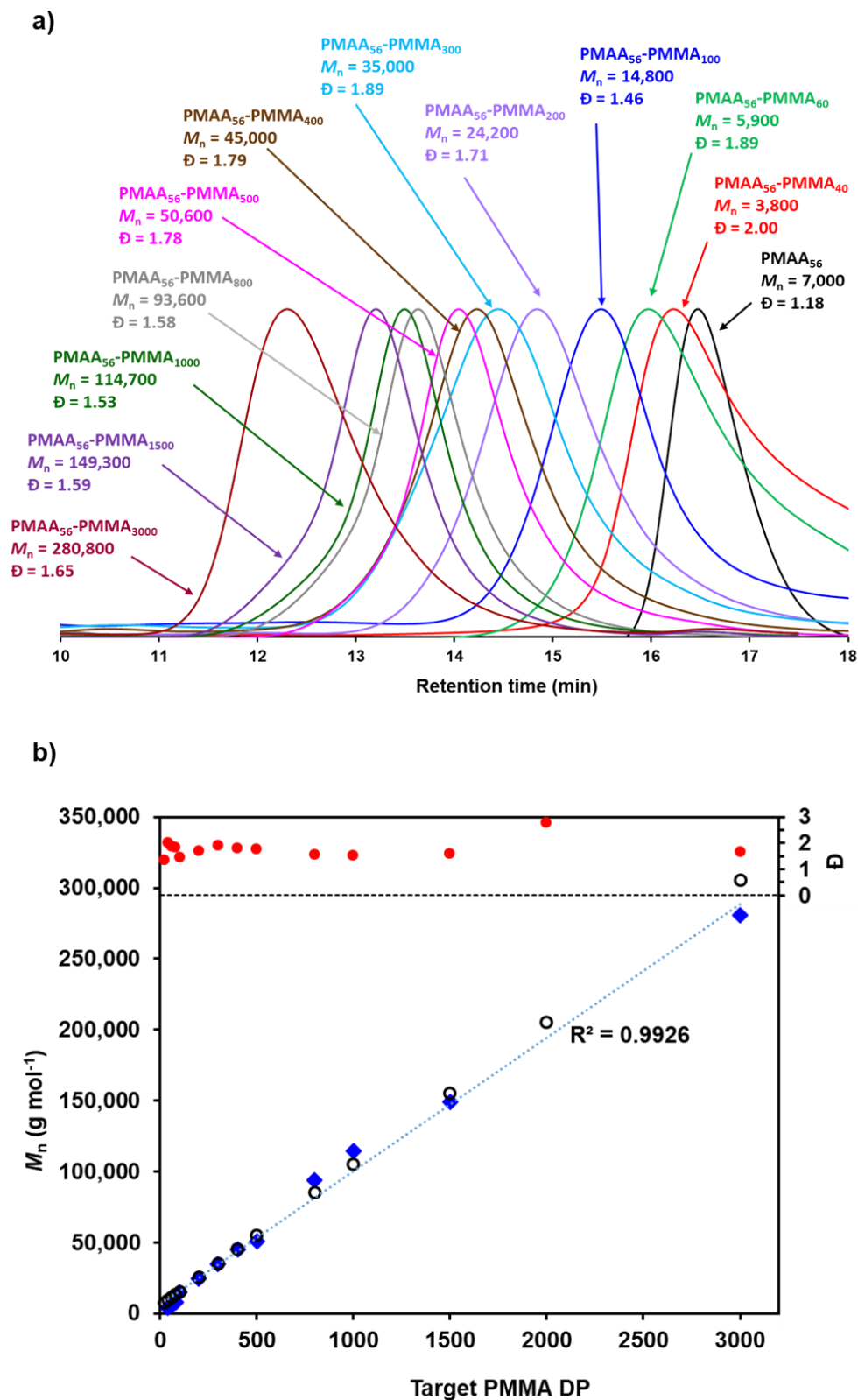


Figure 2.20 THF GPC analysis of methylated $PMAA_{56}-PMMA_y$ diblock copolymers synthesized via RAFT aqueous emulsion polymerization of MMA; (a) THF GPC chromatograms and (b) molecular weight (M_n) and dispersity (\bar{D}) with PMMA DP, where measured M_n = blue filled circles, theoretical M_n = open black circles and \bar{D} = red filled circles. Molecular weights are relative to a series of near-monodisperse PMMA standards.

The particle diameter increases linearly with PMMA DP from 24 nm at DP 40 to 58 nm at PMMA DP 500. Above PMMA DP 500, the particle diameter continues to increase with PMMA DP up to 125 nm at DP 3000 (see Figure 2.22). Similar trends are observed by both DLS and TEM. TEM studies of the PMAA₅₆-PMMA_y diblock copolymer nanoparticles indicated that only spherical nanoparticles were obtained, even for highly asymmetric block compositions ($y = 1000 - 3000$), see Figure 2.22. This demonstrates that, although MMA has a significantly higher aqueous solubility than BzMA (13 g dm^{-3} vs. 0.40 g dm^{-3}), it is still not sufficiently soluble to enable plasticization of the core on the timescale of the polymerization, which is hypothesized to be important for the synthesis of higher order morphology nanoparticles.¹⁸

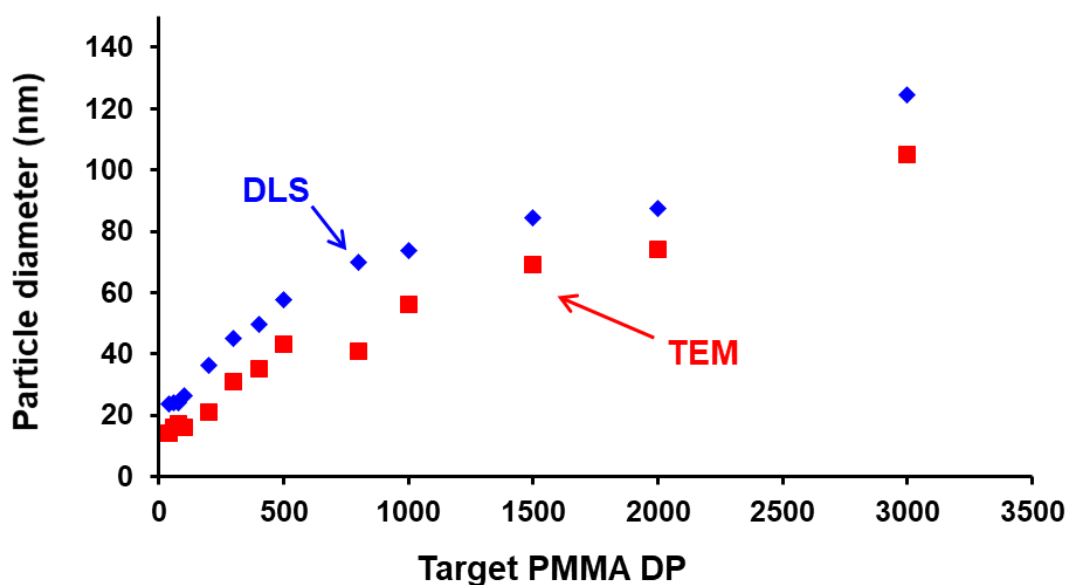


Figure 2.21 Plot of DLS and TEM particle diameter against target PMMA DP showing a linear increase in particle diameter with PMAA DP.

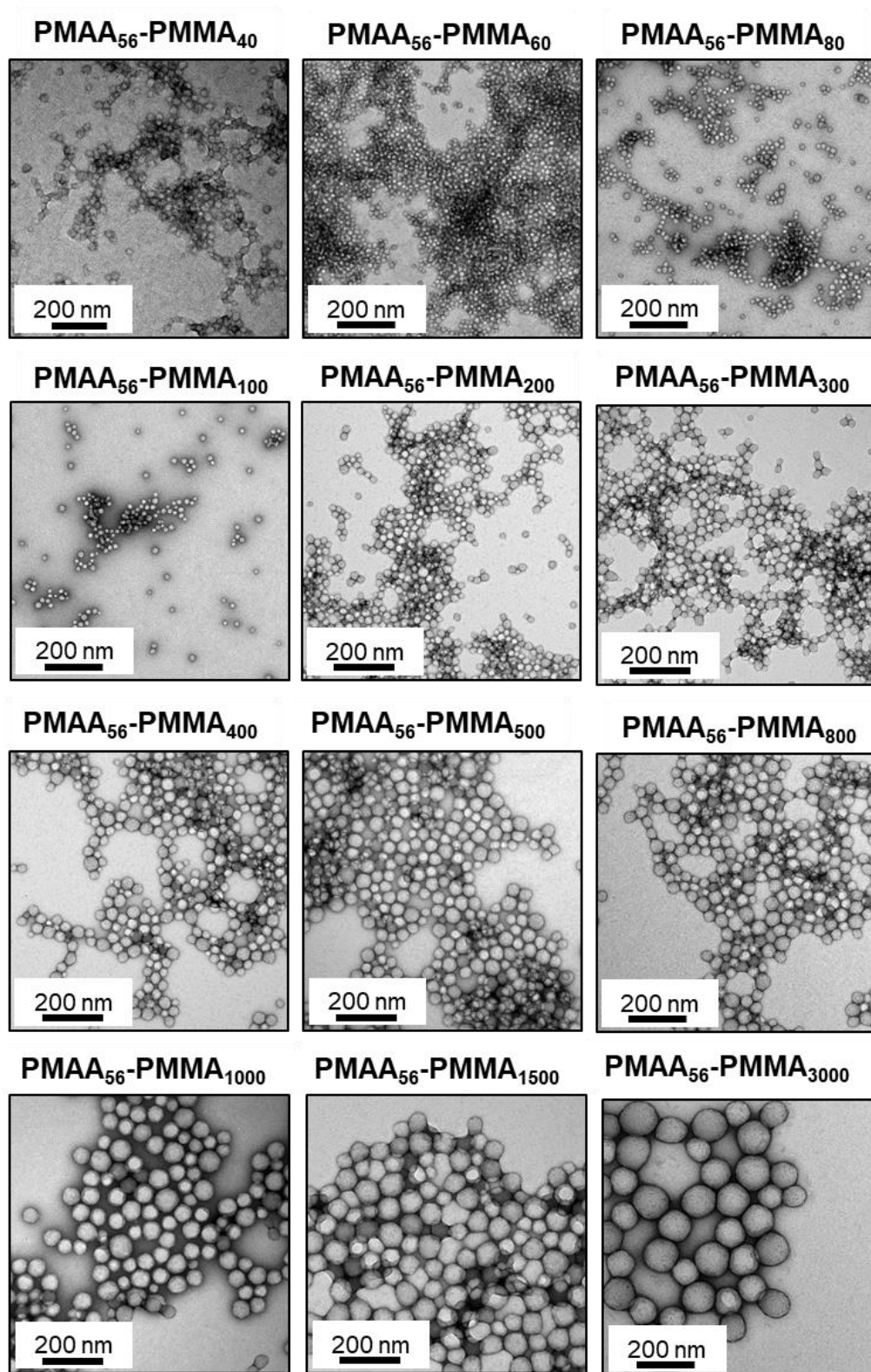


Figure 2.22 TEM images of PMAA₅₆-PMMA_y diblock copolymer nanoparticles (y = 40-3000) prepared at 20% w/w copolymer concentration *via* RAFT aqueous emulsion polymerization of MMA at 70 °C, showing well-defined spherical nanoparticles.

The glass transition temperature (T_g) corresponds to the temperature at which a synthetic polymer transitions from a glass to a rubber state.^{76, 77} Above the T_g polymer chains have sufficient energy to enable chain mobility and limited bond rotation, thus the polymer is in a rubbery state. Below the T_g polymer chain segments are frozen and large scale motions are absent, thus the polymer becomes a glass. The T_g of a polymer depends on its molecular weight, as described by the Flory-Fox Equation (see Equation 2.1), where $T_{g,\infty}$ is the maximum glass transition temperature that can be achieved at a theoretically infinite molecular weight and K is an empirical parameter that is related to the free volume present in the polymer sample.^{78, 79}

$$T_g = T_{g,\infty} - \frac{K}{M_n} \quad 2.1$$

The relationship between T_g and molecular weight is shown in Figure 2.22.

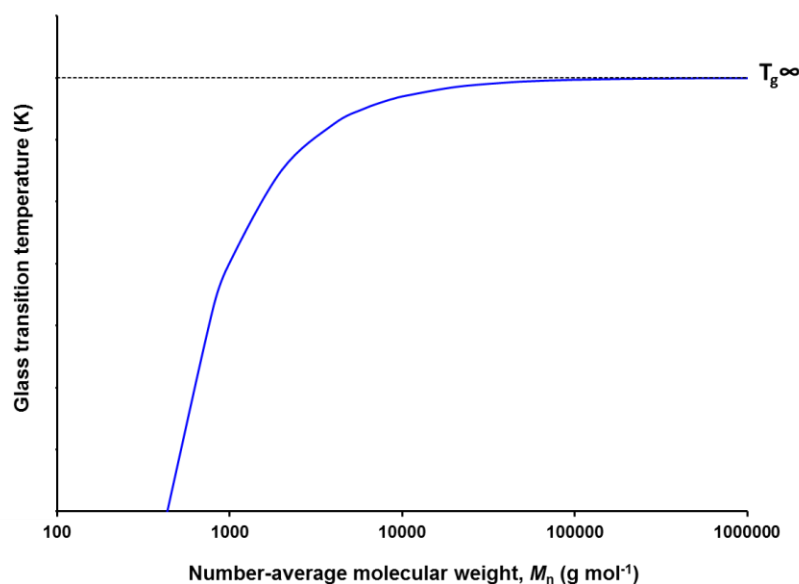


Figure 2.23 Schematic plot demonstrating the relationship between number-average molecular weight (M_n) and glass transition temperature (T_g) as predicted by the Flory-Fox equation, where $T_{g,\infty}$ is the maximum glass transition temperature that can be achieved at a theoretically infinite molecular weight.^{78, 79}

Many techniques can be used to determine T_g including DSC, thermo mechanical analysis or dynamic mechanical analysis. The T_g of the PMAA₅₆-PMMA_y diblock copolymers was determined by differential scanning calorimetry (DSC). The literature value for the T_g of PMMA is between 105 and 120 °C,⁷⁰ which represents the high

molecular weight limit ($T_{g,\infty}$). As some of PMAA₅₆-PMMA_y diblock copolymers in this series are of relatively low molecular weight (14,800 to 281,000 g mol⁻¹) it was thought that the relationship between DP and T_g , suggested in Figure 2.23, might be observed. More specifically, the T_g should increase with PMAA DP before reaching a plateau value of 120 °C. However, this relationship was not observed. DSC analyses indicated that over this molecular weight range the measured T_g value corresponds to the literature value of 120 °C, see Figure 2.24. A small increase in T_g was observed (116 to 127 °C) as the PMMA DP was increased from 40 to 3000. An unusually high T_g value was recorded for the PMAA₅₆-PMMA₆₀ diblock copolymer of 140 °C.

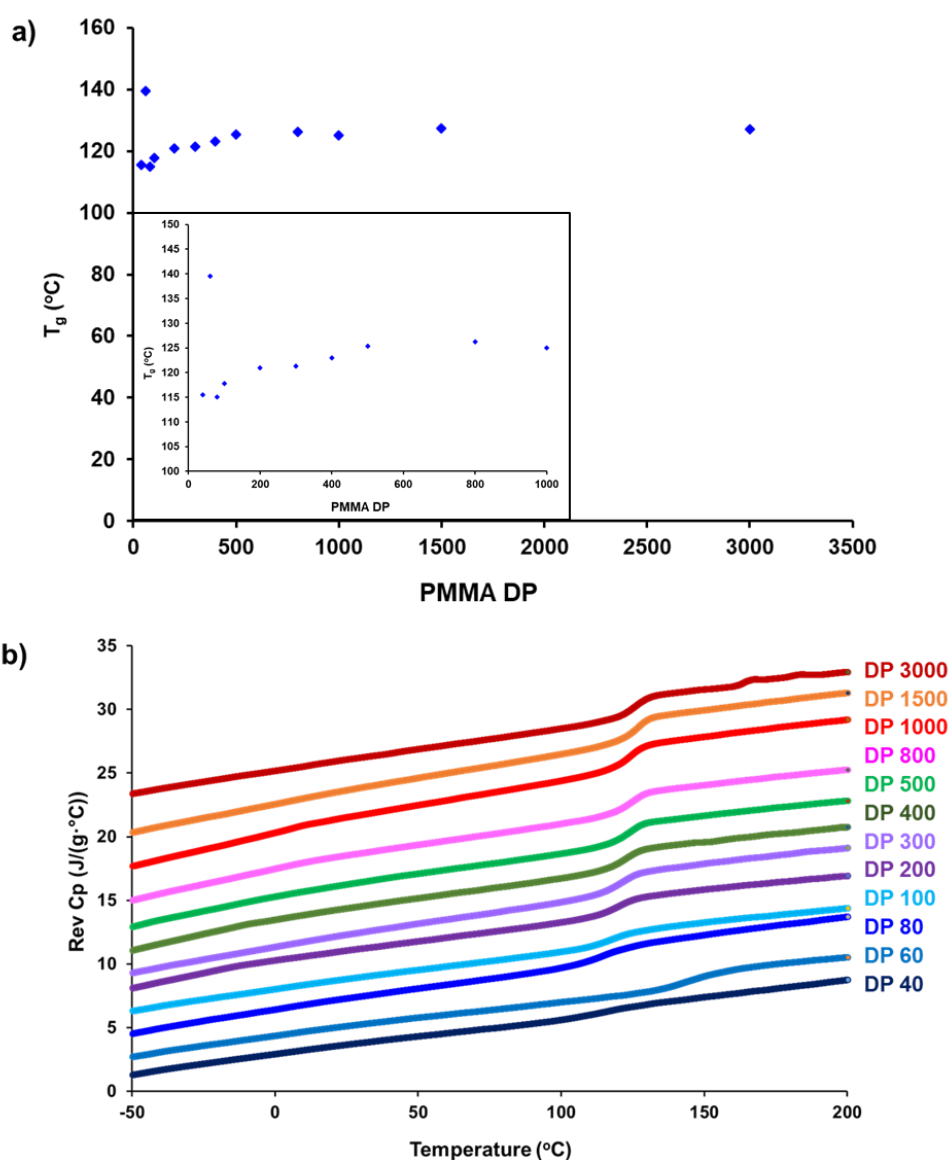


Figure 2.24 (a) Glass transition temperature (T_g) values vs. PMMA DP (40 to 3000) and (b) DSC traces for a series of PMAA₅₆-PMMA_y diblock copolymers synthesized *via* RAFT aqueous emulsion polymerization, where $y = 40$ to 3000.

PMAA₅₆-PMMA₂₀₀ diblock copolymer nanoparticles were evaluated as Pickering emulsifiers, see Table 2.10.^{80, 81} In a Pickering emulsion, oil or water droplets are stabilized by a layer of solid particles adsorbed onto the surface of the droplet. Polymer latex particles⁸²⁻⁸⁵ as well as inorganic clays⁸⁶⁻⁸⁹ and silica⁹⁰⁻⁹² can be used as Pickering emulsifiers. In this case, PMAA₅₆-PMMA₂₀₀ diblock copolymer nanoparticles were used to stabilize oil in water emulsions.

Table 2.10 Details of Pickering emulsions prepared using PMAA₅₆-PMMA₂₀₀ diblock copolymer nanoparticles and the resulting mean droplet diameters.

Oil	Polymer concentration (% w/w)	pH of polymer dispersion before emulsification	Emulsion adjusted to pH	Mean droplet diameter (μm)	Standard deviation
methyl myristate	2.0	2	-	25.0	13.8
	1.5	2	-	24.1	13.7
	1.0	2	-	33.0	26.9
	0.5	2	-	47.8	32.7
	0.1	2	-	85.8	28.7
	0.05	2	-	92.7	29.7
squalene	2.0	2	-	43.9	16.4
	1.5	2	-	50.1	37.5
	1.0	2	-	50.6	38.3
	0.5	2	-	50.5	39.9
	0.1	2	-	91.6	22.8
	0.05	2	-	134.0	36.9
methyl myristate	2.0	2	-	25	14
	2.0	5	-	91	37
	2.0	8	-	38	28
	2.0	2	5	29	23
	2.0	2	8	27	16

Two oils were investigated; methyl myristate and squalene. Initially, emulsions were made using a dispersion of the polymer particles at pH 2. Under these conditions the PMAA residues would be fully protonated and the particles would most likely be aggregated due to a loss of electrosteric stabilization. This pH was chosen as it was thought that the presence of anionic charge on the nanoparticles would hinder their ability to act as efficient Pickering emulsifiers. For each oil six emulsions were prepared utilizing different concentrations of the diblock copolymer nanoparticles (0.05 to 2.0% w/w) and the mean droplet diameter of the resulting emulsions was measured. In both cases, smaller oil droplets were observed at higher copolymer concentrations, see Figure 2.25. This trend has been previously reported for other polymer particles and is indicative of a Pickering emulsifier.^{83, 85}

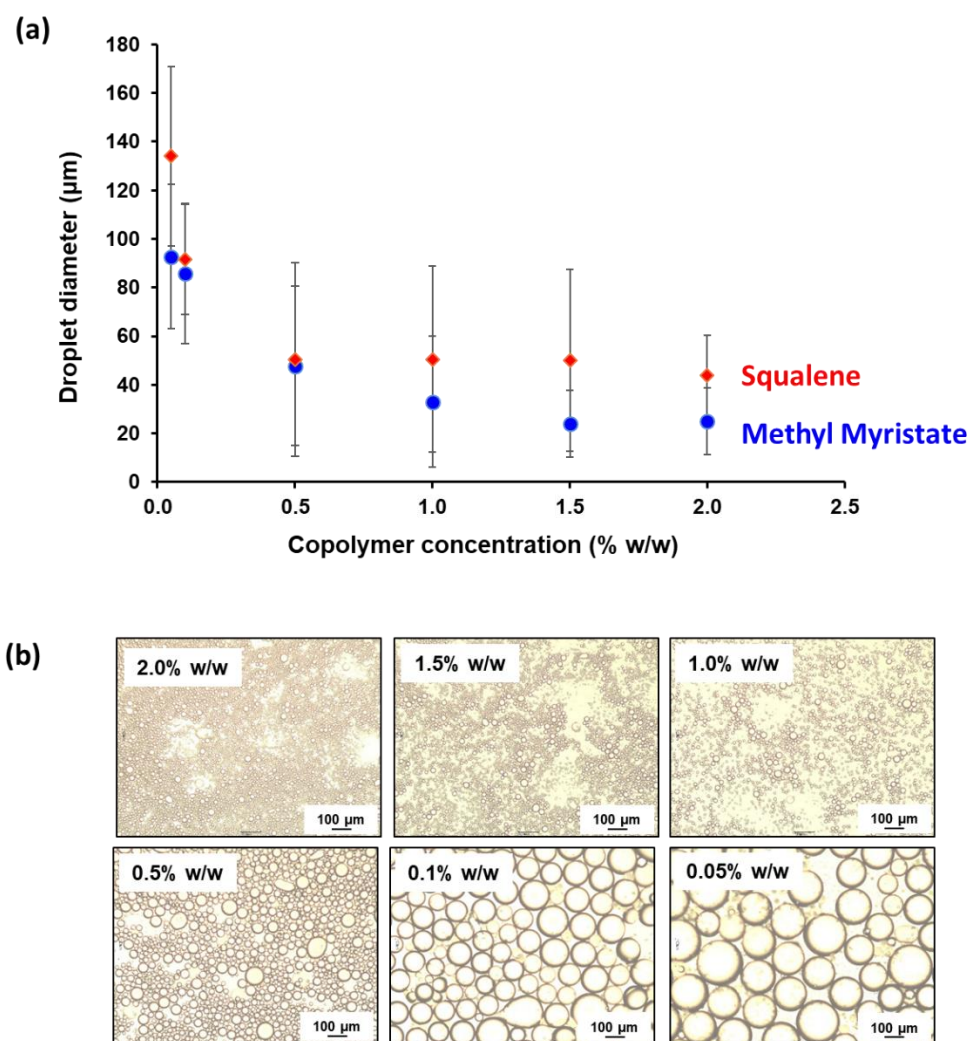


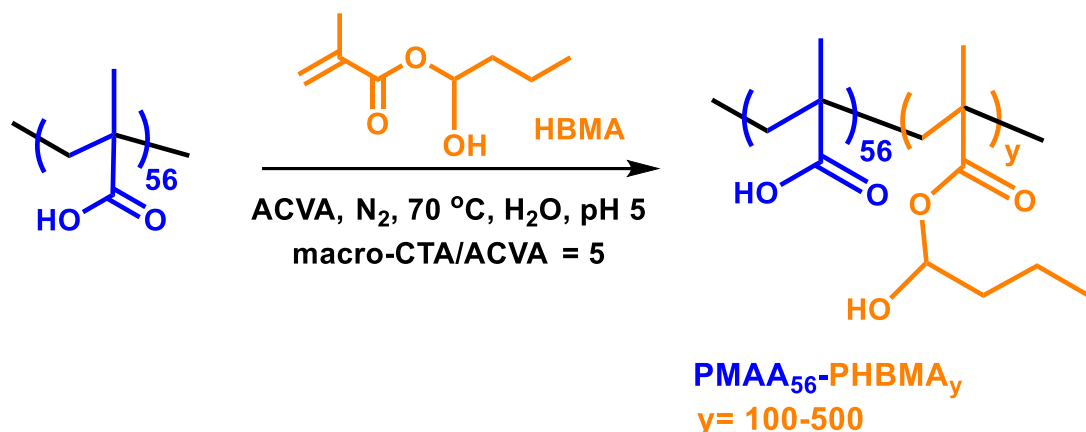
Figure 2.25 (a) mean droplet diameter vs. copolymer concentration for oil in water emulsions stabilized by PMAA₅₆-PMMA₂₀₀ diblock copolymer nanoparticles (at pH 2) made with squalene or methyl myristate. (b) optical microscopy images recorded for emulsion made using methyl myristate.

This behavior also indicates that the PMAA₅₆-PMMA₂₀₀ diblock copolymer nanoparticles are stable to the high shear used during homogenization. If the nanoparticles were not stable, they would dissociate into linear chains resulting in an approximately equal mean droplet diameter being observed at each copolymer concentration.⁸⁴ This has been previously observed for PGMA-PPMA diblock copolymer nanoparticles where crosslinking prior to homogenization was required to prevent dissociation into chains.⁸⁴ Alternatively, utilizing a more hydrophobic PBzMA block enabled the synthesis of nanoparticles with strong hydrophobic interactions that can withstand the high shear of homogenization.⁸⁴ Therefore, our results indicate the PMMA is sufficiently hydrophobic to prevent dissociation of the nanoparticles on homogenization.

The effect of pH on Pickering emulsifier ability was also investigated see Table 2.10. Firstly, methyl myristate in water emulsions were made using a dispersion of PMAA₅₆-PMMA₂₀₀ nanoparticles (2.0% w/w) at pH 5 and at pH 8. The emulsion formed using nanoparticles at pH 5 resulted in a considerable increase in mean droplet diameter relative to the nanoparticles at pH 2 (91 μm vs. 25 μm respectively). This increase in diameter is likely as a result of electrostatic repulsion between neighboring nanoparticles owing to the increased anionic charge. In comparison, the emulsion formed at pH 8 resulted in a smaller mean droplet diameter of 38 μm . This seems surprising owing to the increase negative charge of the diblock copolymer nanoparticles. However, it is well-known that PMAA chains undergo a conformational transition at pH \sim 6.5. Below pH 6.5 PMAA chains are in a hypercoiled confirmation whereas above pH 6.5 the increased ionization of the chains leads to a more extended structure.^{16, 62} Perhaps the PMAA stabilizer chains of the PMAA₅₆-PMMA₂₀₀ diblock copolymer nanoparticles become more extended at pH 8 allowing the nanoparticles to pack closer together and stabilize smaller emulsion droplets.

The pH response of the emulsion was also explored. The methyl myristate-in-water emulsion formed at pH 2 (2.0% w/w polymer concentration) was adjusted to pH 5 and pH 8 after homogenization. It was hypothesized that the change in ionization of the PMAA chains would cause desorption of the nanoparticles from the oil-water interface resulting in demulsification. However, this was not observed and there was minimal change in the mean droplet diameter (25 – 29 μm).

2.4.7.4. *Synthesis of PMAA₅₆-PHBMA_y diblock copolymer nanoparticles via RAFT aqueous emulsion polymerization of HBMA at 20% w/w copolymer concentration*



Scheme 2.6 Synthesis of PMAA₅₆-PHBMA_y diblock copolymer nanoparticles *via* RAFT aqueous emulsion polymerization of HBMA at 20% w/w copolymer concentration. Conditions: 70 °C, pH 5, macro-CTA/ACVA molar ratio = 5.0.

HBMA has an aqueous solubility of 20 g dm⁻³ at 70 °C, making it the most water-soluble of the five methacrylic monomers investigated so far. A series of PMAA₅₆-PHBMA_y diblock copolymer nanoparticles was synthesized *via* RAFT aqueous emulsion polymerization at 20% w/w copolymer concentration, see Scheme 2.6. All reactions were performed at a macro-CTA/ACVA molar ratio of 5.0 and at pH 5. The target PHBMA DP was varied from 100 to 500 and the resulting diblock copolymers were analyzed by ¹H NMR spectroscopy, DLS and TEM, see Table 2.11.

Table 2.11 Monomer conversions, and mean DLS and TEM diameters for a series of PMAA₅₆-PHBMA_y diblock copolymer nanoparticles (y = 100-500) prepared at 20% w/w copolymer concentration.

Target	Conversion (%)	DLS particle diameter (nm)	DLS particle polydispersity	TEM particle diameter (nm)
PMAA ₅₆ -PHBMA ₁₀₀	> 99	167	0.15	45
PMAA ₅₆ -PHBMA ₂₀₀	> 99	251	0.05	174
PMAA ₅₆ -PHBMA ₃₀₀	> 99	252	0.08	210
PMAA ₅₆ -PHBMA ₄₀₀	> 99	245	0.07	240
PMAA ₅₆ -PHBMA ₅₀₀	> 96	295	0.05	266

^aMonomer conversions determined by ¹H NMR spectroscopy.

All syntheses led to high monomer conversions ($\geq 96\%$), as judged by ^1H NMR studies. GPC analysis could not be conducted for this series, as after methylation the diblock copolymer nanoparticles were insoluble in THF.

Particle size analysis by DLS and TEM showed some interesting results. For each PHBMA DP (100-500) a relatively large particle diameter was recorded by DLS (160 - 300 nm). This suggested that $\text{PMAA}_{56}\text{-PHBMA}_y$ nanoparticles might have a vesicular morphology. TEM analysis of these nanoparticles (PHBMA DP 200-500) also suggested the possible synthesis of vesicles. Large monodisperse particles with some evidence for a membrane were observed, see Figure 2.26. These preliminary results suggest that selection of HBMA as a core-forming block might enable the synthesis of higher order morphologies *via* PISA, indicating that the aqueous solubility of the monomer is indeed a key parameter. This new PISA formulation is investigated in more detail in Chapter 3 of this Thesis.

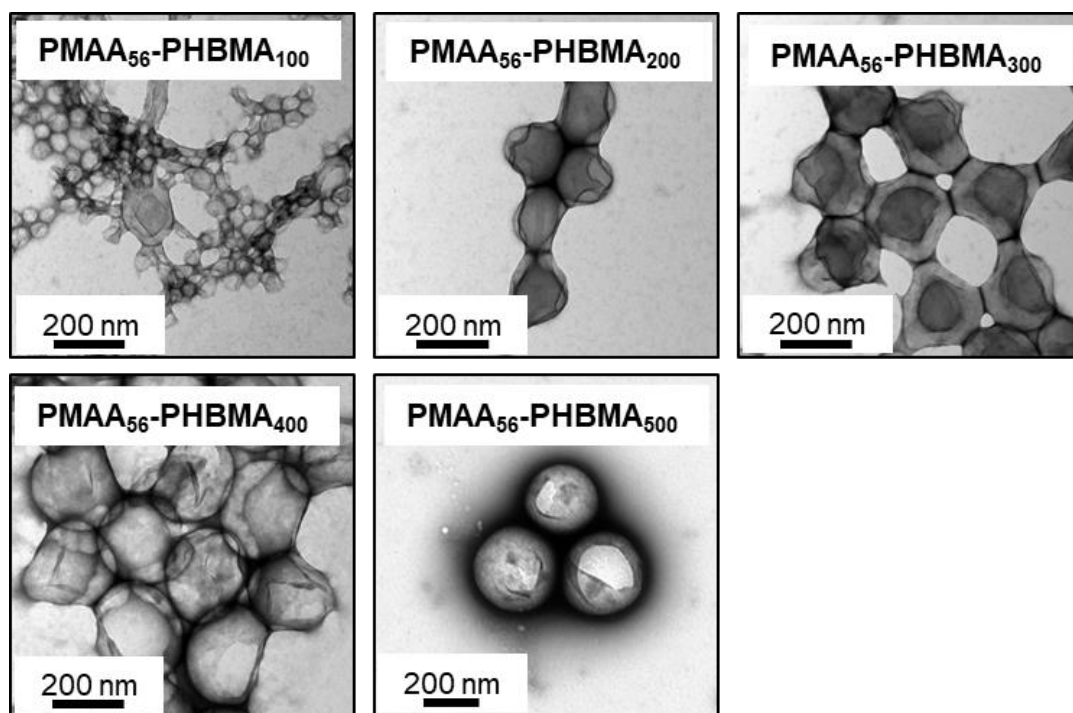
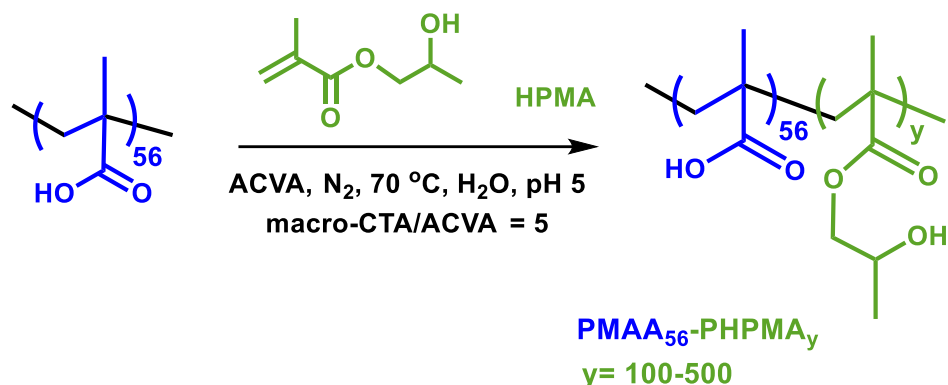


Figure 2.26 TEM images of $\text{PMAA}_{56}\text{-PHBMA}_y$ diblock copolymer nanoparticles synthesized by RAFT aqueous emulsion polymerization of HBMA at 20% w/w copolymer concentration. Conditions: 70 °C, pH 5, macro-CTA/ACVA molar ratio = 5.0

2.4.7.5. Synthesis of PMAA₅₆-PHPMA_y diblock copolymer nanoparticles via RAFT aqueous dispersion polymerization at 20% w/w copolymer concentration



Scheme 2.7 Synthesis of PMAA₅₆-HPMA_y diblock copolymer nanoparticles *via* RAFT aqueous dispersion polymerization of HPMA at 70 °C. Conditions: 20% w/w copolymer concentration, pH 5, macro-CTA/ACVA molar ratio = 5.0.

For comparison, the PMAA₅₆ macro-CTA was also chain-extended with the *water-miscible* monomer HPMA *via* RAFT aqueous dispersion polymerization, see Scheme 2.7. All reactions were performed at 70 °C, using a macro-CTA/ACVA molar ratio of 5.0 targeting 20% w/w copolymer concentration at pH 5. The target PHPMA DP was varied from 100 to 500 and the resulting diblock copolymers were analyzed by ¹H NMR spectroscopy, GPC, DLS and TEM, see Table 2.12.

Table 2.12 Monomer conversions, number-average molecular weights (M_n), dispersities (\mathcal{D}) and mean DLS and TEM diameter for a series of PMAA₅₆-HPMA_y diblock copolymer nanoparticles ($y = 100\text{-}500$) prepared *via* RAFT aqueous dispersion polymerization of HPMA at 20% w/w copolymer concentration.

Target	Conversion ^a (%)	M_n^b (g mol ⁻¹)	\mathcal{D}^b	DLS		TEM
				particle diameter (nm)	DLS polydispersity	particle diameter (nm)
PMAA ₅₆ -HPMA ₁₀₀	> 99	11,100	1.51	178	0.56	18
PMAA ₅₆ -HPMA ₁₅₀	> 99	12,100	2.32	123	0.23	17
PMAA ₅₆ -HPMA ₂₀₀	> 99	19,300	2.31	122	0.13	22
PMAA ₅₆ -HPMA ₂₅₀	> 99	18,300	3.00	148	0.10	96
PMAA ₅₆ -HPMA ₃₀₀	> 99	27,800	3.33	227	0.44	112
PMAA ₅₆ -HPMA ₅₀₀	> 99	34,900	2.52	1523	0.42	> 1000

^aMonomer conversions determined by ¹H NMR spectroscopy.

^bDetermined by THF GPC analysis of copolymers relative to a series of near mono-disperse PMMA calibration standards.

All polymerizations proceeded to $\geq 99\%$ monomer conversion, as judged by ^1H NMR studies. THF GPC analysis of the $\text{PMAA}_{56}\text{-PHPMA}_y$ diblock copolymers reported broad MWDs and poor blocking efficiencies in each case, see Figure 2.27. Further analysis of this diblock copolymer series is required to determine whether the high dispersities reported here ($1.51 \leq \mathcal{D} \leq 3.33$) are truly representative or if the methylation protocol has caused artificial broadening of the MWD. In many of the GPC chromatograms a low molecular weight tail is present, where the trace does not return to the baseline. This could be due to incomplete methylation of the PMAA residues resulting in interactions with the column and a disruption of the size exclusion mechanism. Problems in the methylation of PHPMA-based block copolymer have been observed by previous group members, suggesting that certain monomers may be incompatible with the methylation protocol, leading to artificially high dispersities.⁹³

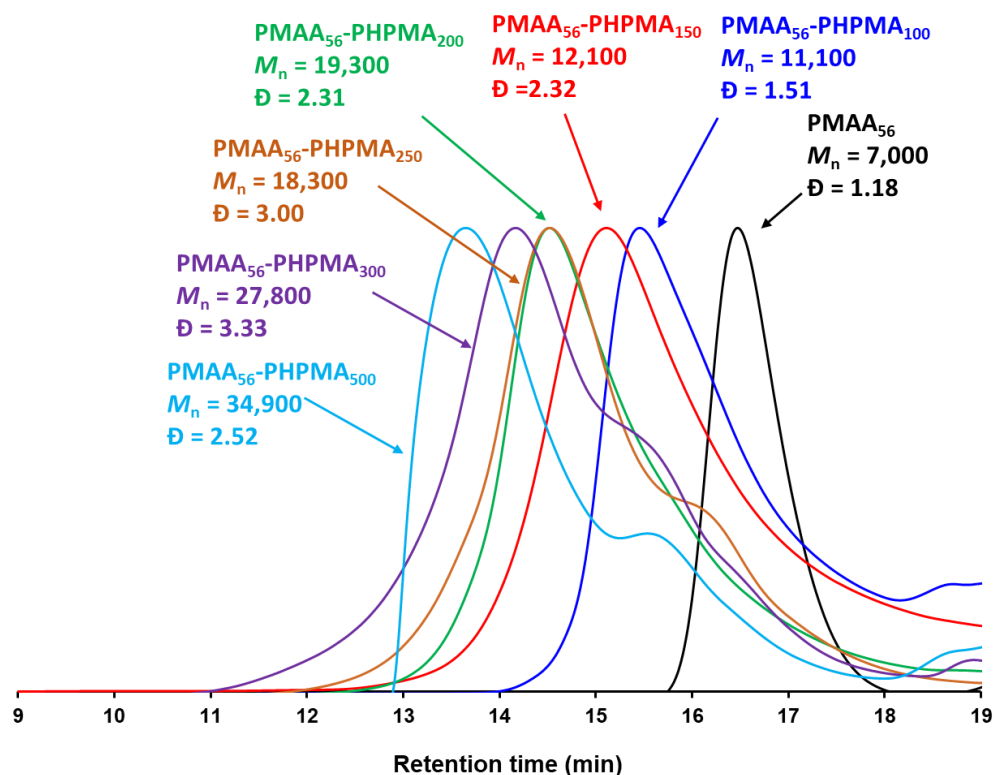


Figure 2.27 THF GPC chromatograms of $\text{PMAA}_{56}\text{-PHPMA}_y$ diblock copolymers ($y = 100$ to 500) synthesized *via* RAFT aqueous dispersion polymerization of HPMA. All molecular weight data calculated relative to a series of near-monodisperse PMAA standards.

DLS analysis indicated that PMAA₅₆-PHPMA_y diblocks with a PHPMA DP of 100 - 250 formed polydisperse spherical nanoparticles of 120 to 180 nm diameter. However, TEM analysis revealed that considerably smaller nanoparticles were formed (18 - 100 nm). The higher particle diameter observed by DLS suggests flocculation of the particles. Targeting a PHPMA DP of 300 led to the formation of larger nanoparticles (~230 nm). On increasing the PHPMA DP up to 500 very large (> 1 μm) spherical nanoparticles are obtained.

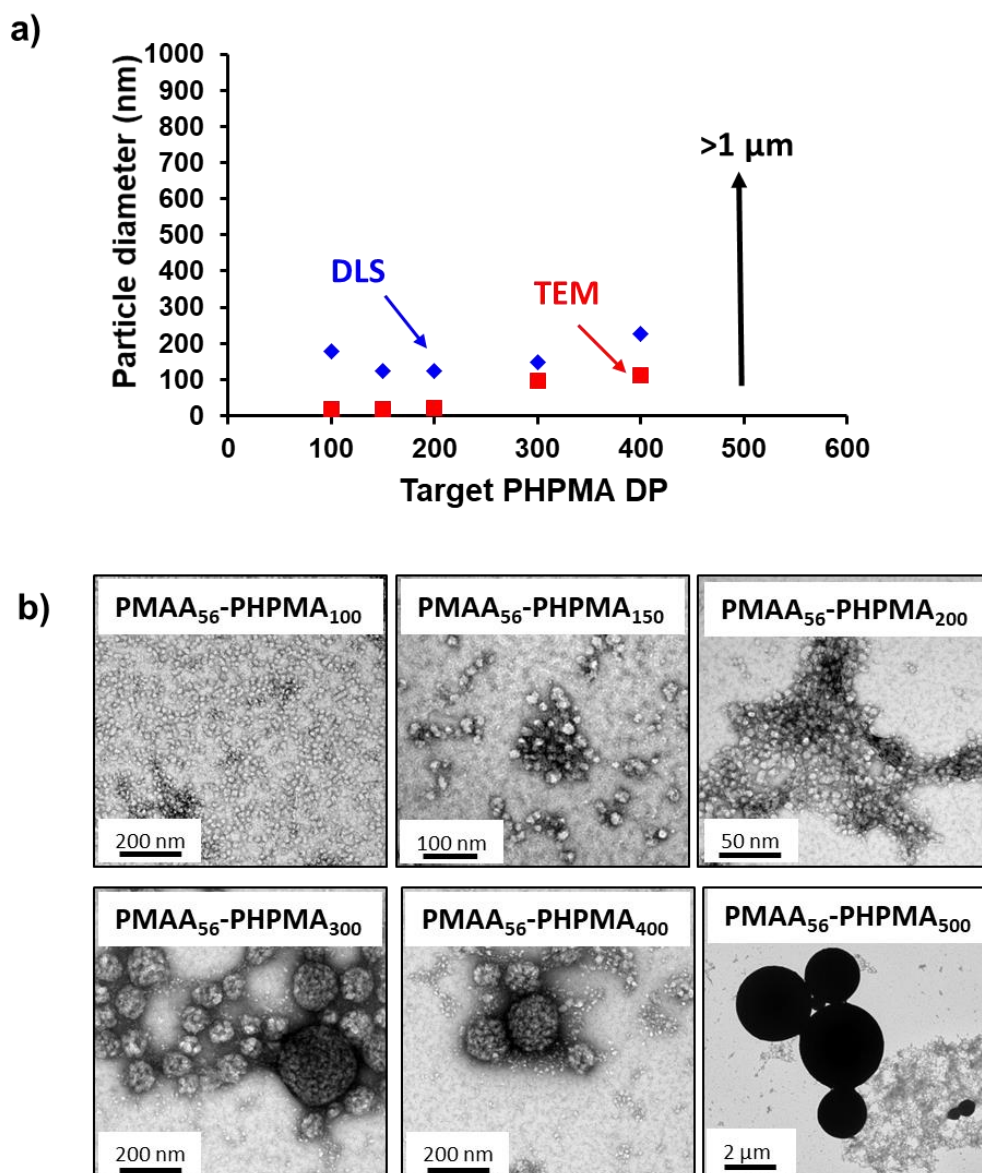


Figure 2.28 Characterization of PMAA₅₆-PHPMA_y diblock copolymer nanoparticles ($y = 100-500$) prepared at 20% w/w copolymer concentration via RAFT aqueous dispersion polymerization of HPMA: (a) mean particle diameter vs. target PHPMA DP by both DLS and TEM and (b) representative TEM images.

Originally, DLS analysis of these PMAA₅₆-PHPMA_y diblock copolymer nanoparticles was performed at pH 8. This pH was selected based on the earlier pH titration of PMAA₅₆-PBzMA₂₀₀ diblock copolymer nanoparticles which indicated that the PMAA chains were highly anionic and hence presumably fully extended under these conditions. TEM analysis of PMAA₅₆-PHPMA₂₅₀ and PMAA₅₆-PHPMA₃₅₀ nanoparticles dried at pH 8 indicated an interesting surface morphology. However, this textured surface is not observed when the particles are analyzed at pH 5, see Figure 2.29. This difference in surface topology might be caused by the markedly differing degrees of ionization of the PMAA chains at pH 5 and pH 8. At pH 5, the PMAA₅₆ chains are only weakly ionized, whereas at pH 8 the PMAA₅₆ chains are almost fully ionized. In the latter, they will be fully-extended taking up more volume. Further analysis of these nanoparticles is required to determine if this observation is an artefact of TEM staining. The change in nanoparticle diameter could be determined by performing a pH titration and monitoring the change in nanoparticle diameter with pH. In addition, SEM analysis could also be used to image the nanoparticles at each pH.

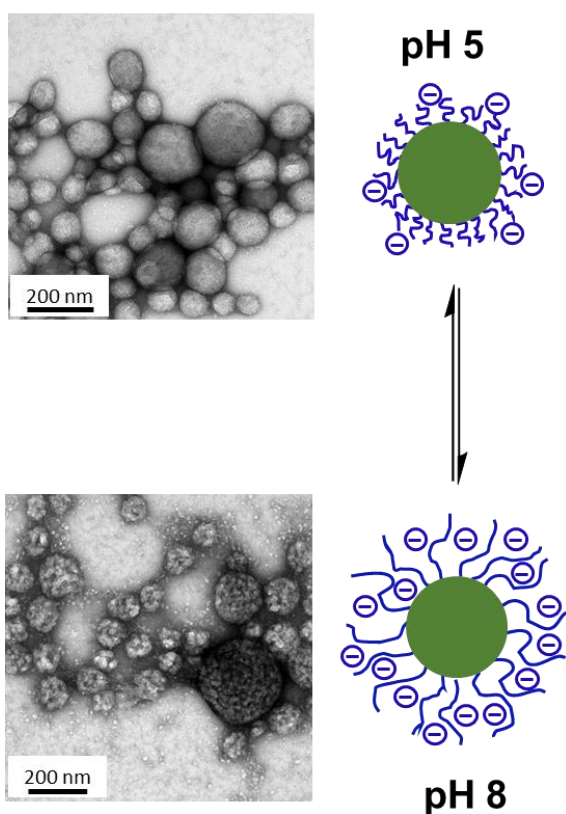


Figure 2.29 Schematic cartoon and TEM images illustrating the apparent change in surface morphology observed for PMAA₅₆-PHPMA₂₅₀ nanoparticles on drying at either pH 5 or pH 8.

2.4.8. Synthesis of PMAA₅₆-PBzMA_y diblock copolymer via RAFT alcoholic dispersion polymerization

PMAA₅₆-PBzMA_y diblock copolymers were also synthesized in ethanol *via* RAFT alcoholic dispersion polymerization at 20% w/w copolymer concentration. These syntheses were performed utilizing the same PMAA₅₆-TTC macro-CTA as in the previous aqueous syntheses, at a macro-CTA/ACVA molar ratio of 5.0. Four different PBzMA DPs were targeted ($y = 50$ to 125) and the resulting diblock copolymers were analyzed by ¹H NMR spectroscopy, GPC, DLS and TEM, see Table 2.13.

Table 2.13 Conversions, number-average molecular weights (M_n), dispersities (\mathcal{D}) and mean DLS diameter for a series of PMAA₅₆-PBzMA_y diblock copolymer nanoparticles ($y = 60$ -160) prepared *via* RAFT alcoholic dispersion polymerization of BzMA at 20% w/w copolymer concentration.

Target Composition	Conversion ^a (%)	M_n^b (g mol ⁻¹)	\mathcal{D}	DLS particle diameter (nm)	DLS particle polydispersity	Morphology
PMAA ₅₆ -PBzMA ₅₀	>99	13,300	1.28	29	0.19	spheres
PMAA ₅₆ -PBzMA ₈₀	>99	17,400	1.33	102	0.26	worms
PMAA ₅₆ -PBzMA ₁₂₅	>99	24,100	1.31	611	0.38	vesicles

^aMonomer conversions determined by ¹H NMR spectroscopy.

^bDetermined by THF GPC analysis of copolymers relative to a series of near mono-disperse PMMA calibration standards.

All polymerizations proceeded to high monomer conversion (>99%), as judged by ¹H NMR spectroscopy in *d*₇-DMF. The polymerizations proceed considerably slower than the equivalent RAFT aqueous emulsion syntheses, requiring a 24 h reaction time to achieve high monomer conversions. THF GPC chromatograms of the methylated block copolymers indicated a linear increase in molecular weight with PBzMA DP, as expected, see Figure 2.30. Importantly, both high blocking efficiencies and low dispersities were observed ($1.28 \leq \mathcal{D} \leq 1.33$). These dispersity values indicate a good level of control over polymerization and are considerably lower than those obtained for the RAFT aqueous emulsion syntheses reported earlier in this Chapter ($1.32 \leq \mathcal{D} \leq 1.89$). These results suggest that the high dispersity values observed for the PMAA_x-PBzMA_y diblock copolymer synthesized *via* RAFT aqueous emulsion polymerization are a result of the polymerization conditions rather than the methylation protocol. Importantly, these results demonstrate the PMAA_x-PBzMA_y

diblock copolymers can be synthesized with a good level of control to give low dispersity polymers.

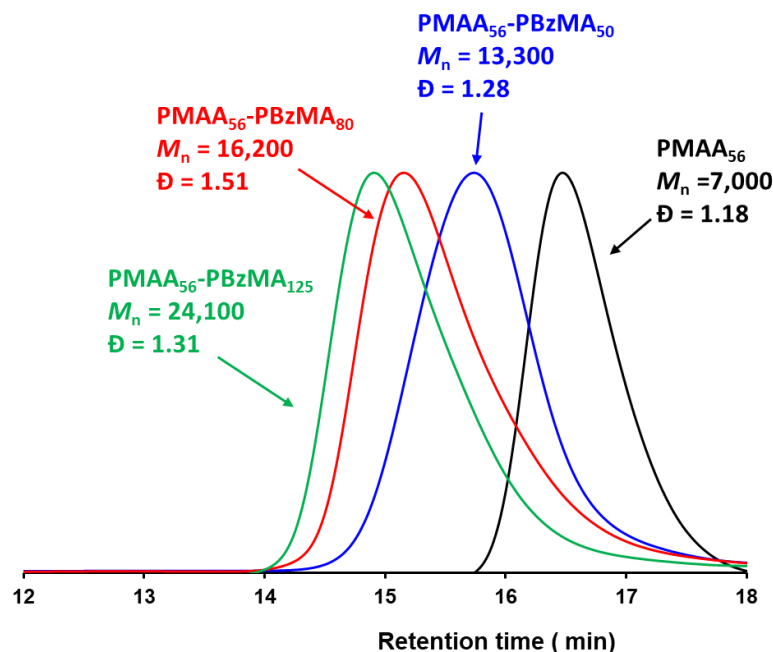


Figure 2.30 THF GPC chromatograms of methylated PMAA₅₆-PBzMA_y diblock copolymer synthesized *via* RAFT alcoholic dispersion polymerization of BzMA at 20% copolymer concentration in ethanol. All molecular weight data are relative to near mono-disperse PMMA standards.

TEM analysis confirmed the formation of nanoparticles by PISA, see Figure 2.31, demonstrating that it is possible to access the full range of nanoparticle morphologies when PMAA₅₆-PBzMA_y diblock copolymers are synthesized in ethanol *via* RAFT alcoholic dispersion polymerization. At the lowest PBzMA DP ($y = 60$), spherical nanoparticles of ~ 30 nm in diameter were obtained. Increasing the PBzMA DP to 80, led to the formation of worms with vesicles being obtained at a PBzMA DP of 125. The only difference between the RAFT aqueous emulsion and the RAFT alcoholic dispersion formulations is the solvent and thus, the monomer solvent solubility. These results clearly indicate the importance of solvent and monomer solubility to the PISA process. The BzMA is significantly more soluble in ethanol and proceeds *via* a RAFT dispersion polymerization. This polymerization is also considerably slower than the analogous RAFT aqueous emulsion polymerization. Both of these factors, could enable the monomer to diffuse through the solvent to core of the growing nanoparticles. Thus, plasticizing the core and facilitating the transition from spheres, to worms, to vesicles on the timescale of polymerization.

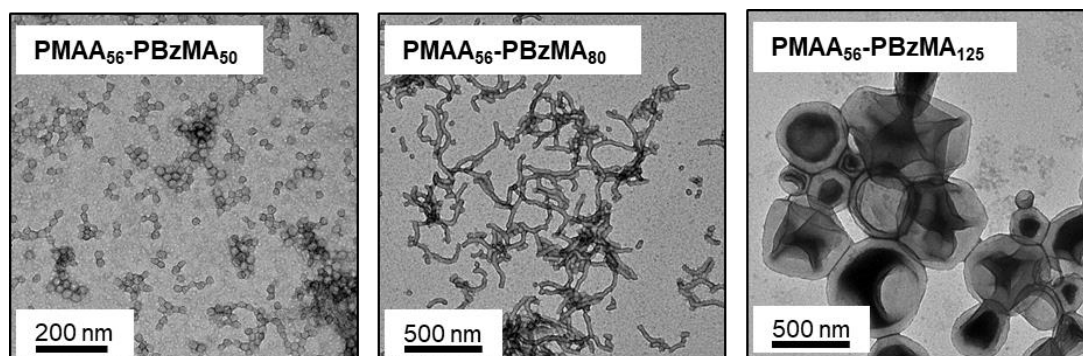


Figure 2.31 Representative TEM images of PMAA₅₆-PBzMA_y diblock copolymer nanoparticles synthesized *via* RAFT alcoholic dispersion polymerization at 20% w/w copolymer concentration in ethanol. The PBzMA DP was varied ($y = 50$ to 125) in order to obtain spheres, worms and vesicles.

2.5. Conclusions

Low dispersity PMAA_x macro-CTAs were synthesized *via* RAFT solution polymerization in ethanol using both CPCP (PMAA₅₄-DB) and PETTC (PMAA₅₆-TTC) as the CTA. Both of these macro-CTAs were then successfully used to synthesize a series of PMAA_x-PBzMA₁₀₀₋₁₅₀₀ diblock copolymers *via* RAFT aqueous emulsion polymerization of BzMA at 10% w/w copolymer concentration. Both series produced well-defined spherical nanoparticles of 30-90 nm in diameter (as judged by DLS and TEM). A comparison of the results from both series indicates better results are achieved when using the PMAA₅₆-TTC macro-CTA, including higher conversions and a slightly improved level of control over the polymerization ($1.32 \leq \bar{D} \leq 1.89$). A more linear increase in the hydrodynamic diameter of the spherical nanoparticles was also observed as the PBzMA DP increased from 100 to 1500 (34 nm up to 92 nm). Finally, PETTC can be made in-house at a reduced cost.

In an effort to obtain higher order morphologies (worms and vesicles) a series of PMAA₅₄-PBzMA₅₀₀ diblock copolymer nanoparticles (utilizing the DB macro-CTA) was synthesized *via* RAFT aqueous emulsion polymerization of BzMA at 10 to 50% w/w copolymer concentration. However, only kinetically-trapped spherical nanoparticles were obtained in each case. A second series of PMAA₅₄-PBzMA_y diblock copolymer nanoparticles ($y = 200$ to 1500) was also synthesized in the presence of salt ($[\text{CaCl}_2] = 0.01$ to 0.04 M). It was hypothesized that the presence of CaCl₂ salt would screen the charge between neighboring PMAA chains aiding sphere-sphere fusion and the evolution of nanoparticle morphology from spheres to worms to vesicles. However, only kinetically-trapped spherical nanoparticles were

obtained. A series of PMAA₅₆-PBzMA_y diblock copolymers were also synthesized *via* RAFT alcoholic dispersion polymerization in ethanol. In contrast to the RAFT aqueous emulsion syntheses, the full range of nanoparticle morphologies could be obtained by PISA. In addition, narrower MWDs were reported ($\bar{D} = 1.28$ to 1.33).

The results from the PMAA₅₆-PBzMA_y system align with previous work on the PGMA₅₁-PBzMA_y system, suggesting that often only kinetically-trapped spherical nanoparticles can be obtained *via* RAFT aqueous emulsion polymerization.¹⁷ In contrast, the full range of morphologies (spheres, worms and vesicles) has been extensively reported for RAFT aqueous dispersion polymerization formulations.^{31, 55, 63-65} Considering that the key difference between these two formulations is the aqueous solubility of the core-forming monomer, this Chapter explored the importance of aqueous solubility on the ability to synthesize higher order morphologies *via* PISA. A series of diblock copolymer nanoparticles was prepared by chain-extending a PMAA₅₆-TTC macro-CTA with six core-forming monomers of increasing aqueous solubility; BzMA, TFEMA, BMA, MMA, HBMA and HPMA. Analysis of the resulting diblock copolymer nanoparticles indicated that only kinetically-trapped spherical nanoparticles were formed for all monomers with the exception of HBMA. The RAFT aqueous emulsion polymerization of TFEMA and BMA resulted in diblock copolymers with broad MWDs (2.94 to 4.45 and 1.69 to 2.44 respectively) indicating a poor level of RAFT control or incompatibility between the core-forming monomer and the methylation protocol. In addition, the spherical nanoparticles obtained for each system did not increase in size with core-forming block DP. Similar results were observed for the RAFT dispersion polymerization of HPMA. Only spherical nanoparticles were observed and broad MWDs were reported (1.51 -3.33). However, incompatibility of HPMA-based block copolymers and the methylation protocol has been previously reported, which could account for the high dispersities.⁹³

The RAFT aqueous emulsion polymerization of MMA was better controlled with dispersities of 1.46 to 2.00. The PMAA₅₆-PMMA_y diblock copolymers showed a very linear increase in molecular weight (M_n) with PMMA DP ($R^2 = 0.9926$). The effect of T_g with PMMA DP was investigated and minimal variation in T_g (116 to 127 °C) was observed as the PMMA DP was increased from 40 to 3000. The PMAA₅₆-PMMA₂₀₀ diblock copolymer nanoparticles were also shown to act as effective Pickering

emulsifiers for both methyl myristate and squalene based oil-in-water emulsion. However, these emulsions were not pH responsive.

The RAFT aqueous emulsion polymerization of HBMA was the only system that enabled the synthesis of non-spherical nanoparticle *via* PISA in aqueous solution suggesting that the aqueous-solubility of the monomer is indeed a key parameter. This new PISA formulation is investigated in more detail in Chapter 3 of this Thesis.

2.6. References

1. E. R. Jones, M. Semsarilar, A. Blanazs and S. P. Armes, *Macromolecules*, 2012, **45**, 5091-5098.
2. M. Semsarilar, E. R. Jones, A. Blanazs and S. P. Armes, *Advanced Materials*, 2012, **24**, 3378-3382.
3. C. Gonzato, M. Semsarilar, E. R. Jones, F. Li, G. J. P. Krooshof, P. Wyman, O. O. Mykhaylyk, R. Tuinier and S. P. Armes, *Journal of the American Chemical Society*, 2014, **136**, 11100-11106.
4. W. Zhao, G. Gody, S. Dong, P. B. Zetterlund and S. Perrier, *Polymer Chemistry*, 2014, **5**, 6990-7003.
5. M. J. Derry, L. A. Fielding and S. P. Armes, *Polymer Chemistry*, 2015, **6**, 3054-3062.
6. L. A. Fielding, J. A. Lane, M. J. Derry, O. O. Mykhaylyk and S. P. Armes, *Journal of the American Chemical Society*, 2014, **136**, 5790-5798.
7. L. A. Fielding, M. J. Derry, V. Ladmiral, J. Rosselgong, A. M. Rodrigues, L. P. D. Ratcliffe, S. Sugihara and S. P. Armes, *Chemical Science*, 2013, **4**, 2081-2087.
8. Y. Pei, O. R. Sugita, L. Thurairajah and A. B. Lowe, *RSC Advances*, 2015, **5**, 17636-17646.
9. Y. Pei, L. Thurairajah, O. R. Sugita and A. B. Lowe, *Macromolecules*, 2015, **48**, 236-244.
10. M. J. Derry, L. A. Fielding and S. P. Armes, *Progress in Polymer Science*, 2016, **52**, 1-18.
11. S. Sugihara, S. P. Armes, A. Blanazs and A. L. Lewis, *Soft Matter*, 2011, **7**, 10787-10793.
12. S. Sugihara, A. Blanazs, S. P. Armes, A. J. Ryan and A. L. Lewis, *Journal of the American Chemical Society*, 2011, **133**, 15707-15713.
13. N. J. Warren, O. O. Mykhaylyk, D. Mahmood, A. J. Ryan and S. P. Armes, *Journal of the American Chemical Society*, 2014, **136**, 1023-1033.
14. M. Semsarilar, V. Ladmiral, A. Blanazs and S. P. Armes, *Langmuir*, 2012, **28**, 914-922.
15. B. Charleux, G. Delaittre, J. Rieger and F. D'Agosto, *Macromolecules*, 2012, **45**, 6753-6765.
16. I. Chaduc, M. Lansalot, F. D'Agosto and B. Charleux, *Macromolecules*, 2012, **45**, 1241-1247.
17. V. J. Cunningham, A. M. Alswieleh, K. L. Thompson, M. Williams, G. J. Leggett, S. P. Armes and O. M. Musa, *Macromolecules*, 2014, **47**, 5613-5623.

18. N. J. Warren and S. P. Armes, *Journal of the American Chemical Society*, 2014, **136**, 10174-10185.
19. J. Tan, H. Sun, M. Yu, B. S. Sumerlin and L. Zhang, *ACS Macro Letters*, 2015, **4**, 1249-1253.
20. C. J. Ferguson, R. J. Hughes, B. T. T. Pham, B. S. Hawkett, R. G. Gilbert, A. K. Serelis and C. H. Such, *Macromolecules*, 2002, **35**, 9243-9245.
21. S. L. Canning, G. N. Smith and S. P. Armes, *Macromolecules*, 2016, **49**, 1985-2001.
22. M. Semsarilar, V. Ladmiral, A. Blanazs and S. P. Armes, *Langmuir*, 2013, **29**, 7416-7424.
23. J. Rieger, F. Stoffelbach, C. Bui, D. Alaimo, C. Jérôme and B. Charleux, *Macromolecules*, 2008, **41**, 4065-4068.
24. M. F. Cunningham, *Progress in Polymer Science*, 2008, **33**, 365-398.
25. C. J. Ferguson, R. J. Hughes, D. Nguyen, B. T. T. Pham, R. G. Gilbert, A. K. Serelis, C. H. Such and B. S. Hawkett, *Macromolecules*, 2005, **38**, 2191-2204.
26. J. Rieger, W. Zhang, F. Stoffelbach and B. Charleux, *Macromolecules*, 2010, **43**, 6302-6310.
27. X. Zhang, S. Boissé, W. Zhang, P. Beaunier, F. D'Agosto, J. Rieger and B. Charleux, *Macromolecules*, 2011, **44**, 4149-4158.
28. N. P. Truong, M. V. Dussert, M. R. Whittaker, J. F. Quinn and T. P. Davis, *Polymer Chemistry*, 2015, **6**, 3865-3874.
29. I. Canton, N. J. Warren, A. Chahal, K. Amps, A. Wood, R. Weightman, E. Wang, H. Moore and S. P. Armes, *ACS Central Science*, 2016, **2**, 65-74.
30. A. Blanazs, S. P. Armes and A. J. Ryan, *Macromolecular Rapid Communications*, 2009, **30**, 267-277.
31. A. Blanazs, R. Verber, O. O. Mykhaylyk, A. J. Ryan, J. Z. Heath, C. W. I. Douglas and S. P. Armes, *Journal of the American Chemical Society*, 2012, **134**, 9741-9748.
32. S. Y. Khor, J. F. Quinn, M. R. Whittaker, N. P. Truong and T. P. Davis, *Macromolecular Rapid Communications*, 2018, **ASAP article**.
33. R. Verber, A. Blanazs and S. P. Armes, *Soft Matter*, 2012, **8**, 9915-9922.
34. G. Liu, Q. Qiu and Z. An, *Polymer Chemistry*, 2012, **3**, 504-513.
35. N. J. W. Penfold, J. R. Lovett, P. Verstraete, J. Smets and S. P. Armes, *Polymer Chemistry*, 2017, **8**, 272-282.
36. J. R. Lovett, N. J. Warren, L. P. D. Ratcliffe, M. K. Kocik and S. P. Armes, *Angewandte Chemie (International Ed. in English)*, 2015, **54**, 1279-1283.
37. W. Zhang, F. D'Agosto, O. Boyron, J. Rieger and B. Charleux, *Macromolecules*, 2011, **44**, 7584-7593.
38. I. Chaduc, W. Zhang, J. Rieger, M. Lansalot, F. D'Agosto and B. Charleux, *Macromolecular Rapid Communications*, 2011, **32**, 1270-1276.
39. I. Chaduc, M. Girod, R. Antoine, B. Charleux, F. D'Agosto and M. Lansalot, *Macromolecules*, 2012, **45**, 5881-5893.
40. I. Chaduc, A. Crepet, O. Boyron, B. Charleux, F. D'Agosto and M. Lansalot, *Macromolecules*, 2013, **46**, 6013-6023.
41. S. Fréal-Saison, M. Save, C. Bui, B. Charleux and S. Magnet, *Macromolecules*, 2006, **39**, 8632-8638.
42. M. Manguian, M. Save and B. Charleux, *Macromolecular Rapid Communications*, 2006, **27**, 399-404.
43. S. Boissé, J. Rieger, K. Belal, A. Di-Cicco, P. Beaunier, M.-H. Li and B. Charleux, *Chemical Communications*, 2010, **46**, 1950-1952.

44. S. Boissé, J. Rieger, G. Pembouong, P. Beaunier and B. Charleux, *Journal of Polymer Science Part A: Polymer Chemistry*, 2011, **49**, 3346-3354.
45. W. Zhang, F. D'Agosto, O. Boyron, J. Rieger and B. Charleux, *Macromolecules*, 2012, **45**, 4075-4084.
46. W. Zhang, F. D'Agosto, P.-Y. Dugas, J. Rieger and B. Charleux, *Polymer*, 2013, **54**, 2011-2019.
47. J. Lesage de la Haye, X. Zhang, I. Chaduc, F. Brunel, M. Lansalot and F. D'Agosto, *Angewandte Chemie International Edition*, 2016, **55**, 3739-3743.
48. N. P. Truong, J. F. Quinn, A. Anastasaki, D. M. Haddleton, M. R. Whittaker and T. P. Davis, *Chemical Communications*, 2016, **52**, 4497-4500.
49. S. Y. Khor, N. P. Truong, J. F. Quinn, M. R. Whittaker and T. P. Davis, *ACS Macro Letters*, 2017, **6**, 1013-1019.
50. L. P. D. Ratcliffe, A. J. Ryan and S. P. Armes, *Macromolecules*, 2013, **46**, 769-777.
51. M. Semsarilar, V. Ladmiral, A. Blanazs and S. P. Armes, *Polymer Chemistry*, 2014, **5**, 3466-3475.
52. D. J. Keddie, G. Moad, E. Rizzardo and S. H. Thang, *Macromolecules*, 2012, **45**, 5321-5342.
53. J. Chiefari, Y. K. B. Chong, F. Ercole, J. Krstina, J. Jeffery, T. P. T. Le, R. T. A. Mayadunne, G. F. Meijs, C. L. Moad, G. Moad, E. Rizzardo and S. H. Thang, *Macromolecules*, 1998, **31**, 5559-5562.
54. J. Chiefari, R. T. A. Mayadunne, C. L. Moad, G. Moad, E. Rizzardo, A. Postma, M. A. Skidmore and S. H. Thang, *Macromolecules*, 2003, **36**, 2273-2283.
55. A. Blanazs, A. J. Ryan and S. P. Armes, *Macromolecules*, 2012, **45**, 5099-5107.
56. K. Matyjaszewski and T. Davis, *Handbook of Radical Polymerization*, Wiley, 2002.
57. S. Perrier and P. Takolpuckdee, *Journal of Polymer Science Part A: Polymer Chemistry*, 2005, **43**, 5347-5393.
58. C. P. Jesson, C. M. Pearce, H. Simon, A. Werner, V. J. Cunningham, J. R. Lovett, M. J. Smallridge, N. J. Warren and S. P. Armes, *Macromolecules*, 2017, **50**, 182-191.
59. L. Couvreur, C. Lefay, J. Belleney, B. Charleux, O. Guerret and S. Magnet, *Macromolecules*, 2003, **36**, 8260-8267.
60. I. Borukhov, D. Andelman, R. Borrega, M. Cloitre, L. Leibler and H. Orland, *The Journal of Physical Chemistry B*, 2000, **104**, 11027-11034.
61. O. Colombani, E. Lejeune, C. Charbonneau, C. Chassenieux and T. Nicolai, *The Journal of Physical Chemistry B*, 2012, **116**, 7560-7565.
62. I. Chaduc, M. Girod, R. Antoine, B. Charleux, F. D'Agosto and M. Lansalot, *Macromolecules*, 2012, **45**, 5881-5893.
63. A. Blanazs, J. Madsen, G. Battaglia, A. J. Ryan and S. P. Armes, *Journal of the American Chemical Society*, 2011, **133**, 16581-16587.
64. P. Chambon, A. Blanazs, G. Battaglia and S. P. Armes, *Macromolecules*, 2012, **45**, 5081-5090.
65. Y. Li and S. P. Armes, *Angewandte Chemie International Edition*, 2010, **49**, 4042-4046.
66. Sigma-Aldrich (Merck) catalogue online, https://www.sigmaaldrich.com/united-kingdom.html?gclid=Cj0KCQjw6rXeBRD3ARIsAD9ni9BAWR_Mty

- G254n9VfZueH7DMdLPjp7HaO5MDOcJW5ibq4IGUfCvEqQaAqbfEALw_wcB, (accessed 22/10/2018).
67. ChemIDplus:A TOXNET DATABASE - Methyl Methacrylate, <https://toxnet.nlm.nih.gov/cgi-bin/sis/search2/r?dbs+hsdb:@term+@rn+@rel+80-62-6>, (accessed 22/10/2018).
 68. Chemical Book - Butyl Methacrylate, https://www.chemicalbook.com/ChemicalProductProperty_EN_CB3321278.htm, (accessed 22/10/2018).
 69. ChemIDplus:A TOXNET DATABASE - 2,2,2-Trifluoroethyl Methacrylate, <https://chem.nlm.nih.gov/chemidplus/rn/352-87-4>, (accessed 22/10/2018).
 70. Thermal Transitions of Homopolymers: Glass Transition & Melting Point, <https://www.sigmaaldrich.com/technical-documents/articles/materials-science/polymer-science/thermal-transitions-of-homopolymers.html>, (accessed 15/10/2018).
 71. Polysciences Monomer Product Guide, http://www.polysciences.com/skin/frontend/default/polysciences/pdf/Monomers_Guide_2012%20.pdf, (accessed 22/10/2018).
 72. J. Brandup and E. H. Immergut, *Polymer Handbook*, John Wiley & Sons, New York, 1975.
 73. M. Semsarilar, E. R. Jones and S. P. Armes, *Polymer Chemistry*, 2014, **5**, 195-203.
 74. B. Akpınar, L. A. Fielding, V. J. Cunningham, Y. Ning, O. O. Mykhaylyk, P. W. Fowler and S. P. Armes, *Macromolecules*, 2016, **49**, 5160-5171.
 75. E. J. Cornel, S. van Meurs, T. Smith, P. S. O'Hora and S. P. Armes, *Journal of the American Chemical Society*, 2018, **140**, 12980-12988.
 76. P. Atkins and J. d. Paula, *Atkins' Physical Chemistry* Oxford University Press, Oxford, 9th Edition edn., 2010.
 77. J. M. G. Cowie, *Polymers: Chemistry & Physics of Modern Materials*, Nelson Thornes, Cheltenham, 2nd edn., 2001.
 78. T. G. Fox and P. J. Flory, *Journal of Applied Physics*, 1950, **21**, 581-591.
 79. T. G. Fox and P. J. Flory, *Journal of Polymer Science*, 1954, **14**, 315-319.
 80. S. U. Pickering, *Journal of the Chemical Society, Transactions*, 1907, **91**, 2001-2021.
 81. W. Ramsden, *Proceedings of the Royal Society of London*, 1904, **72**, 156-164.
 82. B. P. Binks and S. O. Lumsdon, *Langmuir*, 2001, **17**, 4540-4547.
 83. K. L. Thompson, P. Chambon, R. Verber and S. P. Armes, *Journal of the American Chemical Society*, 2012, **134**, 12450.
 84. K. L. Thompson, C. J. Mable, A. Cockram, N. J. Warren, V. J. Cunningham, E. R. Jones, R. Verber and S. P. Armes, *Soft Matter*, 2014, **10**, 8615-8626.
 85. K. L. Thompson, S. P. Armes, J. R. Howse, S. Ebbens, I. Ahmad, J. H. Zaidi, D. W. York and J. A. Burdis, *Macromolecules*, 2010, **43**, 10466-10474.
 86. Y. Cui, M. Threlfall and J. S. van Duijneveldt, *Journal of Colloid and Interface Science*, 2011, **356**, 665-671.
 87. S. A. F. Bon and P. J. Colver, *Langmuir*, 2007, **23**, 8316-8322.
 88. S. Cauvin, P. J. Colver and S. A. F. Bon, *Macromolecules*, 2005, **38**, 7887-7889.
 89. Y. Cui and J. S. van Duijneveldt, *Langmuir*, 2012, **28**, 1753-1757.
 90. S. Levine, B. D. Bowen and S. J. Partridge, *Colloids and Surfaces*, 1989, **38**, 325-343.
 91. B. P. Binks and S. O. Lumsdon, *Physical Chemistry Chemical Physics*, 1999, **1**, 3007-3016.
-

92. B. P. Binks and S. O. Lumsdon, *Physical Chemistry Chemical Physics*, 2000, **2**, 2959-2967.
93. A. Hanisch and S. P. Armes, unpublished work.

Chapter Three

3. Effect of monomer solubility on the evolution of copolymer morphology during polymerization-induced self-assembly in aqueous solution

Reproduced in full from [A. A. Cockram, T. J. Neal, M. J. Derry, O. O. Mykhaylyk, N. S. J. Williams, M. W. Murray, S. N. Emmett and S. P. Armes, *Macromolecules*, 2017, **50**, 796-802]. Copyright [2017] American Chemical Society.

3.1. Introduction

In recent years, PISA has become a widely recognized route for the synthesis of many types of diblock copolymer nano-objects.¹⁻⁵ Compared to post-polymerization processing techniques (solvent exchange, film rehydration or pH switch), PISA is much more efficient and can be performed at relatively high copolymer concentration (10-50% w/w).^{3, 6-8} This approach involves growth of an insoluble block from a soluble homopolymer in a suitable solvent to give well-defined sterically-stabilized diblock copolymer nanoparticles. For example, RAFT aqueous dispersion polymerization involves polymerization of a *water-miscible* monomer such as HPMA from water-soluble PGMA.^{9, 10} Such formulations enable the production of various copolymer morphologies such as spheres, worms and vesicles.¹¹⁻¹⁹ RAFT aqueous emulsion polymerization has similarly received significant attention.^{2, 6, 7, 20-24} In this case, a *water-immiscible* monomer is used to produce the hydrophobic core-forming block, but according to many literature reports only kinetically-trapped spheres can be obtained.^{6, 7, 24-31} Exceptionally, Charleux and co-workers reported the synthesis of diblock copolymer worms (described as ‘nano-fibers’) and vesicles, as well as spheres.^{23, 32-35} Recent empirical experiments have undoubtedly provided some useful insights, but the critical synthesis parameters that determine whether only kinetically-trapped spheres are obtained or the full range of morphologies are observed have not yet been established.³⁶ In this context, Truong *et al.* recently synthesized novel ‘filomicelle nanomaterials’ directly in water by employing RAFT aqueous emulsion polymerization followed by temperature-induced morphological transition (TIMT). Morphological transitions from spherical micelles to filomicelles (worms) and/or vesicles were observed on cooling in the presence of additional monomer, which apparently acts as a plasticizer for the frustrated core-forming block.³⁷ However, this approach does not seem to be particularly attractive from a commercial perspective.

Previous work by the Armes group investigated the effect of varying the nature of the core-forming monomer on particle formation.³⁸ It was shown that chain extending a PGMA₆₀ macro-CTA with *water-miscible* HPMA *via* RAFT aqueous dispersion polymerization lead to the formation of a range of nanoparticle by PISA. However, when HPMA is replaced with hydroxyethyl methacrylate (HEMA) no self-assembly was observed owing to the insufficient hydrophobic character of the PHEMA block.

In contrast, utilizing HBMA as the core-forming block enabled the synthesis of spherical nanoparticles only. Interestingly, polymerizing a 1:1 ratio of HEMA/HBMA to produce diblock copolymers, isomeric to the PHPMA diblock copolymers, enabled access to the whole range of nanoparticle morphologies (spheres, worms and vesicles). Kinetic studies (^1H NMR spectroscopy) indicated that HBMA is consumed faster than HEMA. The polymerization begins as a RAFT aqueous emulsion polymerization of HBMA until particle nucleation occurs. At this point, the HEMA partitions into the growing particle cores and is efficiently copolymerized alongside the HBMA. The study clearly demonstrates that aqueous monomer solubility is an important parameter to consider when investigating the range of morphologies formed by RAFT-mediated PISA.

A study conducted by Figg *et al.*, reported complimentary findings demonstrating that nanoparticle morphology is dictated by the hydrophobic nature of the growing core-forming block.³⁹ A hydrophilic PDMA₆₇ macro-CTA was chain extended with diacetone acrylamide (DAAm) and DMA in varying molar ratios to synthesize a range of statistical copolymers. It was shown that by adjusting the monomer feed and therefore the statistical copolymer compositions, various nanoparticle morphologies (spheres, worms, branched worms and vesicles) could be strategically targeted.

The present work explores the effect of aqueous monomer solubility on copolymer morphology. As noted above, *water-miscible* monomers such as HPMA (aqueous solubility $\sim 100 \text{ g dm}^{-3}$ at $70 \text{ }^\circ\text{C}$) are required for RAFT aqueous dispersion polymerization, whereas *water-immiscible* monomers such as benzyl methacrylate (BzMA; aqueous solubility $\sim 0.40 \text{ g dm}^{-3}$ at $70 \text{ }^\circ\text{C}$) are required for RAFT aqueous emulsion polymerization. Herein we utilize HBMA as a monomer of *intermediate* aqueous solubility ($\sim 20 \text{ g dm}^{-3}$ at $70 \text{ }^\circ\text{C}$) that has been previously reported to undergo RAFT aqueous emulsion polymerization.³⁸ It was suggested in Chapter 2 of this Thesis that selection of HBMA as a core-forming block might enable the synthesis of higher order morphologies *via* PISA. The key question to be addressed is whether such formulations allow access to any copolymer morphologies other than kinetically-trapped spheres.

3.2. Experimental

3.2.1. Materials

2-hydroxybutyl methacrylate (HBMA; actually a 1:1 molar ratio of 2- and 4-isomers as judged by ^1H NMR spectroscopy)¹⁵ and 4,4'-azobis(4-cyanovaleric acid) (ACVA) were purchased from Sigma-Aldrich UK and used as received unless otherwise specified. Deionized water was used in all experiments. The trimethylsilyldiazomethane solution (2.0 M in diethyl ether), THF (HPLC, $\geq 99.9\%$) and glacial acetic acid ($\geq 99.85\%$) used for the preparation and analysis of the methylated diblock copolymers were also purchased from Sigma-Aldrich UK. d_4 -Methanol, d_6 -dimethyl sulfoxide and d_7 -dimethylformamide used for ^1H NMR spectroscopy were purchased from Goss Scientific Instruments Ltd. (Cheshire, UK). All other solvents were purchased from Sigma-Aldrich UK or VWR Chemicals. The TTC-PGMA₂₉ macro-CTA used was prepared by Matt Rymaruk as previously reported.¹⁰

3.2.2. Preparation of poly(methacrylic acid) (PMAA) macro-CTA agent

The same PMAA₅₆-TTC macro-CTA reported in Chapter 2 was also used for all syntheses in this Chapter. The PMAA₂₉ macro-CTA was synthesized and characterized using the same methods.

3.2.3. RAFT polymerization of HBMA in water

A typical protocol for the synthesis of PMAA₅₆-PHBMA₅₀₀ was as follows: PMAA₅₆ macro-CTA (0.0489 g, 0.0094 mmol), ACVA (0.6 mg; 0.0019 mmol, CTA/initiator molar ratio = 5.0) and water (3.20 g, 20% w/w) were weighed into a 14 mL vial. The pH was adjusted to pH 5 using 1 M NaOH. HBMA monomer (0.7500 g, 4.70 mmol) was then added and the reaction vial was sealed and purged for 30 min before being placed in a pre-heated oil bath at 70 °C for 18 h.

3.2.4. Purification of HBMA monomer

As-received HBMA (3.0 g) was dissolved in water (300 g). This aqueous monomer solution was extracted using *n*-hexane to remove the dimethacrylate impurity. The aqueous monomer solution was then salted with NaCl (250 g/L) and HBMA was removed from the aqueous phase by extraction with diethyl ether. MgSO₄ was added to remove traces of water from the ether layer. Hydroquinone (0.1%) was added to prevent thermal polymerization prior to removal of the solvent by distillation under

reduced pressure to afford purified HBMA monomer. The removal of dimethacrylate impurity was quantified by HPLC, see Figure 3.4.

3.3. Copolymer Characterization

3.3.1. ¹H NMR Spectroscopy

All ¹H NMR spectra were recorded using a 400 MHz Bruker Advance-400 spectrometer using either d₄-methanol, d₆-dimethyl sulfoxide or d₇-dimethylformamide.

3.3.2. Methylation of copolymers for GPC Analysis

Prior to GPC analysis, all copolymers were modified by methylation of the carboxylic acid groups in the PMAA block. Excess trimethylsilyldiazomethane was added dropwise to a solution of copolymer (20 mg) in THF (2.0 mL), until the yellow color persisted. This reaction solution was then stirred overnight until all THF had evaporated.

3.3.3. Gel Permeation Chromatography (GPC)

THF GPC at 30 °C was used to determine the molecular weights and dispersities of the modified copolymers containing PMAA. The GPC set-up consisted of two 5 μM Mixed C columns connected to a WellChrom K-2301 refractive index detector. The mobile phase was HPLC-grade THF containing 1.0% glacial acetic acid and 0.05% w/v BHT at a flow rate of 1.0 mL min⁻¹. Molecular weights were calculated with respect to a series of near-monodisperse PMMA standards.

DMF GPC at 60 °C was used to determine the molecular weights and dispersities of the modified copolymers containing PGMA. The GPC set-up consisted of a Varian 290-LC pump injection module connected to two Polymer Laboratories PL gel 5 μm Mixed-C columns connected in series and a Varian 390-LC multi-detector suite (refractive index detector). The mobile phase was HPLC-grade DMF containing 10 mM LiBr at a flow rate of 1.0 mL min⁻¹. Molecular weights were calculated with respect to a series of near-monodisperse PMMA standards.

3.3.4. Dynamic Light Scattering (DLS)

Aqueous copolymer dispersions (0.20% w/w) in disposable plastic cuvettes were analyzed using a Malvern Zetasizer NanoZS instrument. Scattered light was detected at 173° and intensity-average hydrodynamic diameters were calculated using the Stokes-Einstein equation. Data were averaged over three consecutive measurements, comprising a minimum of ten runs per measurement.

3.3.5. Aqueous Electrophoresis

Measurements were performed using a Malvern Zetasizer instrument on dilute (0.20% w/w) copolymer dispersions containing background KCl (1 mM). The solution pH was adjusted by addition of either NaOH or HCl.

3.3.6. Transmission Electron Microscopy (TEM)

One droplet (10 μ L) of a dilute copolymer dispersion (0.20% w/w) were deposited onto a carbon-coated copper grid for 20 seconds. The grid was then stained with 10 μ L uranyl formate for 10 seconds and dried using a vacuum hose. TEM images were then obtained using a Philips CM100 instrument operating at 100 kV and equipped with a Gatan 1 k CCD camera.

3.3.7. Scanning Electron Microscopy (SEM)

Silica or copolymer/silica dispersions were placed on a glass slide and dried overnight, mounted onto SEM stubs using adhesive conducting pads and then gold-coated prior to analysis. Imaging was performed using an Inspect F microscope operating at 15 kV. All SEM analyses were performed by Yin Ning, a postdoctoral researcher in the Armes group.

3.3.8. Reverse-Phase High-Performance Liquid Chromatography (HPLC)

The level of dimethacrylate impurity in the HBMA monomer was quantified by HPLC (Figure 3.4). The experimental set-up consisted of an autosampler (Varian model 410), a solvent delivery module (Varian Module 230), a UV detector (Varian model 310), and an Zorbax Eclipse Plus C18, 3.5 μ m, 4.6 x 100 mm HPLC column. HBMA (5.0 mg) was weighed into an autosampler vial and dissolved in acetonitrile (1.0 mL). The eluent was gradually varied from an initial composition of 5% acetonitrile in water to 95% acetonitrile in water after 15 – 20 min. The UV detector was set to a wavelength of 210 nm.

3.3.9. Shear-Induced Polarized Light Imaging (SIPLI)

Shear alignment experiments were conducted using a mechano-optical rheometer (Anton Paar Physica MCR301 with SIPLI attachment). Measurements were performed using a plate-plate geometry composed of a 25 mm polished steel plate and a fused quartz plate connected to a variable temperature Peltier system. The gap between plates was set at 0.50 mm for all experiments. An additional Peltier hood was used to ensure good control of the sample temperature. Sample illumination was achieved using an Edmund Optics 150 W MI-150 high intensity fibre optic white light

source. The polarizer and analyzer axes were crossed at 90° in order to obtain polarized light images (PLIs), which were recorded using a color CCD camera (Lumenera Lu165c).

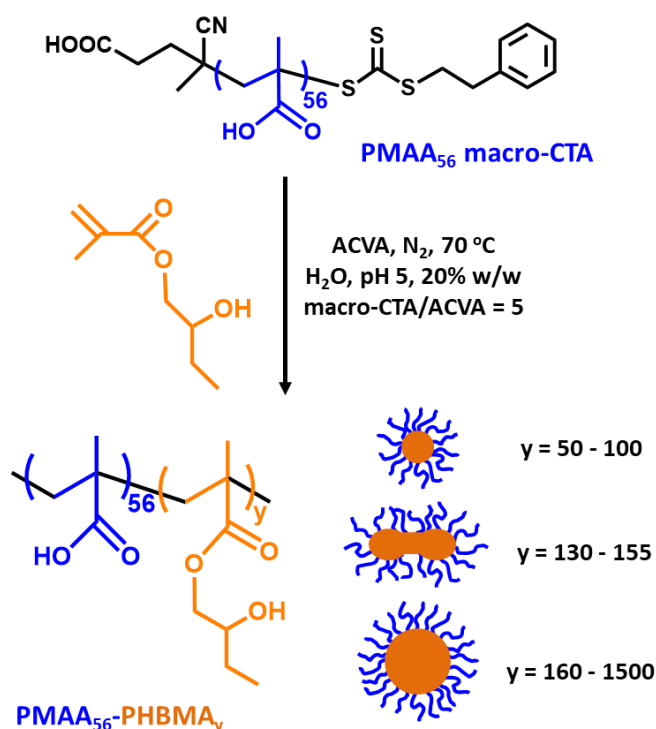
3.3.10. Small-angle x-ray scattering (SAXS)

SAXS patterns for PMAA₅₆-PHBMA_y ($y = 150, 300$ and 1000) were recorded at a synchrotron source (ESRF, station ID02, Grenoble, France) using monochromatic X-ray radiation (wavelength $\lambda = 0.0995$ nm, with q ranging from 0.004 to 2.5 nm⁻¹, where $q = 4\pi \sin \theta/\lambda$ is the length of the scattering vector and θ is one-half of the scattering angle) and a FReLoN Kodak CCD detector. Measurements were conducted on 1.0% w/w aqueous dispersions at pH 5 using glass capillaries of 2.0 mm diameter. X-ray scattering data were reduced using standard routines from the beamline and were further analyzed using Irena SAS macros for Igor Pro. The SAXS pattern for PMAA₅₆-PHBMA₅₀ was obtained using a Bruker AXS Nanostar laboratory instrument modified with a microfocus X-ray tube (GeniX3D, Xenocs) and motorized scatterless slits for the beam collimation (camera length = 1.46 m, Cu K α radiation and “D HiSTAR multiwire gas detector). In this case the SAXS pattern was recorded for a 1.0% w/w aqueous dispersion at pH 5 over a q range of 0.08 nm⁻¹ < q > 1.6 nm⁻¹ using a glass capillary of 2.0 mm diameter and an exposure time of 1.0 h. Raw SAXS data were reduced using Nika macros for Igor Pro written by J. Ilavsky. All SAXS patterns were analyzed (background subtraction, data modelling and fitting) using Irena SAS macros for Igor Pro.⁴⁰ Further information obtained from SAXS analysis can be found in Appendix 2. All SAXS analyses were performed by Tom Neal, a fellow PhD student in the Chemistry Department.

3.4. Results and Discussion

3.4.1. Synthesis of non-spherical nanoparticles via RAFT aqueous emulsion polymerization of HBMA

Preliminary studies indicated that selecting HBMA to form the core-forming block could enable the synthesis of higher order morphologies *via* PISA, see Chapter 2.4.11. Initially, only a limited range of PMAA₅₆-PHBMA_y diblock copolymer compositions were investigated, where $y = 100, 200, 300, 400$ and 500 . To investigate this system further, a wider range of PHBMA DPS was targeted. A PMAA₅₆ macro-CTA was chain-extended with HBMA *via* RAFT polymerization at 70 °C conducted in aqueous solution at pH 5 (see Scheme 3.1). All reactions were conducted at 20% w/w copolymer concentration and with a macro-CTA/ACVA molar ratio = 5.0. The target DP for the structure-directing PHBMA block was varied between 50 and 1500. All polymerizations proceeded to high conversions (> 96%) as judged by ¹H NMR spectroscopy studies in d₇-DMF (see Table 4.2). DLS and TEM studies were conducted to determine the copolymer morphology (see Table 3.1 and Figure 3.1).



Scheme 3.1 Synthesis of poly(methacrylic acid)-poly(2-hydroxybutyl methacrylate) (PMAA₅₆-PHBMA_y) diblock copolymer nanoparticles *via* RAFT polymerization in aqueous solution. Increasing the target degree of polymerization of the PHBMA core-forming block alters both the particle diameter and particle morphology.

Chapter 3: Effect of monomer solubility on the evolution of copolymer morphology during polymerization-induced self-assembly in aqueous solution

Table 3.1 Monomer conversions, mean DLS and TEM diameters and zeta potentials for a series of PMAA₅₆-PHBMA_y diblock copolymer nanoparticles (y = 50 - 1500) prepared *via* RAFT aqueous emulsion polymerization of HBMA at 20% w/w copolymer concentration.

Target composition	Monomer conversion (%) ^a	DLS particle diameter (nm)	DLS polydispersity	TEM particle diameter (nm) ^b	Zeta potential (mV)
PMAA ₅₆ -PHBMA ₅₀	> 99	84	0.39	24	-66
PMAA ₅₆ -PHBMA ₈₀	> 99	114	0.11	40	-56
PMAA ₅₆ -PHBMA ₉₀	> 99	141	0.13	52	-55
PMAA ₅₆ -PHBMA ₁₀₀	> 99	167	0.15	45	-57
PMAA ₅₆ -PHBMA ₁₁₀	> 99	147	0.06	68	-57
PMAA ₅₆ -PHBMA ₁₂₀	> 99	162	0.06	82	-55
PMAA ₅₆ -PHBMA ₁₃₀	> 99	164	0.09	69	-55
PMAA ₅₆ -PHBMA ₁₄₀	> 99	175	0.07	99	-56
PMAA ₅₆ -PHBMA ₁₄₅	> 99	162	0.07	71	-53
PMAA ₅₆ -PHBMA ₁₅₀	> 99	175	0.02	86 (w) 323 (l)	-60
PMAA ₅₆ -PHBMA ₁₅₅	> 99	212	0.08	58 (w) 134 (l)	-57
PMAA ₅₆ -PHBMA ₁₆₀	> 99	232	0.04	115	-56
PMAA ₅₆ -PHBMA ₁₇₀	> 99	226	0.08	155	-57
PMAA ₅₆ -PHBMA ₁₈₀	> 99	194	0.06	283	-55
PMAA ₅₆ -PHBMA ₁₉₀	> 99	230	0.05	254	-63
PMAA ₅₆ -PHBMA ₂₀₀	> 99	251	0.05	174	-52
PMAA ₅₆ -PHBMA ₃₀₀	99	252	0.08	210	-57
PMAA ₅₆ -PHBMA ₄₀₀	> 99	245	0.07	240	-53
PMAA ₅₆ -PHBMA ₅₀₀	96	295	0.05	266	-56
PMAA ₅₆ -PHBMA ₁₀₀₀	> 99	300	0.03	335	-59
PMAA ₅₆ -PHBMA ₁₅₀₀	> 99	385	0.10	329	-63

^a Conversion determined by ¹H NMR spectroscopy

^b for anisotropic particles (w) = width and (l) = length

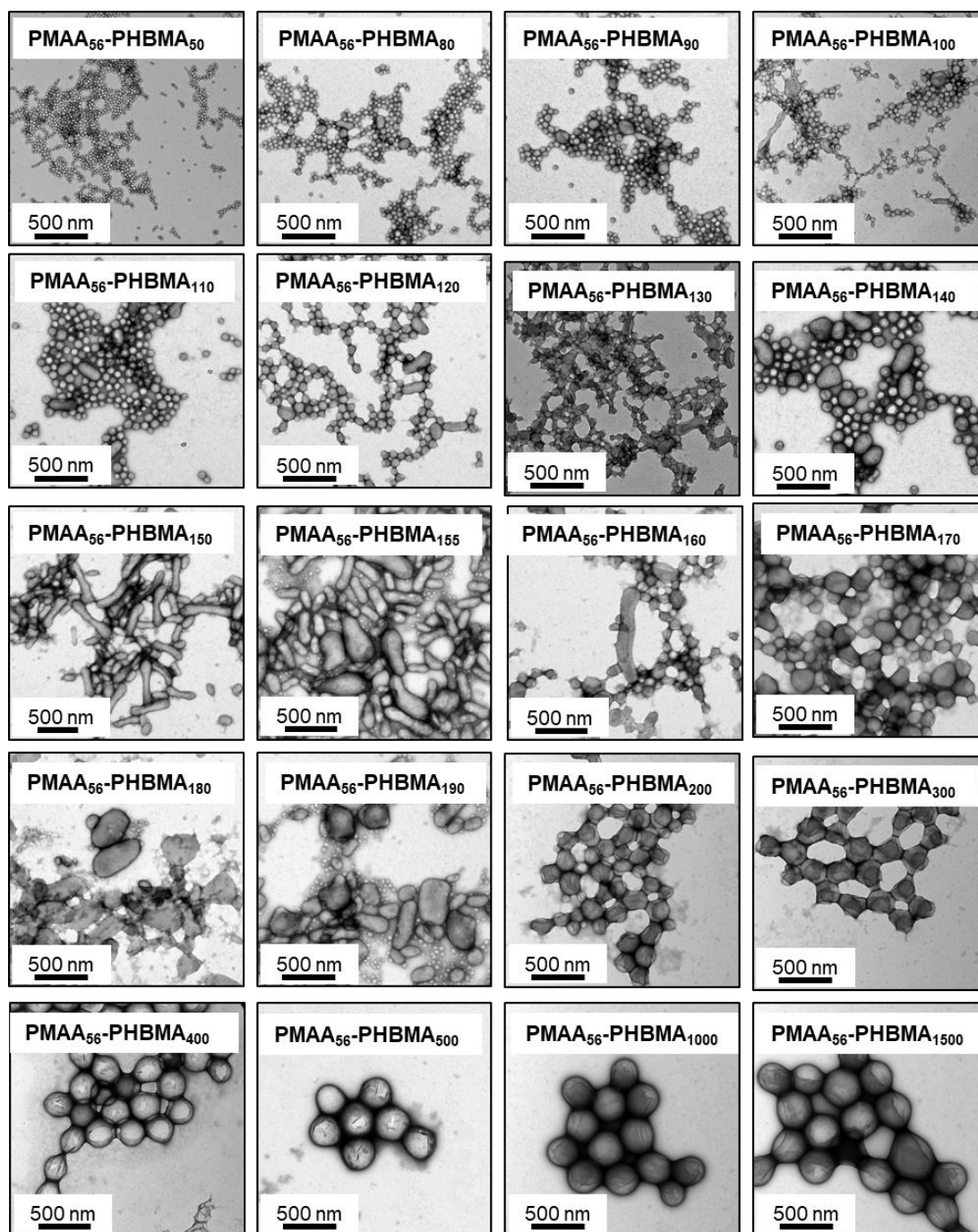


Figure 3.1 Representative TEM images obtained for PMAA₅₆-PHBMA_y diblock copolymer nanoparticles prepared at 20% w/w copolymer concentration *via* RAFT aqueous polymerization of HBMA at 70 °C. PISA leads to the formation of small spherical nanoparticles for y = 50 - 140, a distinctive ‘monkey nut’ morphology for y = 150 – 155 and larger spheres for y = 160 - 1500.

For target PHBMA DP_s of 50 to 145, the PMAA₅₆-PHBMA_y diblock copolymer chains self-assembled to form well-defined spheres of 80 to 175 nm diameter, as judged by DLS and TEM. However, TEM studies indicated that a new ‘monkey nut’ morphology could be obtained over a rather narrow range of y values (y = 150 or 155). These ‘monkey nuts’ are approximately 100 to 800 nm in length, with widths varying from 25 to 125 nm; thus the mean length/width ratio (or particle anisotropy) was approximately four. This unusual non-spherical morphology clearly demonstrates that using a monomer of intermediate aqueous solubility such as HBMA allows access to morphologies other than kinetically-trapped spheres. At higher PHBMA DP_s (y = 160 to 1500), larger spherical nanoparticles were observed with DLS diameters of 160 - 390 nm. TEM analysis of the largest nanoparticles (PHBMA DP = 200 to 1500) suggested the possible synthesis of vesicles, with some evidence for membrane structures, see Figure 3.1. However, such observations could also arise from TEM artefacts. Thus, further analysis of these particles is required.

The PMAA₅₆-PHBMA₁₅₀ ‘monkey-nut’ nanoparticles were also analyzed by SEM, see Figure 3.2. The resulting images confirmed the presence of a new ‘monkey nut’ morphology at a PHBMA DP of 150. SEM analysis indicated the ‘monkey nuts’ are approximately 270 to 700 nm in length, with widths varying from 60 to 130 nm. These values are in agreement with those from TEM analysis but equate to a marginally larger mean length/width ratio of approximately five (ratio approximately four by TEM analysis).

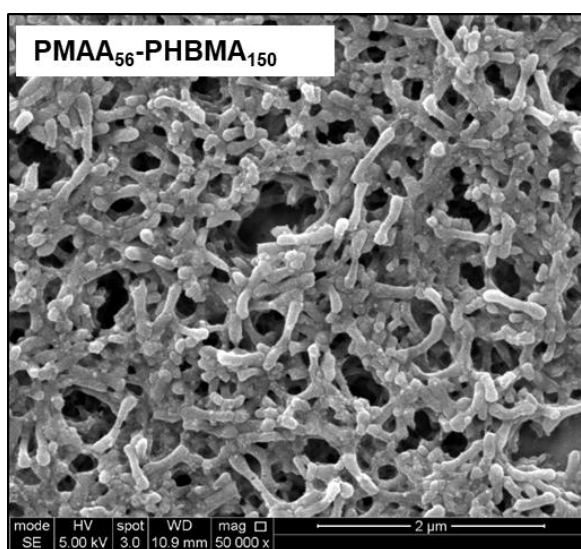


Figure 3.2 SEM image of PMAA₅₆-PHBMA₁₅₀ diblock copolymer nanoparticles confirming the observation of a new ‘monkey nut’ morphology.

3.4.2. Anionic character of monkey nuts

Aqueous electrophoresis was used to assess the mobility and zeta potential of these diblock copolymer nano-objects. The effect of varying pH on the apparent sphere-equivalent particle diameter and zeta potential of the PMAA₅₆-PHBMA₁₅₀ ‘monkey nut’ nanoparticles was evaluated by DLS and aqueous electrophoresis, respectively (see Figure 3.3).

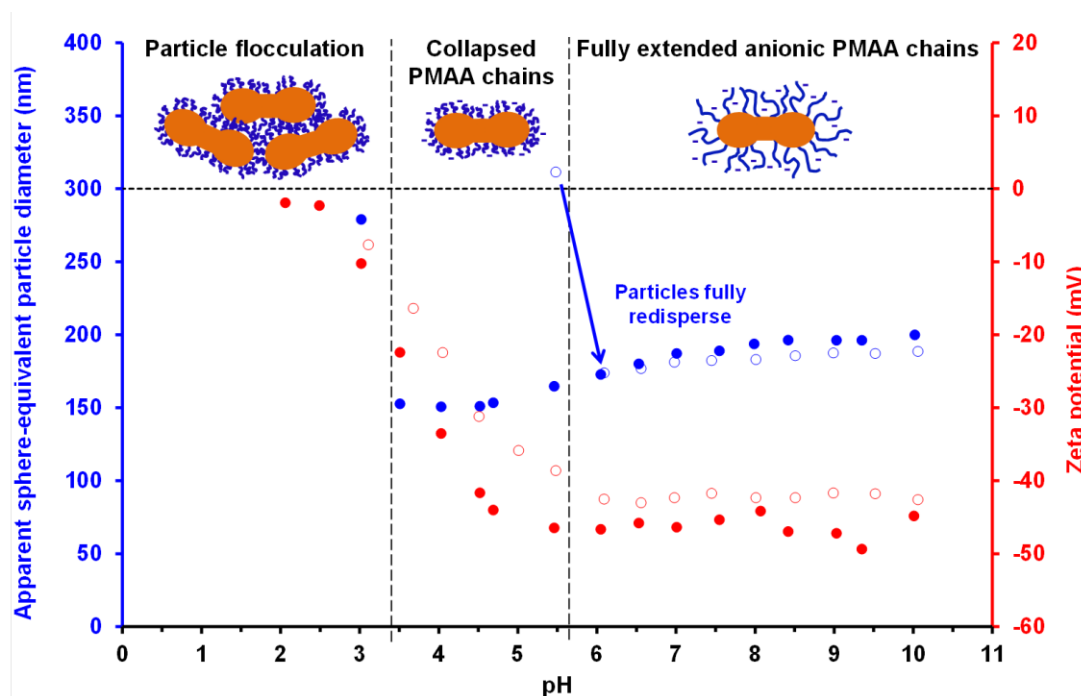


Figure 3.3. Change in apparent sphere-equivalent particle diameter (as judged by DLS) and zeta potential with pH for PMAA₅₆-PHBMA₁₅₀ ‘monkey nut’ nanoparticles. Filled spheres (●) indicate titration from pH 10 to pH 2. Open spheres (○) indicate titration from pH 2 to pH 10. Particle flocculation is observed below pH 3.5 due to the loss of electrosteric stabilization as the PMAA chains become less anionic. This flocculation is reversible on addition of NaOH.

Between pH 10 and pH 5.5, the PMAA stabilizer chains were highly ionized, leading to negative zeta potentials ranging from -50 to -45 mV. The PMAA stabilizer chains remained highly anionic over this pH range, with only a modest reduction in particle diameter (from 200 to 165 nm) being observed. This is consistent with ionized PMAA chains acting as a polyelectrolytic stabilizer block, conferring electrosteric stabilization to the nanoparticles. Between pH 5.5 and pH 3.5 the zeta potential gradually becomes less negative (up to -20 mV) as the PMAA chains become progressively more protonated. A concomitant reduction in apparent hydrodynamic particle diameter to 150 nm occurs as the PMAA chains start to collapse. However, an apparent particle diameter of 5 μm is observed by DLS at approximately pH 2.5. This

is the result of gross flocculation of the PMAA₅₆-PHBMA₁₅₀ nanoparticles, because the near-neutral PMAA stabilizer chains no longer confer effective electrosteric stabilization at this pH. Such aggregation proved to be reversible on raising the solution pH from pH 3.5 to pH 10: the PMAA chains become ionized again and approximately the original sphere-equivalent nanoparticle diameter was obtained, with a corresponding zeta potential of around -40 mV.

3.4.3. Synthesis of non-spherical nanoparticles via RAFT aqueous emulsion polymerization of purified HBMA

In principle, the MWD of the PMAA₅₆-PHBMA_y diblock copolymer chains can be assessed by GPC. However, in practice the MAA residues require methylation to prevent adsorption onto the GPC column. Unfortunately, the methylated PMAA₅₆-PHBMA_y diblock copolymers proved to be insoluble in both THF and DMF, making GPC analysis impossible. This was believed to be the result of extensive cross-linking caused by the ~ 4.4 mol % dimethacrylate impurity in the HBMA monomer. Similar problems have been reported for PISA syntheses involving HPMA.^{10, 13} In order to address this technical problem, the HBMA monomer was purified prior to the preparation of a second series of PMAA₅₆-PHBMA_y diblock copolymers.

Moreover, analysis of such diblock copolymer nano-objects should establish whether the unusual ‘monkey nut’ morphology was merely an artefact caused by *in situ* crosslinking. In this context, it is worth noting that Sugihara and co-workers reported a ‘lumpy rod’ morphology for the synthesis of cross-linked nanoparticles prepared *via* RAFT aqueous dispersion copolymerization of HPMA with EGDMA when targeting more than six EGDMA units per copolymer chain.⁴¹ Thus an aqueous solution of the as-supplied HBMA monomer was extracted using *n*-hexane to remove the dimethacrylate impurity.⁴² The purified HBMA monomer was analyzed by reverse-phase HPLC, which indicated approximately 87% removal of the original dimethacrylate impurity, leaving around 0.57 mol % dimethacrylate still present (see Figure 3.4).

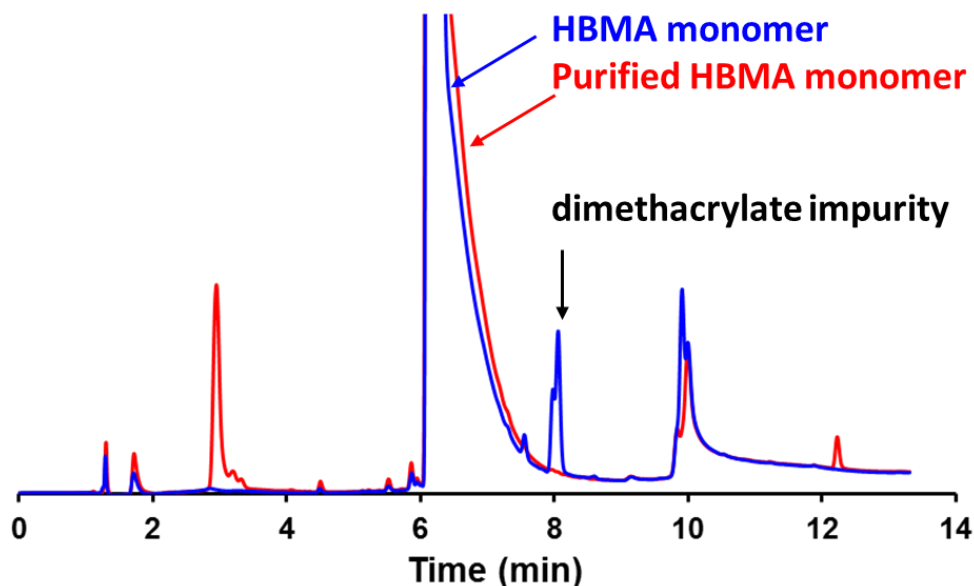


Figure 3.4 HPLC chromatograms of the as-received HBMA monomer and the purified HBMA monomer. An approximately 87% removal of the original dimethacrylate impurity is observed leaving approxing 0.57 mol% dimethacrylate still present in the purified HBMA monomer.

A series of PMAA₅₆-PHBMA_y diblock copolymers (targeting $y = 130$ to 300) was then prepared using this purified HBMA monomer. The MAA residues of the diblock copolymer chains were methylated using excess trimethylsilyl diazomethane and proved to be fully soluble in a THF eluent containing 1.0% glacial acetic acid,⁴³ which indicates a substantial reduction in the degree of crosslinking. The addition of 1.0% glacial acetic acid to the THF GPC eluent, which aids GPC analysis if any residual non-methylated methacrylic acid residues are present. The molecular weight of the diblock copolymer chains increased as the target PHBMA DP was varied from 130 to 300 but dispersities ranged from 1.18 to 6.13, which suggests substantial branching (see Figure 3.5).^{44, 45}

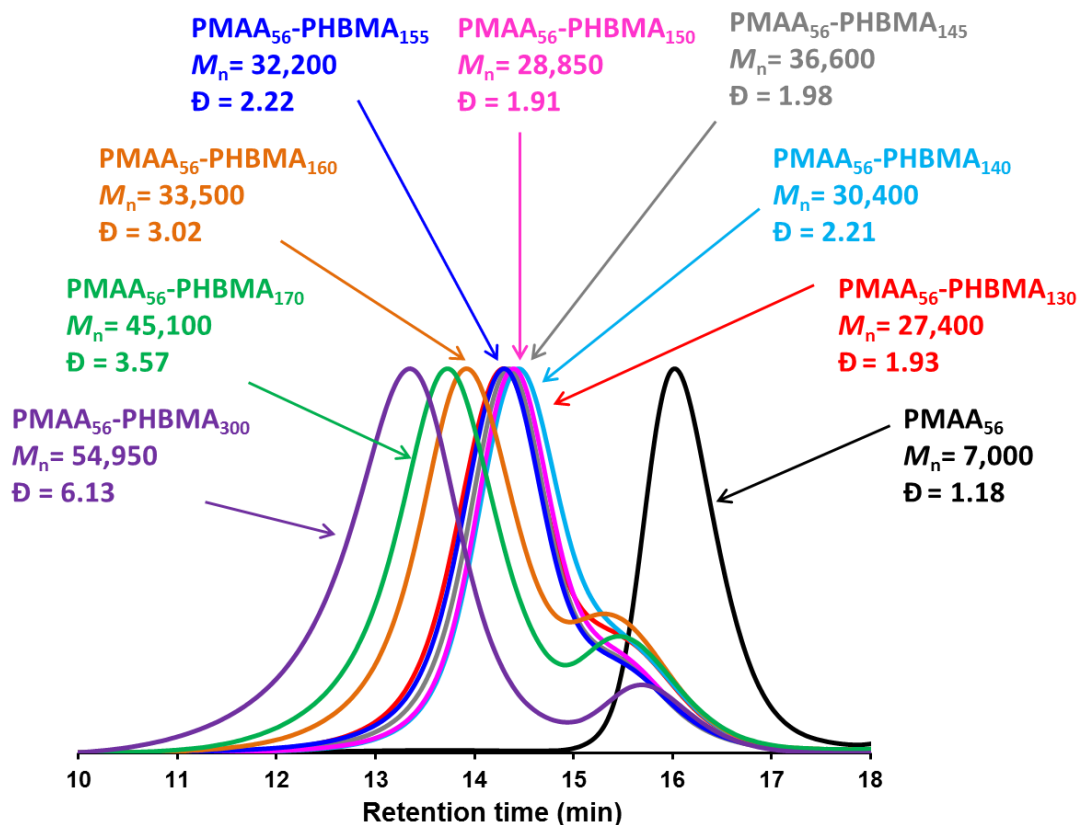


Figure 3.5 THF GPC chromatograms recorded for PMAA₅₆-PHBMA_y diblock copolymers prepared at 20% w/w copolymer concentration *via* RAFT polymerization of purified HBMA monomer in water. All diblock copolymers were modified by methylation of the PMAA block prior to GPC analysis. The THF eluent contained 1.0% glacial acetic acid, which aids GPC analysis if any residual non-methylated methacrylic acid residues are present. Molecular weight data are expressed relative to a series of near-monodisperse PMMA standards. These GPC data indicate substantial branching due to presence of dimethacrylate impurities, which are only partially removed by the HBMA purification protocol. Nevertheless, it is worth emphasizing that no GPC data at all could be obtained for similar diblock copolymers prepared using the as-received HBMA monomer. This is because the dimethacrylate impurity level is so high that extensive cross-linking occurs, which renders these methylated copolymer chains insoluble in THF.

TEM analysis of this second series of PMAA₅₆-PHBMA_y nano-objects prepared using purified HBMA monomer confirmed that a ‘monkey nut’ copolymer morphology could still be obtained, see Figure 3.6. Thus such nano-objects do not appear to be an artefact caused by crosslinking. Moreover, the ‘monkey nut’ morphology is observed for PHBMA DPs of 130 to 155, which is somewhat a broader range than that obtained when using the as-received HBMA monomer.

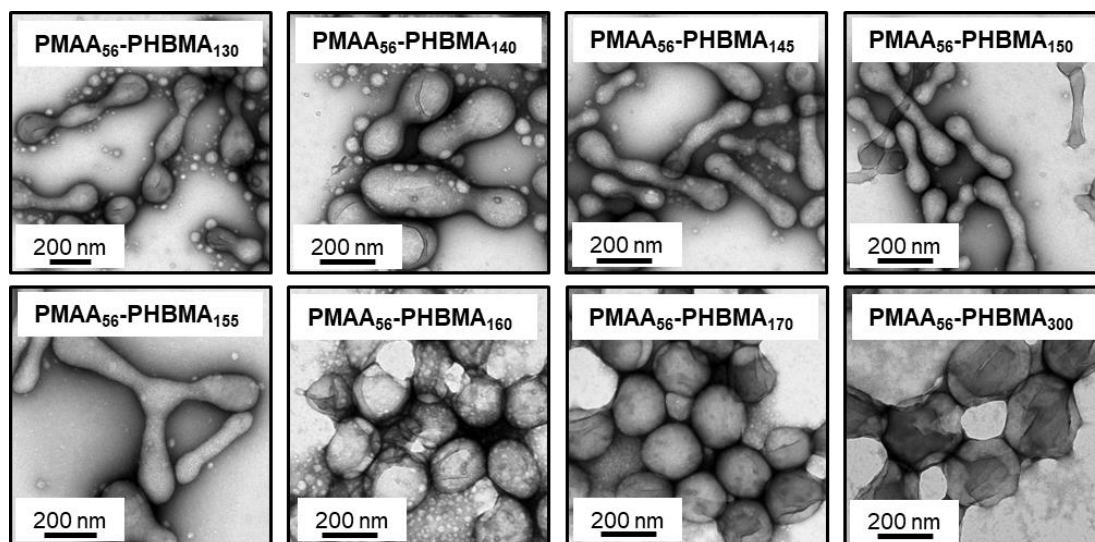


Figure 3.6 PISA syntheses conducted using a purified batch of HBMA monomer also produce a “monkey nut” morphology when targeting $\text{PMAA}_{56}\text{-PHBMA}_y$, where $y = 130$ to 155 . This clearly indicates that this unusual morphology is not simply the result of *in situ* cross-linking as a result of the dimethacrylate impurity in the HBMA monomer.

3.4.4. Analysis using Shear-Induced Polarized Light Imaging to confirm the presence of non-spherical nanoparticles

$\text{PMAA}_{56}\text{-PHBMA}_{150}$ ‘monkey nut’ nanoparticles prepared using purified HBMA monomer were analyzed using the shear-induced polarized light imaging (SIPLI) technique, see Figure 3.7.⁴⁶⁻⁴⁹ It is well-known that anisotropic nanoparticles can be aligned when subjected to an applied shear.^{50, 51} Above a certain critical shear rate, alignment in the direction of flow leads to shear-thinning behavior and the observation of birefringence. In a SIPLI experiment, linearly-polarized white light is directed through a transparent quartz plate on which an aqueous dispersion of $\text{PMAA}_{56}\text{-PHBMA}_{150}$ ‘monkey nuts’ at 20% w/w copolymer concentration is placed. After transmission through the dispersion, the light is reflected by a polished steel plate and then analyzed at 90° to the plane of polarization using a CCD camera. Because the reflected light is analyzed at 90° to the incident light, only rotated light is detected. Particle alignment leads to the observation of a characteristic Maltese cross pattern.

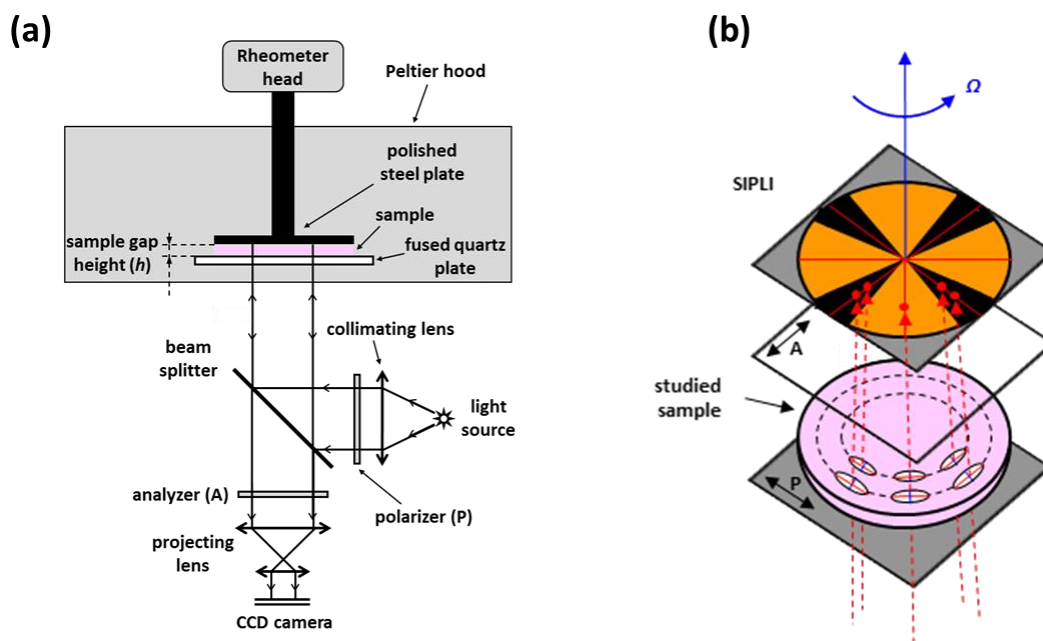


Figure 3.7 Schematic diagram for (a) the experimental set-up for a SIPLI experiment including the arrangement of the light source, polarizer, analyzer and CCD camera in relation to the rheometer, and (b) the formation of shear-induced polarized light imaging (SIPLI), simplified to show a linear arrangement. The perpendicular planes of polarization for the polarizer (P) and the analyzer (A) are indicated by the double-sided arrows. Lines within the white ellipsoids represent the optical axes of the sheared object, with the long axis corresponding to n_1 (red lines) being parallel to the direction of shear-alignment (dashed circles). The angular speed (Ω) indicates the direction of rotation for the polished steel plate.⁴⁶⁻⁴⁹

The PMAA₅₆-PHBMA₁₅₀ ‘monkey nut’ nanoparticles were subjected to shear rates ranging from 50 to 500 s⁻¹ (Figure 3.8). There is a shear rate gradient across the polished steel plate from its center to the periphery, with the maximum shear rate being obtained at the plate edge. A characteristic Maltese cross pattern was observed at maximum shear rates of either 200 or 500 s⁻¹ indicating alignment of anisotropic nanoparticles. The critical shear rate for nanoparticle alignment can be calculated from the image at a maximum shear rate of 100 s⁻¹, where a partial Maltese cross pattern is obtained with a dark circle in the center, see Figure 3.8b. The critical shear rate under these conditions is 40 s⁻¹, which corresponds to a mean relaxation time of approximately 25 ms. This represents the time scale required to produce an isotropic dispersion after cessation of the applied shear.

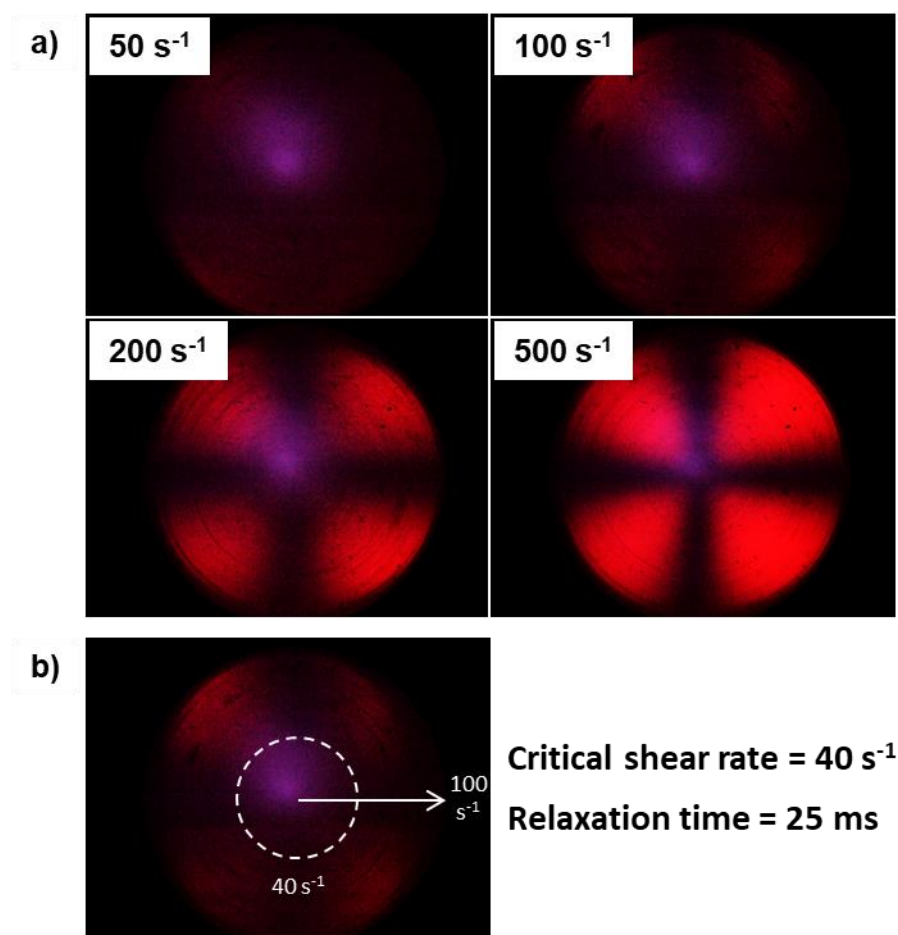


Figure 3.8 (a) Polarized light images obtained for a 20% w/w aqueous dispersion of PMAA₅₆-PHBMA₁₅₀ ‘monkey nut’ nanoparticles at maximum shear rates of 50, 100, 200 and 500 s⁻¹. (b) A Maltese cross is observed above a critical shear rate of 40 s⁻¹, indicating shear-induced alignment. Thus the mean relaxation time of the ‘monkey nut’ nanoparticles corresponds to approximately 25 ms.

3.4.5. Confirmation of diblock copolymer nanoparticle morphologies by Small Angle X-ray Scattering (SAXS)

SAXS was used to confirm the copolymer morphologies indicated by TEM studies, see Figure 3.9. To a good first approximation, the copolymer morphology is indicated by the gradient in the low q regime. Spherical micelles are characterized by a gradient of zero and rigid rods possess a gradient of negative unity.⁵² Although they exhibit considerable flexibility, highly anisotropic diblock copolymer worms prepared *via* PISA behave more or less like rigid rods in terms of their SAXS patterns.^{53, 54} Inspecting Figure 3.9, the $I(q)$ vs. q scattering pattern recorded for a 1.0% w/w dispersion of PMAA₅₆-PHBMA₅₀ diblock copolymer nanoparticles can be satisfactorily fitted to a previously reported spherical micelle model, with a

volume-average core diameter of 19 ± 3 nm (Figure 3.9(a)).⁵⁵ The same spherical micelle model also provided good fits to the scattering patterns obtained for the PMAA₅₆-PHBMA₃₀₀ and PMAA₅₆-PHBMA₁₀₀₀ nanoparticles. In each case, the gradient at low q of approximately zero confirms the spherical morphology indicated by TEM studies, with SAXS volume-average diameters estimated to be 262 ± 26 nm and 330 ± 22 nm, respectively (Figure 3.9(d) and (e) respectively). These analyses enable us to reject our initial hypothesis that the latter nano-objects might be thick-walled vesicles, not least because there is no evidence for any membrane structure. Moreover, the presence of multiple fringes in these latter two scattering patterns suggest relatively narrow size distributions in each case. In contrast, the scattering patterns recorded for the PMAA₅₆-PHBMA₁₅₀ ‘monkey nut’ nanoparticles (synthesized with either the as-received or the purified HBMA monomer) cannot be fitted using the spherical model (Figure 3.9(b) and (c)). These patterns have low q gradients of -0.82 and -0.71 respectively, confirming that these nanoparticles possess significant anisotropic character (as suggested by TEM analysis and SIPLI). In addition, the lack of a well-defined local minimum at high q suggests that these ‘monkey nut’ nanoparticles are relatively polydisperse in terms of their mean widths. Although not yet fully analyzed, these preliminary SAXS data are important, because they are much more statistically robust than TEM analyses. They confirm a unique evolution in copolymer morphology for this PMAA₅₆-PHBMA_x PISA formulation from small spheres to monkey nuts to large spheres with increasing x values. Further information obtained from SAXS analysis can be found in Appendix 2.

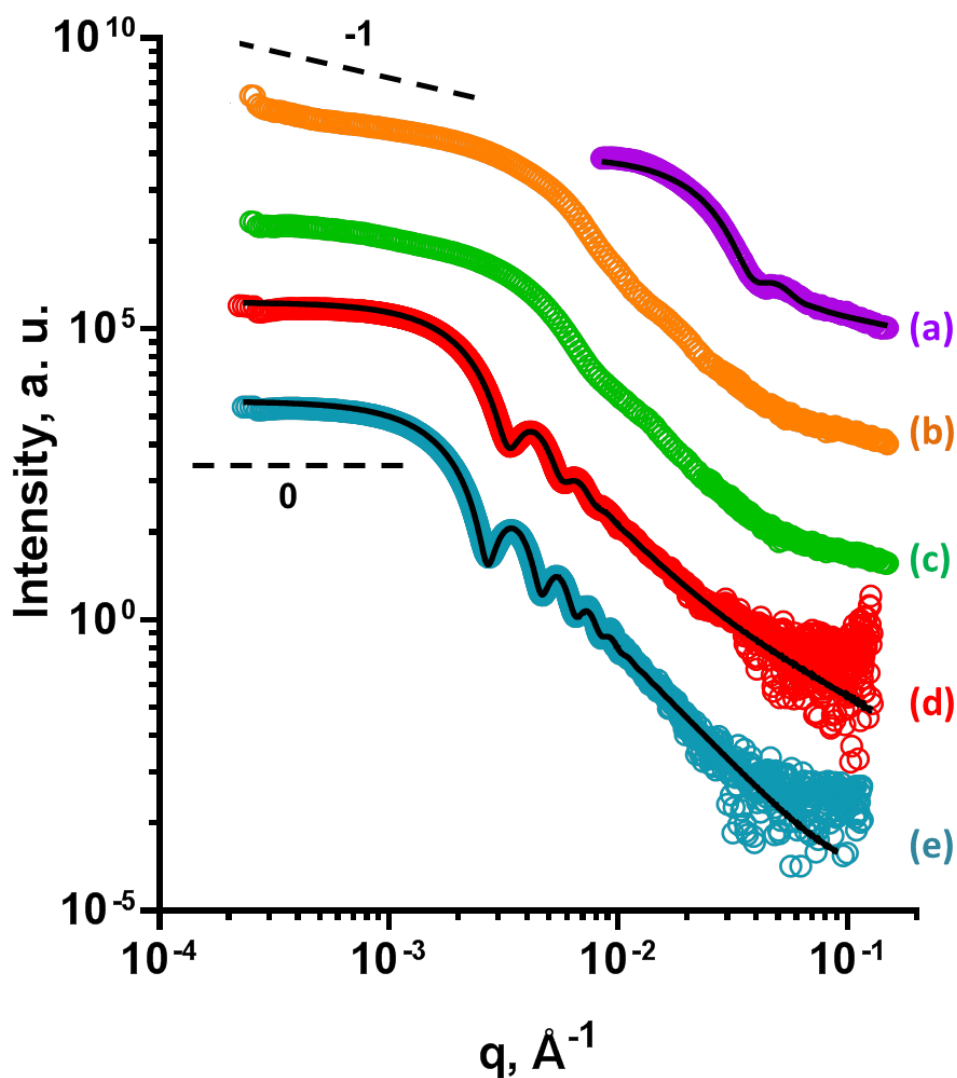


Figure 3.9 SAXS patterns recorded for from 1.0% w/w aqueous dispersions of PMAA₅₆-PHBMA_y diblock copolymer nano-objects at pH 5: (a) PMAA₅₆-PHBMA₅₀ spheres, (b) PMAA₅₆-PHBMA₁₅₀ ‘monkey nut’ nanoparticles (prepared using purified HBMA monomer), (c) PMAA₅₆-PHBMA₁₅₀ ‘monkey nut’ nanoparticles (prepared using as-received HBMA monomer), (d) PMAA₅₆-PHBMA₃₀₀ spheres and (e) PMAA₅₆-PHBMA₁₀₀₀ spheres. SAXS patterns (a), (d) and (e) are fitted to a spherical micelle model. SAXS patterns (b) and (c) cannot be fitted using a spherical model

3.4.6. Synthesis of PMAA₅₆-PHBMA₁₅₀ diblock copolymer nanoparticles at varying copolymer concentrations

As discussed in Chapter 2, it has been previously reported that the particle morphology obtained by PISA can be affected by the copolymer concentration. Typically, higher copolymer concentrations favor the formation of worms and vesicles.¹⁴ Thus, the synthesis of PMAA₅₆-PHBMA₁₅₀ diblock copolymer nanoparticles was repeated at copolymer concentrations of 10, 20 and 30% w/w for comparison, see Table 3.2. High monomer conversions (> 99%) were achieved in all three cases. These syntheses were conducted using purified HBMA, thus enabling analysis by THF GPC after methylation. The resulting GPC chromatograms are similar to those reported above, with relatively high dispersities indicating substantial branching despite purification of the HBMA monomer, see Figure 3.10.

Table 3.2 Monomer conversions, number-average molecular weights (M_n), dispersities (\mathcal{D}) and mean DLS and TEM diameters for a series of PMAA₅₆-PHBMA₁₅₀ diblock copolymer nanoparticles prepared *via* RAFT aqueous emulsion polymerization of HBMA at 10, 20 and 30% w/w copolymer concentration.

Copolymer concentration (% w/w)	Monomer conversion (%) ^a	DLS particle diameter (nm)	DLS particle polydispersity	TEM particle diameter (nm) ^b	Zeta potential (mV)	M_n^c (g mol ⁻¹)	\mathcal{D}^c
10	> 99	230	0.02	82	-57	33,700	3.67
20	> 99	199	0.07	85 (w) 270 (l)	-60	28,800	1.91
30	> 99	127	0.21	48	-65	36,500	1.67

^aConversion determined by ¹H NMR spectroscopy

^bFor anisotropic particles (w) = width and (l) = length

^cMolecular weight data determined by GPC using THF eluent containing 1% v/v glacial acetic acid (calibrated using a series of near-monodisperse PMMA standards).

DLS and TEM studies indicate that the ‘monkey nut’ morphology was only formed at 20% w/w, see Figure 3.11. For RAFT aqueous dispersion polymerization, such as the well-studied PGMA-PPMA system, higher order morphologies are often obtained at higher copolymer concentrations.^{10, 13, 14, 53, 56} In contrast, RAFT aqueous emulsion polymerization systems are often limited to spherical nanoparticles, as reported by Cunningham *et al.* for the PGMA-PBzMA system.⁶

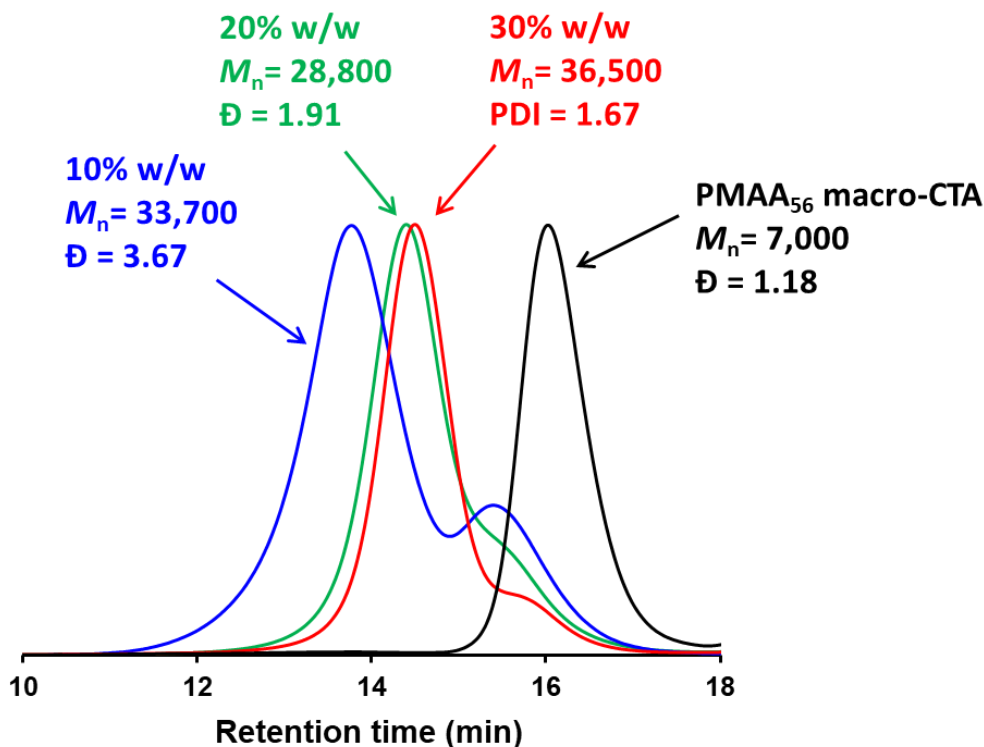


Figure 3.10 THF GPC chromatograms of PMAA₅₆-PHBMA₁₅₀ diblock copolymers synthesized *via* RAFT aqueous emulsion polymerization of HBMA at 10, 20 and 30% copolymer concentration. Eluent contained 1.0% w/w acetic acid. Molecular weight data are expressed relative to a series of near-monodisperse PMMA standards.

Given that HBMA reacts *via* RAFT aqueous emulsion polymerization we would perhaps expect to obtain only spherical nanoparticles. However, the non-spherical ‘monkey nut’ morphology is observed at 20% w/w copolymer concentration, see Figure 3.11. Therefore, we anticipated that the nanoparticles formed at 30% w/w copolymer concentration would also be non-spherical. Somewhat surprisingly this proved not to be the case. This result indicates that there is a rather precise set of conditions required to enable the synthesis of these ‘monkey nut’ particles. In principle, at 30% w/w copolymer concentration there should be more monomer available to plasticize nanoparticle cores, which should facilitate the transition from spheres to higher-order morphologies. However, it does not appear that the presence of additional monomer aids this morphological transition in this case.

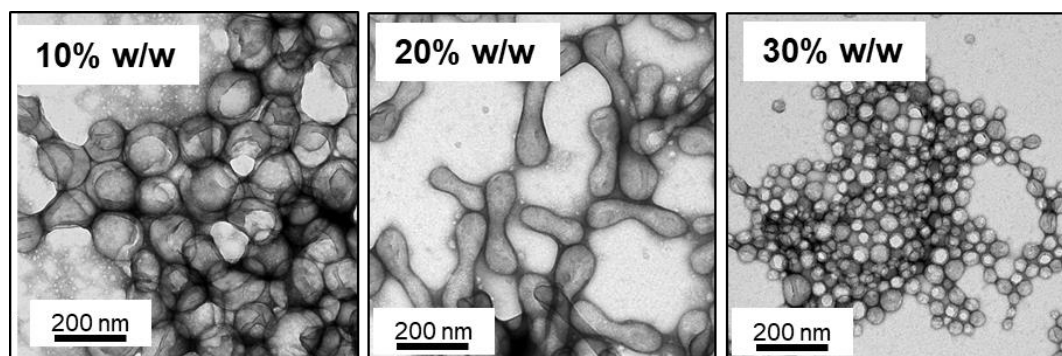


Figure 3.11 Representative TEM images of PMAA₅₆-PHBMA₁₅₀ diblock copolymer nanoparticles synthesized *via* RAFT aqueous emulsion polymerization of HBMA at copolymer concentrations of 10, 20 and 30% w/w. These PISA syntheses were conducted using purified HBMA monomer.

3.4.7. Comparison of reaction kinetics for the RAFT aqueous emulsion polymerization of HPMA and HBMA

The work reported so far in this Thesis indicates that the aqueous solubility of the core-forming monomer appears to be an important parameter for access to non-spherical morphologies during aqueous PISA. We hypothesize that RAFT aqueous emulsion polymerization is limited to spherical nanoparticles owing to the relatively low aqueous solubility of the monomer. In a RAFT aqueous dispersion polymerization, a *water-miscible* monomer is polymerized (e.g. HPMA). This monomer can readily diffuse through the aqueous phase into the growing particles, thus plasticizing the core-forming block and so aiding sphere-sphere fusions which is the first step for the formation of worms and vesicles. In contrast, the *water-immiscible* monomers polymerized *via* RAFT aqueous emulsion polymerization cannot diffuse as quickly through the aqueous phase on the time scale of the polymerization to plasticize the particle cores, resulting in the formation of kinetically-trapped spheres.

To investigate the effect of aqueous monomer solubility on polymerization kinetics, kinetic data were obtained for the synthesis of PMAA₅₆-PHBMA₁₅₀ nanoparticles at 20% w/w copolymer concentration and PMAA₅₆-PHPMA₁₅₀ nanoparticles at 18.8% w/w. The latter concentration provides the same molar concentration of HPMA as that of HBMA.³⁸ Both diblock copolymers were prepared *via* RAFT polymerization in water at 70 °C.

Both polymerizations reached > 98% conversion within 90 min, see Figure 3.12. The semi-log plot data indicates that the reaction kinetics are very similar for each monomer. Initially, mild retardation is observed as expected (but not well understood) for RAFT polymerization of methacrylates.⁵⁷ At ~ 40 min in both polymerizations an increase in slope of the semi-log plot is observed. For the HBMA this indicates that the rate of polymerization increases by a factor of ~ 4 whereas, for the HPMA polymerization the rate increases by a factor of ~ 2.5. This rate increase corresponds to the onset of particle nucleation. As the particles form, unreacted monomer migrates to the growing particle cores causing an increase in effective monomer concentration and thus, an observed rate enhancement.¹⁰

The PMAA₅₆-PHPMA₁₅₀ diblock copolymers form spherical nanoparticles, whereas the PMAA₅₆-PHBMA₁₅₀ diblock copolymers self-assemble to form the ‘monkey nut’ morphology discussed above, see Figure 3.13. This seems rather surprising given that the aqueous solubility of HPMA is significantly higher than that of HBMA. However, for this kinetic experiment the HPMA monomer concentration during the polymerization (18.8% w/w) was higher than the aqueous solubility of HPMA (10% w/w at 70 °C). Thus, at least initially the polymerization could proceed *via* a RAFT aqueous emulsion polymerization mechanism owing to the presence of undissolved HPMA monomer at the start of the polymerization.

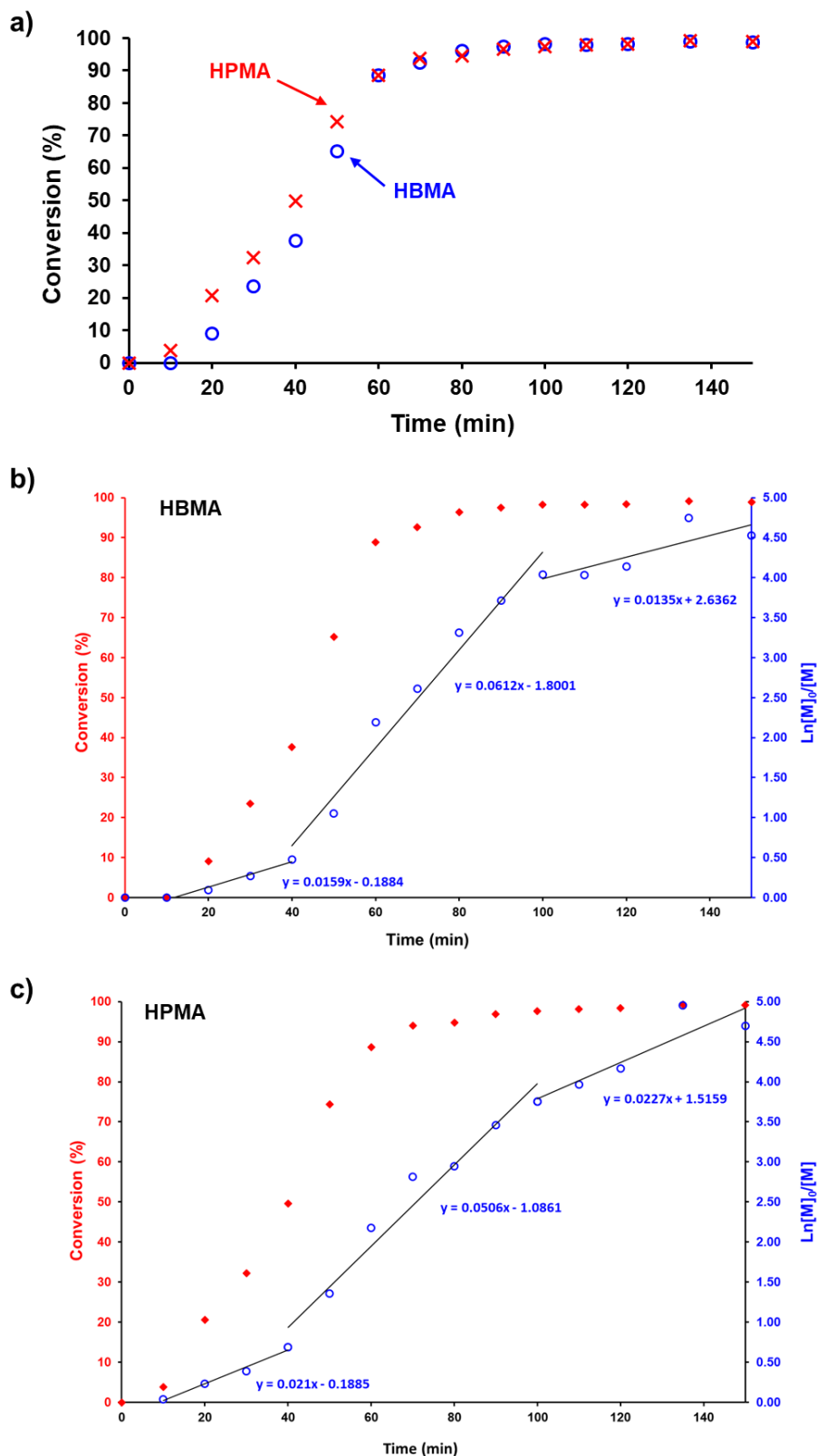


Figure 3.12 Kinetic data obtained for the synthesis of PMAA₅₆-PHBMA₁₅₀ at 20% w/w and PMAA₅₆-PHPMA₁₅₀ at 18.82% w/w. Both diblock copolymers were prepared *via* RAFT polymerization in water at 70 °C. The copolymer concentration of the latter formulation was adjusted to maintain the same molar concentration of monomer. (a) monomer conversion vs. time, (b) monomer conversion and semi-log plot vs. time for the synthesis of PMAA₅₆-PHBMA₁₅₀ and (c) monomer conversion and semi-log plot vs. time for the synthesis of PMAA₅₆-PHPMA₁₅₀.

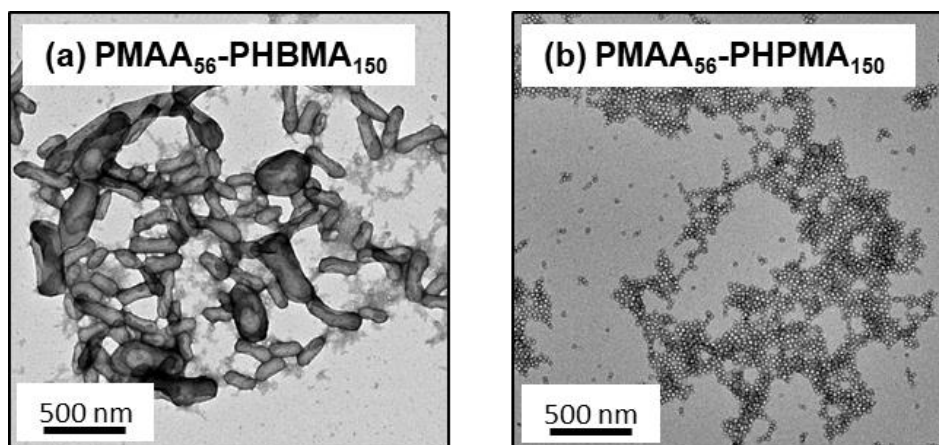


Figure 3.13 Representative TEM images of (a) PMAA₅₆-PHBMA₁₅₀ ‘monkey-nut’ nanoparticles and (b) PMAA₅₆-PHPMA₁₅₀ spherical nanoparticles synthesized *via* RAFT aqueous polymerization at 70 °C.

3.4.8. *Changing the stabilizer block to a shorter PMAA₂₉ macro-CTA or to a PGMA₅₀ macro-CTA.*

Previous literature indicates that using a shorter stabilizer block can lead to the formation of higher order morphologies over a wide range of core-forming block DPs.¹⁴ To try and obtain higher order morphologies, a shorter PMAA₂₉ macro-CTA with a DP of 29 was selected for chain extension with HBMA *via* RAFT aqueous emulsion polymerization. A range of PHBMA DPs was targeted from 50 to 150 and each polymerization proceeded to high conversion (> 99%), as judged by ¹H NMR spectroscopy, see Table 3.3. Analysis by DLS, suggested the formation of reasonably large (125 to 190 nm) and polydisperse particles (0.15 to 0.92), with no discernable trend in particle size. TEM analysis of the resulting diblock copolymer nanoparticles indicated that only spherical nanoparticles (24 to 110 nm) were formed by PISA, see Figure 3.14. It is possible that the ‘monkey nut’ phase was missed and could be obtained with further investigation owing to the very small phase space it occupies. As these particles were synthesized with the as-received HBMA monomer GPC analysis was not conducted.

Chapter 3: Effect of monomer solubility on the evolution of copolymer morphology during polymerization-induced self-assembly in aqueous solution

Table 3.3 Monomer conversions and mean DLS and TEM diameters for a series of PMAA₂₉-PHBMA_y diblock copolymer nanoparticles (y = 50 – 150) and a series of PGMA₅₀-PHBMA_y diblock copolymer nanoparticles (y = 50 – 400) both prepared *via* RAFT aqueous emulsion polymerization at 20% w/w copolymer concentration.

Target composition	Monomer conversion (%) ^a	DLS particle diameter (nm)	DLS particle polydispersity	TEM particle diameter (nm)
PMAA ₂₉ -PHBMA ₅₀	> 99	158	0.47	24
PMAA ₂₉ -PHBMA ₆₀	> 99	161	0.28	27
PMAA ₂₉ -PHBMA ₇₀	> 99	127	0.56	26
PMAA ₂₉ -PHBMA ₈₀	> 99	158	0.45	29
PMAA ₂₉ -PHBMA ₁₀₀	> 99	144	0.92	41
PMAA ₂₉ -PHBMA ₁₂₅	> 99	126	0.21	70
PMAA ₂₉ -PHBMA ₁₅₀	> 99	187	0.15	111
PGMA ₅₀ -PHBMA ₅₀	> 99	26	0.28	24
PGMA ₅₀ -PHBMA ₁₅₀	> 99	39	0.30	33
PGMA ₅₀ -PHBMA ₂₀₀	> 99	82	0.17	39
PGMA ₅₀ -PHBMA ₄₀₀	> 99	94	0.17	50

^a Conversion determined by ¹H NMR spectroscopy

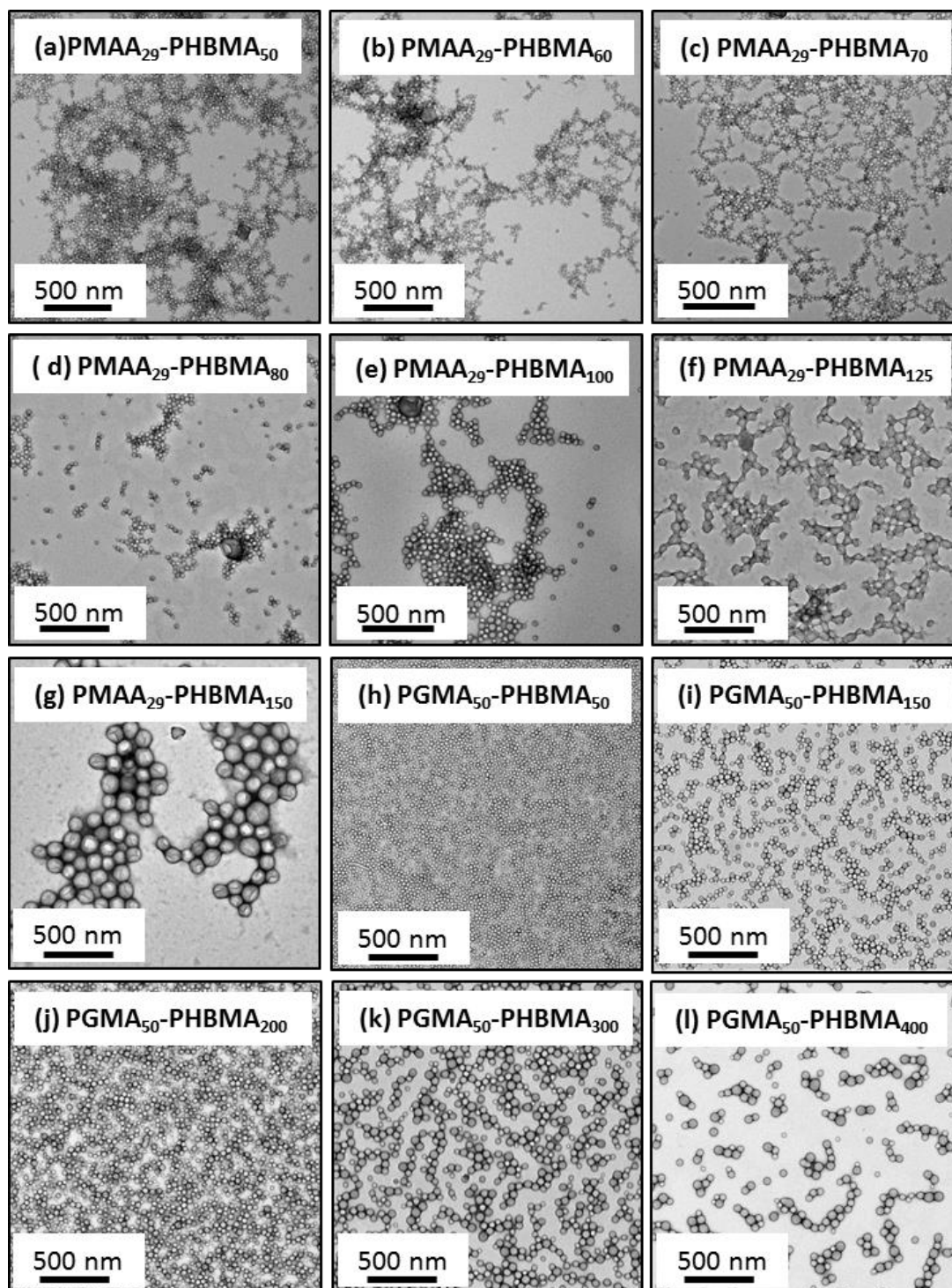


Figure 3.14 TEM images obtained for PMAA₂₉-PHBMA_y (a – g) and PGMA₅₀-PHBMA_y (h – k) diblock copolymer nanoparticles prepared at 20% w/w copolymer concentration *via* RAFT aqueous emulsion polymerization of HBMA at 70 °C. PISA leads only to the formation of spherical nanoparticles for PMAA₂₉-PHBMA_y diblocks with a PHBMA DP (a) 50, (b) 60, (c) 70, (d) 80, (e) 100, (f) 125 and (g) 150 and for PGMA₅₀-PHBMA_y with a PHBMA DP of (h) 50, (i) 150, (j) 200, (k) 300, (l) 400.

In addition to these experiments, a PGMA₅₀ macro-CTA was also chain-extended with HBMA *via* RAFT aqueous emulsion polymerization at 20% w/w copolymer concentration. PGMA was selected as an alternative stabilizer block owing to its non-ionic character. The use of a non-ionic stabilizer block should aid the formation of non-spherical nanoparticles by PISA, as sphere-sphere fusion is considered to be a key step in the transition from spherical nanoparticles to worms. A series of PGMA₅₀-PHBMA_y diblock copolymers was synthesized targeting a range of PHBMA DPs from 50 to 400. All syntheses proceeded to high conversion (> 99%), as judged by ¹H NMR spectroscopy, see Table 3.3. For this series of PGMA₅₀-PHBMA_y diblock copolymers DMF GPC analysis was possible, see Figure 3.15. However, the resulting GPC chromatograms indicate relatively high dispersities indicating substantial branching caused by the dimethacrylate impurity of the HBMA monomer. Analysis of the resulting nanoparticles by DLS showed an increasing particle diameter from 26 to 102 nm with PHBMA DP. TEM analysis of the particles indicated that only spherical nanoparticles were formed, despite the use of a non-ionic PGMA macro-CTA, see Figure 3.14. Unpublished work in the Armes group, has shown that sometimes very small vesicles are indistinguishable from spheres by TEM. Therefore, it would be worth analyzing these particles by SAXS to confirm the morphology.

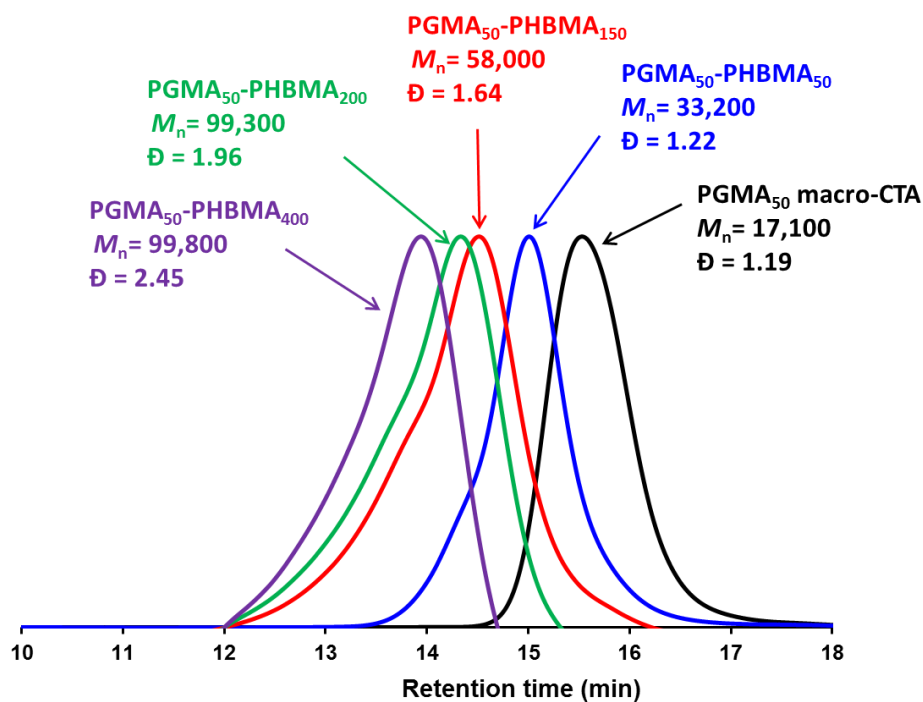


Figure 3.15 DMF GPC chromatograms for a series of PGMA₅₀-PHBMA_y diblock copolymers ($y = 50$ to 400) synthesized *via* RAFT aqueous emulsion polymerization of HBMA at 70 °C. Molecular weight data are expressed relative to a series of near-monodisperse PMMA standards.

3.5. Conclusions

In summary, the RAFT aqueous polymerization of HBMA at pH 5 using a PMAA₅₆ macro-CTA leads to the formation of elongated nanoparticles with an unusual ‘monkey nut’ morphology over a relatively narrow range of core-forming block DPs. This nanoparticle anisotropy is confirmed by SAXS analysis and is sufficient to enable shear alignment, as indicated by SIPL studies. These observations suggest that the aqueous solubility of the monomer can play an important role in determining the copolymer morphology during aqueous PISA syntheses. Sufficiently high monomer solubility enables the restrictive paradigm of kinetically-trapped spheres to be broken. Presumably this is because additional monomer can diffuse into the growing nanoparticle cores on the time scale of the polymerization, thus leading to greater solvation and hence mobility for the PHBMA chains. This aids sphere-sphere fusion, which is a prerequisite for the formation of the ‘monkey nut’ morphology. In future work, we plan to fit the SAXS scattering patterns obtained for these ‘monkey nut’ nanoparticles using an appropriate new analytical model.

3.6. References

1. B. Charleux, G. Delaittre, J. Rieger and F. D’Agosto, *Macromolecules*, 2012, **45**, 6753-6765.
2. S. L. Canning, G. N. Smith and S. P. Armes, *Macromolecules*, 2016, **49**, 1985-2001.
3. M. J. Derry, L. A. Fielding and S. P. Armes, *Progress in Polymer Science*, 2016, **52**, 1-18.
4. W. Cai, W. Wan, C. Hong, C. Huang and C. Pan, *Soft Matter*, 2010, **6**, 5554-5561.
5. N. J. Warren and S. P. Armes, *Journal of the American Chemical Society*, 2014, **136**, 10174-10185.
6. V. J. Cunningham, A. M. Alswieleh, K. L. Thompson, M. Williams, G. J. Leggett, S. P. Armes and O. M. Musa, *Macromolecules*, 2014, **47**, 5613-5623.
7. J. Rieger, W. Zhang, F. Stoffelbach and B. Charleux, *Macromolecules*, 2010, **43**, 6302-6310.
8. S. Binauld, L. Delafresnaye, B. Charleux, F. D’Agosto and M. Lansalot, *Macromolecules*, 2014, **47**, 3461-3472.
9. A. Blanazs, S. P. Armes and A. J. Ryan, *Macromolecular Rapid Communications*, 2009, **30**, 267-277.
10. A. Blanazs, J. Madsen, G. Battaglia, A. J. Ryan and S. P. Armes, *Journal of the American Chemical Society*, 2011, **133**, 16581-16587.
11. G. Liu, Q. Qiu and Z. An, *Polymer Chemistry*, 2012, **3**, 504-513.
12. G. Liu, Q. Qiu, W. Shen and Z. An, *Macromolecules*, 2011, **44**, 5237-5245.

13. Y. Li and S. P. Armes, *Angewandte Chemie International Edition*, 2010, **49**, 4042-4046.
14. A. Blanazs, A. J. Ryan and S. P. Armes, *Macromolecules*, 2012, **45**, 5099-5107.
15. L. P. D. Ratcliffe, A. J. Ryan and S. P. Armes, *Macromolecules*, 2013, **46**, 769-777.
16. W. Shen, Y. Chang, G. Liu, H. Wang, A. Cao and Z. An, *Macromolecules*, 2011, **44**, 2524-2530.
17. W. Zhou, Q. Qu, Y. Xu and Z. An, *ACS Macro Letters*, 2015, **4**, 495-499.
18. S. Sugihara, A. H. Ma'Radzi, S. Ida, S. Irie, T. Kikukawa and Y. Maeda, *Polymer*, 2015, **76**, 17-24.
19. S. Sugihara, A. Blanazs, S. P. Armes, A. J. Ryan and A. L. Lewis, *Journal of the American Chemical Society*, 2011, **133**, 15707-15713.
20. M. F. Cunningham, *Progress in Polymer Science*, 2008, **33**, 365-398.
21. C. J. Ferguson, R. J. Hughes, B. T. T. Pham, B. S. Hawkett, R. G. Gilbert, A. K. Serelis and C. H. Such, *Macromolecules*, 2002, **35**, 9243-9245.
22. C. J. Ferguson, R. J. Hughes, D. Nguyen, B. T. T. Pham, R. G. Gilbert, A. K. Serelis, C. H. Such and B. S. Hawkett, *Macromolecules*, 2005, **38**, 2191-2204.
23. X. Zhang, S. Boissé, W. Zhang, P. Beaunier, F. D'Agosto, J. Rieger and B. Charleux, *Macromolecules*, 2011, **44**, 4149-4158.
24. N. P. Truong, M. V. Dussert, M. R. Whittaker, J. F. Quinn and T. P. Davis, *Polymer Chemistry*, 2015, **6**, 3865-3874.
25. J. Rieger, F. Stoffelbach, C. Bui, D. Alaimo, C. Jérôme and B. Charleux, *Macromolecules*, 2008, **41**, 4065-4068.
26. W. Zhang, F. D'Agosto, O. Boyron, J. Rieger and B. Charleux, *Macromolecules*, 2011, **44**, 7584-7593.
27. I. Chaduc, W. Zhang, J. Rieger, M. Lansalot, F. D'Agosto and B. Charleux, *Macromolecular Rapid Communications*, 2011, **32**, 1270-1276.
28. I. Chaduc, M. Girod, R. Antoine, B. Charleux, F. D'Agosto and M. Lansalot, *Macromolecules*, 2012, **45**, 5881-5893.
29. I. Chaduc, A. Crepet, O. Boyron, B. Charleux, F. D'Agosto and M. Lansalot, *Macromolecules*, 2013, **46**, 6013-6023.
30. S. Fréal-Saison, M. Save, C. Bui, B. Charleux and S. Magnet, *Macromolecules*, 2006, **39**, 8632-8638.
31. M. Manguian, M. Save and B. Charleux, *Macromolecular Rapid Communications*, 2006, **27**, 399-404.
32. S. Boissé, J. Rieger, K. Belal, A. Di-Cicco, P. Beaunier, M.-H. Li and B. Charleux, *Chemical Communications*, 2010, **46**, 1950-1952.
33. S. Boissé, J. Rieger, G. Pembouong, P. Beaunier and B. Charleux, *Journal of Polymer Science Part A: Polymer Chemistry*, 2011, **49**, 3346-3354.
34. W. Zhang, F. D'Agosto, O. Boyron, J. Rieger and B. Charleux, *Macromolecules*, 2012, **45**, 4075-4084.
35. W. Zhang, F. D'Agosto, P.-Y. Dugas, J. Rieger and B. Charleux, *Polymer*, 2013, **54**, 2011-2019.
36. J. Lesage de la Haye, X. Zhang, I. Chaduc, F. Brunel, M. Lansalot and F. D'Agosto, *Angewandte Chemie International Edition*, 2016, **55**, 3739-3743.
37. N. P. Truong, J. F. Quinn, A. Anastasaki, D. M. Haddleton, M. R. Whittaker and T. P. Davis, *Chemical Communications*, 2016, **52**, 4497-4500.
38. L. P. D. Ratcliffe, A. Blanazs, C. N. Williams, S. L. Brown and S. P. Armes, *Polymer Chemistry*, 2014, **5**, 3643-3655.

39. C. A. Figg, R. N. Carmean, K. C. Bentz, S. Mukherjee, D. A. Savin and B. S. Sumerlin, *Macromolecules*, 2017, **50**, 935-943.
40. J. Illavsky and P. R. Jemian, *Journal of Applied Crystallography*, 2009, **42**, 347-353.
41. S. Sugihara, S. P. Armes, A. Blanazs and A. L. Lewis, *Soft Matter*, 2011, **7**, 10787-10793.
42. S. Coca, C. B. Jasieczek, K. L. Beers and K. Matyjaszewski, *Journal of Polymer Science: Part A: Polymer Chemistry*, 1998, **36**, 1417-1424.
43. L. Couvreur, C. Lefay, J. Belleney, B. Charleux, O. Guerret and S. Magnet, *Macromolecules*, 2003, **36**, 8260-8267.
44. I. Bannister, N. C. Billingham, S. P. Armes, S. P. Rannard and P. Findlay, *Macromolecules*, 2006, **39**, 7483-7492.
45. J. Rosselgong, S. P. Armes, W. R. S. Barton and D. Price, *Macromolecules*, 2010, **43**, 2145-2156.
46. O. O. Mykhaylyk, *Soft Matter*, 2010, **6**, 4430-4440.
47. O. O. Mykhaylyk, P. Chambon, C. Impradice, J. P. A. Fairclough, N. J. Terrill and A. J. Ryan, *Macromolecules*, 2010, **43**, 2389-2405.
48. O. O. Mykhaylyk, A. J. Parnell, A. Pryke and J. P. A. Fairclough, *Macromolecules*, 2012, **45**, 5260-5272.
49. O. O. Mykhaylyk, N. J. Warren, A. J. Parnell, G. Pfeifer and J. Laeuger, *Journal of Polymer Science Part B: Polymer Physics*, 2016, **54**, 2151-2170.
50. W. J. Orts, *Macromolecules*, 1998, **31**, 5717-5725.
51. B. Z. Tang and H. Xu, *Macromolecules*, 1999, **32**, 2569-2576.
52. O. Glatter and O. Kratky, *Small-angle X-ray scattering*, Academic Press, London, 1982.
53. A. Blanazs, R. Verber, O. O. Mykhaylyk, A. J. Ryan, J. Z. Heath, C. W. I. Douglas and S. P. Armes, *Journal of the American Chemical Society*, 2012, **134**, 9741-9748.
54. L. A. Fielding, J. A. Lane, M. J. Derry, O. O. Mykhaylyk and S. P. Armes, *Journal of the American Chemical Society*, 2014, **136**, 5790-5798.
55. J. S. Pedersen and M. C. Gerstenberg, *Macromolecules*, 1996, **29**, 1363-1365.
56. P. Chambon, A. Blanazs, G. Battaglia and S. P. Armes, *Macromolecules*, 2012, **45**, 5081-5090.
57. G. Moad, E. Rizzardo and S. H. Thang, *Accounts of Chemical Research*, 2008, **41**, 1133-1142.

Chapter Four

4. Optimization of the high-throughput synthesis of multiblock copolymer nanoparticles in aqueous media *via* polymerization-induced self-assembly

Reproduced in full from [A. A. Cockram, R. D. Bradley, S. A. Lynch, P. C. D. Fleming, N. S. J. Williams, M. W. Murray, S. N. Emmet and S. P. Armes, *React. Chem. Eng.*, 2018, **3**, 645-657]. Copyright [2018] The Royal Society of Chemistry.

4.1. Introduction

RAFT polymerization can be conducted in aqueous media to synthesize a remarkably wide range of block copolymer nanoparticles *via* PISA.¹⁻¹³ PISA enables the *rational* synthesis of diblock copolymer nanoparticles directly in water at relatively high concentrations ($\leq 50\%$ w/w).^{3, 14} Various block copolymer morphologies (e.g. spheres,^{4, 15, 16} worms,¹⁷ nanofibers,⁵ vesicles,^{4, 18} framboidal vesicles,¹⁹ monkey nuts,²⁰ jellyfish⁶ and lamellae¹¹) can be obtained, often simply by varying the DP of the respective blocks.^{2, 7, 10, 11} In principle, such nanoparticles offer a wide range of potential applications, including use as super flocculants,²¹ stem-cell storage media,²² Pickering emulsifiers^{23, 24} and coatings.^{25, 26}

Many important properties of the final block copolymer nanoparticles can be readily tuned by choosing appropriate monomers, targeting suitable block DPs and adjusting the block order.^{1, 7, 19, 27, 28} Additional synthesis parameters such as copolymer concentration, solution pH, polymerization temperature, reaction time, and RAFT agent/initiator molar ratio can also play important roles in determining a successful outcome for a given PISA synthesis.^{7, 11, 15, 29, 30} Given this complexity, optimization of new PISA formulations can be a time-consuming and laborious task, particularly if the construction of phase diagrams is desired.^{3, 7, 10, 31, 32} In principle, this ‘bottleneck’ problem can be addressed by using a high-throughput strategy to perform parallel syntheses of multiple reactions under similar conditions.³³⁻³⁵ For example, the Chemspeed Autoplant A100 automated synthesizer (Figure 4.7) can perform up to twenty parallel syntheses, which enables several parameters to be explored simultaneously. This high-throughput approach has been successfully applied in many fields such as the pharmaceutical industry, materials research, and polymer science.^{33, 34, 36-45} More specifically, pharmaceutical research has benefited from rapid screening of large libraries of potential lead compounds, which can cause a considerable reduction in time-to-market for novel drugs.^{34, 36, 37} In the case of materials research,³⁸ high-throughput strategies have aided the discovery of novel superconducting materials,³⁹ inorganic phosphorous compounds for use in flat-panel displays, lighting and X-ray imaging⁴⁰⁻⁴³ and new polymer catalysts.⁴⁴⁻⁴⁷ Of particular relevance to the present study are high-throughput studies based on living radical polymerization.⁴⁸⁻⁵² For example, a library of acrylic diblock copolymers was synthesized using the so-called macromolecular design *via* the interchange of

xanthates (MADIX) process.⁴⁸ The RAFT solution polymerization of MMA in toluene was successfully transferred to an automated synthesizer (Chemspeed Accelerator™ SLT00) to produce a series of well-defined homopolymers.⁴⁹ Such precursors were subsequently chain-extended in turn with various methacrylic comonomers to generate a range of well-defined AB diblock copolymers.⁵⁰ Similarly, Hoogenboom and co-workers chain-extended poly(methyl acrylate), poly(*n*-butyl acrylate), PMMA or PDEAEMA in turn with 1-ethoxyethyl acrylate using the same equipment.⁵¹ The same team reported a standard protocol for the parallel optimization of RAFT polymerizations.⁵² This body of prior work indicates that RAFT polymerizations are amenable to a high-throughput approach. However, as far as we are aware, high-throughput RAFT polymerizations have not yet been performed in water. Moreover, there appears to be no reports of the high-throughput synthesis of diblock copolymer nanoparticles *via* RAFT-mediated PISA. In principle, coupling RAFT aqueous emulsion polymerization with a high-throughput approach should enable the rapid, convenient synthesis of a library of block copolymer nanoparticles. However, in addition to standard deoxygenation protocols for these air-sensitive polymerizations, it is noteworthy that such *heterogeneous* formulations require adequate stirring to ensure the formation of sufficiently small monomer droplets for the efficient production of colloidally stable dispersions.⁵³

In this chapter, we demonstrate that successful PISA syntheses can be performed with good reproducibility using a Chemspeed Autoplant A100, which is a commercial high-throughput robot synthesizer (Figure 4.7). More specifically, the RAFT aqueous emulsion polymerization of BzMA or BMA is conducted using a water-soluble PMAA macro-CTA to generate a series of sterically-stabilized diblock, triblock and tetrablock copolymer nanoparticles at up to 45% w/w copolymer concentration. This work was conducted at the AkzoNobel site in Slough, as part of a six-month work placement during this PhD project.

4.2. Experimental

4.2.1. Materials

Methacrylic acid (MAA, 99%), benzyl methacrylate (BzMA, 96%), *n*-butyl methacrylate (BMA, 99%), 4,4'-azobis(4-cyanovaleric acid) (ACVA, $\geq 98\%$), THF (HPLC, $\geq 99.9\%$) and glacial acetic acid ($\geq 99.85\%$) were purchased from Sigma-Aldrich (UK) and used as received. The 4-cyano-4-(2-phenylethanesulfanylthiocarbonyl)sulfanyl-pentanoic acid (PETTC) RAFT agent was prepared as described previously.⁵⁴ The *d*₄-methanol and *d*₈-tetrahydrofuran used for ¹H NMR studies were purchased from Goss Scientific Instruments Ltd. (Cheshire, UK). All other solvents were purchased from Sigma-Aldrich (UK) or VWR Chemicals (UK) and used as received. Deionized water was used in all experiments.

4.2.2. Synthesis of poly(methacrylic acid) (PMAA) macro-CTA at 40% w/w polymer concentration.

PETTC RAFT agent (21.77 g, 0.064 mol, assuming 80% efficiency), MAA (230 g, 2.67 mol, target DP 50) and absolute ethanol ($\geq 99.5\%$, 376.7 g, 40% w/w) were weighed into a 1 L round-bottom flask. The flask was covered with a five-necked lid and fitted with a condenser, overhead anchor-type stirrer, N₂ inlet and temperature probe (see Figure 4.1). In a separate vial, ACVA (3.00 g, 10 mmol; CTA/initiator molar ratio = 5.0) was dissolved in a small volume of ethanol (~10 mL). Both reaction mixtures were degassed with N₂ for 90 min while stirring at room temperature. After 90 min, the initiator solution was injected into the round-bottomed flask under a N₂ atmosphere using a syringe. The reaction mixture was further degassed for 20 min before being heated at 70 °C by immersion in a pre-heated water bath. After 3 h, the flask was removed from the water bath, allowed to cool, and its contents were exposed to air to quench the polymerization. The resulting PMAA macro-CTA was then purified by precipitation into a five-fold excess of diethyl ether. The crude polymer was collected by filtration and redissolved in the minimum amount of ethanol, before a second precipitation into excess diethyl ether. The purified polymer was allowed to dry overnight before being redissolved in the minimum amount of water, followed by lyophilization. The mean degree of polymerization for this macro-CTA was calculated to be 56 by ¹H NMR (see Figure 4.2). GPC analysis of methylated PMAA₅₆ macro-CTA (using THF eluent containing 4% v/v glacial acetic acid, against

poly(methyl methacrylate) standards) indicated $M_n = 6,000 \text{ g mol}^{-1}$ and $\mathcal{D} = 1.17$, (see Figure 4.3).

4.2.3. Laboratory-scale synthesis of PMAA₅₆-PBzMA₅₀₀ diblock copolymer nanoparticles at 20% w/w copolymer concentration via RAFT aqueous emulsion polymerization of benzyl methacrylate.

A typical protocol for the synthesis of PMAA₅₆-PBzMA₅₀₀ nanoparticles was as follows: PMAA₅₆ macro-CTA (0.1171 g, 0.02 mmol), ACVA (0.0013 g; 0.05 mmol, macro-CTA/initiator molar ratio = 5.0) and water (8.47 g, 20% w/w) were weighed into a 15 mL vial. The solution pH was adjusted to pH 5 using 1 M NaOH and BzMA monomer (2.00 g, 0.01 mol) was then added. The final mass of liquid reagents was ~10 - 11 g. A magnetic flea was added and the reaction vial was sealed using a rubber septum. The reaction solution was purged under N₂ for 15 min and the vial was then placed in a pre-heated water bath at 70 °C for 2 h, prior to its removal and exposure to air to quench the polymerization. In all the laboratory experiments, magnetic stirring was conducted at 500 rpm.

4.2.4. Laboratory-scale one-pot synthesis of tetrablock copolymer nanoparticles via RAFT aqueous emulsion polymerization.

A typical protocol for the synthesis of PMAA₅₆-PBzMA₅₀₀-PBMA₅₀₀-PBzMA₅₀₀ nanoparticles was as follows. PMAA₅₆ macro-CTA (0.1757 g, 0.03 mmol), ACVA (1.9 mg; 0.01 mmol, macro-CTA/initiator molar ratio = 5.0) and water (7.42 g, 30% w/w) were weighed into a 25 mL round-bottomed flask. The solution pH was adjusted to pH 5 using 1 M NaOH, followed by addition of BzMA monomer (3.00 g, 0.02 mol). A magnetic flea was added and the reaction flask was sealed using a rubber septum. The reaction solution was then purged under N₂ for 20 min before placing the flask in a pre-heated water bath at 70 °C for 120 min. A 1.0 mL sample of the diblock copolymer dispersion was removed using a syringe under a N₂ atmosphere for analysis. Previously degassed BMA monomer (2.10 g, 0.02 mol) and water (0.85 g, 40% w/w) were then injected into the flask using a syringe under a N₂ atmosphere. The second-stage polymerization was allowed to proceed for a further 180 min at 70 °C. A 1.0 mL sample of the triblock copolymer dispersion was removed using a syringe under a N₂ atmosphere for analysis. Previously degassed BzMA monomer (2.24 g, 0.01 mol) and water (1.58 g, 45% w/w) were then injected into the flask using a syringe under a N₂ atmosphere. The third-stage polymerization was allowed to

proceed for a further 18 h at 70 °C, before removing the flask from the water bath and exposing its contents to air to quench the reaction.

4.2.5. High-throughput syntheses of diblock copolymer nanoparticles via RAFT aqueous emulsion polymerizations using the Chemspeed Autoplant A100.

A typical protocol for the synthesis of PMAA₅₆-PBzMA₅₀₀ nanoparticles was as follows: Firstly, an aqueous stock solution containing PMAA₅₆ macro-CTA (38.3 mg dm⁻³, 7.4 μmol dm⁻³) and ACVA initiator (0.40 mg dm⁻³, 1.42 μmol dm⁻³, macro-CTA/ACVA ratio = 5.0) was prepared and adjusted to pH 5 using 1 M NaOH. Up to twenty reactor vessels were then charged with this stock solution (17.75 g). The monomer (BzMA, 5.12 g) was then added over 10 min, while further water was added (3.95 g) to adjust to the desired overall copolymer concentration (20% w/w). A stream of N₂ gas was blown through all the reaction vessels for 20 min. The reaction vessels were then sealed and heated up to 70 °C. Each vessel was equipped with an overhead stirrer. Either a propeller-type stirrer (at 350-650 rpm) or an anchor-type stirrer (at 150-350 rpm) was used (Figure 4.7). The stirring range used for each stirrer geometry was selected to afford efficient mixing with minimal splashing, as judged by visual inspection. The anchor stirrer generates significantly higher shear rates than the propeller stirrer at an equivalent stirring speed (rpm). All reaction vessels were maintained at 70 °C for 1 h before cooling to room temperature and decanting into 100 mL sample bottles. These reactions were also performed using BMA monomer. Batch sizes for the synthesis of PMAA₅₆-PBzMA₅₀₀ and PMAA₅₆-PBMA₅₀₀ were ~27 g and ~22 g respectively. In further experiments, these syntheses were also conducted at a higher overall copolymer concentration of 30% w/w.

4.2.6. High-throughput syntheses of triblock and tetrablock copolymers via RAFT aqueous emulsion polymerization using the Chemspeed Autoplant A100.

Initially, the same protocol as that described above for the diblock copolymer syntheses was employed. Then, at the end of the 1 h reaction time, a second water-immiscible monomer (BzMA or BMA) was injected into the reaction solution for the second-stage polymerization. Further water was also added to adjust the overall copolymer concentration to 40% w/w. The reaction solution was then held at 70 °C for 2 h. For the synthesis of tetrablock copolymer nanoparticles (45% w/w copolymer concentration), a third water-immiscible monomer (BzMA or BMA) and further water was added after completion of the triblock copolymer synthesis. Each reaction vessel

was then held at 70 °C for 2 h before cooling to room temperature and exposing to air to quench the polymerization.

4.3. Instrumentation and Copolymer Characterization

4.3.1. *The Chemspeed Autoplant A100 high-throughput robot.*

This apparatus was equipped with a four-needle head, 10 mini-plant modules and 10 pump modules (see Figure 4.7). Each mini-plant module can house two 100 mL steel reactors that can be heated and stirred independently as well as connecting to a refluxing 80:20 water/ethanol mixture to allow reactor head cooling. Stirrer blades were available with either anchor or propeller geometries and stirrer speeds could be varied from 50 to 1000 rpm. Heating is controlled by individual electrically-heated jackets around each vessel that can be individually heated from ambient temperature up to 200 °C with valves connected to chilled fluid for cooling. The cooling fluid (silicone oil) is provided by a dynamic temperature control system/circulation thermostat (Huber Unistat Tango). An inert atmosphere was maintained by applying a 1.1 bar flow of N₂ through all the reactors, at a flow rate of 0.8 L min⁻¹. With additional pump modules, the A100 can feed up to three liquid materials to each reactor in parallel. The liquid feeding (dosing) is completed using syringe pumps that are capable of continuous cycles of aspiration and dispensation (one 100 µL syringe and two 50 µL syringes). The software used to control the A100 was ‘Chemspeed Autosuite 1.11.2.24’.

4.3.2. *¹H NMR Spectroscopy.*

All ¹H NMR spectra were recorded using a 400 MHz Bruker Advance-400 spectrometer using *d*₄-methanol or *d*₈-tetrahydrofuran as the solvent.

4.3.3. *Dynamic Light Scattering (DLS).*

Aqueous copolymer dispersions (0.20% w/w) in disposable plastic cuvettes were analyzed at 20 °C using a Malvern Zetasizer NanoZS instrument. Scattered light was detected at 173° and intensity-average hydrodynamic diameters were calculated using the Stokes-Einstein equation. Data were averaged over three consecutive measurements, comprising a minimum of ten runs per measurement. The particle diameter standard deviations were calculated from the DLS polydispersity index (PDI).

4.3.4. Transmission Electron Microscopy (TEM).

Each sample was prepared by depositing 10 μL (0.20% w/w) of 0.1% w/w aqueous copolymer dispersion onto a glow-discharged carbon-coated copper grid for 20 seconds. The grid was then stained with 10 μL uranyl formate solution (0.75% w/w) for 10 seconds and carefully dried using a vacuum hose. TEM images were recorded using a Philips CM100 instrument operating at 100 kV and connected to a Gatan 1 k CCD camera. ImageJ software was used to determine mean nanoparticle diameters from TEM images (at least 100 nanoparticles were analyzed per sample). Standard deviations were calculated using Microsoft Excel.

4.3.5. High-Performance Liquid Chromatography (HPLC) for Monomer Conversion

A stock solution was made up comprising both BzMA (0.100 g) and BMA (0.100 g) dissolved in acetonitrile (100 mL). This stock solution was serially diluted to afford four calibration solutions with concentrations ranging from $5.68 \times 10^{-2} \text{ mmol dm}^{-3}$ to $1.41 \text{ mmol dm}^{-3}$ for BzMA and from $7.03 \times 10^{-2} \text{ mmol dm}^{-3}$ to $1.41 \text{ mmol dm}^{-3}$ for BMA. Samples (0.100 g) were dissolved in acetonitrile (10 mL), before filtering through a $0.45 \mu\text{m}$ filter. The experimental set-up comprised an Agilent 1200 quaternary pump operating at a flow rate of 0.50 mL min^{-1} in series with an Agilent 1200 evaporative light scattering detector maintained at $40 \text{ }^\circ\text{C}$, and a diode array variable wavelength UV detector (set to wavelengths of 205 and 254 nm). The eluent was initially 60:40 v/v acetonitrile/water (for 11 min) before being gradually increased to 90:10 v/v acetonitrile/water over 4 min and then held constant for the final 5 min. Linear calibration plots were obtained for both BMA and BzMA monomers using this protocol (see Appendix 3).

4.3.6. Gel Permeation Chromatography (GPC).

THF GPC was used to determine copolymer molecular weights and dispersities at $30 \text{ }^\circ\text{C}$. For analysis of polymers synthesized *via* the high-throughput protocol the GPC set-up consisted of an autosampler, Viscotex 2001 GPC max pump, PSS SDV analytical pre-column column ($10 \mu\text{m}$, $50 \text{ mm} \times 8.0 \text{ mm}$), 3 PSS SDV analytical columns ($10 \mu\text{m}$, $300 \text{ mm} \times 8.0 \text{ mm}$, 1000 \AA ; $10 \mu\text{m}$, $300 \text{ mm} \times 8.0 \text{ mm}$, 10^5 \AA ; $10 \mu\text{m}$, $300 \text{ mm} \times 8.0 \text{ mm}$, 10^7 \AA), connected to a Viscotek TDA 305 refractive index detector. For analysis of polymers synthesized on a laboratory-scale the GPC set-up consisted of an Agilent 1260 Infinity II GPC/SEC system fitted with an autosampler

and two 5 μM Mixed-B columns connected to a refractive index detector. In both protocols, the mobile phase was HPLC-grade THF containing 4.0% v/v glacial acetic acid at a flow rate of 1.0 mL min⁻¹. Molecular weights were calculated using a series of near-monodisperse PMMA calibration standards. The PMAA₅₆ macro-CTA and the block copolymers synthesized on a laboratory-scale were modified by methylation of the carboxylic acid groups to render them THF-soluble. This was achieved by adding excess trimethylsilyldiazomethane dropwise to a solution of copolymer (20 mg) in THF (2.0 mL) until a persistent yellow coloration was observed. This reaction solution was then stirred overnight until all THF had evaporated, prior to GPC analysis.

4.4. Results and Discussion

4.4.1. Synthesis of PMAA macro-CTA on a large scale

The specific RAFT aqueous emulsion polymerization formulations explored in this study involve the chain extension of a water-soluble PMAA macro-CTA with a *water-immiscible* monomer (either BzMA or BMA) in water at pH 5, see Scheme 2.1. As the polymerization proceeds the *water-immiscible* monomer forms a *water-insoluble* polymer leading to *in situ* self-assembly of the propagating diblock copolymer chains to form sterically-stabilized nanoparticles *via* PISA.^{5, 15, 20, 27, 29, 30, 55-67}

A PMAA_x macro-CTA, similar to that used in Chapters 2 and 3 was chosen for this set of experiments. Ideally, precisely the same PMAA_x macro-CTA would be utilized for every block copolymer nanoparticle synthesis to mitigate any difference in particle morphology caused by minor variations in the macro-CTA DP. In addition, a relatively large number of syntheses were planned owing to the high-throughput nature of the project and the need to optimize formulations. For these reasons, one large batch of PMAA_x macro-CTA was synthesized. PETTC was chosen as the RAFT agent to minimize cost, as this reagent can be readily synthesized in-house.⁶⁸

The synthetic protocol was identical to that discussed in Chapter 2 but conducted on a considerably larger scale. MAA was polymerized using PETTC and ACVA in ethanol at 70 °C. The reaction was conducted on a 600 g scale to yield 250 g of PMAA_x macro-CTA with a target DP of 50. The reaction was carried out in a 1 L round-bottomed flask sealed with a five-necked lid (Figure 4.1). The lid was fitted with a N₂ inlet (N₂ was bubbled through the reaction mixture throughout the reaction),

a condenser, an overhead anchor stirrer and a temperature probe. Owing to the large solution volumes, both ethanol and MAA monomer (containing the CTA) were degassed separately for 90 min. The ACVA initiator was dissolved in ethanol (5-10 mL) and degassed for 30 min. The MAA and ethanol were then combined and this solution was degassed for 10 min. Finally, the initiator solution was added and degassed for 5 min, prior to heating to 70 °C in a water bath for 3 h.

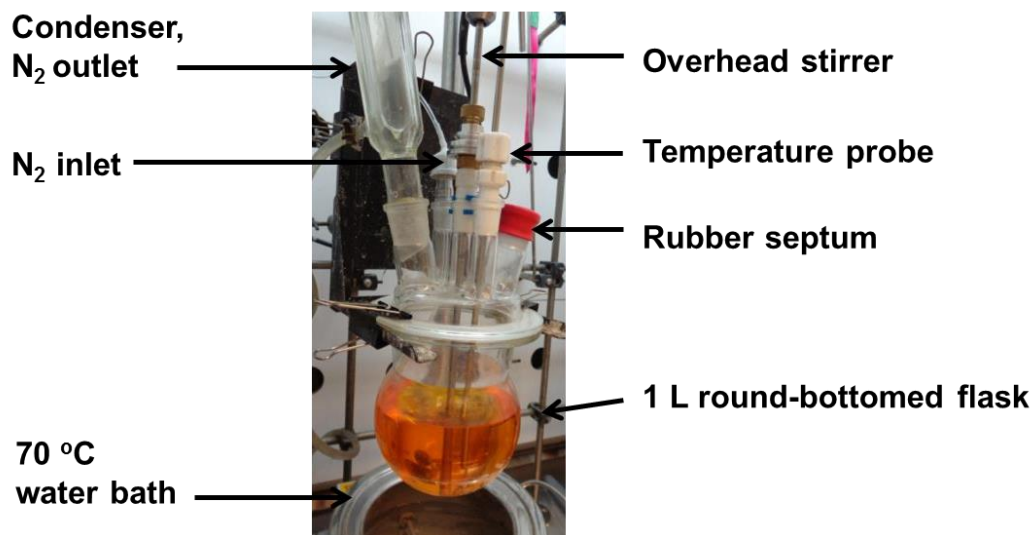


Figure 4.1 Digital photograph of the experimental set-up for the synthesis of the PMAA₅₆ macro-CTA on a large scale (250 g). The 1 L round-bottomed flask was fitted with a N₂ inlet, a condenser, an overhead stirrer and a temperature probe.

The PMAA macro-CTA was then purified by precipitation into diethyl ether. This was performed in several batches owing to the large volume of ether required. The PMAA_x macro-CTA was precipitated from ethanol into a round-bottomed flask. After precipitation the majority of ether was decanted and any residual ether was allowed to evaporate overnight. The PMAA_x macro-CTA was dissolved in the minimum amount of methanol and precipitated again into ether. After removal of the ether the viscous PMAA_x macro-CTA was redispersed in water, owing to the high viscosity of the PMAA_x macro-CTA this required the use of overhead stirring. Once redissolved in water, the PMAA_x macro-CTA was freeze-dried overnight and a fine yellow powder was obtained. ¹H NMR analysis of the purified macro-CTA indicated a mean PMAA DP of 56, see Figure 4.2.

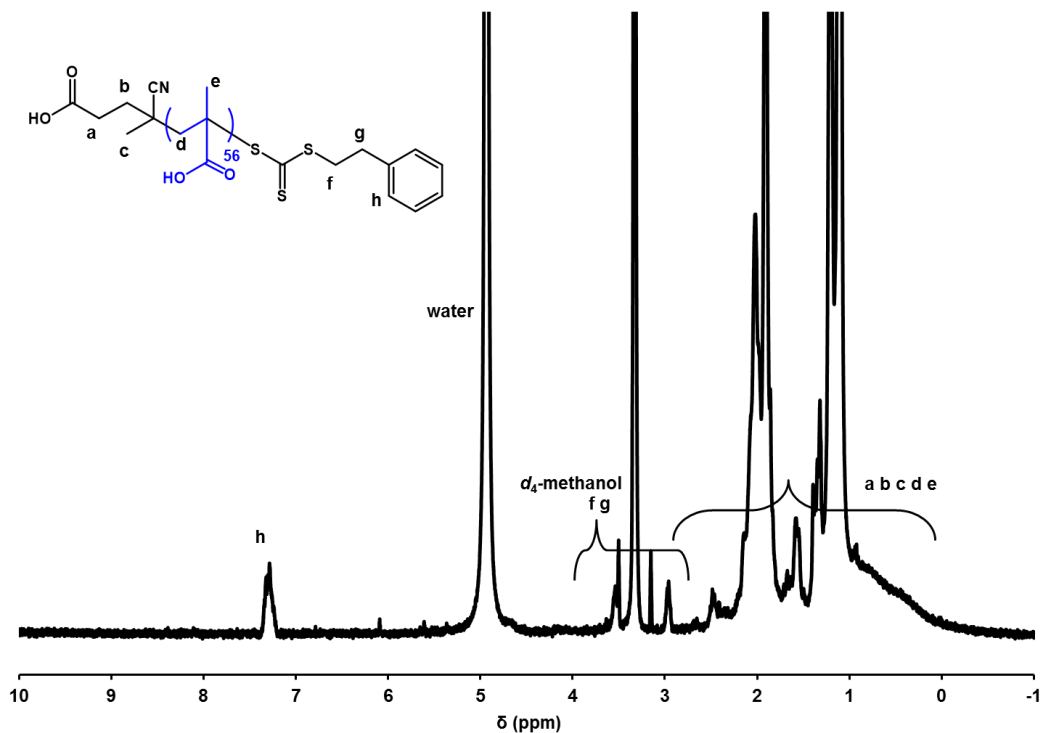


Figure 4.2 ^1H NMR of PMAA₅₆ macro-CTA synthesized on a large scale (250 g). Spectra was recorded in *d*₄-methanol.

GPC analysis of the methylated PMAA₅₆ macro-CTA (using THF eluent containing 4% v/v glacial acetic acid, against poly(methyl methacrylate) standards) conducted at the AkzoNobel site in Slough indicated an M_n of 6,000 g mol⁻¹ and $\mathcal{D} = 1.17$, (see Figure 4.3). GPC analysis of the same methylated PMAA₅₆ macro-CTA at the University of Sheffield indicated an M_n of 5,700 g mol⁻¹ and $\mathcal{D} = 1.30$. This PMAA₅₆ macro-CTA was used for both laboratory-scale and high-throughput syntheses. It is important to note that two different GPC set-ups were used during the analysis of all subsequent block copolymers, see the Experimental for more details.

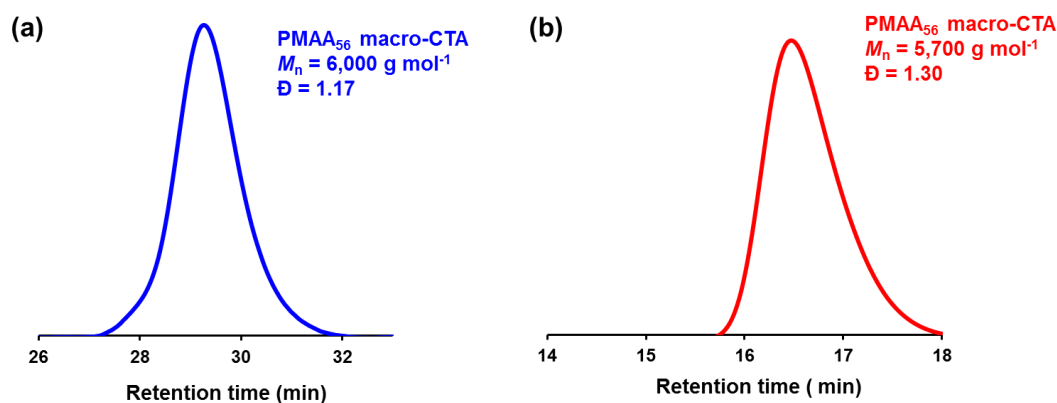


Figure 4.3 THF GPC chromatograms of methylated PMAA₅₆ macro-CTA synthesized on a large scale (250 g). PETTC was used as the CTA. Molecular weight and dispersity data are expressed relative to PMMA standards. (a) was analyzed using the THF GPC at the AkzoNobel site in Slough and (b) was analyzed on the THF GPC at the University of Sheffield.

4.4.2. Laboratory-scale syntheses of di-, tri- and tetra-block copolymers

Laboratory-scale syntheses of PMAA₅₆-PBzMA₅₀₀ and PMAA₅₆-PBMA₅₀₀ diblock copolymer nanoparticles were typically performed on a ~10–11 g scale using 15 mL glass vials. PMAA₅₆ macro-CTA, ACVA initiator and water were weighed into each vial and the solution pH was adjusted to pH 5 prior to addition of BzMA monomer (according to Chaduc and co-workers, this solution pH is optimal for the synthesis of PMAA-containing diblock copolymer nanoparticles *via* RAFT aqueous emulsion polymerization, as discussed in Chapter 2).^{30, 63} The vial was then sealed and degassed in ice by bubbling N₂ through the reaction mixture for 15 min with continuous magnetic stirring at approximately 500 rpm, prior to heating to 70 °C using an oil bath. Both polymerizations proceeded to more than 99% conversion within 2 h and led to the formation of spherical nanoparticles *via* PISA, see Table 4.1.

Table 4.1 Conversions, number-average molecular weights (M_n), dispersities (\mathcal{D}) and mean DLS and TEM diameters for PMAA₅₆-PBzMA₅₀₀ and PMAA₅₆-PBMA₅₀₀ diblock copolymers prepared at 20% w/w copolymer concentration on a laboratory-scale.

Composition	Conversion (%) ^a	DLS particle diameter (nm)	DLS polydispersity	M_n^b (g mol ⁻¹)	\mathcal{D}^b
PMAA ₅₆ -PBzMA ₅₀₀	> 99	51	0.14	82,600	1.73
PMAA ₅₆ -PBMA ₅₀₀	> 99	37	0.15	50,500	2.01

^aConversion determined by ¹H NMR for laboratory-scale syntheses.

^bMolecular weight data determined by GPC using THF eluent containing 4% v/v glacial acetic acid (calibrated using a series of near-monodisperse PMMA standards). The copolymers obtained from the laboratory-scale syntheses were methylated using excess trimethylsilyldiazomethane.

The GPC data obtained for the laboratory-scale syntheses of the PMAA₅₆-PBzMA₅₀₀ and the PMAA₅₆-PBMA₅₀₀ diblock copolymers indicated relatively broad molecular weight distributions ($\mathcal{D} = 1.73$ and 2.01 respectively), see Figure 4.4. However, unimodal distributions and high blocking efficiencies were achieved in both cases. The synthesis of spherical nanoparticles by PISA was confirmed by DLS and TEM analysis, see Appendix 4.

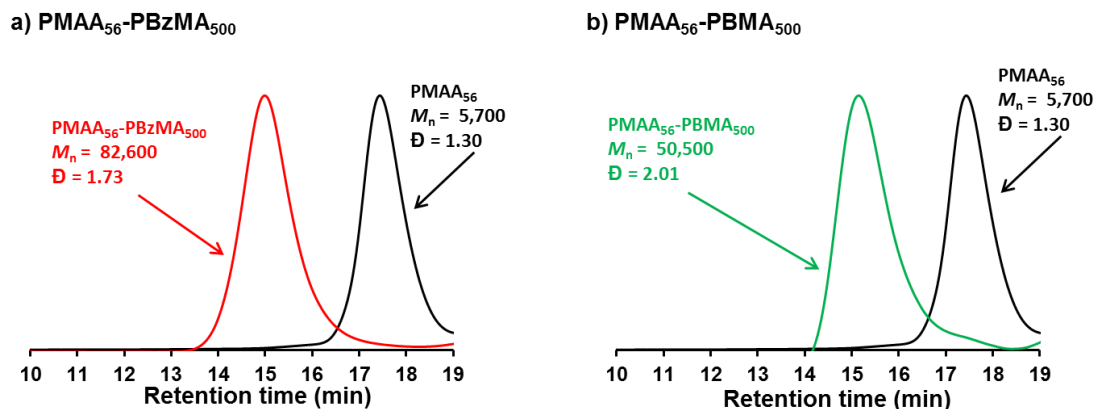
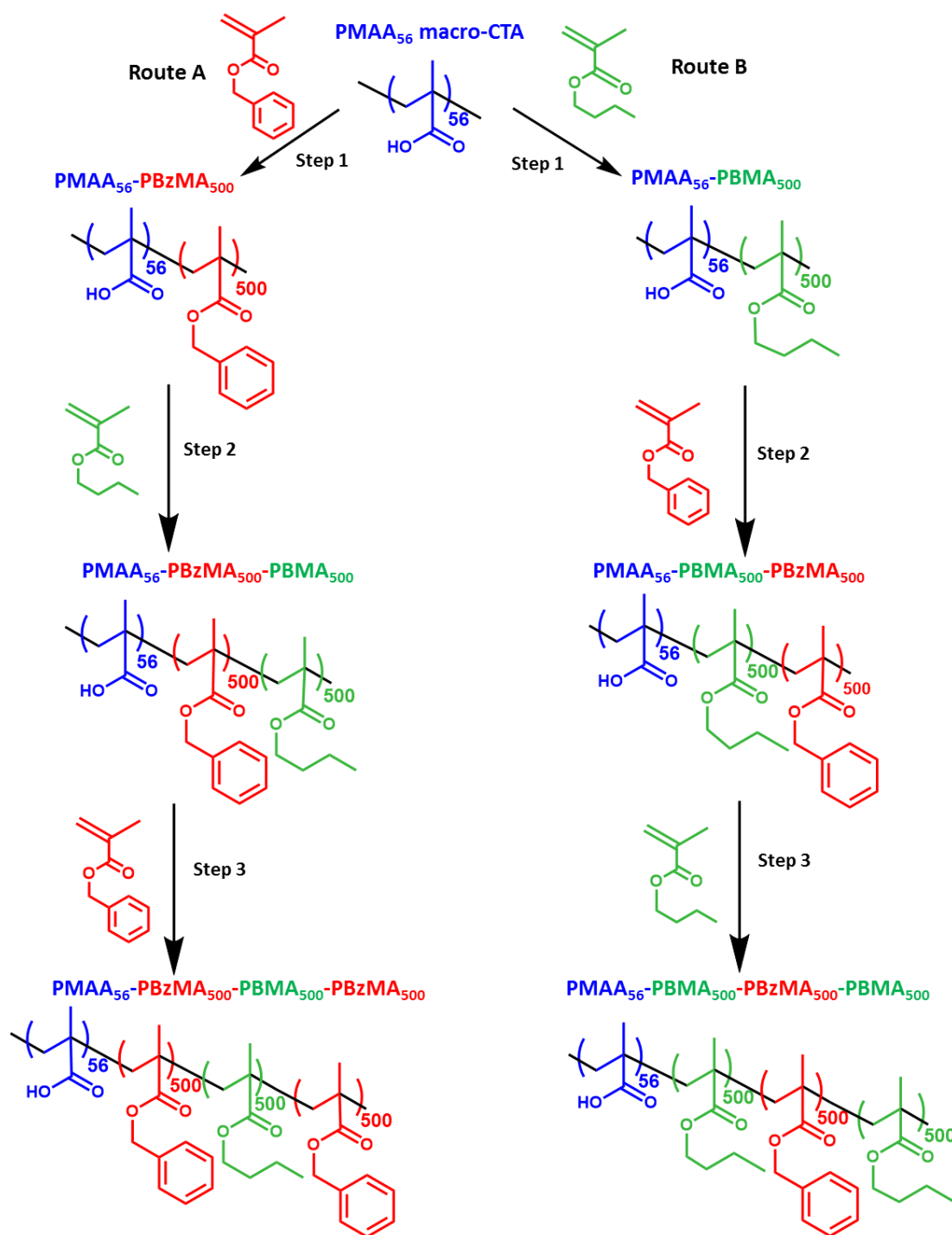


Figure 4.4 THF GPC chromatograms of methylated (a) PMAA₅₆-PBzMA₅₀₀ and (b) PMAA₅₆-PBMA₅₀₀ diblock copolymers synthesized *via* RAFT aqueous emulsion polymerization on a laboratory-scale. Samples were analyzed relative to PMMA standards.

Following the successful synthesis of PMAA₅₆-PBzMA₅₀₀ and PMAA₅₆-PBMA₅₀₀ diblock copolymer nanoparticles, various triblock and tetrablock copolymer nanoparticles were prepared *via* a one-pot protocol using sequential monomer addition. In this case, the same PMAA₅₆ macro-CTA was chain-extended with BzMA, followed by BMA and then (in the case of the tetrablocks) BzMA, with a DP of 500 being targeted for each block (Scheme 4.1, Route A). The sequence of the two core-forming blocks was then reversed; the PMAA₅₆ macro-CTA was chain-extended first with BMA, followed by BzMA and finally with BMA (see Scheme 4.1, Route B).

The synthesis of the tetrablock copolymer nanoparticles was initially identical to that of the diblock copolymer nanoparticles. After the diblock copolymer synthesis had reached high conversion (within 2 h), a 1 mL aliquot was removed under N₂ for analysis by ¹H NMR, GPC, DLS and TEM. To synthesize the triblock copolymers, previously degassed monomer and additional water (to adjust the copolymer concentration) were added to the diblock copolymer dispersion under a N₂ atmosphere. This second-stage polymerization was then allowed to proceed for a further 2 h at 70 °C, before removal of a 1 mL aliquot for analysis by ¹H NMR, GPC, DLS and TEM.) For the synthesis of the tetrablock copolymers, the final monomer and water were injected and the polymerization was allowed to continue overnight (18 h) to ensure high monomer conversion.



Scheme 4.1. Synthesis of diblock, triblock and tetrablock copolymers prepared *via* RAFT aqueous emulsion polymerization either on a laboratory-scale or *via* a high-throughput approach using the Chemspeed A100 robot synthesizer. A PMAA₅₆ macro-CTA was chain-extended with BzMA, followed by BMA and then (in the case of the tetrablocks) BzMA, with each insoluble block having a target DP of 500. The sequence of the two core-forming blocks was also reversed; thus the PMAA₅₆ macro-CTA was chain-extended first with BMA, followed by BzMA and then BMA. These multiblock syntheses were performed at 70 °C using a PMAA₅₆ macro-CTA/initiator of 5.0, in aqueous solution at pH 5. Timings for each step are different for the laboratory-scale and high-throughput approach, see Experimental section for specific conditions used in each step. RAFT CTA end-groups have been omitted for simplicity, all block copolymers are capped with PETTC end-groups (as shown in Figure 4.2).

Table 4.2 Summary of diblock, triblock and tetrablock copolymers prepared *via* RAFT aqueous emulsion polymerization. These syntheses were performed either on a laboratory-scale. These multiblock copolymer syntheses were performed at 70 °C using a PMAA₅₆ macro-CTA/initiator of 5.0, in aqueous solution at pH 5.

	Target Composition	Overall Monomer Conversion ^a (%)		DLS particle diameter (nm)	DLS particle polydispersity	TEM particle diameter (nm)	M_n^b (g mol ⁻¹)	\bar{D}^b
		BzMA	BMA					
Laboratory-Scale Syntheses	PMAA ₅₆ -PBzMA ₅₀₀	> 99	-	64	0.16	40	79,900	1.55
	PMAA ₅₆ -PBzMA ₅₀₀ -PBMA ₅₀₀	> 99	> 99	80	0.13	57	130,800	1.59
	PMAA ₅₆ -PBzMA ₅₀₀ -PBMA ₅₀₀ -PBzMA ₅₀₀	96	> 99	121	0.17	63	192,700	1.64
	PMAA ₅₆ -PBMA ₅₀₀	-	> 99	62	0.15	48	87,800	1.62
	PMAA ₅₆ -PBMA ₅₀₀ -PBzMA ₅₀₀	> 99	> 99	90	0.17	52	205,700	1.85
	PMAA ₅₆ -PBMA ₅₀₀ -PBzMA ₅₀₀ -PBMA ₅₀₀	>99	> 99	109	0.16	67	280,200	1.84

^aConversion determined by ¹H NMR for laboratory-scale syntheses.

^bMolecular weight data determined by GPC using THF eluent containing 4% v/v glacial acetic acid (calibrated using a series of near-monodisperse PMMA standards). The copolymers obtained from the laboratory-scale syntheses were methylated using excess trimethylsilyldiazomethane prior to GPC analysis.

The resulting diblock, triblock and tetrablock copolymers were analyzed by ^1H NMR, GPC, DLS and TEM, see Table 4.2. High monomer conversions ($> 99\%$) were achieved at Step 1 and 2 of the polymerization for both Route A and Route B. However, during the final stage of the synthesis (Step 3) of the $\text{PMAA}_{56}\text{-PBzMA}_{500}\text{-PBMA}_{500}\text{-PBzMA}_{500}$ tetrablock the BzMA conversion was only 96 % after 18 h. THF GPC analysis of the various methylated block copolymers indicated a progressive increase in molecular weight after addition of each block, as expected. However, dispersities were always significantly higher than those typically reported for RAFT aqueous emulsion polymerization syntheses.^{16, 59, 62, 69-76} There are a number of literature reports of relatively broad molecular weight distributions for such PISA formulations.^{5, 27, 29, 30, 64, 66} Frankly, we are not sure why relatively high dispersities are observed in the present studies. Nevertheless, the GPC data shown in Figure 4.5 indicate unimodal distributions and high blocking efficiencies. Thus well-defined, albeit relatively polydisperse, block copolymers are obtained with minimal macro-CTA contamination.

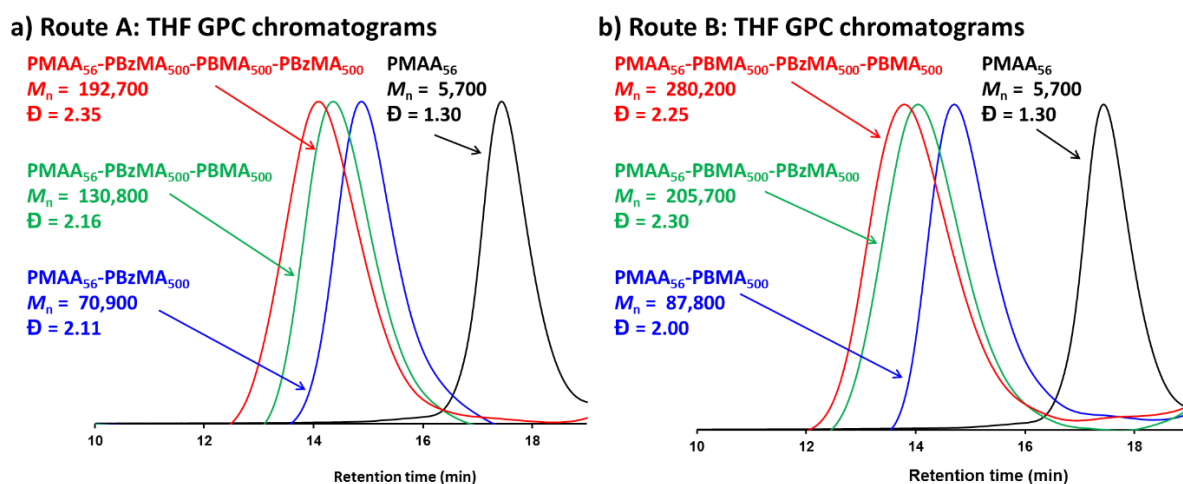


Figure 4.5 THF GPC chromatograms for diblock, triblock and tetrablock copolymers prepared *via* RAFT aqueous emulsion polymerization on a laboratory-scale. These block copolymers were prepared via either (a) Route A or (b) Route B as outlined in Scheme 2.

DLS and TEM studies of the block copolymer nanoparticles confirm that colloiddally stable spherical nanoparticles were obtained in all cases, see Table 4.2, Figure 4.6 and Appendix 4. Moreover, the mean particle diameter increased after addition of each successive block.

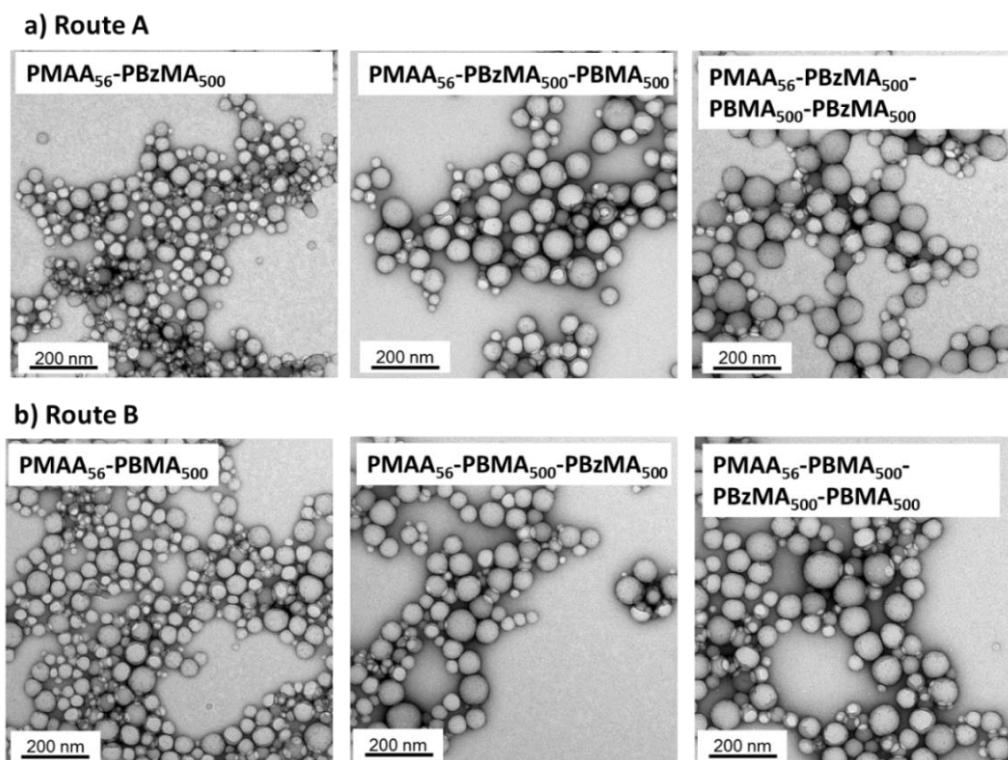


Figure 4.6. Representative TEM images obtained for the synthesis of diblock, triblock and tetrablock copolymers prepared on a laboratory-scale by RAFT aqueous emulsion polymerization. Spherical morphologies were obtained in all cases and an increase in mean nanoparticle diameter was observed by DLS and TEM with each subsequent block addition.

4.4.3. Optimization of high-throughput protocol

For the successful transfer of such PISA formulations from individual lab-scale syntheses to high-throughput syntheses, three essential differences need to be taken into consideration. Firstly, weighing out four components and adjusting the solution pH in all 20 reaction vessels is simply too time-consuming. Secondly, it is not possible to bubble N_2 through the reaction mixture contained in each of the twenty reaction vessels. Thirdly, using an overhead mechanical stirrer instead of a magnetic flea should enable more efficient stirring, but additional factors such as stirrer geometry may be important.

To avoid weighing out each reagent individually into all twenty reaction vessels, a stock aqueous solution containing the PMAA₅₆ macro-CTA, ACVA initiator and water (adjusted to pH 5) was used to charge each reactor vessel. This stock solution comprised PMAA₅₆ macro-CTA (38.3 mg dm^{-3} , $7.4 \text{ } \mu\text{mol dm}^{-3}$) and ACVA initiator (0.40 mg dm^{-3} , $1.42 \text{ } \mu\text{mol dm}^{-3}$), giving a macro-CTA/initiator molar ratio of 5.0. A predetermined volume of the stock solution (5-20 mL) was injected into each reaction vessel to produce the PISA

formulation required for a given target diblock copolymer composition. The monomer was then injected, along with further water (0-25 mL) to adjust the final copolymer concentration. Thorough deoxygenation of the reaction solution is required prior to synthesis for RAFT polymerizations, if oxygen is present, it can react with the polymer radicals and retard the rate of polymerization.⁷⁷⁻⁷⁹ This is typically achieved by bubbling N₂ gas directly through the reaction mixture. However, this is not possible with the Chemspeed A100 synthesizer. Instead, N₂ gas was blown through the reaction chamber for 20 min (at 20 °C) while stirring the reaction mixture at 200 rpm prior to initiation of the polymerization. Initial experiments confirmed that this modified protocol provided sufficient protection from aerial oxygen to enable high monomer conversions (> 94%) to be achieved during RAFT aqueous emulsion polymerization.

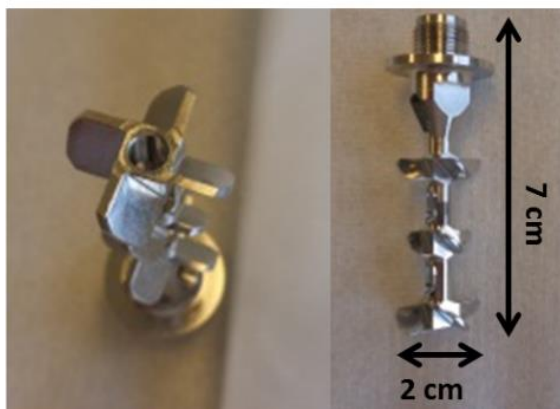
a) Chemspeed Autoplant A100 synthesizer



b) 100 mL reactor vessel and stirrer module



c) Propeller Stirrer



d) Anchor Stirrer



Figure 4.7 Digital photographs showing (a) the Chemspeed A100 automated synthesizer, (b) a 100 mL reaction vessel and stirrer module, (c) a propeller-type stirrer and (d) an anchor-type stirrer.

4.4.4. *Stirring*

In conventional emulsion polymerization, it is well-documented that efficient stirring is of critical importance.^{80, 81} Firstly, inefficient stirring can lead to the formation of relatively large monomer droplets which can potentially act as the locus of polymerization. This leads to suspension polymerization, rather than emulsion polymerization. Secondly, the stirring rate may influence both the rate of polymerization and the final particle diameter.⁸² Indeed, Charleux and co-workers reported that the stirring rate can have a significant impact on the success of RAFT aqueous emulsion polymerization formulations.²⁹ Moreover, colloidally stable dispersions could not be obtained in the present study when using *unstirred* reaction mixtures in laboratory-scale control experiments, see Figure 4.8. In the *unstirred* reaction solution of either BzMA or BMA no significant polymerization was observed by ¹H NMR spectroscopy, evidenced by the presence of unreacted monomer, see Figure 4.8. In contrast, when repeated with stirring (generated by a magnetic flea at 500 rpm) polymerization did occur, resulting in the formation of diblock copolymer nanoparticles *via* PISA. The presence of these nanoparticles is clearly demonstrated by the increased turbidity of the final reaction solution, see Figure 4.8.

	Before Reaction	After Reaction	
		No Stirring	With Stirring (500 rpm)
a) PMAA₅₆-PBzMA₅₀₀	 monomer	 unreacted monomer	 diblock copolymer nanoparticles
b) PMAA₅₆-PBMA₅₀₀	 monomer	 unreacted monomer	 diblock copolymer nanoparticles

Figure 4.8 Digital photographs showing initial reaction mixtures and final diblock copolymer nanoparticle dispersions for the laboratory-scale synthesis of (a) PMAA₅₆-PBzMA₅₀₀ and (b) PMAA₅₆-PBMA₅₀₀. Reactions were either unstirred or stirred at 500 rpm with a magnetic flea. No significant polymerization was obtained for the unstirred reaction solution as judged by ¹H NMR spectroscopy.

When using the Chemspeed A100, reaction mixtures were mechanically stirred at 150 to 650 rpm using an overhead stirrer unit with either anchor or propeller stirrers (Figure 4.7). Ideally, our high-throughput protocol for RAFT aqueous emulsion polymerization should be applicable for a wide range of formulations. Thus, two *water-immiscible* methacrylic monomers (BzMA

and BMA) were selected to have differing densities: BzMA is slightly more dense than water (1.04 g cm^{-3} at $25 \text{ }^\circ\text{C}$), whereas BMA is slightly less dense than water (0.89 g cm^{-3} at $25 \text{ }^\circ\text{C}$). Therefore, the former monomer droplets tend to sediment, whereas the latter tend to cream; ideally, the stirrer type should be able to cope with this difference in droplet buoyancy. A PMAA₅₆ macro-CTA was chain-extended using each monomer while targeting a mean core-forming block DP of 500; all reaction conditions were kept constant while evaluating the two stirrer geometries for a range of stirring rates. Each RAFT aqueous emulsion polymerization was conducted on a 15 to 20 mL scale using a propeller stirrer at stirring speeds of 350, 450, 550 and 650 rpm and with an anchor stirrer at stirring speeds of 150, 250 and 350 rpm (see Table 4.3). For the former stirrer, only the lowest propeller blade was immersed in the reaction mixture, thus mimicking the stirring achieved with a magnetic flea. This set-up provided adequate stirring and enabled more than 98% conversion to be achieved for both monomers (BzMA and BMA) at all stirring speeds, with both stirrer geometries (see Table 4.3). The single exception to this was during the synthesis of PMAA₅₆-PBzMA₅₀₀ with the anchor stirrer at 350 rpm, where significantly *lower* conversion (78%) were observed (see Table 4.3). Furthermore, GPC analysis indicated that reduced RAFT control was achieved ($\text{Đ} = 1.39\text{-}1.84$) with the anchor stirrer compared to the propeller stirrer ($\text{Đ} = 1.36\text{-}1.48$), see Table 4.3.

Finally, the GPC data obtained for the laboratory-scale syntheses of these diblock copolymers differ significantly from those obtained from the corresponding high-throughput syntheses, with the latter giving narrower molecular weight distributions (see Figure 4.4 and Figure 4.9). However, it is worth emphasizing that these two data sets were analyzed using separate GPC instruments with differing column sets. The analysis of the methylated PMAA₅₆ macro-CTA on both GPC instruments was reported in Figure 4.3. This Figure clearly demonstrated that despite the reported M_n values being comparable ($6,000$ and $5,000 \text{ g mol}^{-1}$), the dispersity value was significantly higher when analyzed on the GPC instrument at the University of Sheffield compared to when analyzed on the AkzoNobel instrument ($\text{Đ} = 1.30$ vs. 1.17 respectively). Moreover, the copolymers obtained from the laboratory-scale syntheses were methylated using excess trimethylsilyldiazomethane, whereas those prepared using the high-throughput protocol were not subjected to this chemical derivatization.

Chapter 4: Optimization of the high-throughput synthesis of multiblock copolymer nanoparticles in aqueous media *via* polymerization-induced self-assembly

Table 4.3. Summary of the effect of stirrer geometry and stirring rate (rpm) on the synthesis of PMAA₅₆-PBzMA₅₀₀ and PMAA₅₆-PBMA₅₀₀ diblock copolymer nanoparticles *via* high-throughput RAFT aqueous emulsion polymerization at 70 °C. All reactions were performed at 20% w/w copolymer concentration using a macro-CTA/initiator molar ratio of 5.0.

Monomer	Monomer density at 20 °C (g cm ⁻³)	Water solubility at 20 °C (g dm ⁻³)	Scale	Stirrer geometry	Stirring rate (rpm)	Conversion (%) ^a	DLS	DLS	GPC ^b	
							particle diameter (nm)	polydispersity	<i>M</i> _n (g mol ⁻¹)	Đ
BzMA	1.04	0.19	High-Throughput	Propeller	350	99	39	0.19	57,000	1.38
					450	98	43	0.17	56,500	1.36
					550	99	48	0.16	60,300	1.39
					650	99	48	0.16	59,100	1.40
			High-Throughput	Anchor	150	99	45	0.14	68,900	1.39
					250	99	52	0.14	62,200	1.49
					350	78	61	0.18	39,400	1.47
BMA	0.89	0.20	High-Throughput	Propeller	350	99	45	0.25	57,900	1.36
					450	99	45	0.20	59,900	1.44
					550	99	45	0.18	58,100	1.48
					650	99	45	0.16	58,300	1.46
			High-Throughput	Anchor	150	99	47	0.21	63,800	1.56
					250	99	42	0.18	43,000	1.84
					350	99	45	0.17	57,700	1.47

^a Conversion determined by HPLC

^b Molecular weight data determined by GPC using THF eluent containing 4% v/v glacial acetic acid (calibrated using a series of near-monodisperse PMMA standards)

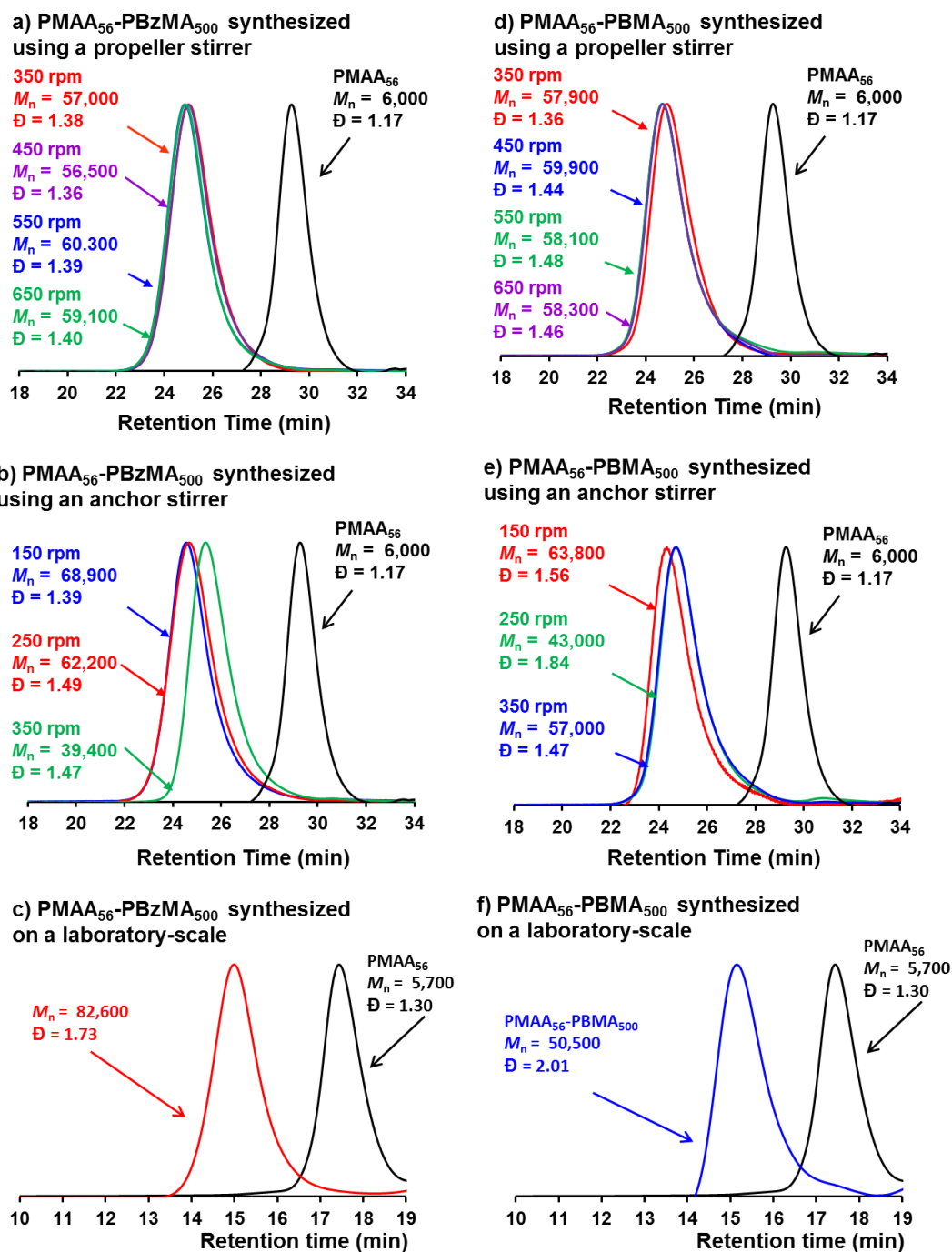


Figure 4.9 THF GPC chromatograms corresponding to the data reported in Table 2. This data demonstrates the effect of stirrer geometry and stirring rate (rpm) on the synthesis of PMAA₅₆-PBzMA₅₀₀ and PMAA₅₆-PBMA₅₀₀ diblock copolymer nanoparticles *via* high-throughput RAFT aqueous emulsion polymerization at 70 °C. All reactions were performed at 20% w/w copolymer concentration using a macro-CTA/initiator molar ratio of 5.0. (a), (b), (d) and (e) were analyzed at AkzoNobel in Slough, whereas (c) and (f) were analyzed at the University of Sheffield.

For the BzMA polymerizations, some variation in the intensity-average diameter was observed when adjusting the stirring rate for both stirrer geometries (Figure 4.10 and Table 4.3). When using the anchor stirrer, a modest increase in nanoparticle diameter from 45 to 61 nm was observed as the stirring rate was increased from 150 to 350 rpm. A smaller increase in nanoparticle diameter (from 39 to 45 nm) with stirring rate was observed for polymerizations using the propeller stirrer. In contrast, the stirrer geometry and stirring rate had minimal effect on the intensity-average diameter for BMA polymerizations (Figure 4.10 and Table 4.3). In addition, the particle size was comparable to those achieved during laboratory scale syntheses of the PMAA₅₆-PBzMA₅₀₀ and PMAA₅₆-PBMA₅₀₀ diblock copolymer nanoparticles (which afforded intensity-average diameters of 51 nm and 37 nm, respectively). Overall, it seems that the propeller stirrer provides more effective stirring than the anchor stirrer for these RAFT aqueous emulsion polymerizations and that the monomer density has little influence on the formation of monomer droplets under shear.

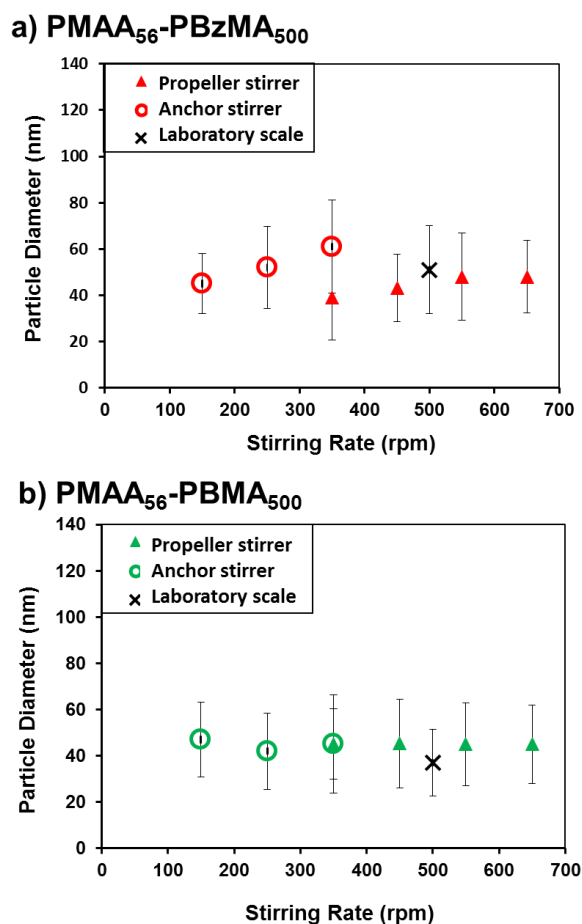


Figure 4.10 Summary of dynamic light scattering (DLS) data showing the effect of stirrer geometry and stirring rate (rpm) on the intensity-average particle diameter (nm) for (a) PMAA₅₆-PBzMA₅₀₀ and (b) PMAA₅₆-PBMA₅₀₀ diblock copolymer nanoparticles prepared *via* high-throughput RAFT aqueous emulsion polymerization using the Chemspeed AutoPlant A100 synthesizer. Filled triangles indicate syntheses conducted using the propeller stirrer, open circles indicate syntheses performed using the anchor stirrer and crosses indicate laboratory-scale syntheses. Error bars indicate the standard deviations for each particle size distribution, rather than the experimental error.

4.4.5. Reproducibility of high-throughput syntheses

The reproducibility of such high-throughput syntheses using the Chemspeed A100 was then evaluated by preparing both PMAA₅₆-PBzMA₅₀₀ and PMAA₅₆-PBMA₅₀₀ nanoparticles five times using precisely the same formulation in each case. These formulations were conducted in randomized locations on the Chemspeed A100. The resulting diblock copolymer dispersions were then analyzed by HPLC, DLS and TEM for comparison, along with THF GPC analyses of the copolymer chains (see Table 4.4). All five PMAA₅₆-PBzMA₅₀₀ syntheses proceeded to high conversion within 1 h (> 98%) while GPC analyses indicated comparable molecular weight distributions in each case ($M_n = 56\,700 \pm 500 \text{ g mol}^{-1}$ and $\text{Đ} = 1.48 - 1.57$) (Figure 4.11a).

Chapter 4: Optimization of the high-throughput synthesis of multiblock copolymer nanoparticles in aqueous media via polymerization-induced self-assembly

Table 4.4. Assessment of the reproducibility of the PISA synthesis of diblock copolymer nanoparticles *via* high-throughput RAFT aqueous emulsion polymerization of either benzyl methacrylate (BzMA) or *n*-butyl methacrylate (BMA) at 70 °C using a PMAA₅₆ macro-CTA at pH 5.

Monomer	Experiment number	Conversion (%) ^a	DLS particle diameter (nm)	DLS PDI ^b	TEM particle diameter (nm)	M_n^b (g mol ⁻¹)	\mathcal{D}^b
BzMA	1	99	44	0.15	31	56,900	1.57
	2	99	46	0.14	31	58,400	1.55
	3	98	45	0.13	31	57,300	1.49
	4	99	45	0.14	34	58,000	1.50
	5	99	45	0.14	34	57,700	1.48
BMA	1	98	45	0.20	33	51,300	1.67
	2	98	43	0.18	37	50,300	1.62
	3	98	43	0.16	36	55,900	1.54
	4	98	45	0.16	34	53,100	1.60
	5	98	46	0.18	35	54,600	1.60

^a Conversion determined by high-performance liquid chromatography (HPLC)

^b Molecular weight data determined by GPC using THF eluent containing 4% v/v glacial acetic acid (calibrated using a series of near-monodisperse PMMA standards).

Similarly, each of the five PMAA₅₆-PBMA₅₀₀ syntheses proceeded to 98% conversion within 1 h ($M_n = 53,400 \pm 2,100 \text{ g mol}^{-1}$ and $\bar{D} = 1.54 - 1.67$, Figure 4.11b). THF GPC chromatograms also confirm high blocking efficiencies and unimodal traces in all cases.

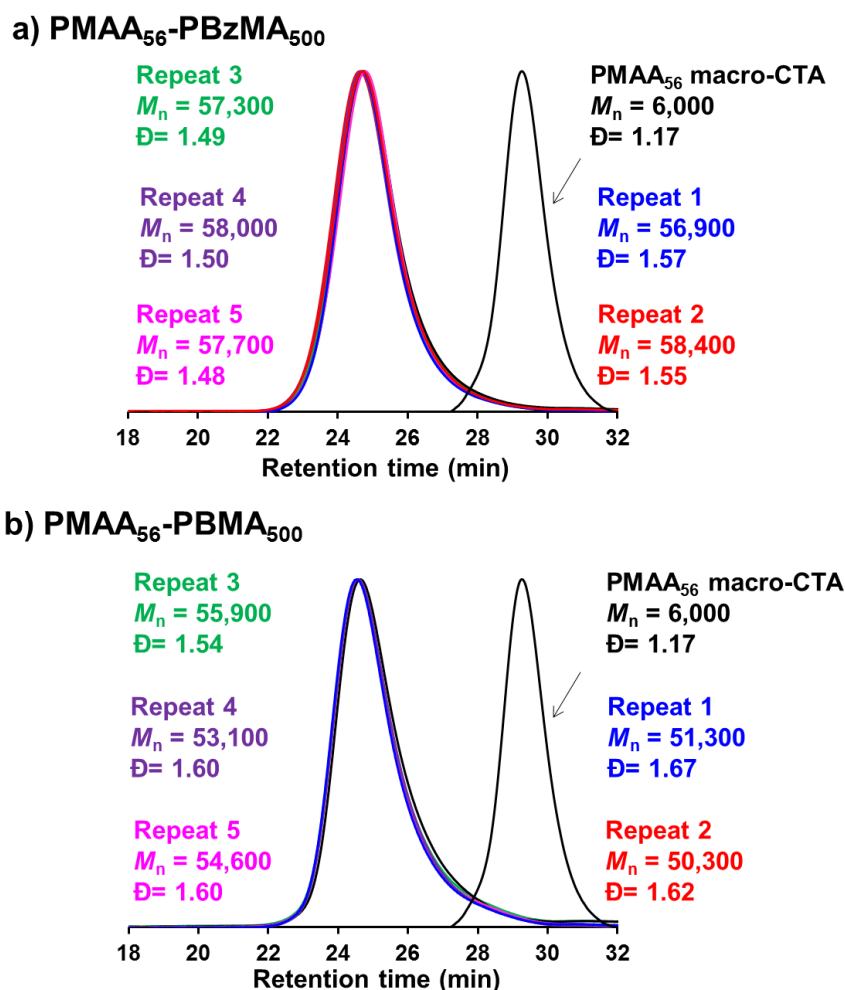


Figure 4.11. THF GPC chromatograms confirm that good reproducibility is achieved for molecular weight distributions when targeting (a) PMAA₅₆-PBzMA₅₀₀ and (b) PMAA₅₆-PBMA₅₀₀ nanoparticles via high-throughput RAFT aqueous emulsion polymerizations performed using the Chemspeed A100. Each synthesis was conducted five times and the corresponding chromatograms are overlaid. Tables summarize the M_n and \bar{D} data calculated from each chromatogram.

Moreover, there was generally minimal variation in the intensity-average particle diameter between the PMAA₅₆-PBzMA₅₀₀ series (44 nm to 46 nm) and the PMAA₅₆-PBMA₅₀₀ series (43 to 46 nm), see Figure 4.12 and Appendix 5. However, TEM analysis (which is only sensitive to the nanoparticle cores, and so underestimates relative to the hydrodynamic diameter reported by DLS) indicated the formation of spherical nanoparticles with comparable particle diameters in all cases, see Figure 4.13.

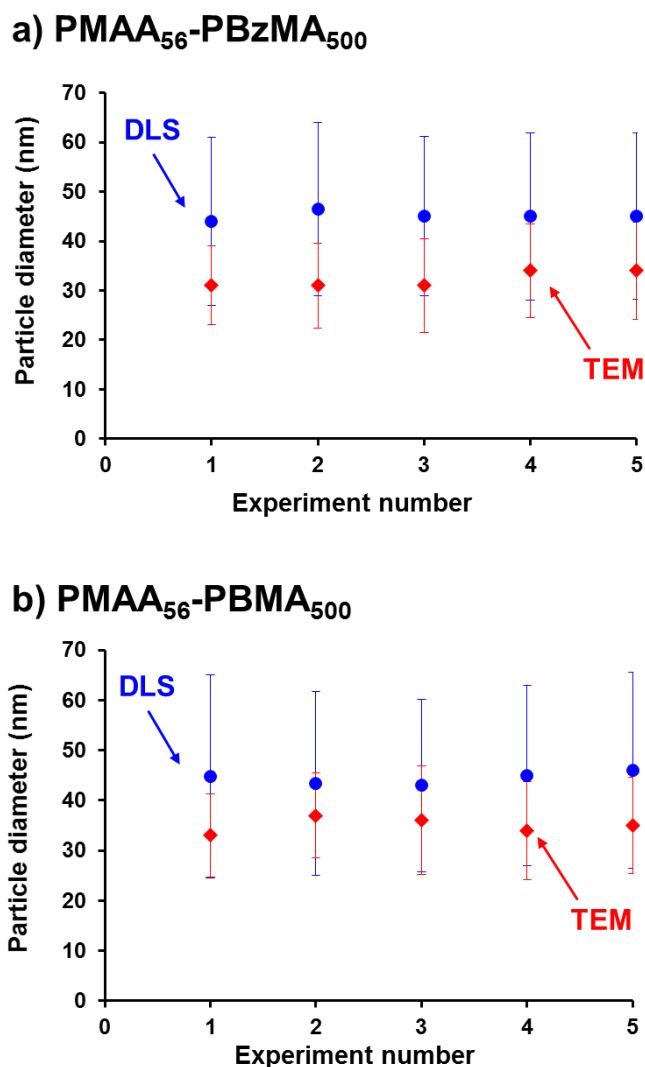


Figure 4.12. Particle size analysis of diblock copolymer nanoparticles synthesized *via* high-throughput RAFT aqueous emulsion polymerization using the Chemspeed Autoplant A100 automated synthesizer: (a) PMAA₅₆-PBzMA₅₀₀ and (b) PMAA₅₆-PBMA₅₀₀. Particle diameter as measured by DLS (blue circles) and by TEM (red diamonds). Error bars indicate standard deviations for each particle size distribution, rather than the experimental error.

In summary, the observed minimal variation in conversion, molecular weight, dispersity and mean particle diameter indicate rather good reproducibility for the high-throughput RAFT aqueous emulsion polymerizations performed using the Chemspeed A100.

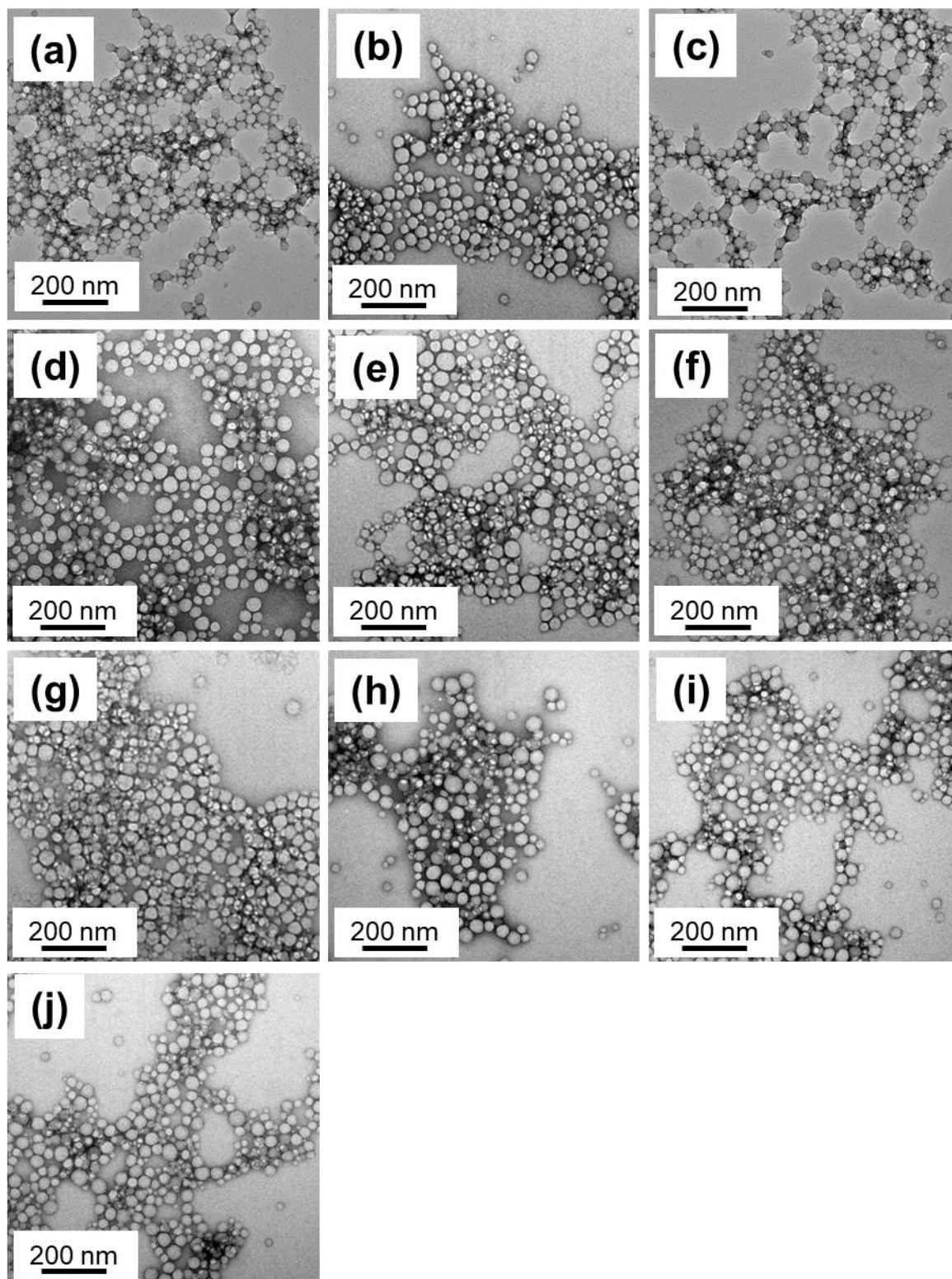


Figure 4.13. Representative TEM images of diblock copolymer nanoparticles synthesized *via* high-throughput RAFT aqueous emulsion polymerization using the Chemspeed Autoplant A100 automated synthesizer. The reproducibility of such high-throughput syntheses are assessed by preparing both (a-e) PMAA₅₆-PBzMA₅₀₀ and (f-j) PMAA₅₆-PBMA₅₀₀ nanoparticle five times using exactly the same formulation in each case.

4.4.6. Synthesis of diblock, triblock and tetra-block copolymers via high-throughput method

Having demonstrated reproducible RAFT aqueous emulsion polymerization syntheses for both PMAA₅₆-PBzMA₅₀₀ and PMAA₅₆-PBMA₅₀₀ diblock copolymer nanoparticles, the versatility of this optimized high-throughput approach was assessed for the synthesis of methacrylic-based multiblock nanoparticles.⁸³ Triblock and tetrablock copolymer nanoparticles were prepared *via* a high-throughput one-pot protocol using sequential monomer addition. The multiblock copolymers were of the same compositions as those synthesized previously on a laboratory-scale, see Scheme 4.1. These PISA syntheses were completed within 3 h in the case of the triblock copolymer nanoparticles (40% w/w copolymer concentration; > 99% overall conversion), see Table 4.5 and Figure 4.14. However, tetrablocks (45% w/w copolymer concentration) suffer from incomplete conversions (87-96% within 5 h) and hence most likely represent the upper limit for this approach, see Table 4.5 and Figure 4.14.

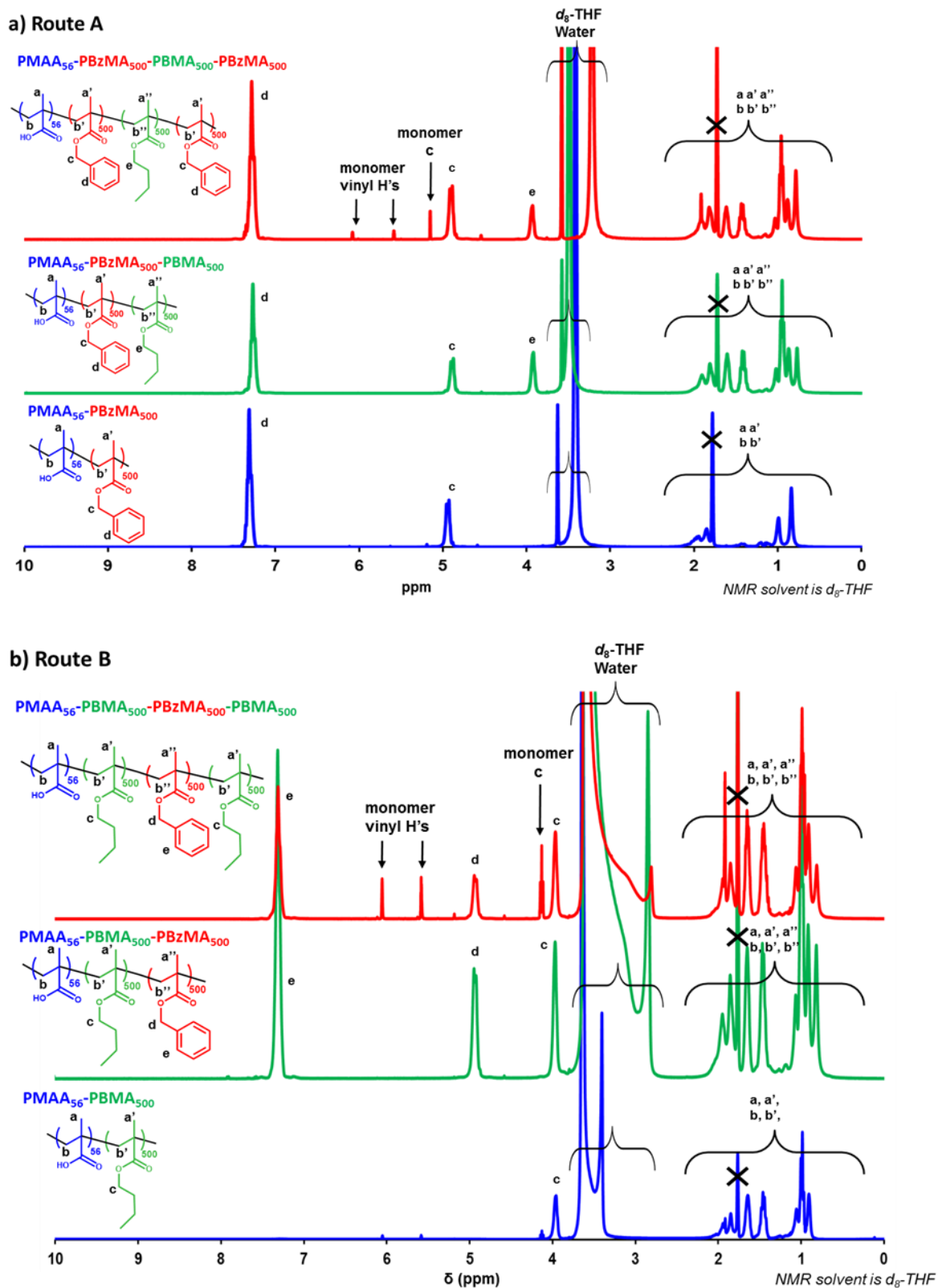


Figure 4.14 ^1H NMR spectra for diblock, triblock and tetrablock copolymers prepared *via* RAFT aqueous emulsion polymerization. These syntheses were performed on the high-throughput Chemspeed A100 robot synthesizer *via* either (a) Route A or (b) Route B as outlined in Scheme 2. The peaks labelled with a black cross correspond to solvent peaks from d_8 -tetrahydrofuran (1.73 ppm and 3.58 ppm) and water (~3.5 ppm).

Table 4.5 Summary of diblock, triblock and tetrablock copolymers prepared *via* RAFT aqueous emulsion polymerization. These syntheses were performed on the high-throughput Chemspeed A100 robot synthesizer. These multiblock copolymer syntheses were performed at 70 °C using a PMAA₅₆ macro-CTA/initiator of 5.0, in aqueous solution at pH 5.

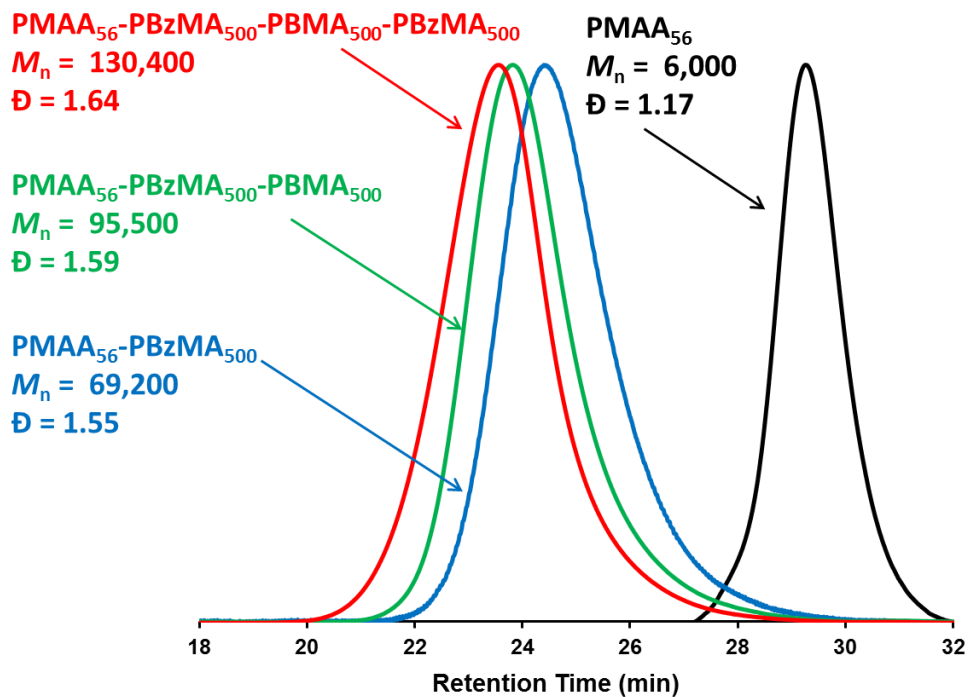
	Target Composition	Overall Monomer Conversion ^a (%)		DLS particle diameter (nm)	DLS particle polydispersity	TEM particle diameter (nm)	M_n^b (g mol ⁻¹)	\mathcal{D}^b
		BzMA	BMA					
High-Throughput Syntheses	PMAA ₅₆ -PBzMA ₅₀₀	99	-	49	0.17	38	69,200	1.55
	PMAA ₅₆ -PBzMA ₅₀₀ -PBMA ₅₀₀	> 99	> 99	86	0.09	60	95,500	1.59
	PMAA ₅₆ -PBzMA ₅₀₀ -PBMA ₅₀₀ -PBzMA ₅₀₀	96	> 99	106	0.10	64	130,400	1.64
	PMAA ₅₆ -PBMA ₅₀₀	-	94	47	0.21	40	69,000	1.62
	PMAA ₅₆ -PBMA ₅₀₀ -PBzMA ₅₀₀	> 99	> 99	82	0.16	49	103,900	1.85
	PMAA ₅₆ -PBMA ₅₀₀ -PBzMA ₅₀₀ -PBMA ₅₀₀	> 99	87	117	0.17	61	129,400	1.84

^a Conversion determined by high-performance liquid chromatography (HPLC)^b Molecular weight data determined by GPC using THF eluent containing 4% v/v glacial acetic acid (calibrated using a series of near-monodisperse PMMA standards).

THF GPC analysis indicated a progressive increase in molecular weight during the synthesis of the tetrablock copolymer, see Figure 4.15. Clearly, the dispersity values obtained throughout this study ($\mathcal{D} = 1.35$ to 1.85) are generally higher than those normally reported for RAFT aqueous emulsion polymerization syntheses. As discussed above, there are a number of literature reports that also report relatively broad molecular weight distributions for such PISA formulations.^{5, 27, 29, 30, 64, 66} Although, we are not sure why such high dispersity values are observed in this work, well-defined, albeit relatively disperse, block copolymers are obtained as evidence by the unimodal distributions and high blocking efficiencies are achieved, see Figure 4.15.

Finally, the GPC data obtained for the laboratory-scale synthesis of the tetrablock copolymers differ significantly from that obtained from the corresponding high-throughput syntheses, with the former giving broader molecular weight distributions (compare Figure 4.5 and Figure 4.15). However, such discrepancies may well be attributable to differing GPC analytical protocols and instrument set-ups, as noted earlier (see page 170).

a) Route A: THF GPC chromatograms



b) Route B: THF GPC chromatograms

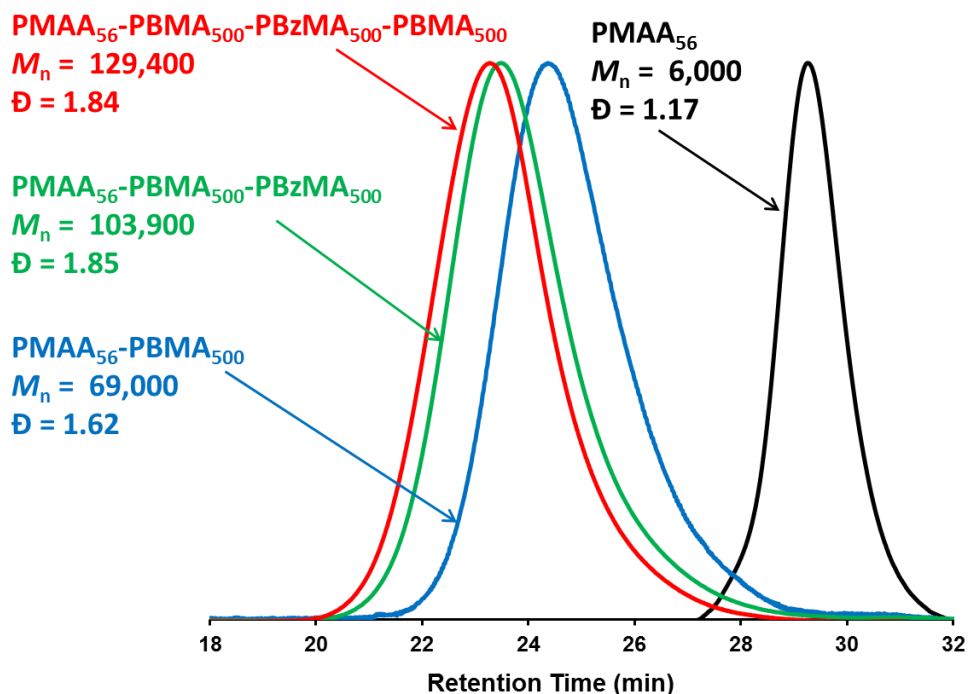


Figure 4.15. THF GPC chromatograms illustrating the monotonic increase in block copolymer molecular weight achieved with each subsequent block addition during the high-throughput synthesis of diblock, triblock and tetrablock copolymer nanoparticles by RAFT aqueous emulsion polymerization using the Chemspeed A100. All M_n values are expressed relative to PMMA calibration standards.

TEM and DLS studies confirmed that colloiddally stable spherical nanoparticles were obtained in all cases (see Figure 4.16, and Appendix 6). Owing to the larger (~30 mL) scale and higher copolymer concentrations (30-45% w/w) used for these reactions, the stirring rate was raised to 700 rpm for the diblock copolymer syntheses and to 900 rpm for the triblock and tetrablock syntheses.

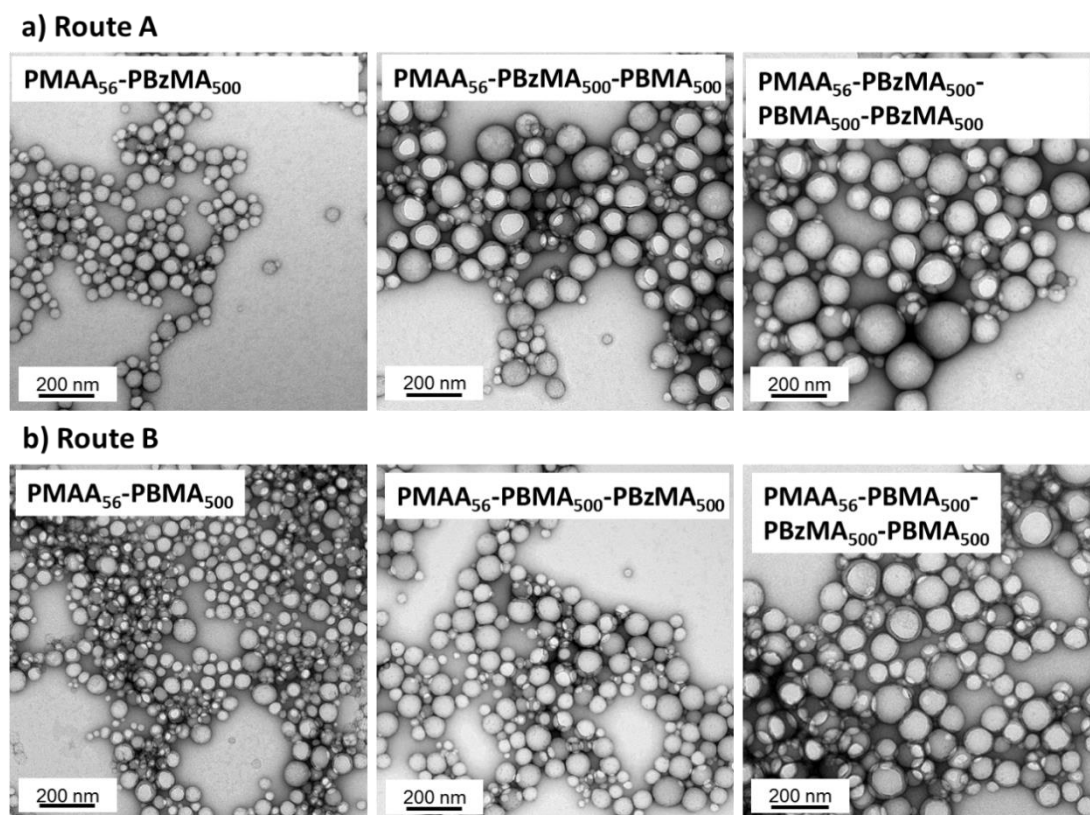


Figure 4.16. Representative TEM images obtained for the synthesis of diblock, triblock and tetrablock copolymers using the Chemspeed A100 automated synthesizer by RAFT aqueous emulsion polymerization. Spherical morphologies were obtained in all cases and an increase in mean nanoparticle diameter was observed by DLS and TEM with each subsequent block addition.

In summary, RAFT aqueous emulsion polymerization can be used for the synthesis of methacrylic tetrablock nanoparticles at up to 45% w/w copolymer concentration within 5 h, which is comparable to industrial latex formulations based on conventional emulsion polymerization. However, the latter technique cannot be used to access diblock copolymer architectures, so RAFT aqueous emulsion polymerization may offer new potential applications in terms of nanoscale phase separation.

4.5. Conclusions

The synthesis of a PMAA₅₆ macro-CTA *via* RAFT solution polymerization in ethanol was successfully conducted on a 250 g scale. ¹H NMR analysis indicated a mean PMAA DP of 56. Whilst, GPC analysis (of the methylated polymer) confirmed that the RAFT polymerization was well-controlled, resulting in a M_n of 6,000 g mol⁻¹ and a dispersity of 1.17 (analysis conducted at the AkzoNobel site in Slough). This PMAA₅₆ macro-CTA was chain-extended with BzMA and/or BMA *via* RAFT aqueous emulsion polymerization to synthesize a series of diblock, triblock and tetrablock copolymers on a laboratory-scale. These polymerizations proceeded to high monomer conversions (> 96%) for each sequential block and resulted in the formation of spherical nanoparticles, as judged by DLS and TEM.

Optimized protocols for performing high-throughput RAFT aqueous emulsion polymerizations using a commercial automated robot synthesizer (Chemspeed A100) are reported. In addition to thorough deoxygenation of the reaction solution, reproducible formulations required the use of a propeller-type stirrer at stirring rates of 550 to 900 rpm to produce sufficiently small droplets of the water-immiscible benzyl methacrylate or *n*-butyl methacrylate monomer. Various sterically-stabilized diblock copolymer nanoparticles could be prepared with final monomer conversions of $\geq 94\%$ within 1 h. GPC studies indicated very high blocking efficiencies but relatively broad molecular weight distributions ($\mathcal{D} 1.48 \leq 1.67$). TEM studies confirm that a well-defined spherical morphology was obtained in each case but DLS analyses indicated relatively broad size distributions. These high-throughput syntheses were shown to be reproducible with minimal variation in conversion, molecular weight, dispersity and mean particle diameter observed. A library of various triblock and tetrablock copolymer nanoparticles were also prepared *via* a convenient one-pot protocol using sequential monomer addition. For the tetrablock copolymers, final conversions of 87 - 96% within 5 h at 70 °C and good colloidal stability being achieved even at 45% w/w copolymer concentration. GPC studies indicate high blocking efficiencies but relatively broad molecular weight distributions ($\mathcal{D} = 1.64 - 1.85$), suggesting well-defined (albeit rather disperse) tetrablock copolymers. These preliminary studies provide the basis for further high-throughput screening of RAFT-mediated PISA formulations, which is likely to be required for commercialization of this promising technology.

4.6. References

1. B. Charleux, G. Delaittre, J. Rieger and F. D'Agosto, *Macromolecules*, 2012, **45**, 6753-6765.
2. S. L. Canning, G. N. Smith and S. P. Armes, *Macromolecules*, 2016, **49**, 1985-2001.
3. N. J. Warren and S. P. Armes, *Journal of the American Chemical Society*, 2014, **136**, 10174-10185.
4. Y. Li and S. P. Armes, *Angewandte Chemie International Edition*, 2010, **49**, 4042-4046.
5. S. Boissé, J. Rieger, K. Belal, A. Di-Cicco, P. Beaunier, M.-H. Li and B. Charleux, *Chemical Communications*, 2010, **46**, 1950-1952.
6. A. Blanazs, J. Madsen, G. Battaglia, A. J. Ryan and S. P. Armes, *Journal of the American Chemical Society*, 2011, **133**, 16581-16587.
7. A. Blanazs, A. J. Ryan and S. P. Armes, *Macromolecules*, 2012, **45**, 5099-5107.
8. J.-T. Sun, C.-Y. Hong and C.-Y. Pan, *Soft Matter*, 2012, **8**, 7753.
9. J.-T. Sun, C.-Y. Hong and C.-Y. Pan, *Polymer Chemistry*, 2013, **4**, 873-881.
10. N. J. Warren, O. O. Mykhaylyk, D. Mahmood, A. J. Ryan and S. P. Armes, *Journal of the American Chemical Society*, 2014, **136**, 1023-1033.
11. J. Rieger, *Macromolecular Rapid Communications*, 2015, **36**, 1458-1471.
12. M. R. Hill, R. N. Carmean and B. S. Sumerlin, *Macromolecules*, 2015, **48**, 5459-5469.
13. M. J. Derry, L. A. Fielding and S. P. Armes, *Progress in Polymer Science*, 2016, **52**, 1-18.
14. M. Semsarilar, E. R. Jones, A. Blanazs and S. P. Armes, *Advanced Materials*, 2012, **24**, 3378-3382.
15. V. J. Cunningham, A. M. Alswieleh, K. L. Thompson, M. Williams, G. J. Leggett, S. P. Armes and O. M. Musa, *Macromolecules*, 2014, **47**, 5613-5623.
16. B. Akpınar, L. A. Fielding, V. J. Cunningham, Y. Ning, O. O. Mykhaylyk, P. W. Fowler and S. P. Armes, *Macromolecules*, 2016, **49**, 5160-5171.
17. A. Blanazs, R. Verber, O. O. Mykhaylyk, A. J. Ryan, J. Z. Heath, C. W. I. Douglas and S. P. Armes, *Journal of the American Chemical Society*, 2012, **134**, 9741-9748.
18. C. Gonzato, M. Semsarilar, E. R. Jones, F. Li, G. J. P. Krooshof, P. Wyman, O. O. Mykhaylyk, R. Tuinier and S. P. Armes, *Journal of the American Chemical Society*, 2014, **136**, 11100-11106.
19. P. Chambon, A. Blanazs, G. Battaglia and S. P. Armes, *Macromolecules*, 2012, **45**, 5081-5090.
20. A. A. Cockram, T. J. Neal, M. J. Derry, O. O. Mykhaylyk, N. S. J. Williams, M. W. Murray, S. N. Emmett and S. P. Armes, *Macromolecules*, 2017, **50**, 796-802.
21. N. J. W. Penfold, Y. Ning, P. Verstraete, J. Smets and S. P. Armes, *Chemical Science*, 2016, **7**, 6894-6904.
22. I. Canton, N. J. Warren, A. Chahal, K. Amps, A. Wood, R. Weightman, E. Wang, H. Moore and S. P. Armes, *ACS Central Science*, 2016, **2**, 65-74.
23. K. L. Thompson, C. J. Mable, A. Cockram, N. J. Warren, V. J. Cunningham, E. R. Jones, R. Verber and S. P. Armes, *Soft Matter*, 2014, **10**, 8615-8626.

24. M. J. Rymaruk, K. L. Thompson, M. J. Derry, N. J. Warren, L. P. D. Ratcliffe, C. N. Williams, S. L. Brown and S. P. Armes, *Nanoscale*, 2016, **8**, 14497-14506.
25. M. Chenal, J. Rieger, C. Véchambre, J.-M. Chenal, L. Chazeau, C. Creton and L. Bouteiller, *Macromolecular Rapid Communications*, 2013, **34**, 1524-1529.
26. M. Chenal, C. Véchambre, J.-M. Chenal, L. Chazeau, V. Humblot, L. Bouteiller, C. Creton and J. Rieger, *Polymer*, 2017, **109**, 187-196.
27. X. Zhang, S. Boissé, W. Zhang, P. Beaunier, F. D'Agosto, J. Rieger and B. Charleux, *Macromolecules*, 2011, **44**, 4149-4158.
28. S. Sugihara, A. Blanzs, S. P. Armes, A. J. Ryan and A. L. Lewis, *Journal of the American Chemical Society*, 2011, **133**, 15707-15713.
29. S. Boissé, J. Rieger, G. Pembouong, P. Beaunier and B. Charleux, *Journal of Polymer Science Part A: Polymer Chemistry*, 2011, **49**, 3346-3354.
30. I. Chaduc, A. Crepet, O. Boyron, B. Charleux, F. D'Agosto and M. Lansalot, *Macromolecules*, 2013, **46**, 6013-6023.
31. L. D. Blackman, K. E. B. Doncom, M. I. Gibson and R. K. O'Reilly, *Polymer Chemistry*, 2017, **8**, 2860-2871.
32. M. Williams, N. J. W. Penfold, J. R. Lovett, N. J. Warren, C. W. I. Douglas, N. Doroshenko, P. Verstraete, J. Smets and S. P. Armes, *Polymer Chemistry*, 2016, **7**, 3864-3873.
33. R. Hoogenboom, M. A. R. Meier and U. S. Schubert, *Macromolecular Rapid Communications*, 2003, **24**, 15-32.
34. H. E. Tuinstra and C. H. Cummins, *Advanced Materials*, 2000, **23**, 1819-1822.
35. M. A. R. Meier, R. Hoogenboom and U. S. Schubert, *Macromolecular Rapid Communications*, 2004, **25**, 21-33.
36. S. P. Rohrer, E. T. Birzin, R. T. Mosley, S. C. Berk, S. M. Hutchins, D.-M. Shen, Y. Xiong, E. C. Hayes, R. M. Parmar, F. Foor, S. W. Mitra, S. J. Degrado, M. Shu, J. M. Klopp, S.-J. Cai, A. Blake, W. W. S. Chan, A. Pasternak, L. Yang, A. A. Patchett, R. G. Smith, K. T. Chapman and J. M. Schaeffer, *Science*, 1998, **282**, 737-740.
37. K. C. Nicolaou, A. J. Roecker, S. Barluenga, J. A. Pfefferkorn and G.-Q. Cao, *ChemBioChem*, 2001, **2**, 460-465.
38. B. Jandeleit, D. J. Schaefer, T. S. Powers, H. W. Turner and W. H. Weinberg, *Science*, 1999, **268**, 1738-1740.
39. X. D. Xiang, X.-D. Sun, G. Briceno, Y. Lou, K.-A. Wang, H. Chang, W. G. Wallace-Freedman, S.-W. Chen and P. G. Schultz, *Science*, 1995, **268**, 1738-1740.
40. E. Danielson, J. H. Golden, E. W. McFarland, C. M. Reaves, W. H. Weinberg and X. D. Wu, *Angewandte Chemie International Edition*, 1997, **38**, 2494-2532.
41. X.-D. Sun, C. Gao, J. Wang and X. D. Xiang, *Applied Physics Letters*, 1997, **70**, 3353-3355.
42. J. Wang, Y. Yoo, C. Gao, I. Takeuchi, X.-D. Sun, H. Chang, X.-D. Xiang and P. G. Schultz, *Science*, 1998, **279**, 1712-1714.
43. P. G. Schultz and X.-D. Xiang, *Current Opinion in Solid State and Materials Science*, 1998, **3**, 153-158.
44. S. M. Senkan, *Angewandte Chemie International Edition*, 1998, **40**, 284-310.
45. M. T. Reetz, *Nature*, 1998, **394**, 350-353.
46. T. R. Boussie, G. M. Diamond, C. Goh, K. A. Hall, A. M. LaPointe, M. Leclerc, C. Lund, V. Murphy, J. A. W. Shoemaker, U. Tracht, H. Turner, J.

- Zhang, T. Uno, R. K. Rosen and J. C. Stevens, *Journal of the American Chemical Society*, 2003, **125**, 4306-4317.
47. T. R. Boussie, G. M. Diamond, C. Goh, K. A. Hall, A. M. LaPointe, M. K. Leclerc, V. Murphy, J. A. W. Shoemaker, H. Turner, R. K. Rosen, J. C. Stevens, F. Alfano, V. Busico, R. Cipullo and G. Talarico, *Angewandte Chemie International Edition*, 2006, **45**, 3278-3283.
48. P. Chapon, M. Catherine, L. Gilda and D. Mathias, *Macromolecular Rapid Communications*, 2003, **24**, 87-91.
49. M. W. M. Fijten, M. A. R. Meier, R. Hoogenboom and U. S. Schubert, *Journal of Polymer Science Part A: Polymer Chemistry*, 2004, **42**, 5775-5783.
50. M. W. M. Fijten, R. M. Paulus and U. S. Schubert, *Journal of Polymer Science Part A: Polymer Chemistry*, 2005, **43**, 3831-3839.
51. R. Hoogenboom and U. S. Schubert, *Macromolecules*, 2005, **38**, 7653-7659.
52. C. R. Becer, A. M. Groth, R. Hoogenboom, R. M. Paulus and U. S. Schubert, *QSAR & Combinatorial Science*, 2008, **27**, 977-983.
53. S. Boissé, J. Rieger, G. Pembouong, P. Beaunier and B. Charleux, *Journal of Polymer Science Part A: Polymer Chemistry*, 2011, **49**, 3346-3354.
54. M. Semsarilar, V. Ladmiral, A. Blanazs and S. P. Armes, *Polymer Chemistry*, 2014, **5**, 3466-3475.
55. S. W. Prescott, M. J. Ballard, E. Rizzardo and R. G. Gilbert, *Australian Journal of Chemistry*, 2002, **55**, 415.
56. C. J. Ferguson, R. J. Hughes, B. T. T. Pham, B. S. Hawkett, R. G. Gilbert, A. K. Serelis and C. H. Such, *Macromolecules*, 2002, **35**, 9243-9245.
57. C. J. Ferguson, R. J. Hughes, D. Nguyen, B. T. T. Pham, R. G. Gilbert, A. K. Serelis, C. H. Such and B. S. Hawkett, *Macromolecules*, 2005, **38**, 2191-2204.
58. S. Fréal-Saison, M. Save, C. Bui, B. Charleux and S. Magnet, *Macromolecules*, 2006, **39**, 8632-8638.
59. M. Manguian, M. Save and B. Charleux, *Macromolecular Rapid Communications*, 2006, **27**, 399-404.
60. M. F. Cunningham, *Progress in Polymer Science*, 2008, **33**, 365.
61. W. Zhang, F. D'Agosto, O. Boyron, J. Rieger and B. Charleux, *Macromolecules*, 2011, **44**, 7584-7593.
62. I. Chaduc, W. Zhang, J. Rieger, M. Lansalot, F. D'Agosto and B. Charleux, *Macromolecular Rapid Communications*, 2011, **32**, 1270-1276.
63. I. Chaduc, M. Girod, R. Antoine, B. Charleux, F. D'Agosto and M. Lansalot, *Macromolecules*, 2012, **45**, 5881-5893.
64. W. Zhang, F. D'Agosto, O. Boyron, J. Rieger and B. Charleux, *Macromolecules*, 2012, **45**, 4075-4084.
65. W. Zhang, F. D'Agosto, P.-Y. Dugas, J. Rieger and B. Charleux, *Polymer*, 2013, **54**, 2011-2019.
66. N. P. Truong, M. V. Dussert, M. R. Whittaker, J. F. Quinn and T. P. Davis, *Polymer Chemistry*, 2015, **6**, 3865-3874.
67. J. Lesage de la Haye, X. Zhang, I. Chaduc, F. Brunel, M. Lansalot and F. D'Agosto, *Angewandte Chemie International Edition*, 2016, **55**, 3739-3743.
68. M. Semsarilar, V. Ladmiral, A. Blanazs and S. P. Armes, *Polymer Chemistry*, 2014, **5**, 3466-3475.
69. I. Chaduc, A. Crepet, O. Boyron, B. Charleux, F. D'Agosto and M. Lansalot, *Macromolecules*, 2013, **46**, 6013.
70. J. Zhou, R. He and J. Ma, *Polymers*, 2016, **8**, 207-220.

71. E. Velasquez, J. Rieger, F. Stoffelbach, F. D'Agosto, M. Lansalot, P.-E. Dufils and J. Vinas, *Polymer*, 2016, **106**, 275-284.
72. I. Chaduc, M. Girod, R. Antoine, B. Charleux, F. D'Agosto and M. Lansalot, *Macromolecules*, 2012, **45**, 5881-5893.
73. F. L. Hatton, J. R. Lovett and S. P. Armes, *Polymer Chemistry*, 2017, **8**, 4856-4868.
74. C. P. Jesson, V. J. Cunningham, M. J. Smallridge and S. P. Armes, *Macromolecules*, 2018, **51**, 3221-3232.
75. J. Rieger, F. Stoffelbach, C. Bui, D. Alaimo, C. Jérôme and B. Charleux, *Macromolecules*, 2008, **41**, 4065-4068.
76. J. Rieger, G. Osterwinter, C. Bui, F. o. Stoffelbach and B. Charleux, *Macromolecules*, 2009, **42**, 5518-5525.
77. J. Chiefari, Y. K. B. Chong, F. Ercole, J. Krstina, J. Jeffery, T. P. T. Le, R. T. A. Mayadunne, G. F. Meijs, C. L. Moad, G. Moad, E. Rizzardo and S. H. Thang, *Macromolecules*, 1998, **31**, 5559-5562.
78. F. A. Bovey and I. M. Kolthoff, *Chemical Reviews*, 1948, **42**, 491-525.
79. V. A. Bhanu and K. Kishore, *Chemical Reviews*, 1991, **91**, 99-115.
80. J. W. Goodwin, J. Hearn, C. C. Ho and R. H. Ottewill, *Colloid and Polymer Science*, 1974, **252**, 464-471.
81. S. Fathi Roudsari, R. Dhib and F. Ein-Mozaffari, *Polymer Engineering & Science*, 2015, **55**, 945-956.
82. K. Matyjaszewski and T. Davis, *Handbook of Radical Polymerization*, Wiley, 2002.
83. , There has been considerable recent interest in the synthesis of multiblock copolymers via living radical polymerization in the literature (e.g. G. Gody, T. Maschmeyer, P. B. Zetterlund and S. Perrier, *Macromolecules*, 2014, 2047, 3451-3460 and N. G. Engelis, A. Anastasaki, G. Nurumbetov, N. P. Truong, V. Nikolaou, A. Shegiwal, M. R. Whittaker, T. P. Davis and D. M. Haddleton, *Nature Chemistry*, 2016, 2019).

Chapter Five

5. Synthesis and characterization of film-forming block copolymer nanoparticles *via* RAFT aqueous emulsion polymerization

5.1. Introduction

Polymers are a key component of coatings formulations; they act as a ‘binder’ for the pigment particles and strongly influence the physical properties of the coating. For a high-performance coating, important characteristics include hardness, impact resistance, adhesion, stress/strain properties, anti-corrosion properties and good weathering resistance.¹ For many years, film formation was achieved by dissolving the polymer (along with dispersed pigments and additives) in a volatile organic solvent.¹ However, government legislation now restricts the level of volatile organic compounds (VOCs) allowed in such formulations. This has led to such solvent-borne coatings being gradually phased out. Waterborne coatings, where polymers are synthesized as latex particles directly in water, are one strategy that complies with zero-VOC regulations.² For the industrial scale production of coatings, conventional emulsion polymerization is the most widely used technique for the synthesis of polymers directly in water.^{1, 3-5} In such formulations, surfactant is usually required to stabilize the latex particles.⁵ Although widely used in industry, migration and segregation of free surfactant during the process of film formation can have a negative impact on many properties of the final polymer film including gloss, water sorption, permeability and adhesion to a substrate.⁵⁻⁹ This has led to design of so-called ‘surfactant-free’ latexes with comparable properties to those of the surfactant-stabilized counterparts.¹⁰⁻¹³ In reality such formulations typically involve the synthesis of a surface-active species *in situ* during the polymerization which can also migrate during film formation resulting in similar negative effects.

Synthesizing block copolymers by RDRP techniques (e.g. RAFT polymerization) usually affords excellent control over mean block length (DP) and the MWD. This enables the properties of block copolymers to be fine-tuned for their desired application. In particular, the spontaneous microphase separation of block copolymers can have a significant impact on their physical and mechanical properties in the solid state. This has been exploited for specific applications such as nanoscale lithography, ionic conductivity, organic photovoltaics and energy storage.¹⁴⁻²⁰

The microphase separation of an AB diblock copolymer is caused by the mutual enthalpic incompatibility of the two blocks, and has been extensively studied.²⁰⁻²⁴ The microdomains of each block typically form a periodic structure with long-range order.

The resulting copolymer morphology depends on three parameters. Firstly, the relative volume fraction of each block (f_A and f_B), where the total volume fraction equals unity ($f_A + f_B = 1$). Secondly, the total DP (N) of the two blocks (where $N = DP_A + DP_B$). Thirdly, the Flory-Huggins parameter (χ_{AB}), which indicates the degree of enthalpic incompatibility between the two blocks, as defined in Equation 1.18.^{21, 24-26} It is worth noting that morphologies resulting from AB diblock copolymer microphase separation are only observed for diblock copolymers of low dispersity ($\mathcal{D} < 1.2$).^{26, 27} As the dispersity increases the morphology is lost and segregation of the block occurs more randomly.²⁷

ABA triblock copolymers comprising a long rubbery (low T_g) B block capped by two short glassy (high T_g) A blocks are often used for elastomeric applications in areas such as coatings, textiles, footwear, adhesives, roofing and road surfaces.^{28, 29} When microphase separated, the B blocks act as physical crosslinks for the A block creating a physically cross-linked network, see Figure 5.1.^{27, 30-32} Thus, increasing the dimensional stability of ABA triblock relative to AB diblock copolymers. This increased stability enables ABA triblock copolymers to offer a wide range of desirable physical properties, including toughness, extensibility and ease of processing.²⁹

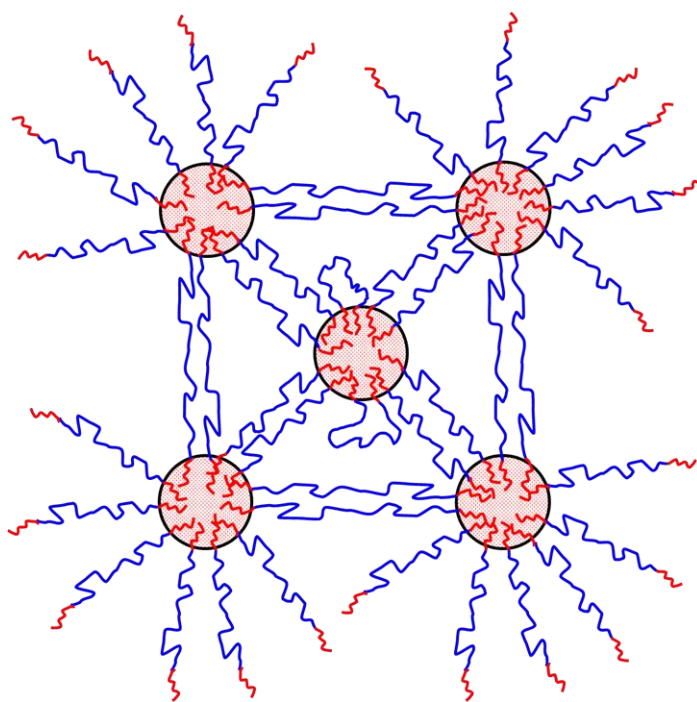


Figure 5.1 Cartoon of a physically cross-linked network created during microphase separation of ABA triblock copolymers, where the low T_g B blocks (shown in blue) act as physical crosslinks between the high T_g domains of the A blocks (shown in red).^{27, 30-32}

In recent years, multiblock copolymers have been the subject of increasing academic attention. The phase separation of $(AB)_n$ linear multiblock copolymers is similar to that of AB diblock copolymers and a range of morphologies can be observed including lamellar, cylindrical, spherical and gyroid phases.^{28, 33-39} This literature suggests that, relative to diblock and triblock copolymers, multiblock copolymers have superior mechanical properties such as toughness, tensile strength.³⁷⁻⁴² This enhancement is caused by the ability of the copolymer chains to bridge multiple nanoscale domains.^{28, 29, 35, 37, 39, 41, 43-48} In principle, phase separation in multiblock copolymers makes them ideal candidates for many applications.¹⁶

Of particular significance to this Thesis, are literature reports of transparent copolymer films formed by block copolymer nanoparticles synthesized *via* RAFT aqueous emulsion polymerization.⁴⁹⁻⁵² The transparent copolymer films reported by Lansalot and co-workers were obtained from block copolymer nanoparticles comprising a mixture of MAA, BA, MMA and styrene (S).⁴⁹ Spherical nanoparticles were formed *via* PISA, whereby the PMAA chains acted as an anionic stabilizer block for the nanoparticles, eliminating the need for added surfactant. Similarly, Velasquez *et al.* utilized PAA, PMAA or poly(sodium 4-styrenesulfonate) as the stabilizer block for the RAFT aqueous emulsion copolymerization of vinylidene chloride with methyl acrylate. The resulting block copolymer nanoparticles afforded transparent films.⁵⁰ Chenal *et al.* also reported utilizing PAA-PBA diblock copolymer nanoparticles to form transparent films.⁵¹ These films were shown to have a honey-comb structure after drying at room temperature, see Figure 5.2. Thermally annealing these films enabled rearrangement to a more thermodynamically stable inverted structure, see Figure 5.2.

Spherical nanoparticles comprising self-assembled block copolymers containing alternating hard and soft blocks (e.g. high and low T_g blocks) have also been recently reported.^{51, 52} Using a combination of hard and soft blocks created a percolating nanostructure within the copolymer film. The hard blocks conferred stiffness while the soft blocks ensured high extensibility and film formation at room temperature. In addition to phase separation behavior, the T_g of a copolymer can also largely influence its material properties.⁵³⁻⁵⁸ It has recently been shown that monomer choice,⁵⁹ number of blocks^{36, 39, 60} and block DP^{36, 39} all significantly affect the T_g of a block copolymer. It is particularly important to consider the glass transition temperature (T_g) of the

copolymer to ensure that film formation occurs at room temperature on the removal of solvent.

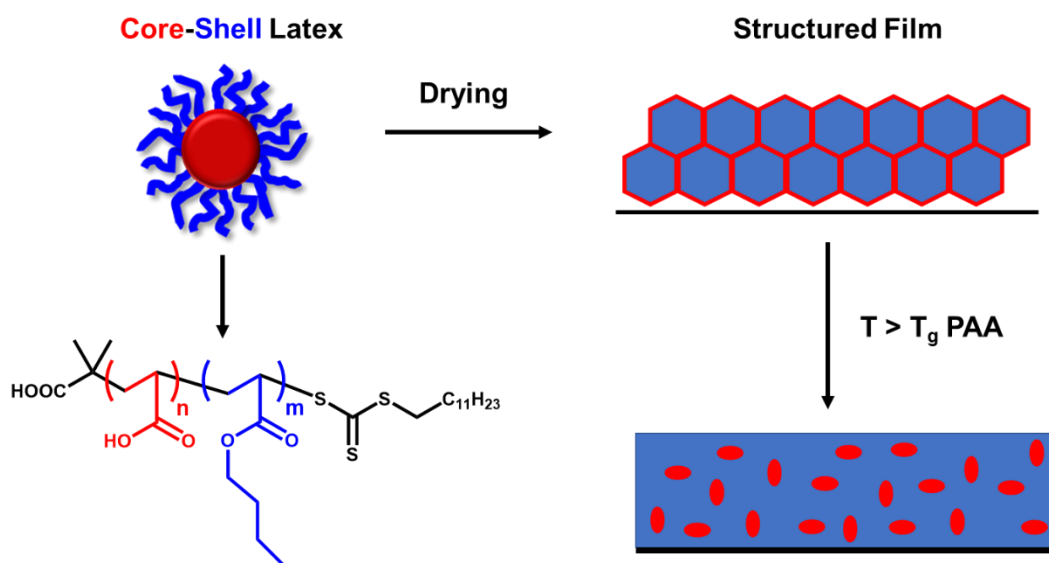


Figure 5.2 Schematic representation of the waterborne PAA-PBA core-shell latex synthesized *via* RAFT aqueous emulsion polymerization and the nanostructured film generated upon drying. Reproduced from Reference.⁵¹

Block copolymers composed of MAA, BzMA and BMA have been reported in Chapter 4 of this Thesis.⁶¹ These monomers were chosen to provide a model system for the transfer of RAFT aqueous emulsion polymerization from laboratory-scale syntheses to a high-throughput protocol. However, they are unsuitable for the synthesis of film-forming block copolymer compositions because none of the three corresponding homopolymers (i.e. PMAA, PBzMA, PBMA) has a T_g below ambient temperature. In this Chapter, the synthesis of diblock, triblock and tetrablock copolymer nanoparticles *via* RAFT aqueous emulsion polymerization directly in water is described. These block copolymer nanoparticles consist of a very high T_g PMAA stabilizer block ($T_g = 228\text{ }^\circ\text{C}$)⁶² and a core composed of alternating blocks of PBzMA and poly(hexyl methacrylate) (PHxMA). For the target tetrablock copolymers, two high T_g PBzMA blocks ($T_g = 54\text{ }^\circ\text{C}$)⁶² are separated by a low T_g PHxMA_y block ($T_g = -5\text{ }^\circ\text{C}$).⁶² The PBzMA blocks have a fixed DP of 100, while the PHxMA block DP is systematically varied from 200 to 800. This is expected to produce a range of film formation behavior.

5.2. Experimental

Benzyl methacrylate (BzMA, 96%), hexyl methacrylate (HxMA, 99%), butyl methacrylate (BMA, 99%), 4,4'-azobis(4-cyanovaleric acid) (ACVA, $\geq 98\%$), benzyl bromide, caesium carbonate and THF (HPLC, $\geq 99.9\%$) were purchased from Sigma-Aldrich (UK) and used as received. The same PMAA₅₆ macro-CTA reported in Chapter 4 was also used for all syntheses in this Chapter.⁶¹ The *d*₈-tetrahydrofuran used for ¹H NMR studies was purchased from Goss Scientific Instruments Ltd. (Cheshire, UK). All other solvents were purchased from Sigma-Aldrich (UK) or VWR Chemicals (UK) and used as received. Deionized water was used in all experiments.

5.2.1. Preparation of poly(methacrylic acid) (PMAA) macro-CTA agent

The same PMAA₅₆-TTC macro-CTA reported in Chapter 4 was also used for all syntheses in this Chapter.

5.2.2. Synthesis of precursor PMAA₅₆-PzMA₁₀₀ diblock copolymer nanoparticles *via* RAFT aqueous emulsion polymerization

A typical protocol for the synthesis of PMAA₅₆-PBzMA₁₀₀ nanoparticles was as follows. PMAA₅₆ macro-CTA (2.93 g, 0.57 mmol), ACVA (3.2 mg; 0.11 mmol, CTA/initiator molar ratio = 5.0) and water (38.88 g, 25% w/w) were weighed into a 100 mL round-bottomed flask. The solution pH was adjusted to pH 5 using 1 M NaOH, followed by addition of BzMA monomer (10.00 g, 0.06 mol; target DP = 100). A magnetic flea was added and the flask was sealed using a rubber septum. The reaction solution was then purged under N₂ for 20 min before placing the flask in a pre-heated water bath at 70 °C for 120 min. The flask was then removed from the water bath and its contents exposed to air to quench the BzMA polymerization.

5.2.3. Synthesis of PMAA₅₆-PBzMA₁₀₀-PHxMA_y triblock copolymer nanoparticles *via* seeded RAFT aqueous emulsion polymerization

A typical protocol for the synthesis of PMAA₅₆-PBzMA₁₀₀-PHxMA₈₀₀ nanoparticles was as follows. Precursor PMAA₅₆-PBzMA₁₀₀ diblock copolymer dispersion (25% w/w, 5.0 g, 0.05 mmol), ACVA (3.1 mg; 0.01 mmol, CTA/initiator molar ratio = 5.0), HxMA (7.47 g, 0.04 mol; target DP = 800) and water (7.47 g, 34% w/w) were weighed into a 50 mL round-bottomed flask. A magnetic flea was added and the flask was sealed using a rubber septum. The reaction solution was then purged under N₂ for 20 min before placing the flask in a pre-heated water bath at 70 °C for 18 h. The

flask was then removed from the water bath and its contents exposed to air to quench the HxMA polymerization. In order to synthesize triblock copolymers with a range of PHxMA DPs ($y = 200$ to 800), the mass of the precursor diblock copolymer dispersion was kept constant (5.0 g) and the amount of HxMA monomer was increased from 1.87 g to 7.47 g, alongside the mass of water to keep the copolymer concentration constant.

5.2.4. Synthesis of PMAA₅₆-PBzMA₁₀₀-PHxMA_y-PBzMA₁₀₀ tetrablock copolymer nanoparticles via seeded RAFT aqueous emulsion polymerization

A typical protocol for the synthesis of PMAA₅₆-PBzMA₁₀₀-PHxMA₂₀₀-PBzMA₁₀₀ nanoparticles was as follows. Precursor PMAA₅₆-PBzMA₁₀₀-PHxMA₂₀₀ triblock copolymer dispersion (5.0 g, 0.03 mol), ACVA (1.7 mg; 0.002 mmol, CTA/initiator molar ratio = 5.0), BzMA (0.19 g, 0.001 mol; target DP = 100) and water (0.36 g, 35% w/w) were weighed into a 50 mL round-bottomed flask. A magnetic flea was added and the reaction flask was sealed using a rubber septum. The reaction solution was then purged under N₂ for 20 min before placing the flask in a pre-heated water bath at 70 °C for 18 h. The flask was then removed from the water bath and its contents exposed to air to quench the BzMA polymerization.

5.2.5. ¹H NMR Spectroscopy

All ¹H NMR spectra were recorded using a 400 MHz Bruker Advance-400 spectrometer using *d*₈-THF as the solvent.

5.2.6. Dynamic Light Scattering (DLS)

Aqueous copolymer dispersions (0.20% w/w) in disposable plastic cuvettes were analyzed at 20 °C using a Malvern Zetasizer NanoZS instrument. Scattered light was detected at 173° and intensity-average hydrodynamic diameters were calculated using the Stokes-Einstein equation. Data were averaged over three consecutive measurements, comprising a minimum of ten runs per measurement.

5.2.7. Differential Scanning Calorimetry (DSC)

Aqueous copolymer dispersions were dried overnight on a glass slide. An accurate mass (between 6 and 10 mg) was weighed into an aluminium pan and sealed with a lid. Each copolymer sample was heated under N₂ in a TA instruments Q2000 model calorimeter. Thermograms were acquired at a rate of 10 °C per min from -80 °C to

220 °C, 3 cycles were performed. The mid-point T_g values are reported. These analyses were conducted by members of the analytical department at AkzoNobel (Slough).

5.2.8. Transmission Electron Microscopy (TEM)

Each sample was prepared by depositing a 10 μ L (0.20% w/w) droplet of a 0.1% w/w aqueous copolymer dispersion onto a glow-discharged carbon-coated copper grid for 20 seconds. The grid was then stained with 10 μ L uranyl formate solution (0.75% w/w) for 10 seconds and carefully dried using a vacuum hose. TEM images were recorded using a Philips CM100 instrument operating at 100 kV and equipped with a Gatan 1 k CCD camera. ImageJ software was used to determine mean nanoparticle diameters from TEM images, with at least 100 nanoparticles being analyzed per sample.

5.2.9. Methylation of copolymers for GPC Analysis

Prior to THF GPC analysis, all copolymers were modified by methylation of the carboxylic acid groups in the PMAA block.⁶³ Excess trimethylsilyldiazomethane was added dropwise to a solution of copolymer (20 mg) in THF (2.0 mL), until the yellow color persisted. This reaction solution was then stirred overnight until all THF had evaporated. Degrees of methylation of the PMAA block were determined by ¹H NMR spectroscopy.

5.2.10. Benzylation of copolymers for GPC Analysis

Prior to DMF GPC analysis, all copolymers were modified by benzylation of the carboxylic acid groups in the PMAA block. Benzyl bromide and caesium carbonate (~ 1.1 mol eq. w.r.t. MAA content) was added to a solution of copolymer (0.25 g) in DMF (5 mL). This reaction solution was then stirred overnight, before filtration to remove the salt byproduct. Degrees of benzylation of the PMAA block were determined by ¹H NMR spectroscopy.

5.2.11. Gel Permeation Chromatography (GPC)

THF GPC was used to determine copolymer molecular weights and dispersities. The GPC set-up consisted of an Agilent 1260 Infinity II GPC/SEC system operating at 30 °C and fitted with an autosampler and two 5 μ M Mixed-C columns connected to a refractive index detector. The mobile phase was HPLC-grade THF at a flow rate of 1.0 mL min⁻¹. Molecular weights were calculated using a series of near-monodisperse PMMA calibration standards. All copolymers were modified by methylation prior to THF GPC analysis.

DMF GPC at 60 °C was used to determine the molecular weights and dispersities of the PMAA-based copolymers modified by benzylation. The GPC set-up consisted of a Varian 290-LC pump injection module connected to two Polymer Laboratories PL gel 5 µm Mixed-C columns connected in series and a Varian 390-LC multi-detector suite (refractive index detector). The mobile phase was HPLC-grade DMF containing 10 mM LiBr at a flow rate of 1.0 mL min⁻¹. Molecular weights were calculated with respect to a series of near-monodisperse PMMA standards.

5.2.12. Casting and annealing of films

Copolymer films were prepared at room temperature (20 °C) by dropping ~ 0.1 mL of aqueous copolymer dispersion (at 20, 30 or 35% w/w copolymer concentration) onto a mica disk and allowing to dry overnight. Copolymer films cast at 20 °C were annealed by heating for 2 h at 200 °C in a vacuum oven.

5.2.13. Optical transmission measurements on copolymer films

Visible absorption spectra were recorded between 200 and 800 nm using a Shimadzu UV-1800 spectrophotometer. Copolymer films were analyzed by mounting the mica disk on the sample holder inside the spectrophotometer. The mean thickness of each film was measured using a micrometer screw gauge. Reported thickness values are an average of three measurements taken in different locations across the film.

5.2.14. SAXS analysis

SAX patterns were collected using Xuess 2.0 laboratory beamline (Xenocs, Sassenage, France) equipped with FOX 3D multilayered X-ray mirror and two sets of scatterless slits for beam collimation, two hybrid pixel area detectors (Pilatus 1M for SAXD and Pilatus 100k for WAXD, Dectris, Baden-Dattwil, Switzerland) and a liquid gallium MetalJet X-ray source (Excillum, Kista, Sweden), wavelength $\lambda = 1.341 \text{ \AA}$. SAXS patterns were recorded using a sample-to-detector distance of 5.121 m (calibrated using silver behenate standard). The block copolymer films were dried onto mica discs which were then mounted onto an array stage for data collection. Two-dimensional SAXS patterns were azimuthally integrated, normalized and background-subtracted using the Foxtrot software package (supplied with the laboratory beamline) to obtain 1D scattering profiles. All SAXS analyses were performed by Dr. James Jennings, a postdoctoral researcher in the Armes group.

5.3. Results and Discussion

5.3.1. Synthesis of diblock, triblock and tetrablock copolymers

As discussed earlier, the glass transition temperature (T_g) corresponds to the temperature at which a synthetic polymer transitions from a glass to a rubber state.^{64, 65} The T_g of a polymer depends on its molecular weight, as described by the Flory-Fox Equation (see Equation 2.1).^{66, 67} The relationship between T_g and molecular weight is shown in Figure 2.22., where the $T_{g,\infty}$ is the maximum glass transition temperature that can be achieved at a theoretically infinite molecular weight.

The overall T_g of a statistical copolymer can be calculated by considering the contribution from each individual comonomer, as outlined by Equation 5.2 (the Fox Equation), where F_n is the weight fraction and T_g^n is the T_g of component n .⁶⁸ Thus, the overall T_g can be tuned by appropriate monomer selection and also by adjusting the relative proportion of each comonomer within the statistical copolymer.

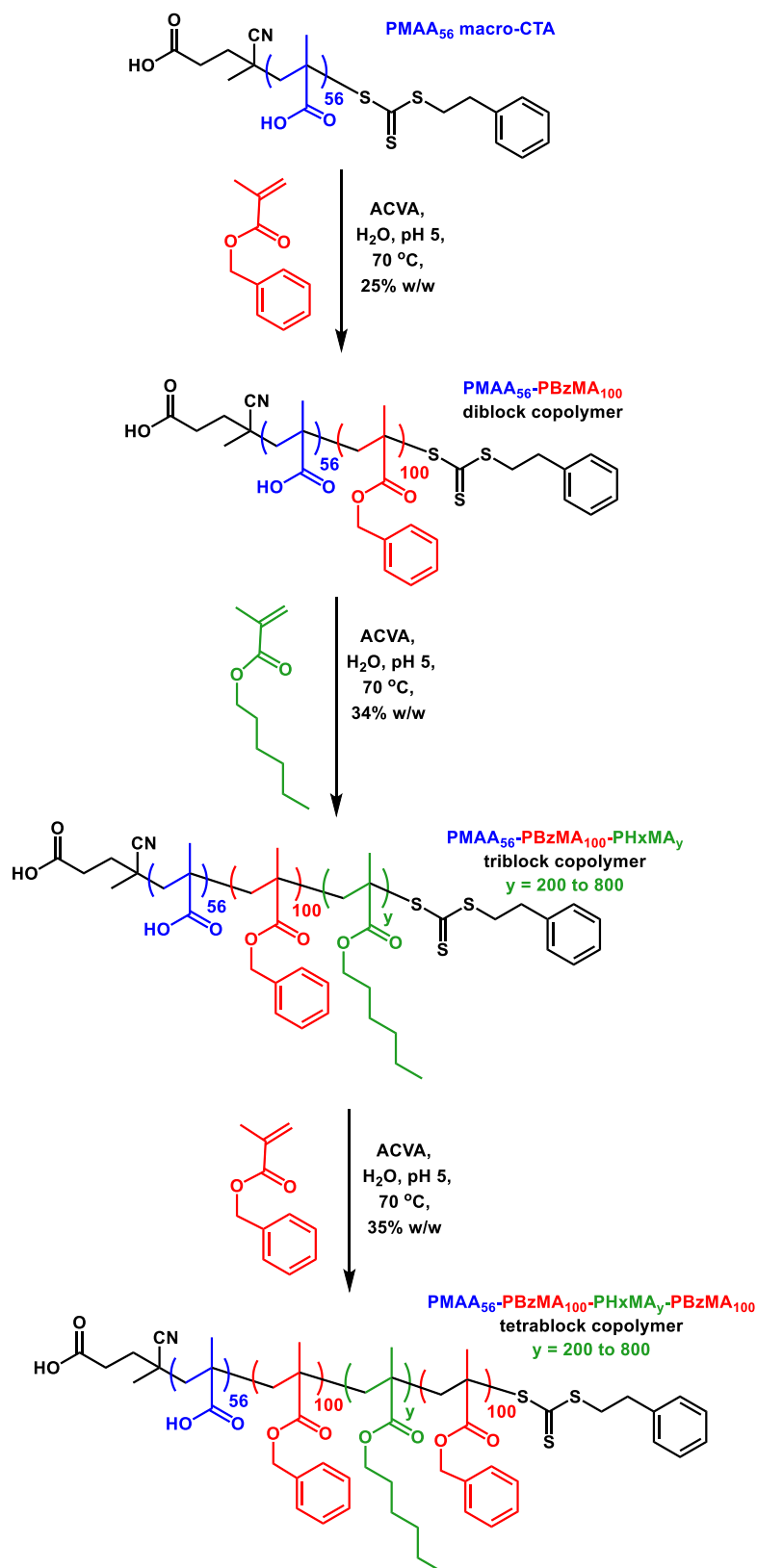
$$\frac{1}{T_g^*} = \frac{F_1}{T_g^1} + \frac{F_2}{T_g^2} + \frac{F_3}{T_g^3} + \dots + \frac{F_n}{T_g^n} \quad 5.2$$

For block copolymers, microphase separation caused by the mutual enthalpic incompatibility between blocks results in the observation of two or more T_g values, corresponding to each core-forming block.⁶⁰ However, the temperature at which the block copolymers forms a film will be influenced by the relative contribution of each block. This temperature is described as the minimum film-forming temperature (MFFT); the lowest temperature at which a latex or emulsion will coalesce to form a thin film on a substrate.⁶⁹ As previously mentioned, PMAA and PBzMA have relatively high T_g values (228 °C and 56 °C, respectively). By introducing a third block with a substantially lower T_g , the MFFT of the block copolymer can be reduced to enable film formation to occur at room temperature. In this study, *n*-hexyl methacrylate (HxMA) was chosen as a suitable methacrylic monomer to ensure a sufficiently low MFFT (PHxMA has a T_g of -5 °C).⁶²

A series of diblock, triblock and tetrablock copolymer nanoparticles were synthesized *via* RAFT aqueous emulsion polymerization, see Scheme 5.1. These block copolymers comprised a PMAA stabilizer block and hydrophobic core-forming blocks of PBzMA and/or PHxMA (namely, PMAA₅₆-PBzMA₁₀₀, PMAA₅₆-PBzMA₁₀₀-PHxMA_y and

PMAA₅₆-PBzMA₁₀₀-PHxMA_y-PBzMA₁₀₀). The DP of the PHxMA block was systematically varied between 200 and 800 in order to determine the block DP required to enable film formation at room temperature and also to investigate the effect of varying PHxMA block DP on film properties. The final PBzMA₁₀₀ block was added to produce a tetrablock copolymer, thus emulating the hard-soft-hard block arrangement found in ABA thermoplastic elastomers that deliver desirable mechanical properties for coatings applications.

To synthesize such block copolymers, the PMAA₅₆ macro-CTA was first chain-extended *via* RAFT aqueous emulsion polymerization of BzMA, targeting a PBzMA DP of 100, see Scheme 5.1. This PISA synthesis was conducted under essentially the same conditions described previously (i.e. 70 °C, using a macro-CTA/ACVA molar ratio of 5.0 and pH 5). However, the copolymer concentration was increased from 20% w/w to 25% w/w, because higher copolymer concentrations are strongly preferred for industrial paints and coatings. These PMAA₅₆-PBzMA₁₀₀ diblock copolymer nanoparticles were then used as a precursor for the seeded RAFT aqueous emulsion polymerization of HxMA at 34% w/w copolymer concentration, see Scheme 5.1. Four PHxMA DPs were targeted to yield a series of PMAA₅₆-PBzMA₁₀₀-PHxMA_y triblock copolymer nanoparticles, where $y = 200, 400, 600$ or 800 . Each of these triblock copolymer nanoparticles was then further reacted with BzMA to give a series of PMAA₅₆-PBzMA₁₀₀-PHxMA_y-PBzMA₁₀₀ tetrablock copolymer nanoparticles at 35% w/w copolymer concentration, see Scheme 5.1. This series of diblock, triblock and tetrablock copolymers was analyzed by ¹H NMR, DLS, TEM, GPC and DSC, see Table 5.1.



Scheme 5.1 Synthesis of PMAA₅₆-PBzMA₁₀₀ diblock copolymer, PMAA₅₆-PBzMA₁₀₀-PHxMA_y triblock copolymer and PMAA₅₆-PBzMA₁₀₀-PHxMA_y-PBzMA₁₀₀ tetrablock copolymer nanoparticles *via* RAFT aqueous emulsion polymerization ($y = 200, 400, 600$ or 800).

Table 5.1 Summary of diblock, triblock and tetrablock copolymer nanoparticles prepared *via* RAFT aqueous emulsion polymerization at 70 °C using a PMAA₅₆ macro-CTA/initiator of 5.0 at pH 5.

Target Composition	Monomer conversion for final block ^a (%)	DLS particle diameter (nm)	DLS particle polydispersity	TEM particle diameter (nm)	M_n^b (g mol ⁻¹)	\bar{D}^b	T_g^c (°C)
PMAA ₅₆ -PBzMA ₁₀₀	>99	42	0.11	26	15,900	3.05	- 69
PMAA ₅₆ -PBzMA ₁₀₀ -PHxMA ₂₀₀	>99	74	0.33	38	36,000	3.46	- 70
PMAA ₅₆ -PBzMA ₁₀₀ -PHxMA ₄₀₀	>99	83	0.27	52	63,500	5.01	2 68
PMAA ₅₆ -PBzMA ₁₀₀ -PHxMA ₆₀₀	>99	78	0.17	53*	70,400	4.70	0 68
PMAA ₅₆ -PBzMA ₁₀₀ -PHxMA ₈₀₀	98	82	0.20	44*	98,800	5.86	-4 63
PMAA ₅₆ -PBzMA ₁₀₀ -PHxMA ₂₀₀ -PBzMA ₁₀₀	>99	72	0.28	56	48,400	4.19	0 69
PMAA ₅₆ -PBzMA ₁₀₀ -PHxMA ₄₀₀ -PBzMA ₁₀₀	>99	86	0.23	52	64,800	4.24	4 71
PMAA ₅₆ -PBzMA ₁₀₀ -PHxMA ₆₀₀ -PBzMA ₁₀₀	99	94	0.26	52	72,900	4.66	3 68
PMAA ₅₆ -PBzMA ₁₀₀ -PHxMA ₈₀₀ -PBzMA ₁₀₀	99	118	0.26	57	67,300	5.75	3 68

^a Conversion determined by ¹H NMR^b GPC data of methylated block copolymers expressed relative to a series of near-monodisperse PMMA calibration standards^c The quoted T_g values refer to mid-point values from the DSC analysis

*These values are not considered to be reliable given that these particles are susceptible to beam damage owing to their low MFFT, see Figure 5.6

Monomer conversions of more than 98% were achieved in all cases, as judged by ^1H NMR studies in d_8 -THF. Representative ^1H NMR spectra are shown in Figure 5.3 for the $\text{PMAA}_{56}\text{-PBzMA}_{100}$ diblock copolymer, $\text{PMAA}_{56}\text{-PBzMA}_{100}\text{-PHxMA}_{800}$ triblock copolymer and $\text{PMAA}_{56}\text{-PBzMA}_{100}\text{-PHxMA}_y\text{-PBzMA}_{100}$ tetrablock copolymer.

THF GPC analysis of the methylated copolymers indicated a progressive increase in molecular weight during the syntheses of each tetrablock copolymer, see Figure 5.4. Unfortunately, the dispersities at each stage of the polymerization are very high ($\mathcal{D} \sim 3.05$ to 5.86). In addition, the blocking efficiency is imperfect, with evidence for unreacted precursor blocks. The best set of data was observed for the shortest PHxMA DP of 200, which afforded the lowest dispersity and highest blocking efficiency. At higher PHxMA DPs, dispersities increase and the blocking efficiency is reduced. These GPC data suggest limited control over the polymerization and suggest premature loss of the RAFT chain-ends. It is likely that the high dispersities of these block copolymers has a significant impact on their microphase separation. This is supported by both theoretical and experimental studies in the literature.⁷⁰⁻⁷²

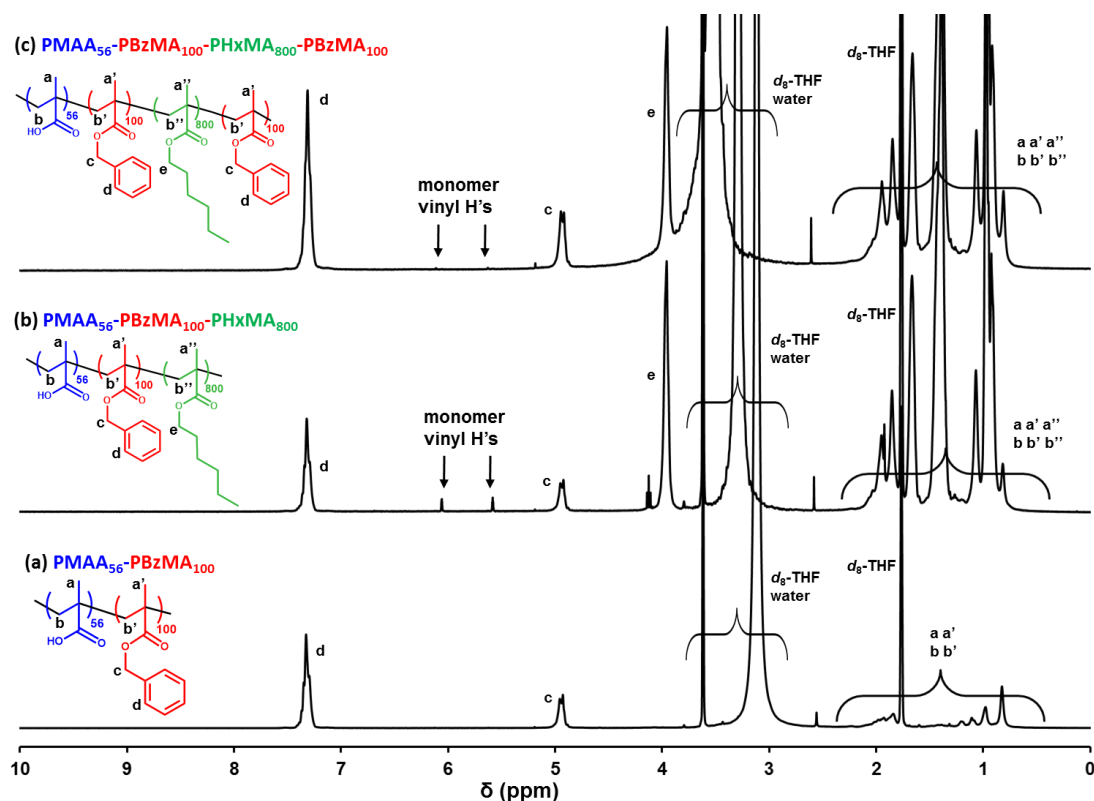


Figure 5.3 ^1H NMR spectra recorded for $\text{PMAA}_{56}\text{-PBzMA}_{100}$ diblock copolymer, $\text{PMAA}_{56}\text{-PBzMA}_{100}\text{-PHxMA}_{800}$ triblock copolymer and $\text{PMAA}_{56}\text{-PBzMA}_{100}\text{-PHxMA}_{800}\text{-PBzMA}_{100}$ tetrablock copolymer all synthesized *via* RAFT aqueous emulsion polymerization. All spectra were recorded in d_8 -THF.

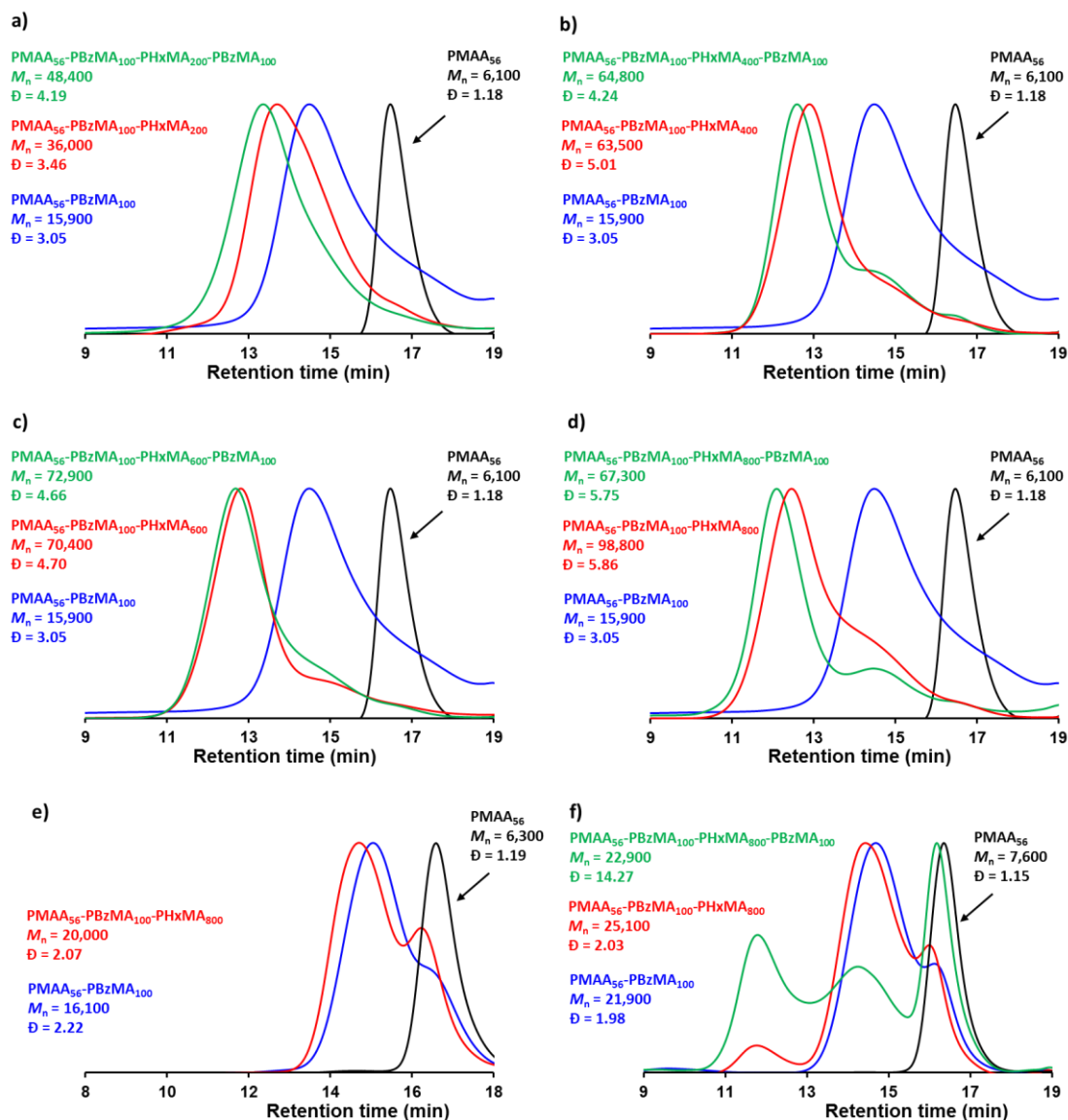
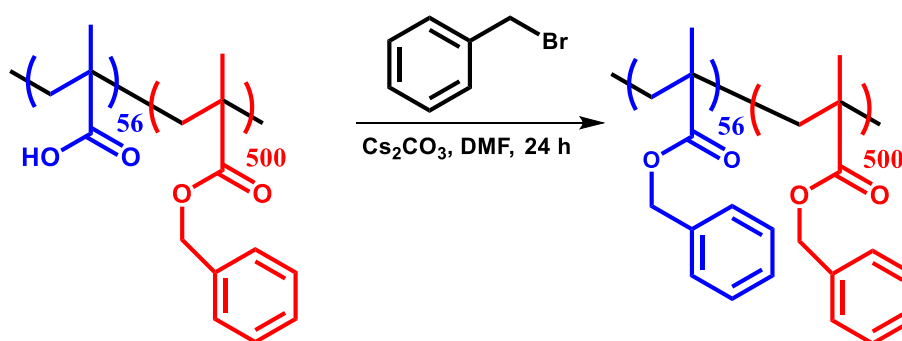


Figure 5.4 (a-d) THF GPC chromatograms recorded for *methylated* PMAA₅₆-PBzMA₁₀₀ diblock copolymer, PMAA₅₆-PBzMA₁₀₀-PHxMA_y triblock copolymer and PMAA₅₆-PBzMA₁₀₀-PHxMA_y-PBzMA₁₀₀ tetrablock copolymer prepared *via* RAFT aqueous emulsion polymerization: (a) *y* = 200, (b) *y* = 400, (c) *y* = 600, (d) *y* = 800. (e) DMF GPC chromatograms recorded for *benzylated* PMAA₅₆-PBzMA₁₀₀ diblock copolymer and PMAA₅₆-PBzMA₁₀₀-PHxMA_y triblock copolymer, where *y* = 800. The PMAA₅₆-PBzMA₁₀₀-PHxMA₈₀₀-PBzMA₁₀₀ tetrablock copolymer was insoluble in DMF. (f) THF GPC chromatograms recorded for *benzylated* PMAA₅₆-PBzMA₁₀₀ diblock copolymer, PMAA₅₆-PBzMA₁₀₀-PHxMA_y triblock copolymer and PMAA₅₆-PBzMA₁₀₀-PHxMA_y-PBzMA₁₀₀ tetrablock copolymer where *y* = 800.

So far in this Thesis, all block copolymers containing a PMAA block have been methylated using trimethylsilyldiazomethane prior to THF GPC analysis.⁶³ This modification converts all the anionic PMAA residues to PMMA, thus preventing any interaction or absorption onto the column. Given the very high dispersities observed for the block copolymers synthesized in this Chapter the diblock, triblock and tetrablock copolymers with a PHxMA DP of 800 were also modified by a benzylation reaction to determine whether the broad MWDs observed are in some way caused by the methylation protocol. This benzylation reaction converts the carboxylic acid group on the PMAA residues to a methyl ester, see Scheme 5.2.⁷³



Scheme 5.2 Reaction scheme for the benzylation of PMAA₅₆-PBzMA₁₀₀ diblock copolymer using benzyl bromide and caesium carbonate.⁷³

The benzylated block copolymers were then analyzed by DMF and THF GPC, see Figure 5.4(e and f). A dramatic reduction in the dispersity can be seen when comparing the benzylated samples to the alkylated samples. THF GPC analysis of the *methylated* PMAA₅₆-PBzMA₁₀₀ diblock copolymer reported a \mathcal{D} of 3.05 and low molecular weight tailing can clearly be seen. In contrast, DMF GPC analysis of the benzylated PMAA₅₆-PBzMA₁₀₀ diblock copolymer reported a \mathcal{D} of 2.22 and THF GPC analysis of the same sample indicated a \mathcal{D} of 1.98. Although these values are still high, they are considerably lower than those recorded for the methylated sample.

A similar reduction in dispersity can be observed for the benzylated triblock copolymer. However, a lower than expected M_n is also observed. In addition, the benzylated tetrablock copolymer is not soluble in DMF and THF GPC analysis indicates a very broad MWD. It is thought that the triblock and tetrablock copolymers were not fully soluble in THF or DMF and that the insoluble chains are removed by

filtration prior to GPC analysis. The samples prepared for GPC analysis (in both solvents) were initially cloudy but went clear after filtration. Analysis by ^1H NMR spectroscopy also indicates that the triblock and tetrablock copolymers are only sparingly soluble in both DMF and THF, see Appendix 7 and 8. This is demonstrated by the absence of integrals corresponding to the PHxMA block.

This sparingly low solubility could account for the observation of a lower than expected M_n for both the triblock copolymer samples. The high molecular weight peak observed in the THF GPC chromatograms of the triblock and tetrablock copolymer could also be an artefact owing to the low solubility of the chains or an indication of free radical polymerization.

DLS analysis of these block copolymer nanoparticles indicates a progressive increase in particle diameter with addition of each subsequent block, see Figure 5.5. A relatively large increase in particle diameter (30 – 40 nm) was observed on chain extension of the diblock copolymer with the third HxMA block. In contrast, a relatively modest increase in particle diameter (0 – 36 nm) was observed on addition of the final BzMA block to obtain the tetrablock copolymer. In each case relatively broad nanoparticle particle size distributions were observed (DLS PDI = 0.17 to 0.33). Subsequent analysis of these nanoparticles by TEM indicated that kinetically-trapped spherical nanoparticles were obtained during the synthesis of each block, see Figure 5.6. Some beam damage to the PMAA₅₆-PBzMA₁₀₀-PHxMA₆₀₀ and PMAA₅₆-PBzMA₁₀₀-PHxMA₈₀₀ triblock copolymer nanoparticles was observed during TEM analysis owing to the low T_g of the HxMA block. Thus, resulting in poorer quality images where the nanoparticles are less well-defined.

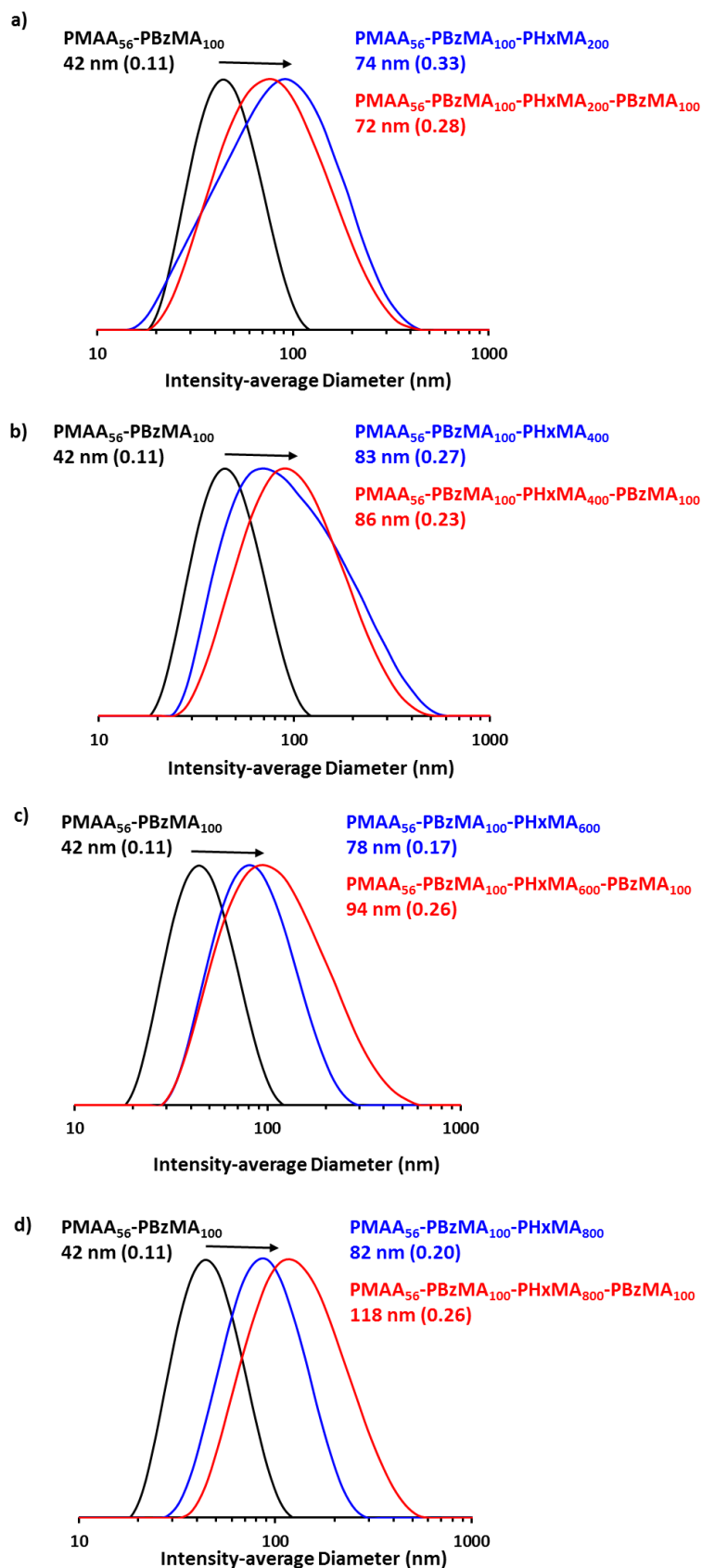


Figure 5.5. DLS particle size distributions showing the increase in particle diameter during the synthesis of PMAA₅₆.PBzMA₁₀₀ diblock copolymer, PMAA₅₆-PBzMA₁₀₀-PHxMA_y triblock copolymer and PMAA₅₆-PBzMA₁₀₀-PHxMA_y-PBzMA₁₀₀ tetrablock copolymer for (a) $y = 200$, (b) $y = 400$, (c) $y = 600$ and (d) $y = 800$.

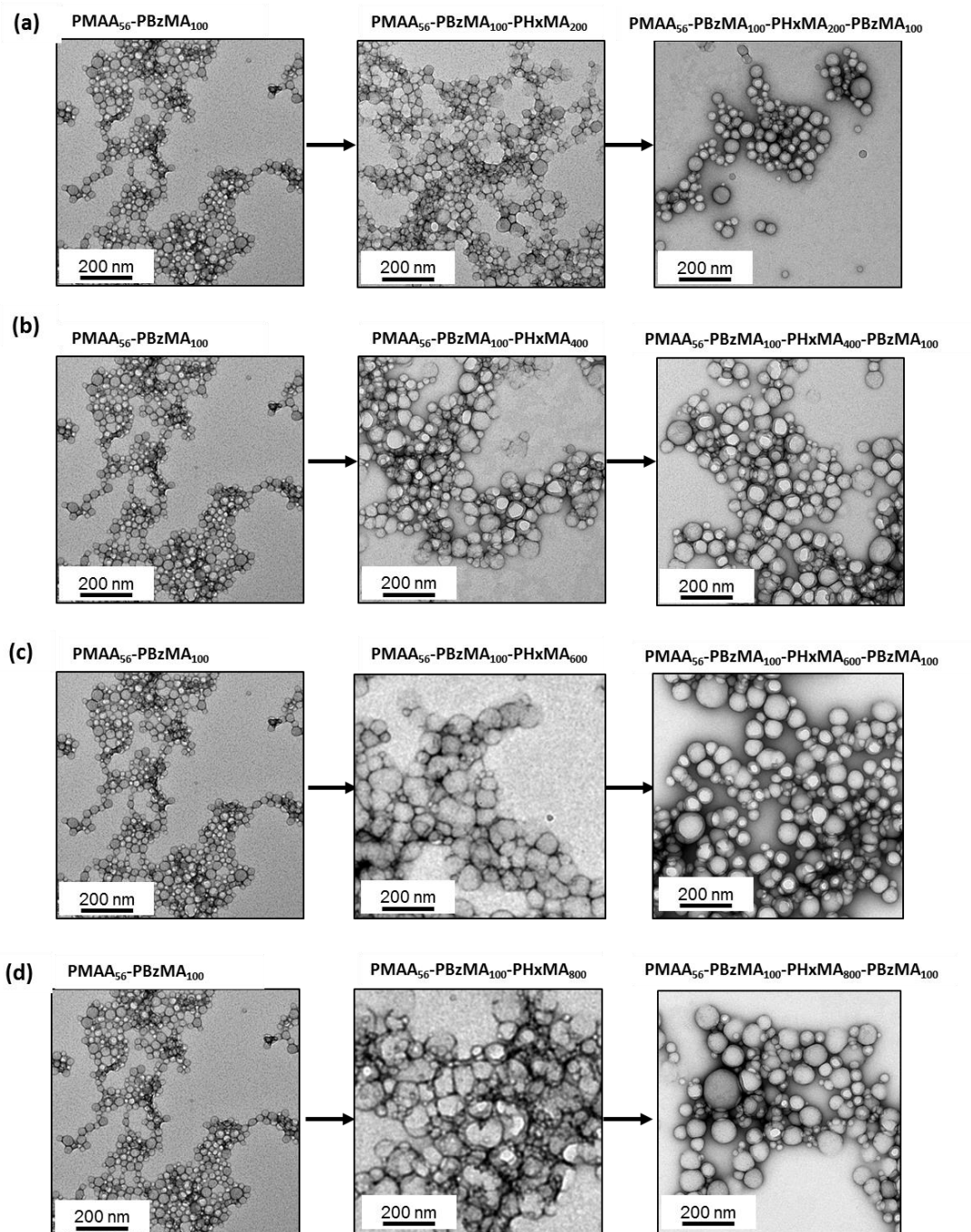


Figure 5.6. Representative TEM images obtained for PMAA₅₆-PBzMA₁₀₀ diblock copolymer precursor nanoparticles, PMAA₅₆-PBzMA₁₀₀-PHxMA_y triblock copolymer nanoparticles and PMAA₅₆-PBzMA₁₀₀-PHxMA_y-PBzMA₁₀₀ tetrablock copolymer nanoparticles, where (a) $y = 200$, (b) $y = 400$, (c) $y = 600$ or (d) $y = 800$. It is worth noting that the PMAA₅₆-PBzMA₁₀₀-PHxMA_y triblock copolymer nanoparticles shown in (c) and (d) are susceptible to beam damage owing to their low MFFT.

5.3.2. Analysis of block copolymer films

The dried copolymers were analyzed by DSC to determine T_g values, see Table 5.1. The DSC data showed that, for a PHxMA DP above 200, phase separation between the PHxMA and PBzMA blocks occurs. This is demonstrated by the observation of two T_g features, relating to each of the hydrophobic blocks of the block copolymer, see Figure 5.7. The DSC trace of the PMAA₅₆-PBzMA₁₀₀ diblock copolymer only showed one single T_g value of 69 °C. This is slightly higher than the literature value for PBzMA (56 °C), see Figure 5.7b. However, the increase in T_g could be caused by the high T_g of the PMAA block (228 °C). DSC analysis of the PMAA₅₆-PBzMA₁₀₀-PHxMA₂₀₀ triblock copolymer also showed only one single T_g value at 70 °C. This demonstrates that a PHxMA DP of 200 is not sufficient to cause microphase separation between the PHxMA and the PBzMA blocks. As the PHxMA DP was increased further ($y = 400, 600$ or 800) two distinct T_g values were observed in each case indicative of phase separation, see Figure 5.7c. The two T_g values corresponded to the T_g of each block, PHxMA $T_g = 2$ to -4 °C and PBzMA $T_g = 68$ to 63 °C. DSC analysis of the PMAA₅₆-PBzMA₁₀₀-PHxMA _{y} -PBzMA₁₀₀ reported two distinct T_g values in each case ($y = 200$ to 800) indicative of phase separation, see Figure 5.7. The T_g values corresponding to the PBzMA block are very similar to those reported for the corresponding triblock copolymers ($T_g = 68$ to 71 °C), whereas the T_g values corresponding to the PHxMA block are marginally higher ($T_g = 0$ to 4 °C). Again this increase in T_g could be attributed to the presence of the other higher T_g blocks.

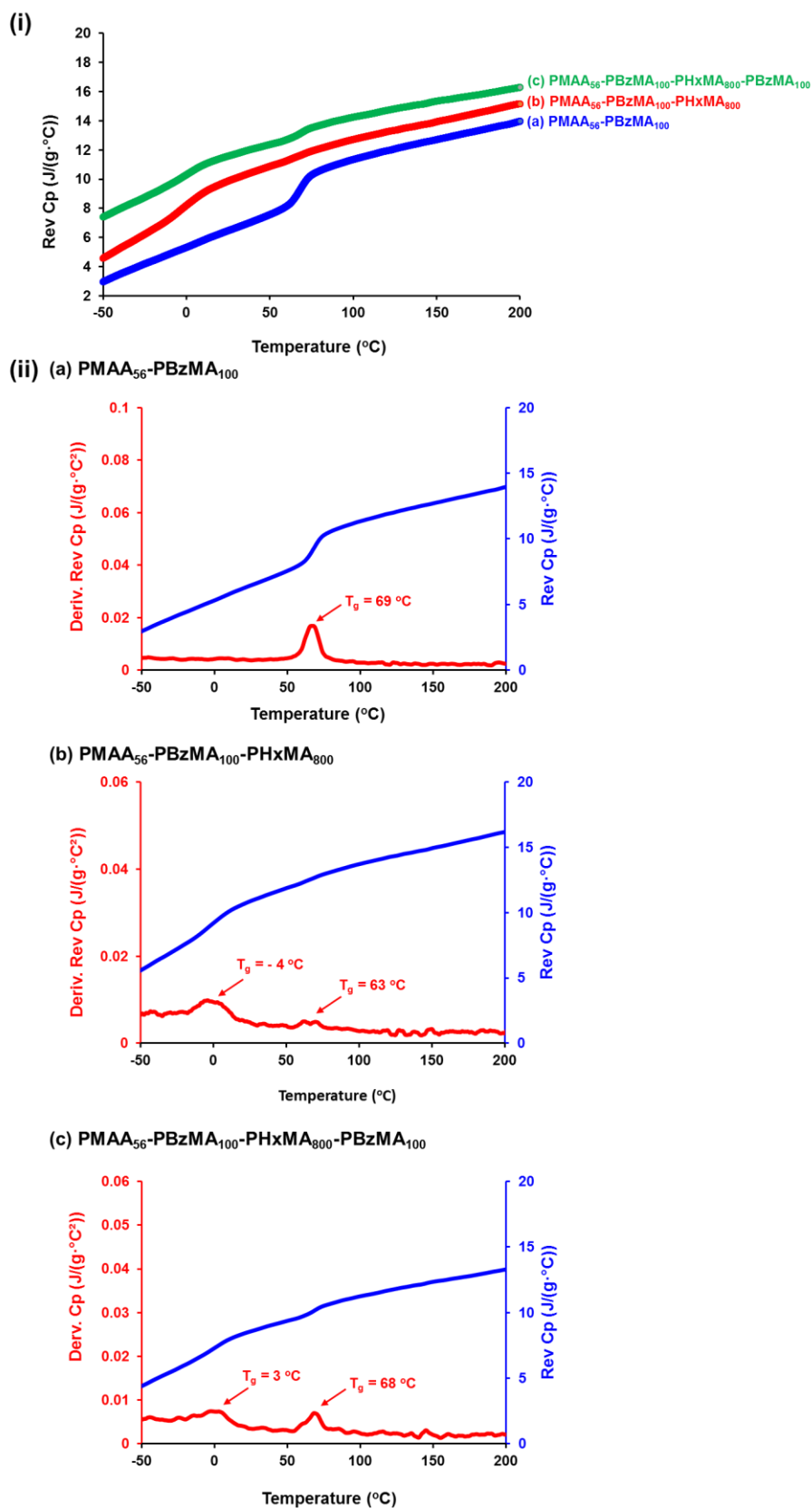


Figure 5.7 (i) Heat capacity (Cp) with temperature for a series of block copolymers (a) PMAA₅₆-PBzMA₁₀₀, (b) PMAA₅₆-PBzMA₁₀₀-PHxMA₈₀₀ and (c) PMAA₅₆-PBzMA₁₀₀-PHxMA₈₀₀-PBzMA₁₀₀ and (ii) individual plots for each block copolymer (a-c) showing Cp and the first derivation of the Cp with temperature.

To assess the film-forming ability of the diblock, triblock and tetrablock copolymers, ~ 0.1 mL of the copolymer dispersion was pipetted onto a mica disc and allowed to dry overnight at room temperature. The mean film thickness was measured to be between 120 and 200 μm , see Table 5.2. As expected, the PMAA₅₆-PBzMA₁₀₀ diblock copolymer did not form a film owing to the high T_g of both blocks. For the series of PMAA₅₆-PBzMA₁₀₀-PHxMA_y triblock copolymers, a PHxMA DP of 200 was insufficient to enable film formation at room temperature. However, at PHxMA DPs of 400 to 800, transparent films were formed at room temperature. Chain extension of the PMAA₅₆-PBzMA₁₀₀-PHxMA_y triblock copolymers with BzMA to give PMAA₅₆-PBzMA₁₀₀-PHxMA_y-PBzMA₁₀₀ copolymers reduces the effect of the PHxMA block, resulting in cracked films at room temperature. Digital photographs of transparent copolymer films are shown in Figure 5.8.

The transparency of the block copolymer films was assessed by visible absorption spectroscopy, see Figure 5.8. The optical transmittance was measured across the visible spectrum from 400 to 800 nm. The transmittance at 600 and 400 nm are reported in Table 5.2. These results demonstrate that the PMAA₅₆-PBzMA₁₀₀-PHxMA_y triblock copolymers ($y = 400, 600, 800$) are highly transparent ($> 95\%$ at 600 nm and $> 92\%$ at 400 nm). However, on addition of the fourth block to give PMAA₅₆-PBzMA₁₀₀-PHxMA_y-PBzMA₁₀₀ tetrablock copolymers ($y = 600, 800$) the film transparency is reduced ($> 89\%$ at 600 nm and $> 82\%$ at 400 nm). The film transmittance was also remeasured after thermal annealing at 200 °C in a vacuum oven for 2 h. The film transmittance decreased after annealing, from $> 95\%$ to $< 94\%$ at 600 nm and (more significantly) from $> 90\%$ to $< 65\%$ at 400 nm. The transmittance of the annealed PMAA₅₆-PBzMA₁₀₀-PHxMA₆₀₀-PBzMA₁₀₀ tetrablock copolymer film was also reduced but by a considerably smaller amount (from 90% to 87%) whereas, the PMAA₅₆-PBzMA₁₀₀-PHxMA₈₀₀-PBzMA₁₀₀ tetrablock copolymer film transmittance was comparable before and after annealing (89-90%).

Table 5.2 Film thickness, transmittance and domain spacing (d) for block copolymer films formed at room temperature and for the same films after annealing at 200 °C in a vacuum oven. Transmittance (%) is reported at both 600 and 400 nm.

Target Composition	Film thickness (μm) ^a		Transmittance (%) ^b				Domain spacing (nm) ^c	
	Film at room temperature	Film annealed at 200 °C	Film at room temperature		Film annealed at 200 °C		Film at room temperature	Film annealed at 200 °C
			600 nm	400 nm	600 nm	400 nm		
PMAA ₅₆ -PBzMA ₁₀₀ -PHxMA ₄₀₀	190	160	95	90	94	65	97	143
PMAA ₅₆ -PBzMA ₁₀₀ -PHxMA ₆₀₀	180	160	95	90	86	63	140	160
PMAA ₅₆ -PBzMA ₁₀₀ -PHxMA ₈₀₀	160	150	100	92	94	65	135	165
PMAA ₅₆ -PBzMA ₁₀₀ -PHxMA ₆₀₀ -PBzMA ₁₀₀	200	180	90	82	87	71	60	177
PMAA ₅₆ -PBzMA ₁₀₀ -PHxMA ₈₀₀ -PBzMA ₁₀₀	120	100	89	84	90	82	66	190

^aMeasured using a micrometer screw gauge^bMeasured by visible absorpotion spectroscopy^cDomain spacing calculated from SAXS analysis using the Bragg equation (Equation 5.3)

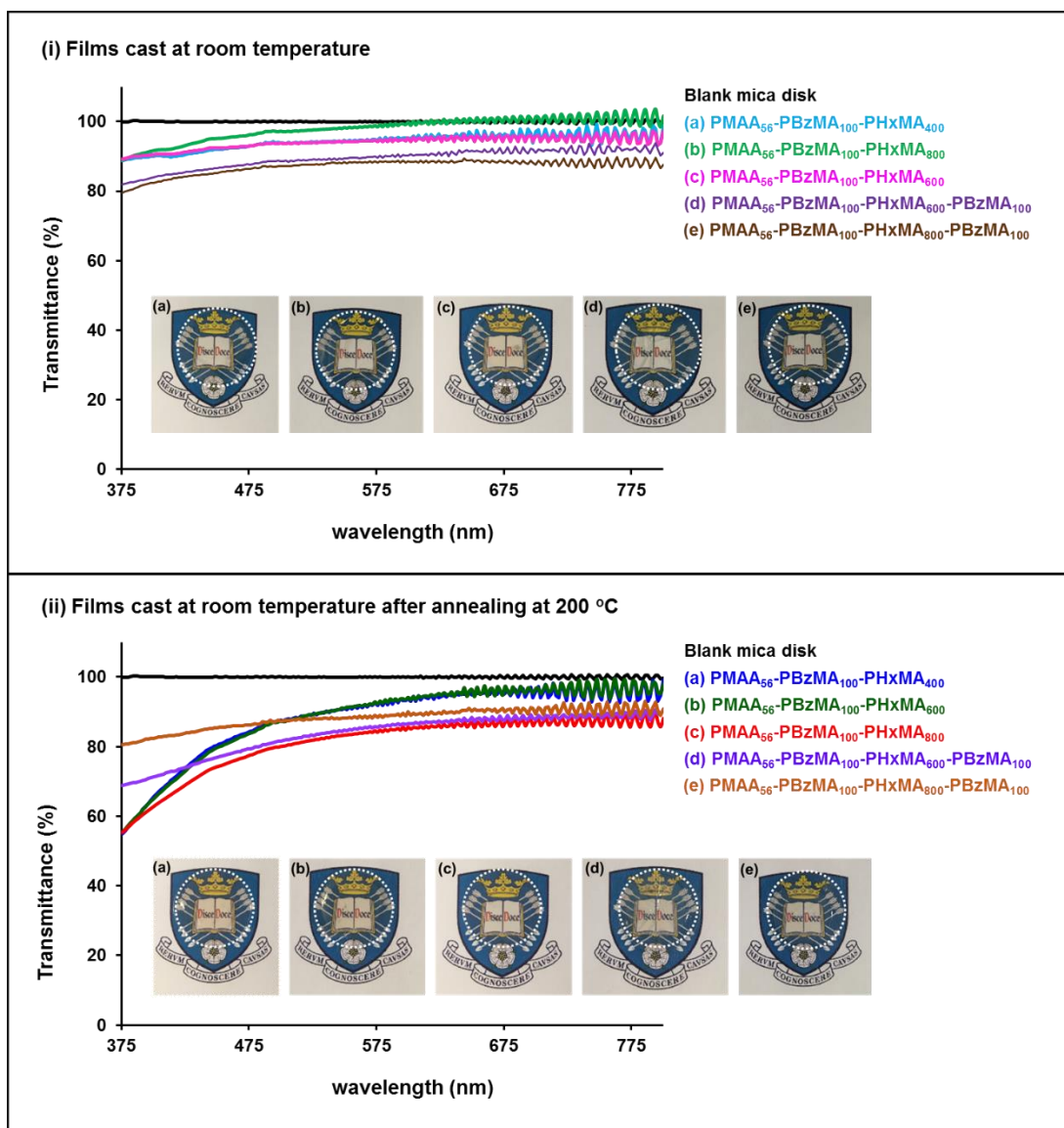


Figure 5.8 Transmittance vs. wavelength plots for (i) films cast at room temperature and (ii) films cast at room temperature and then annealed at 200 °C. Digital photographs showing the transparency of each film when placed over a University of Sheffield logo (white dotted circles indicate positioning of mica disks). The copolymer films are formed from (a) PMAA₅₆-PBzMA₁₀₀-PHxMA₄₀₀, (b) PMAA₅₆-PBzMA₁₀₀-PHxMA₆₀₀, (c) PMAA₅₆-PBzMA₁₀₀-PHxMA₈₀₀, (d) PMAA₅₆-PBzMA₁₀₀-PHxMA₆₀₀-PBzMA₁₀₀ and (e) PMAA₅₆-PBzMA₁₀₀-PHxMA₈₀₀-PBzMA₁₀₀ diblock copolymer nanoparticles.

The films cast at room temperature and the same films annealed at 200 °C were both analyzed by SAXS. In each case, only one main peak was observed, indicating the absence of long-range order. This suggests that all of the multiblock copolymers are in a disordered state. However, as two distinct T_g values are observed in each case, the block copolymers are likely to be microscopically inhomogeneous. Similar observations have been reported previously for multiblock copolymers.⁶⁰ A series of multiblock copolymers composed of alternating poly(ethylene glycol methyl ether acrylate) and poly(*tert*-butyl acrylate) were synthesized *via* RAFT polymerization. SAXS analysis of these multiblock copolymers indicated that, with the exception of diblock copolymers, all copolymers were in a “disordered inhomogeneous state”.⁶⁰

In each scattering pattern, just one peak was observed, see Figure 5.9. The domain spacing was calculated using the Bragg equation, see Equation 5.3 (where q is the scattering vector corresponding to the local maximum).

$$d = \frac{2\pi}{q} \quad 5.3$$

No real trend in domain spacing size is observed for the triblock copolymer films cast at room temperature. Surprisingly the domain spacing for the tetrablock copolymer films is smaller than that observed for the triblock copolymer films. In contrast, after the annealing at 200 °C an increase in domain spacing (from 143 to 165 nm) is observed for the triblock copolymer films as the PHxMA DP was increased from 400 to 800. The domain spacing increases further for the tetrablock copolymers and is larger (190 nm) for PHxMA DP 800 relative to that for the PHxMA DP 600 (177 nm). Heating the copolymer films to above the T_g of each block (200 °C) gives the polymer chains sufficient mobility to rearrange into their most stable thermodynamic conformation.²⁷ The increase in domain spacing observed after annealing the copolymer films correlates with an increase in light scattering, thus reducing the transmittance.

As previously mentioned, dispersity has been shown to have a significant impact on the microphase separation of block copolymers.⁷⁰⁻⁷² More specifically, it has been reported that domain spacing increases with increasing dispersity.⁷⁰ Therefore, the relatively high dispersities obtained for this PISA formulation are likely to be responsible for the large domain spacings indicated by SAXS.

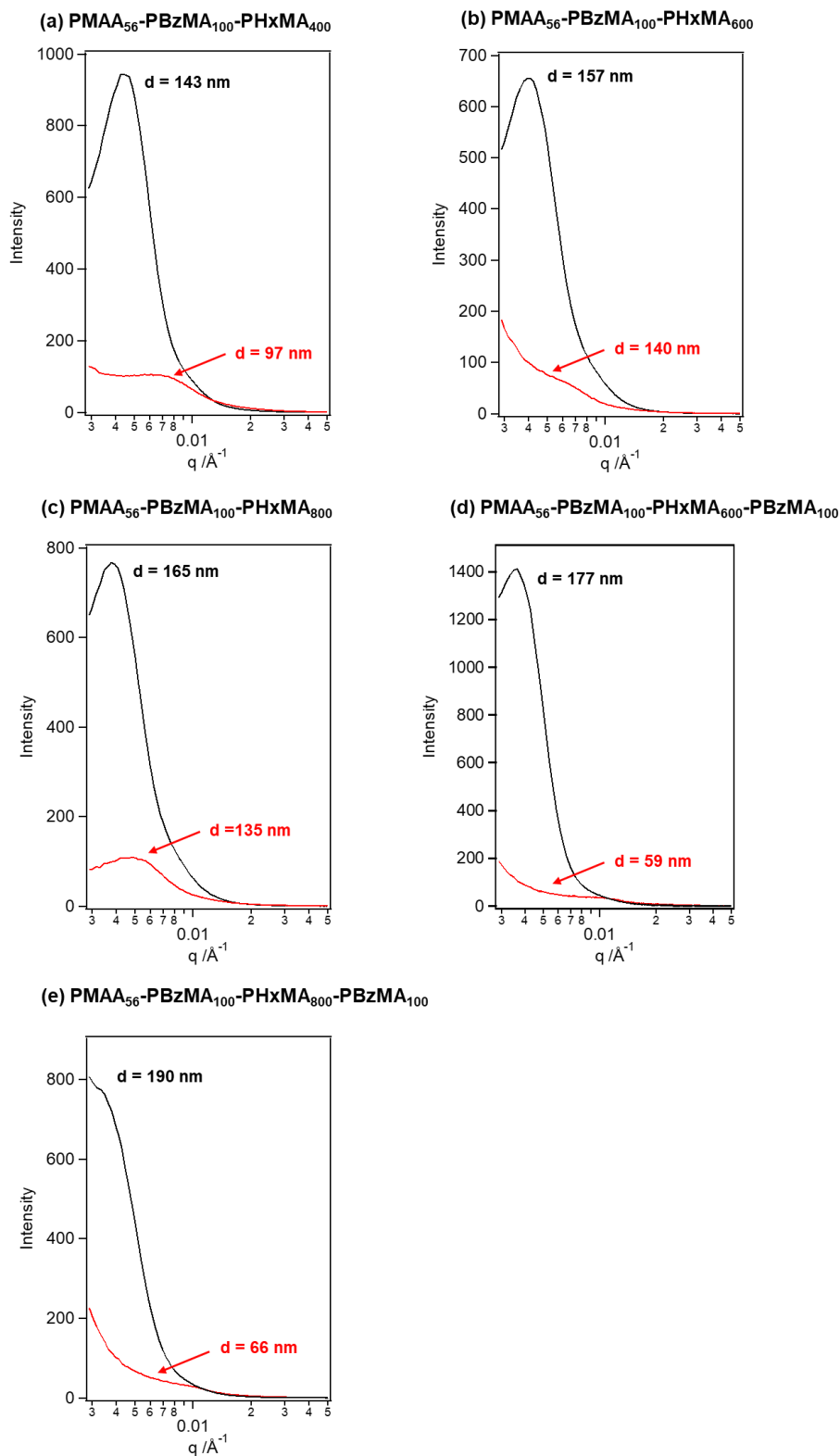


Figure 5.9 Small-angle x-ray scattering (SAXS) data obtained for three PMAA₅₆-PBzMA₁₀₀-PHxMA_y triblock copolymers where $y = 400, 600$ or 800 (a – c) and two PMAA₅₆-PBzMA₁₀₀-PHxMA_y-PBzMA₁₀₀ tetrablock copolymers where $y = 600$ or 800 (d – e). The red traces correspond to copolymer films cast at room temperature and the black traces correspond to the same films after annealing in a vacuum oven for 2 h at 200 °C. The domain spacing (d) was calculated using the Bragg equation ($d = 2\pi/q$, where q is the scattering vector corresponding to the local maximum).

5.4. Conclusions

A series of multiblock copolymer nanoparticles was synthesized *via* RAFT aqueous emulsion polymerization. A PMAA₅₆ macro-CTA was selected owing to its high T_g (228 °C)⁶² and its ability to electrosterically stabilize nanoparticles synthesized by PISA. This macro-CTA was chain-extended with alternating blocks of BzMA (54 °C)⁶² and HxMA (-5 °C)⁶² to give diblock, triblock and tetrablock copolymers. The target PBzMA DP was fixed at 100 and the target PHxMA DP was varied between 200 and 800. PHxMA was selected to reduce the T_g relative to the previous PBzMA/PBMA formulation reported in Chapter 4 hence and enable film formation at ambient temperature.⁶¹ In principle, the tetrablock copolymer should produce elastomeric coatings. The ability to produce such tough, resilient films using a zero-VOC, wholly aqueous formulation is a potentially decisive advantage compared to solvent-borne elastomeric coatings reported in the literature.^{1,2}

Each multiblock copolymer was prepared with a high degree of conversion (> 98%) for each block and the formation of spherical nanoparticles was confirmed by DLS and TEM analysis. However, GPC analysis of the methylated block copolymers indicated relatively high dispersities ($\mathcal{D} = 3.05$ to 5.75) and poor blocking efficiencies suggesting a poor level of control and the presence of some dead chains. The diblock, triblock and tetrablock copolymers with a PHxMA DP of 800 were also modified by a benzylation reaction to determine whether the broad MWDs observed are in some way caused by the methylation protocol. A decrease in dispersity was observed by both DMF and THF GPC analysis of the benzylated diblock copolymer ($\mathcal{D} = 2.22$ and 1.98 respectively). However, the benzylated triblock and tetrablock copolymers were only sparingly soluble in both DMF and THF. Any undissolved chains would be removed by filtration during sample preparation. Thus, the GPC analysis conducted may not be representative of the whole sample.

DSC analysis of the triblock and tetrablock copolymers showed that for a PHxMA DP above 200, phase separation between the PHxMA and PBzMA blocks occurs. This is demonstrated by the observation of two T_g features, relating to each of the hydrophobic blocks of the block copolymer. Despite the broad MWDs, the triblock (PHxMA DP = 400 to 800) and tetrablock copolymer (PHxMA DP = 600 or 800) formed highly transparent films at room temperature. Optical transmittance

(at 600 nm) was determined by visible absorption spectroscopy to be > 95% for the triblock copolymer films and > 89% for the tetrablock copolymer films formed at room temperature. However, lower transmittances (< 94% for the triblock copolymer films and < 87 % for the tetrablock copolymer films) were observed after annealing such films at 200 °C in a vacuum oven for 2 h.

SAXS analysis of these multiblock copolymer films indicated local phase separation but an absence of long-range order. There was no observable trend between domain spacing and PHxMA block DP for films cast at room temperature. However, an increase in domain size with PHxMA DP was observed for triblock copolymer films annealed at 200 °C. In addition, the domain size increased further on the addition of a fourth block (PBzMA).

5.5. References

1. A. Marrion, *The Chemistry and Physics of Coatings*, The Royal Society of Chemistry Cambridge, 1994.
2. T. F. L. McKenna, B. Charleux, E. Bourgeat-Lami, F. D'Agosto and M. Lansalot, *Journal of Coatings Technology and Research*, 2014, **11**, 131.
3. C. S. Chern, *Progress in Polymer Science*, 2006, **31**, 443-486.
4. W. D. Harkins, *Journal of the American Chemical Society*, 1947, **69**, 1428-1444.
5. P. A. Lovell and M. S. El-Aasser, *Emulsion Polymerization and Emulsion Polymers*, John Wiley & Sons Ltd, 1997.
6. R. G. Gilbert, *Emulsion Polymerization: A Mechanistic Approach*, Academic Press, London, 1995.
7. A. Gromer, F. Thalmann, P. Hébraud and Y. Holl, *Langmuir*, 2017, **33**, 561-572.
8. C. Heldmann, R. Ivan Cabrera, B. Momper, R. Kuroпка and K. Zimmerschied, *Progress in Organic Coatings*, 1999, **35**, 69-77.
9. L. N. Butler, C. M. Fellows and R. G. Gilbert, *Journal of Applied Polymer Science*, 2004, **92**, 1813-1823.
10. P. J. Feeney, D. H. Napper and R. G. Gilbert, *Macromolecules*, 1987, **20**, 2922-2930.
11. E. Marc and Z. Rudolf, *Macromolecular Chemistry and Physics*, 2004, **205**, 1479-1488.
12. K. Tauer, R. Deckwer, I. Kühn and C. Schellenberg, *Colloid and Polymer Science*, 1999, **277**, 607-626.
13. J. W. Goodwin, J. Hearn, C. C. Ho and R. H. Ottewill, *Colloid and Polymer Science*, 1974, **252**, 464-471.
14. I. Bitá, J. K. W. Yang, Y. S. Jung, C. A. Ross, E. L. Thomas and K. K. Berggren, *Science*, 2008, **321**, 939-943.
15. J. Sun, A. A. Teran, X. Liao, N. P. Balsara and R. N. Zuckermann, *Journal of the American Chemical Society*, 2013, **135**, 14119-14124.
16. C. Park, J. Yoon and E. L. Thomas, *Polymer*, 2003, **44**, 6725-6760.

17. M. Singh, O. Odusanya, G. M. Wilmes, H. B. Eitouni, E. D. Gomez, A. J. Patel, V. L. Chen, M. J. Park, P. Fragouli, H. Iatrou, N. Hadjichristidis, D. Cookson and N. P. Balsara, *Macromolecules*, 2007, **40**, 4578-4585.
18. H. Erothu, J. Kolomanska, P. Johnston, S. Schumann, D. Deribew, D. T. W. Toolan, A. Gregori, C. Dagron-Lartigau, G. Portale, W. Bras, T. Arnold, A. Distler, R. C. Hiorns, P. Mokarian-Tabari, T. W. Collins, J. R. Howse and P. D. Topham, *Macromolecules*, 2015, **48**, 2107-2117.
19. D. T. W. Toolan, A. J. Parnell, P. D. Topham and J. R. Howse, *Journal of Materials Chemistry A*, 2013, **1**, 3587-3592.
20. J. M. G. Swann and P. D. Topham, *Polymers*, 2010, **2**, 454-469.
21. F. S. Bates and G. H. Fredrickson, *Physics Today*, 1999, **52**, 32-38.
22. L. Leibler, *Macromolecules*, 1980, **13**, 1602-1617.
23. S. Lecommandoux, M. Lazzari and G. Liu, *Block Copolymers in Nanoscience*, Wiley-VCH, Weinheim, 2008.
24. Y. Mai and A. Eisenberg, *Chemical Society Reviews*, 2012, **41**, 5969-5985.
25. F. S. Bates, *Science*, 1991, **251**, 898-905.
26. A. K. Khandpur, S. Förster and F. S. Bates, *Macromolecules*, 1995, **28**, 8796-8806.
27. P. D. Topham, University of Sheffield, 2005.
28. L. Wu, E. W. Cochran, T. P. Lodge and F. S. Bates, *Macromolecules*, 2004, **37**, 3360-3368.
29. C. M. Koo, M. A. Hillmyer and F. S. Bates, *Macromolecules*, 2006, **39**, 667-677.
30. M. Karbarz, Z. Stojek, T. K. Georgiou and C. S. Patrickios, *Polymer*, 2006, **47**, 5182-5186.
31. P. D. Topham, J. R. Howse, O. O. Mykhaylyk, S. P. Armes, R. A. L. Jones and A. J. Ryan, *Macromolecules*, 2006, **39**, 5573-5576.
32. L. Wang, P. D. Topham, O. O. Mykhaylyk, J. R. Howse, W. Bras, R. A. L. Jones and A. J. Ryan, *Advanced Materials*, 2007, **19**, 3544-3548.
33. M. W. Matsen, *Macromolecules*, 2012, **45**, 2161-2165.
34. M. W. Matsen and M. Schick, *Macromolecules*, 1994, **27**, 7157-7163.
35. I. Lee, T. R. Panthani and F. S. Bates, *Macromolecules*, 2013, **46**, 7387-7398.
36. I. Lee and F. S. Bates, *Macromolecules*, 2013, **46**, 4529-4539.
37. T. R. Panthani and F. S. Bates, *Macromolecules*, 2015, **48**, 4529-4540.
38. M. T. Martello, D. K. Schneiderman and M. A. Hillmyer, *ACS Sustainable Chemistry & Engineering*, 2014, **2**, 2519-2526.
39. R. J. Spontak and S. D. Smith, *Journal of Polymer Science Part B: Polymer Physics*, 2001, **39**, 947-955.
40. A. S. Lee, V. Butun, M. Vamvakaki, S. P. Armes, J. A. Pople and A. P. Gast, *Macromolecules*, 2002, **35**, 8540.
41. Y. Matsumiya, H. Watanabe, A. Takano and Y. Takahashi, *Macromolecules*, 2013, **46**, 2681-2695.
42. C. Y. Ryu, J. Ruokolainen, G. H. Fredrickson and E. J. Kramer, *Macromolecules*, 2001, **35**, 2157-2166.
43. T. J. Hermel, S. F. Hahn, K. A. Chaffin, W. W. Gerberich and F. S. Bates, *Macromolecules*, 2003, **36**, 2190-2193.
44. C. Y. Ryu, J. Ruokolainen, G. H. Fredrickson, E. J. Kramer and S. F. Hahn, *Macromolecules*, 2002, **35**, 2157-2166.
45. D. Cohn and A. H. Salomon, *Biomaterials*, 2005, **26**, 2297-2305.

46. J.-O. Lin, W. Chen, Z. Shen and J. Ling, *Macromolecules*, 2013, **46**, 7769-7776.
47. B. Arman, A. S. Reddy and G. Arya, *Macromolecules*, 2012, **45**, 3247-3255.
48. V. Khanna, J. Ruokolainen, E. J. Kramer and S. F. Hahn, *Macromolecules*, 2006, **39**, 4480-4492.
49. J. Lesage de la Haye, I. Martin-Fabiani, M. Schulz, J. L. Keddie, F. D'Agosto and M. Lansalot, *Macromolecules*, 2017, **50**, 9315-9328.
50. E. Velasquez, J. Rieger, F. Stoffelbach, F. D'Agosto, M. Lansalot, P.-E. Dufils and J. Vinas, *Polymer*, 2016, **106**, 275-284.
51. M. Chenal, J. Rieger, C. Véchambre, J.-M. Chenal, L. Chazeau, C. Creton and L. Bouteiller, *Macromolecular Rapid Communications*, 2013, **34**, 1524-1529.
52. M. Chenal, C. Véchambre, J.-M. Chenal, L. Chazeau, V. Humblot, L. Bouteiller, C. Creton and J. Rieger, *Polymer*, 2017, **109**, 187-196.
53. R. P. White and J. E. G. Lipson, *Macromolecules*, 2016, **49**, 3987-4007.
54. K. Geng and O. K. C. Tsui, *Macromolecules*, 2016, **49**, 2671-2678.
55. C. N. Walker, J. M. Sarapas, V. Kung, A. L. Hall and G. N. Tew, *ACS Macro Letters*, 2014, **3**, 453-457.
56. C. J. Ellison, M. K. Mundra and J. M. Torkelson, *Macromolecules*, 2005, **38**, 1767-1778.
57. A. C. Boukis, A. Llevot and M. A. R. Meier, *Macromolecular Rapid Communications*, 2016, **37**, 643-649.
58. M. E. Vanderlaan and M. A. Hillmyer, *Macromolecules*, 2016, **49**, 8031-8040.
59. Y. Shi, X. Cao, S. Luo, X. Wang, R. W. Graff, D. Hu, R. Guo and H. Gao, *Macromolecules*, 2016, **49**, 4416-4422.
60. J. Zhang, R. Deubler, M. Hartlieb, L. Martin, J. Tanaka, E. Patyukova, P. D. Topham, F. H. Schacher and S. Perrier, *Macromolecules*, 2017, **50**, 7380-7387.
61. A. A. Cockram, R. D. Bradley, S. A. Lynch, P. C. D. Fleming, N. S. J. Williams, M. W. Murray, S. N. Emmett and S. P. Armes, *Reaction Chemistry & Engineering*, 2018, **3**, 645-657.
62. Thermal Transitions of Homopolymers: Glass Transition & Melting Point, <https://www.sigmaaldrich.com/technical-documents/articles/materials-science/polymer-science/thermal-transitions-of-homopolymers.html>, (accessed 15/10/2018).
63. L. Couvreur, C. Lefay, J. Belleney, B. Charleux, O. Guerret and S. Magnet, *Macromolecules*, 2003, **36**, 8260-8267.
64. P. Atkins and J. d. Paula, *Atkins' Physical Chemistry* Oxford University Press, Oxford, 9th Edition edn., 2010.
65. J. M. G. Cowie, *Polymers: Chemistry & Physics of Modern Materials*, Nelson Thornes, Cheltenham, 2nd edn., 2001.
66. T. G. Fox and P. J. Flory, *Journal of Applied Physics*, 1950, **21**, 581-591.
67. T. G. Fox and P. J. Flory, *Journal of Polymer Science*, 1954, **14**, 315-319.
68. T. G. Fox, *Bulletin of the American Physical Society*, 1956, **1**, 123-132.
69. G. Sewell, *Pigment & Resin Technology*, 1998, **27**, 173-174.
70. N. A. Lynd and M. A. Hillmyer, *Macromolecules*, 2005, **38**, 8803-8810.
71. N. A. Lynd, A. J. Meuler and M. A. Hillmyer, *Progress in Polymer Science*, 2008, **33**, 875-893.
72. D. M. Cooke and A.-C. Shi, *Macromolecules*, 2006, **39**, 6661-6671.
73. J. Clayden, N. Greeves, S. Warren and P. Wothers, *Organic Chemistry*, Oxford University Press, Oxford, 2001.

Chapter Six

6. Conclusions and Future Work

The synthesis of nanoparticles directly in water (over organic solvents or alcohols) is desirable for a diverse range of applications including low-VOC coatings,¹⁻³ and for biomedical applications.⁴ It is well known that PISA conducted by RAFT aqueous dispersion polymerization leads to the synthesis of a range of diblock copolymer morphologies such as spheres, worms and vesicles.⁵⁻⁷ Such morphologies can be reproducibly targeted by systematically varying the stabilizer block DP, the core-forming block DP and the copolymer concentration.⁶ In contrast, PISA conducted by RAFT aqueous emulsion polymerization is often limited to the synthesis of kinetically-trapped spherical nanoparticles. The key difference between these two formulations is the aqueous solubility of the monomer; RAFT aqueous dispersion polymerization involves the polymerization of a *water-miscible* monomer, whereas RAFT aqueous emulsion polymerization involves the polymerization of a *water-immiscible* monomer (with a relatively low aqueous solubility).

In this Thesis a water-soluble anionic PMAA_x macro-CTA has been chain-extended with a range of core-forming monomers *via* RAFT aqueous polymerization to assess the effect of varying the aqueous solubility of the core-forming monomer on the ability to access higher order morphologies *via* aqueous PISA. Polymerization of HBMA (~20 g dm⁻³ at 70 °C) led to the synthesis of a novel non-spherical ‘monkey nut’ morphology, thus breaking the restrictive paradigm of kinetically-trapped spheres. It is believed that HBMA has sufficiently high aqueous solubility to enable its diffusion into the growing nanoparticle cores on the time scale of the polymerization. This provides greater solvation and hence increased mobility of the growing core-forming chains located within the nanoparticle cores. This in turn aids sphere-sphere fusion, which is a prerequisite for the formation of the ‘monkey nut’ morphology.

Following publication of this initial finding in 2017⁸, the effect of varying the aqueous monomer solubility has been validated by further unpublished work within the Armes group. More specifically, a non-ionic PGMA macro-CTA has been chain-extended with two other monomers exhibiting a similar aqueous solubility to that of HBMA (~20 g dm⁻³). Firstly, glycidyl methacrylate (GlyMA) was investigated as a core-forming monomer. Initial results, suggested that only spherical nanoparticles could be obtained when using a PGMA₄₅ macro-CTA.⁹ However, further study has confirmed that a worm phase could be obtained *via* a convenient three-step one-pot protocol.¹⁰ By utilizing a shorter PGMA₂₅ macro-CTA and targeting a composition of

PGMA₂₅-PGlyMA₄₅ at 15% w/w copolymer concentration, the synthesis of epoxy-functionalized diblock copolymer worms was achieved. Such worms can be derivatized with 4-amino-TEMPO to give nitroxide-functionalized diblock copolymer worms, which could offer potential applications for charge storage and transport.¹¹⁻¹³

More recently, the RAFT aqueous emulsion polymerization of 2-methoxyethyl methacrylate (MOEMA) using a PGMA₂₉ macro-CTA was studied.¹⁴ This PISA formulation enabled the full range of morphologies to be reproducibly targeted by varying the target PMOEMA DP from 35 to 110 and the copolymer concentration from 10 to 30% w/w. The evolution in copolymer morphology during the synthesis of PGMA₂₉-PMOEMA₇₀ vesicles was also studied by *in situ* SAXS using a bespoke stirrable reaction cell. A manuscript describing this work is currently in preparation.¹⁵ There is also some evidence to suggest that PGMA₂₉-PMOEMA_y nanoparticles could exhibit stimulus-responsive behavior. In order for diblock copolymer nanoparticles to be stimulus-responsive the stabilizer block and/or core-forming block volume must change, thus triggering a morphological transition. This change in block volume can occur either by solvent entering the core of the nanoparticles or by end-group ionization.⁷ Nanoparticles synthesized *via* RAFT aqueous emulsion polymerization typically possess highly hydrophobic cores, so such nanoparticles are not normally stimulus-responsive.^{7, 16} Thus, these subsequent experiments have further highlighted the importance of aqueous monomer solubility when targeting higher order morphologies *via* PISA. Another important parameter to consider is the T_g of the core-forming block. For high T_g blocks, chain mobility within the nanoparticle cores will be restricted, which may hinder the evolution of morphology from spheres to worms to vesicles. In principle, this evolution in morphology should be more likely for lower T_g blocks based on acrylates.

PMAA was originally chosen as the stabilizer block for this work owing to its anionic character and high glass transition temperature, which are attractive properties for potential applications in paints and coatings. Although such anionic macro-CTAs are well-known to confer good electrosteric stabilization, electrostatic repulsion between neighboring PMAA chains is likely to hinder the sphere-sphere fusion required for the formation of higher-order morphologies. In addition, as the reaction pH (5) is very close to the pK_a of the PMAA (pK_a PMAA₅₆ macro-CTA = 5.97) and the ‘monkey nut’ morphology was only observed over a small PHBMA DP range ($y = 150$ to 155),

slight variations in the pH of the reaction solution may also affect whether this morphology is observed or not. In hindsight, it would have perhaps been better to utilize a non-ionic macro-CTA such as PGMA or PEO eliminate the polyelectrolytic character that is known to favor kinetically-trapped spheres.¹⁷

The second issue with using PMAA as the macro-CTA is that it requires derivatization prior to GPC analysis. The anionic MAA residues can interact with or adsorb onto the GPC column, thus disrupting the size exclusion mechanism and adversely affecting the molecular weight and dispersity data. To enable GPC analysis of the block copolymers synthesized in this Thesis, all PMAA-based block copolymers were subjected to methylation *via* reaction with excess trimethylsilyldiazomethane, thus converting PMAA to PMMA.¹⁸ GPC analysis of methylated PMAA_x-PBzMA_y diblock copolymers synthesized *via* RAFT alcoholic dispersion polymerization has been previously reported and low dispersities were observed ($\mathcal{D} \leq 1.26$).^{19, 20} GPC analysis of methylated block copolymers prepared by RAFT aqueous emulsion polymerization in this Thesis yielded higher than expected dispersities ($\mathcal{D} \leq 1.32$). More specifically, for PMAA_x-PBzMA_y diblock copolymers dispersities of 1.32 to 1.89 were obtained which are significantly higher than those achieved by RAFT aqueous dispersion polymerization synthesized for comparison ($1.28 \leq \mathcal{D} \leq 1.33$). Additionally, methylation of block copolymers containing other core-forming blocks based on HPMA, HBMA, TFEMA or BMA also resulted in higher than expected dispersities ($1.56 \leq \mathcal{D} \leq 3.33$). These results suggest that certain monomers may be incompatible with the methylation protocol, leading to artificially high dispersities. Problems in the methylation of PHPMA-based block copolymer have been observed by previous group members.²¹ All methylated block copolymers were analyzed by ¹H NMR spectroscopy. However, calculation of the degree of methylation proved to be difficult. Not-least owing to the overlap of the THF and methyl ester peaks, see Appendix 9 to 14. It is therefore possible that the degree of methylation was not quantitative. If this is indeed the case, MAA residues would still be present which could account for the broad MWDs observed.

In addition, PMAA₅₆-PHBMA_y diblock copolymers synthesized using the as-received HBMA monomer were not soluble in THF and thus could not be analyzed by GPC. This was originally attributed to high levels of dimethacrylate impurity in the ‘technical grade’ HBMA monomer, PMAA₅₆-PHBMA_y diblock copolymers prepared

using a purified batch of HBMA monomer were THF-soluble and could be analyzed by GPC. However, analogous PGMA₅₀-PHBMA_y diblock copolymers prepared utilizing the as-received HBMA monomer could be analyzed by GPC. This suggests that cross-linking is more likely caused by the methylation reaction than by dimethacrylate impurities. In addition, subsequent work on the PGMA-PHBMA system within the Armes group has shown that spheres, worms and vesicles can be obtained. A phase diagram was created by chain-extending a PGMA₄₁ macro-CTA with HBMA *via* RAFT aqueous emulsion polymerization and varying both the PHBMA DP (between 10 and 120) and the copolymer concentration (between 5 and 20% w/w).²²

In an effort to better understand the reasons for the broad MWDs reported in this Thesis, selected copolymers were analyzed by different methods. Firstly, some block copolymers were analyzed using a THF eluent containing 1 to 4% glacial acetic acid, see Appendix 15 and 16. The addition of acetic acid to the GPC eluent ensured that all MAA residues were in their protonated (non-ionic) state and thus should not interact with the GPC column. This analysis technique is frequently used by the sponsor company of this PhD project, AkzoNobel, to analyze MAA (or AA) based statistical polymers, as the use of trimethylsilyl diazomethane is not considered appropriate in an industrial context. In Chapter 4, all copolymers synthesized using the high-throughput protocol were analyzed by GPC at AkzoNobel using a THF eluent containing 4% v/v acetic acid. THF GPC analysis of the laboratory-scale methylated copolymers indicated broader MWDs relative to the high-throughput samples. There are three possible explanations for these higher dispersities. Firstly, the high-throughput protocol might afford more control over the polymerization. Secondly, the methylation artificially broadens the MWD. Thirdly, the GPC instrument used to analyze the high-throughput samples at AkzoNobel performs better than the GPC instrument at Sheffield. The THF plus acetic acid protocol was also used to analyze the PMAA₅₆-PBzMA₁₀₀ diblock, PMAA₅₆-PBzMA₁₀₀-PHxMA₈₀₀ triblock and PMAA₅₆-PBzMA₁₀₀-PHxMA₈₀₀-PBzMA₁₀₀ tetrablock copolymers. In each case the dispersities were lower than those reported for the corresponding methylated copolymers, see Appendices 15 and 16. This suggests that the methylation protocol artificially broadens the MWD.

A second method of chemical derivatization was also investigated. Instead of methylating the block copolymers, selected copolymers were modified *via* benzylation (Appendices 7 to 15 and Appendix 17). The PMAA₅₆ macro-CTA, PMAA₅₆-PBzMA₁₀₀ diblock, PMAA₅₆-PBzMA₁₀₀-PHxMA₈₀₀ triblock and PMAA₅₆-PBzMA₁₀₀-PHxMA₈₀₀-PBzMA₁₀₀ tetrablock copolymers were modified by reaction with excess benzyl bromide in DMF and analyzed by both DMF and THF GPC, see Figure 5.4. Analysis of the benzylated PMAA₅₆ macro-CTA reported very similar results to those obtained for the methylated macro-CTA. For the diblock and triblock copolymers, a reduction in dispersity was observed relative to the corresponding methylated copolymers analyzed by THF GPC. However, a lower than expected M_n is also observed. Additionally, the benzylated PMAA₅₆-PBzMA₁₀₀-PHxMA₈₀₀-PBzMA₁₀₀ tetrablock was insoluble in DMF and only sparingly soluble in THF. The removal of undissolved chains by filtration prior to GPC analysis would make the GPC analysis not representative of the whole sample. The low solubility of the block copolymers in both THF and DMF also prevents the degree of benzylation from being calculated by ¹H NMR spectroscopy, Appendix 7 and 8.

The dramatic reduction in dispersity observed on analysis of the benzylated diblock copolymer suggests that methylation artificially broadens the MWD. This hypothesis was supported by DMF GPC analyses of other PMAA-based diblock copolymers; PMAA₅₆-PHPMA₁₀₀, PMAA₅₆-PMMA₄₀₀, PMAA₅₆-PBMA₁₀₀ and PMAA₅₆-PTFEMA₁₀₀. In all cases, comparable or lower dispersities were reported by DMF GPC analysis of the benzylated copolymers in relation to THF GPC analysis of the methylated copolymers, see Appendix 15 and 17.

With the benefit of hindsight, it would have been advisable to synthesize analogous block copolymers utilizing a PGMA macro-CTA alongside those prepared using the PMAA macro-CTA for direct comparison. This would have provided a clearer understanding of the effect of the anionic charge density on the PMAA chains and also enabled the cause of the high dispersities to be more clearly established.

The high-throughput experiments reported in this Thesis provide the basis for further high-throughput screening of RAFT-mediated PISA formulations, which is likely to be required for commercialization of this promising technology.²³ This could be achieved by using the Chemspeed A100 automated synthesizer to further explore the

design space. By systematically varying the monomer choice, the DP of each block, the number of blocks and the copolymer concentration, the relationship between the copolymer compositions and desired physical properties (e.g. hardness, flexibility, impact resistance, adhesion) could be established. Utilizing the high-throughput approach would enable this work to be conducted more efficiently and faster than serial laboratory experiments.

Following the high-throughput studies conducted at AkzoNobel, it was shown that replacing the PBMA block in these formulations with a lower T_g PHxMA block enabled film formation to be achieved at room temperature. So far, only the effect of varying the PHxMA DP has been studied. There are many other parameters that could be investigated further to produce high-quality block copolymer films. Firstly, the PBzMA DP could be varied or alternative core-forming monomers could be explored such as 2-ethylhexyl methacrylate. As mentioned earlier, the PMAA macro-CTA could be replaced with a PGMA macro-CTA. PGMA has a lower T_g than PMAA and would also enable easier GPC analysis, without the need for chemical derivatization. Optimization studies could also be conducted in order to minimize the dispersities of the block copolymers. Modification of this protocol to develop a one-pot formulation would also be highly advantageous, particularly from an industrial viewpoint. In addition, evaluating all acrylic block copolymer formulations would increase the number of potential low T_g monomers available to aid film formation and microphase separation at room temperature.

Further analysis of the block copolymer films could also be conducted. Ideally, optical transmittance studies should be repeated on films of comparable thickness as this parameter also influences the transmittance.²⁴ Atomic force microscopy could also be used to assess the surface morphology of the phase-separated films to determine the extent of particle coalescence. Mechanical testing could also be conducted to probe the hardness, flexibility, impact resistance, adhesion of these new block copolymer films.² Additionally, SAXS and TEM analysis could be conducted on the wet particle dispersions to look for evidence of internal microphase separation within the nanoparticles.

6.1. References

1. Z. Qiao, T. Qiu, W. Liu, L. Zhang, J. Tu, L. Guo and X. Li, *Polymer Chemistry*, 2017, **8**, 3013-3021.
2. A. Marrion, *The Chemistry and Physics of Coatings*, The Royal Society of Chemistry Cambridge, 1994.
3. J. Lesage de la Haye, I. Martin-Fabiani, M. Schulz, J. L. Keddie, F. D'Agosto and M. Lansalot, *Macromolecules*, 2017, **50**, 9315-9328.
4. S. Y. Khor, J. F. Quinn, M. R. Whittaker, N. P. Truong and T. P. Davis, *Macromolecular Rapid Communications*, 2018, **ASAP article**.
5. A. Blanazs, J. Madsen, G. Battaglia, A. J. Ryan and S. P. Armes, *Journal of the American Chemical Society*, 2011, **133**, 16581-16587.
6. A. Blanazs, A. J. Ryan and S. P. Armes, *Macromolecules*, 2012, **45**, 5099-5107.
7. N. J. Warren and S. P. Armes, *Journal of the American Chemical Society*, 2014, **136**, 10174-10185.
8. A. A. Cockram, T. J. Neal, M. J. Derry, O. O. Mykhaylyk, N. S. J. Williams, M. W. Murray, S. N. Emmett and S. P. Armes, *Macromolecules*, 2017, **50**, 796-802.
9. F. L. Hatton, J. R. Lovett and S. P. Armes, *Polymer Chemistry*, 2017, **8**, 4856-4868.
10. F. L. Hatton, A. M. Park, Y. Zhang, G. D. Fuchs, C. K. Ober and S. P. Armes, *Polymer Chemistry*, 2018, submitted for publication.
11. K. Oyaizu and H. Nishide, *Advanced Materials*, 2009, **21**, 2339-2344.
12. K.-A. Hansen and J. P. Blinco, *Polymer Chemistry*, 2018, **9**, 1479-1516.
13. J. Lutkenhaus, *Science*, 2018, **359**, 1334.
14. E. Brotherton, University of Sheffield, 2018.
15. E. E. Brotherton, F. L. Hatton, A. A. Cockram, M. J. Derry, P. D. Topham, O. O. Mykhaylyk and S. P. Armes, *manuscript in preparation*, 2018.
16. S. L. Canning, G. N. Smith and S. P. Armes, *Macromolecules*, 2016, **49**, 1985-2001.
17. M. Semsarilar, V. Ladmiral, A. Blanazs and S. P. Armes, *Langmuir*, 2012, **28**, 914-922.
18. L. Couvreur, C. Lefay, J. Belleney, B. Charleux, O. Guerret and S. Magnet, *Macromolecules*, 2003, **36**, 8260-8267.
19. M. Semsarilar, V. Ladmiral, A. Blanazs and S. P. Armes, *Polymer Chemistry*, 2014, **5**, 3466-3475.
20. M. Semsarilar, E. R. Jones, A. Blanazs and S. P. Armes, *Advanced Materials*, 2012, **24**, 3378-3382.
21. A. Hanisch and S. P. Armes, unpublished work.
22. S. Hunter, unpublished work.
23. A. A. Cockram, R. D. Bradley, S. A. Lynch, P. C. D. Fleming, N. S. J. Williams, M. W. Murray, S. N. Emmett and S. P. Armes, *Reaction Chemistry & Engineering*, 2018, **3**, 645-657.
24. A. Schmid, P. Scherl and S. P. Armes, *Macromolecules*, 2009, **42**, 3721-3728.

Chapter Seven

7. Appendices

Appendix 1. Calculation used to determine the degree of ionization of the PMAA₅₄-DB and PMAA₅₆-TTC macro-CTAs under the reaction conditions (pH 5).

For a weak acid:



Consider PMAA_x macro-CTA as a weak acid:



The dissociation constant (k_a) can be calculated from the pK_a

$$k_a = 10^{-pK_a}$$

K_a is relative to the concentration of each species:

$$k_a = \frac{[H^+][A^-]}{[HA]}$$

The $[H^+]$ can be calculated from the pH value:

$$[H^+] = 10^{-pH}$$

For a monoprotic acid:

$$[H^+] = [A^-]$$

The $[HA]$ can be calculated by rearranging the equation for k_a :

$$[HA] = \frac{[H^+][A^-]}{k_a}$$

Once we have determine $[H^+]$ and $[HA]$ we can be calculated the percentage dissociation:

$$\% \text{ dissociation} = \frac{[H^+]}{[HA]} \times 100$$

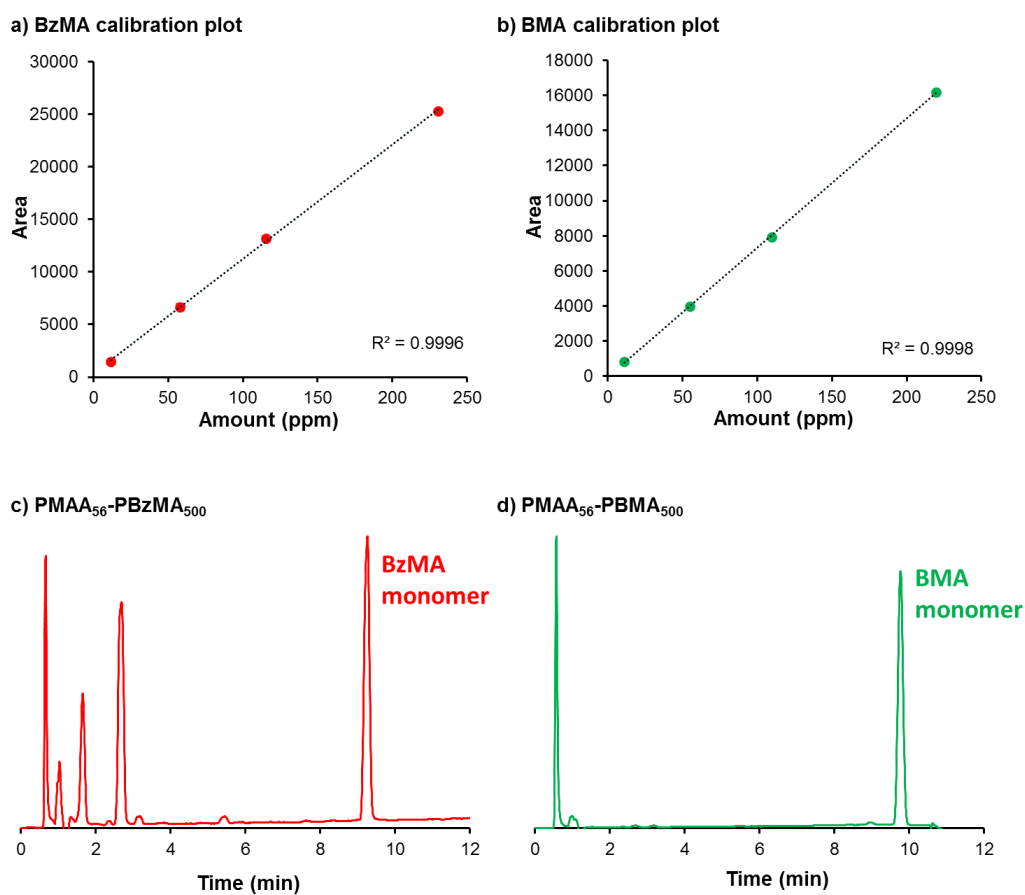
Appendix 2. Structural parameters obtained from SAXS analysis of 1.0 % w/w aqueous dispersions of PMAA₅₆-PHBMA_y diblock copolymer nano-objects at pH 5 using the spherical micelle model. R_g is the radius of gyration of the PMAA₅₆ corona chains while x_{sol} denotes the volume fraction of solvent in the core.

Population of Spheres							
	Scale	Radius (nm)	Std dev (nm)	a_1 (mixing coeff)	R_g (nm)	x_{sol}	Sigma interface
PMAA ₅₆ -PHBMA ₅₀	0.0009	9.6	1.3	2.5	1.0	0	2

Population of Chains						
	Scale	R_g (nm)	Theta sol	Volume (nm ³)	Scattering length density (sol)	Scattering length density (poly)
PMAA ₅₆ -PHBMA ₅₀	0.0016	1.3	0.5	6.90	9.42	10.70

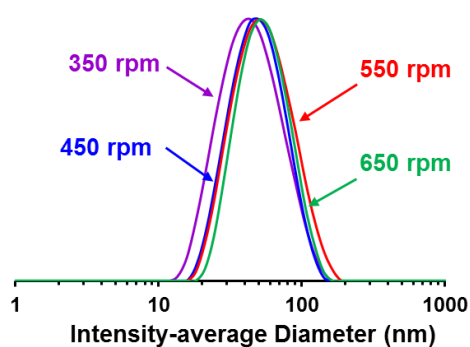
	Scale	Radius (nm)	Std dev (nm)	a_1 (mixing coeff)	R_g (nm)	x_{sol}	Sigma interface
PMAA ₅₆ -PHBMA ₃₀₀	0.0020	131	13	2.5	1.0	0	2
PMAA ₅₆ -PHBMA ₁₀₀₀	0.0023	165	11	2.5	1.0	0	2

Appendix 3. Monomer conversions for all high-throughput syntheses were determined by using HPLC to calculate the amount of residual monomer (ppm). Example calibration plots for (a) BzMA monomer and (b) BMA monomer and example chromatograms for (c) PMAA₅₆-PBzMA₅₀₀ and (d) PMAA₅₆-PBMA₅₀₀ are shown in this figure.

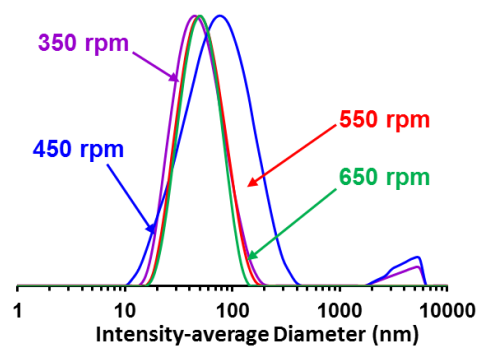


Appendix 4. Intensity-average size distribution plots for dynamic light scattering data reported in Table 1 and Figure 2. This data demonstrates the effect of stirrer geometry and stirring rate (rpm) on the synthesis of PMAA₅₆-PBzMA₅₀₀ and PMAA₅₆-PBMA₅₀₀ diblock copolymer nanoparticles *via* high-throughput RAFT aqueous emulsion polymerization at 70 °C. All reactions were performed at 20 % w/w solids using a macro-CTA/initiator molar ratio of 5.0. Intensity-average size distribution plots for the equivalent laboratory-scale syntheses (c) and (f) are also included for comparison.

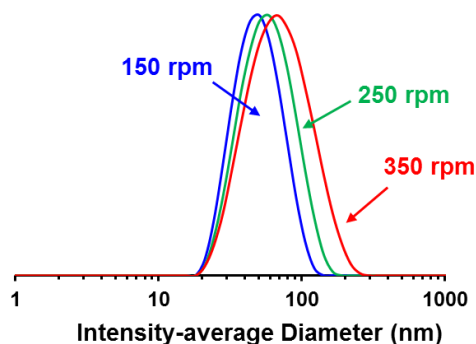
a) PMAA₅₆-PBzMA₅₀₀ synthesized using a *propeller* stirrer



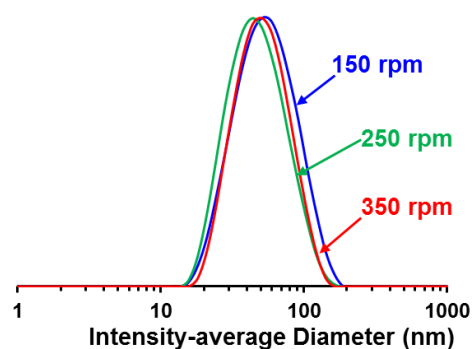
d) PMAA₅₆-PBMA₅₀₀ synthesized using a *propeller* stirrer



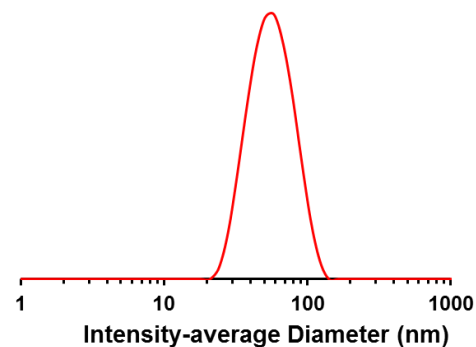
b) PMAA₅₆-PBzMA₅₀₀ synthesized using an *anchor* stirrer



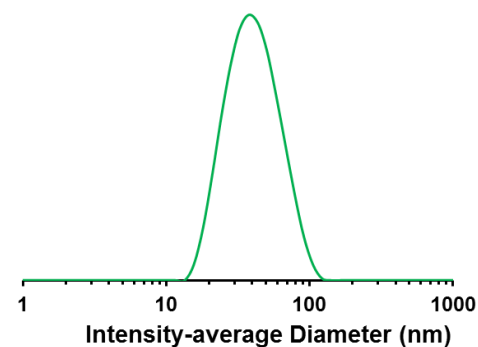
e) PMAA₅₆-PBMA₅₀₀ synthesized using an *anchor* stirrer



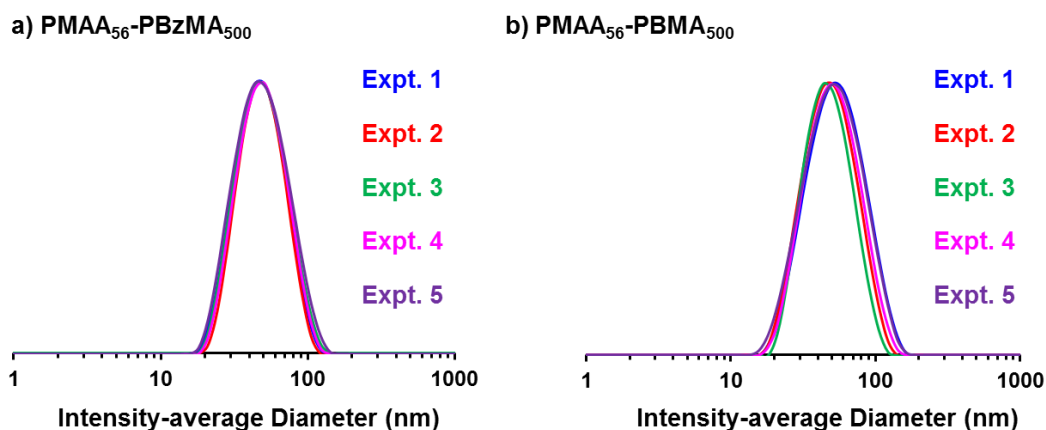
c) PMAA₅₆-PBzMA₅₀₀ synthesized on a laboratory scale



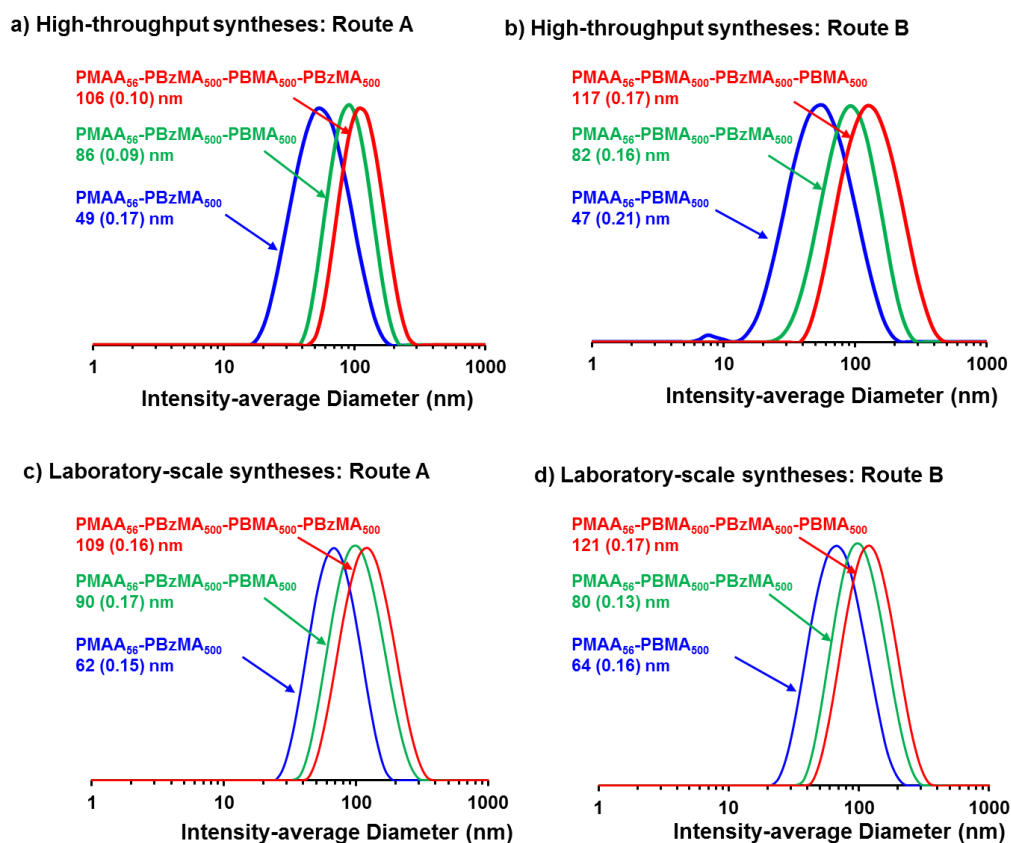
f) PMAA₅₆-PBzMA₅₀₀ synthesized on a laboratory scale



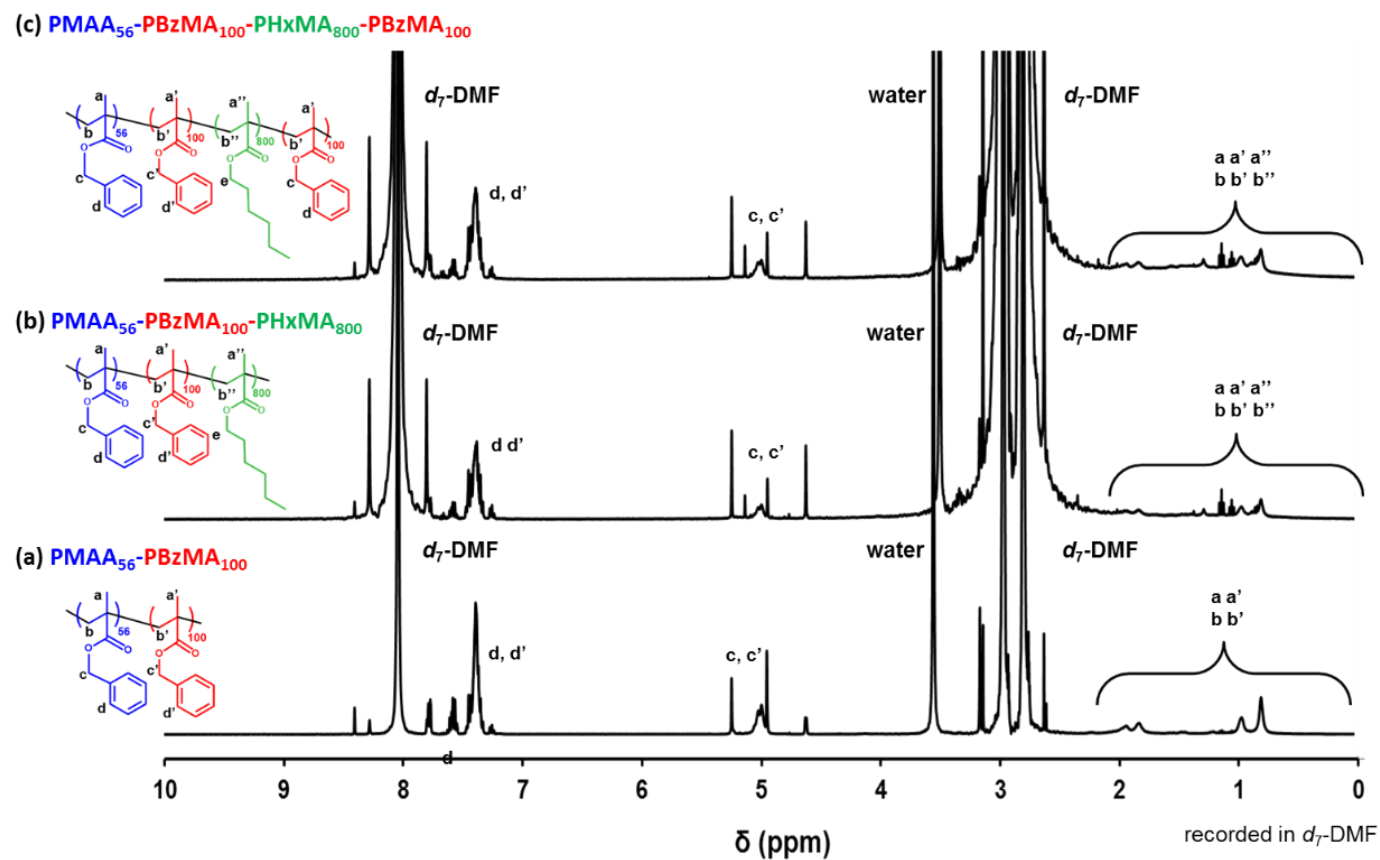
Appendix 5. Intensity-average size distribution plots for dynamic light scattering data reported in Table 2. This data demonstrates the reproducibility of the PISA synthesis of diblock copolymer nanoparticles *via* high-throughput RAFT aqueous emulsion polymerization of either benzyl methacrylate (BzMA) or *n*-butyl methacrylate (BMA) at 70 °C using a PMAA₅₆ macro-CTA at pH 5.



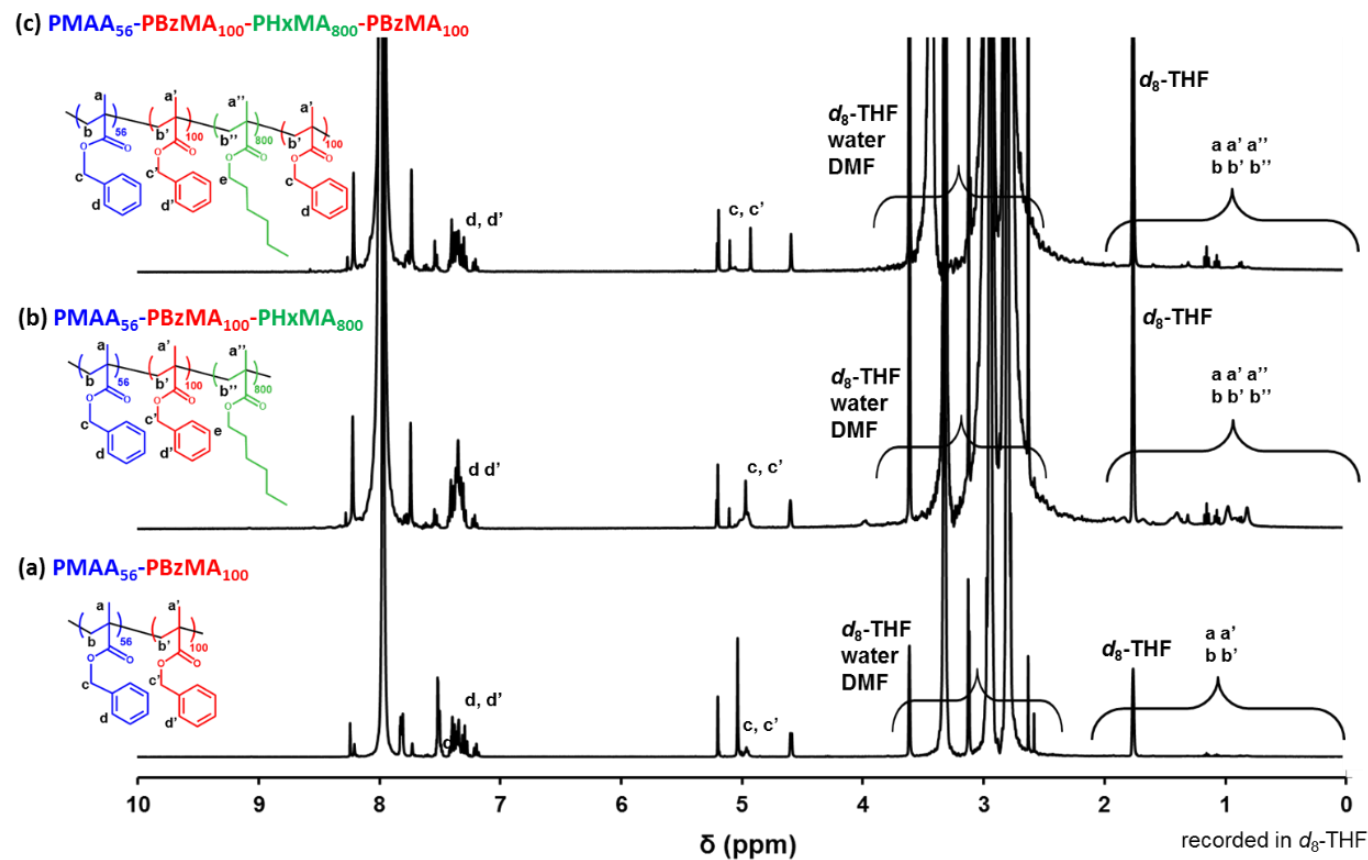
Appendix 6. Intensity-average size distribution plots for dynamic light scattering data for diblock, triblock and tetrablock copolymers prepared *via* RAFT aqueous emulsion polymerization. These syntheses were performed either on the high-throughput Chemspeed A100 robot synthesizer or on a laboratory-scale. These block copolymers were prepared via either (a) Route A or (b) Route B as outlined in Scheme 2.



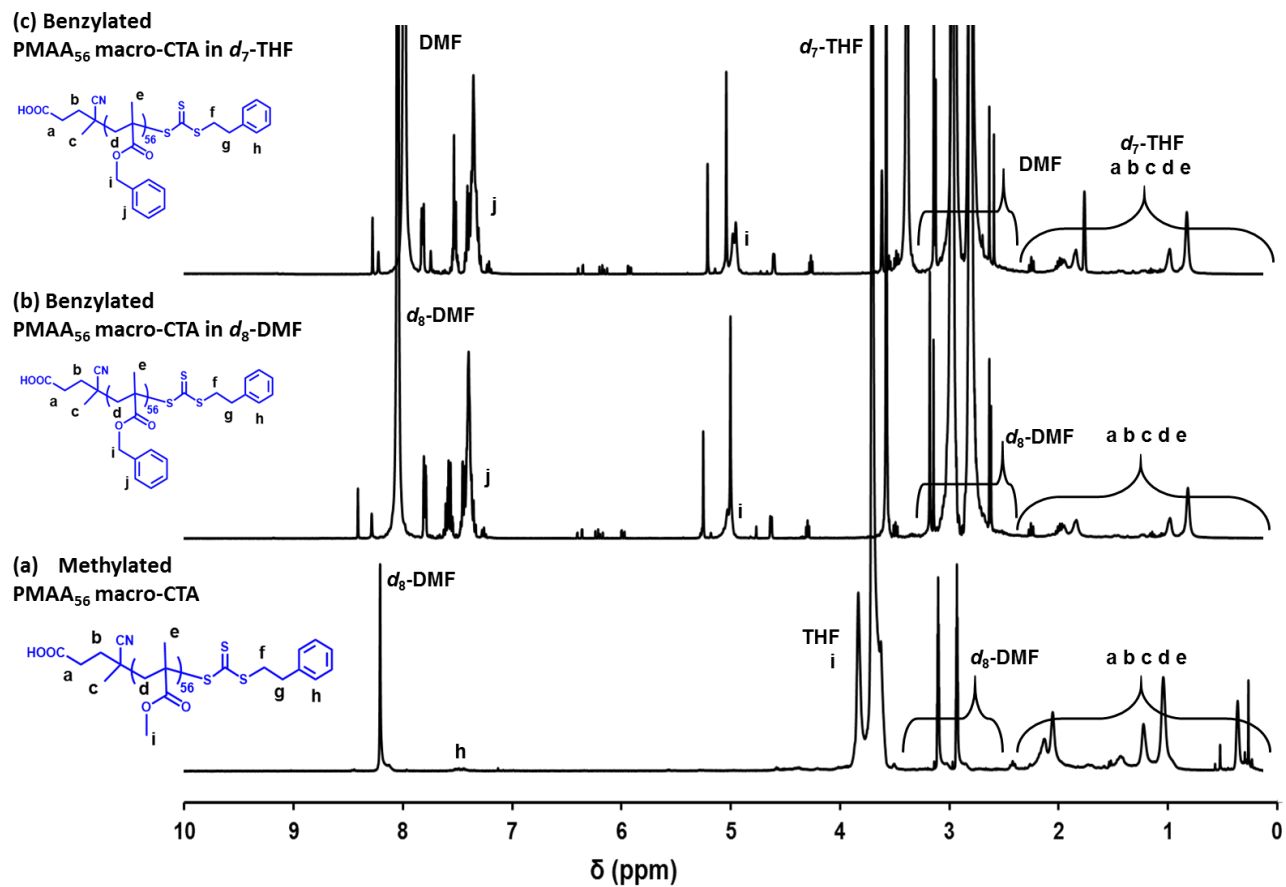
Appendix 7. ^1H NMR spectra recorded for *benzylated* PMAA₅₆-PBzMA₁₀₀ diblock copolymer, PMAA₅₆-PBzMA₁₀₀-PHxMA₈₀₀ triblock copolymer and PMAA₅₆-PBzMA₁₀₀-PHxMA₈₀₀-PBzMA₁₀₀ tetrablock copolymer all synthesized *via* RAFT aqueous emulsion polymerization. All spectra were recorded in d_7 -DMF.



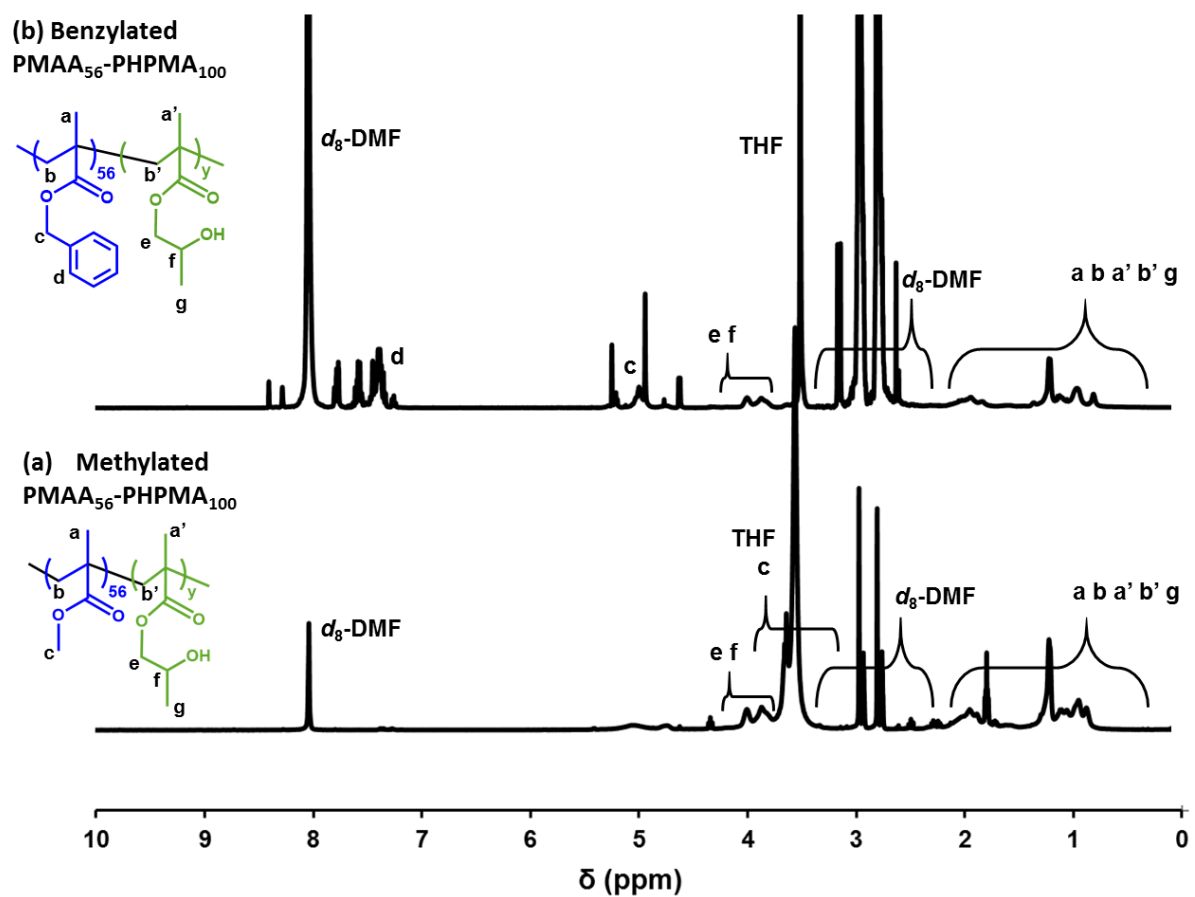
Appendix 8. ^1H NMR spectra recorded for *benzylated* PMAA₅₆-PBzMA₁₀₀ diblock copolymer, PMAA₅₆-PBzMA₁₀₀-PHxMA₈₀₀ triblock copolymer and PMAA₅₆-PBzMA₁₀₀-PHxMA₈₀₀-PBzMA₁₀₀ tetrablock copolymer all synthesized *via* RAFT aqueous emulsion polymerization. All spectra were recorded in d_8 -THF.



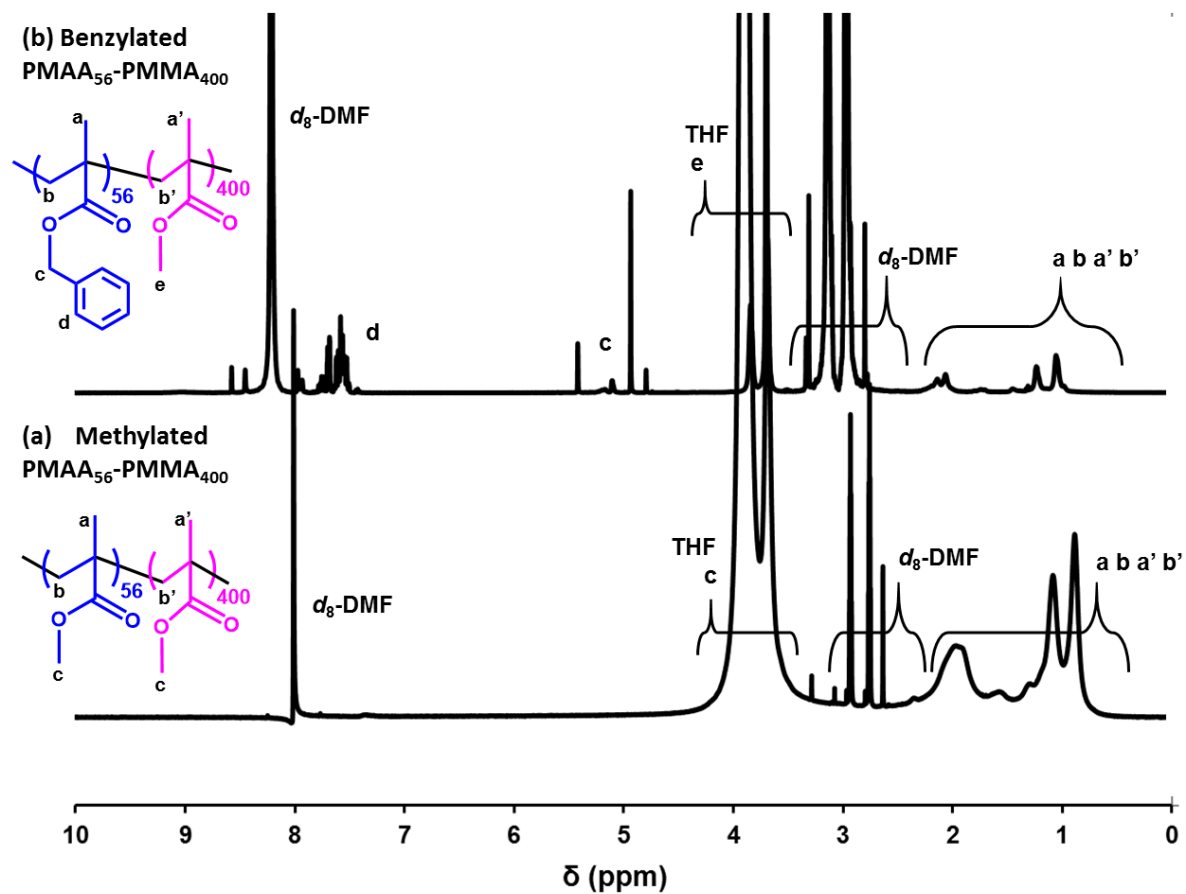
Appendix 9. ^1H NMR spectra recorded for (a) *methylated* and (b) *benzylated* PMAA₅₆ macro-CTA diblock copolymer synthesized *via* RAFT aqueous emulsion polymerization. Spectra were recorded in d_8 -DMF.



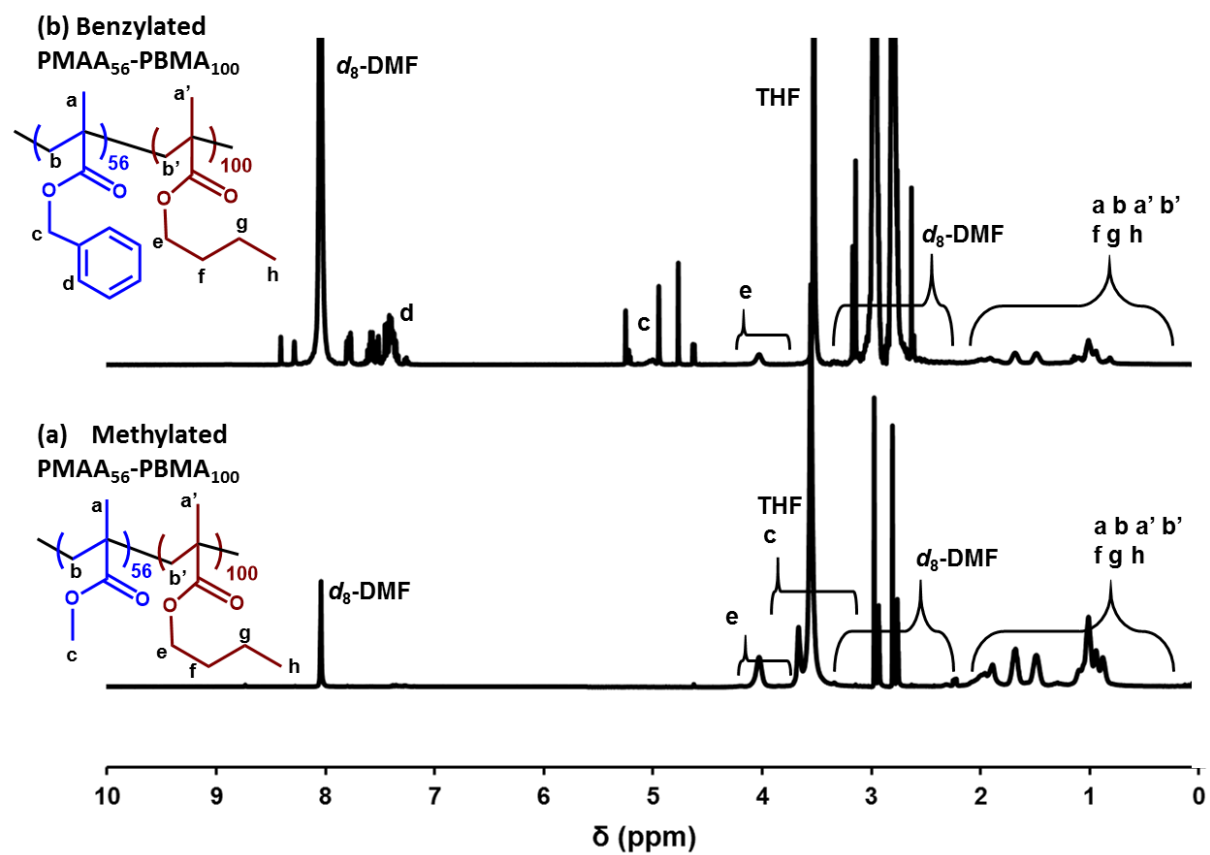
Appendix 10. ^1H NMR spectra recorded for (a) *methylated* and (b) *benzylated* PMAA₅₆-PHPMA₁₀₀ diblock copolymer synthesized *via* RAFT aqueous emulsion polymerization. Spectra were recorded in d_8 -DMF.



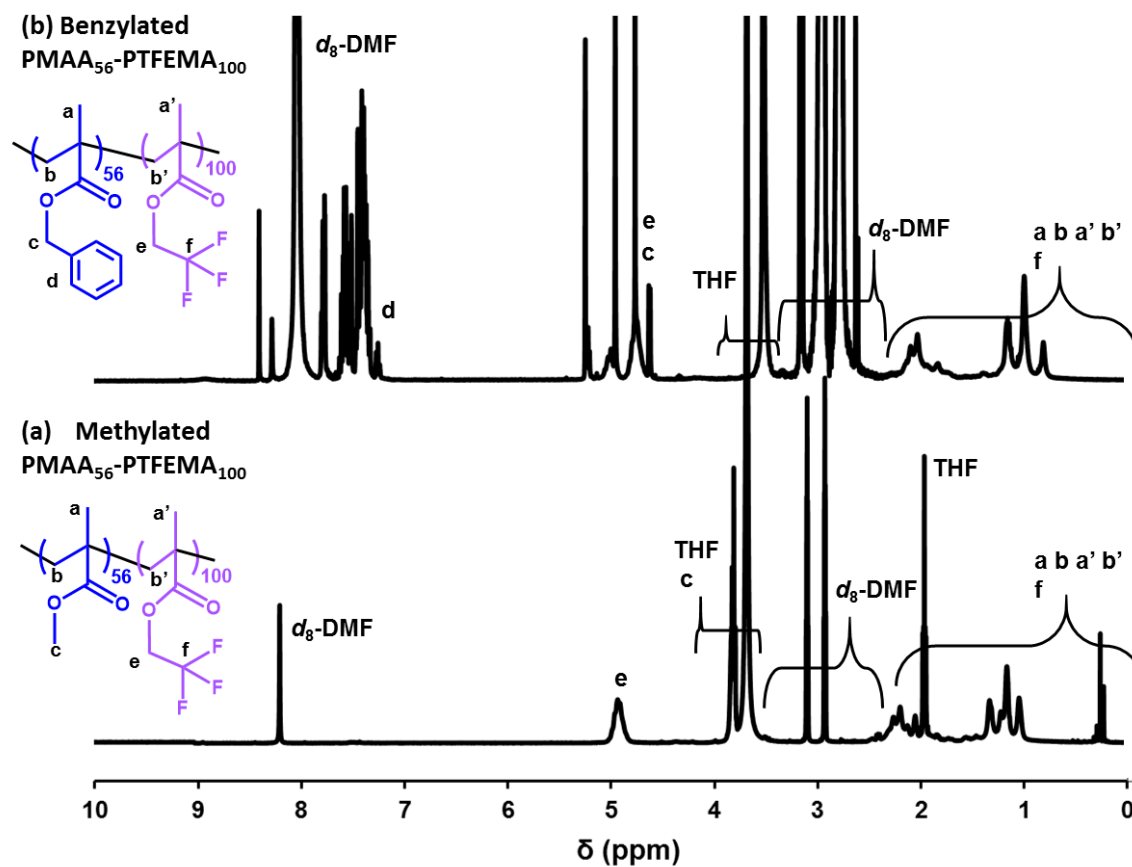
Appendix 11. ^1H NMR spectra recorded for (a) *methylated* and (b) *benzylated* PMAA₅₆-PMMA₄₀₀ diblock copolymer synthesized *via* RAFT aqueous emulsion polymerization. Spectra were recorded in d_8 -DMF.



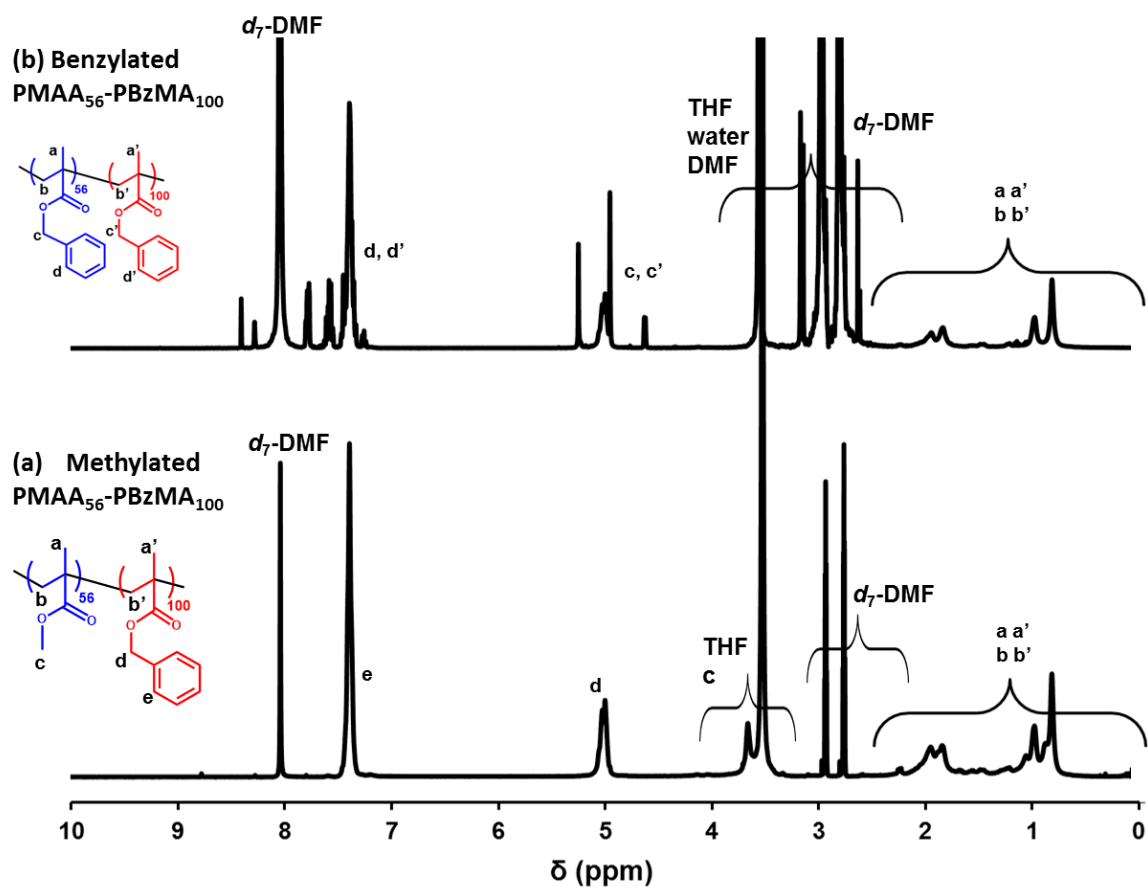
Appendix 12. ^1H NMR spectra recorded for (a) *methylated* and (b) *benzylated* PMAA₅₆-PBMA₁₀₀ diblock copolymer synthesized *via* RAFT aqueous emulsion polymerization. Spectra were recorded in d_8 -DMF.



Appendix 13. ^1H NMR spectra recorded for (a) *methylated* and (b) *benzylated* PMAA₅₆-PTFEMA₁₀₀ diblock copolymer synthesized *via* RAFT aqueous emulsion polymerization. Spectra were recorded in d_8 -DMF.



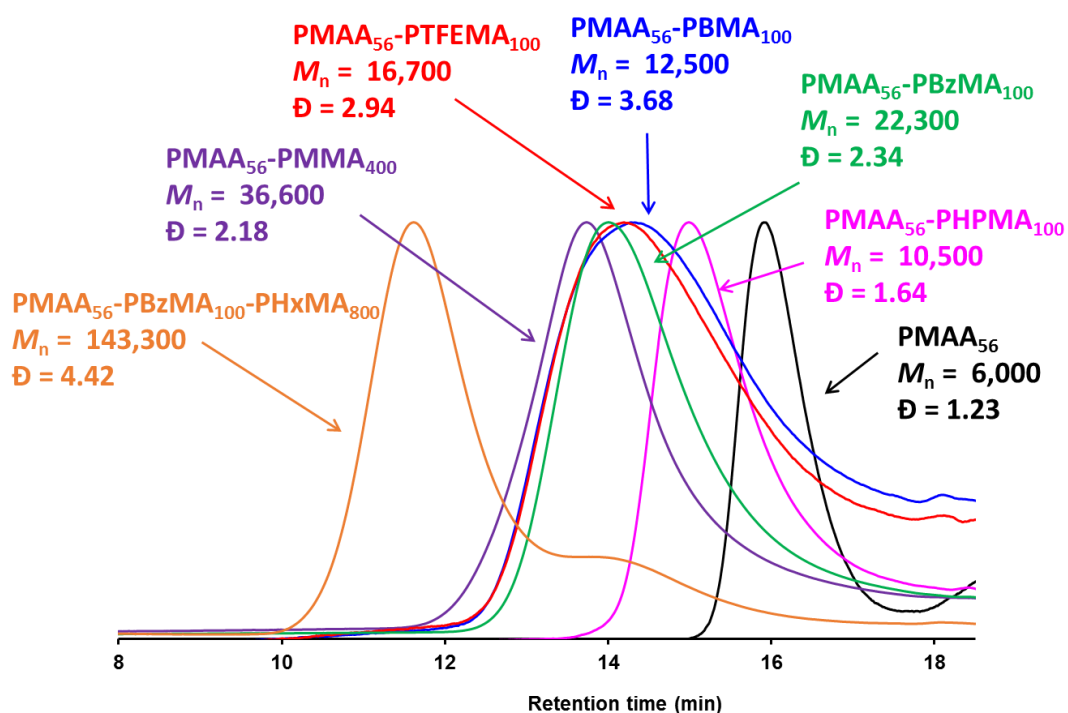
Appendix 14. ^1H NMR spectra recorded for (a) *methylated* and (b) *benzylated* PMAA₅₆-PBzMA₁₀₀ diblock copolymer synthesized *via* RAFT aqueous emulsion polymerization. Spectra were recorded in d_8 -DMF.



Appendix 15. Number-average molecular weights (M_n) and dispersities for a range of PMAA-based block copolymers synthesized *via* RAFT aqueous emulsion polymerization. Block copolymers were either modified by a methylation or benzylation reaction prior to THF GPC analysis or not modified and analyzed using THF eluent containing 4% v/v acetic acid.

Composition	Methylated block copolymers		Benzylated block copolymers		Not modified, analyzed using THF + 4% v/v acetic acid eluent	
	M_n	\bar{D}	M_n	\bar{D}	M_n	\bar{D}
PMAA ₅₆ -macro-CTA	7,000	1.18	6,300	1.19	6,000	1.23
PMAA ₅₆ -PHPMA ₁₀₀	11,100	1.51	20,800	1.57	10,500	1.64
PMAA ₅₆ -PMMA ₄₀₀	45,000	1.79	30,600	1.77	36,000	2.18
PMAA ₅₆ -PBMA ₁₀₀	18,600	2.44	9,400	1.45	12,500	3.68
PMAA ₅₆ -PTFEMA ₁₀₀	11,400	2.94	9,100	2.13	16,700	2.94
PMAA ₅₆ -PBzMA ₁₀₀	15,900	3.05	16,100	2.22	22,300	2.34
PMAA ₅₆ -PBzMA ₁₀₀ -PHxMA ₈₀₀	98,800	5.86			143,300	4.42
PMAA ₅₆ -PBzMA ₁₀₀ -PHxMA ₈₀₀ -PBzMA ₁₀₀	67,300	5.75			132,700	4.46

Appendix 16. THF GPC chromatograms of a selection of PMAA-based block copolymers synthesized *via* RAFT polymerization in water. Block copolymers are not modified prior to GPC analysis but analyzed using a THF eluent containing 4% v/v acetic acid. Molecular weight (M_n) and dispersity (\mathcal{D}) are calculated relative to a series of near-monodisperse PMMA calibration standards.



Appendix 17. DMF GPC chromatograms of a selection of PMAA-based block copolymers synthesized *via* RAFT polymerization in water. Block copolymers are modified by a benzylation reaction prior to analysis. Molecular weight (M_n) and dispersity (\mathcal{D}) are calculated relative to a series of near-monodisperse PMMA calibration standards.

